

CONJUGATED POLYELECTROLYTES: SYNTHESIS, PHOTOPHYSICAL STUDIES AND
APPLICATIONS TO SENSORS AND BIOCIDAL ACTIVITY

By

EUNKYUNG JI

A DISSERTATION PRESENTED TO THE GRADUATE SCHOOL
OF THE UNIVERSITY OF FLORIDA IN PARTIAL FULFILLMENT
OF THE REQUIREMENTS FOR THE DEGREE OF
DOCTOR OF PHILOSOPHY

UNIVERSITY OF FLORIDA

2009

© 2009 Eunkyung Ji

To my family

ACKNOWLEDGMENTS

During my long journey toward this point of my academic career, there are many people who I sincerely want to acknowledge. First of all, I really would like to thank my advisor, Dr. Kirk Schanze for his support, advice and encouragement. His enthusiasm to science encouraged me to keep on studying fascinating areas of photophysics and conjugated polymers which I barely knew before I joined his group.

I also would like to acknowledge all the former and current members of the Schanze group. When I first started experiments Eric Silverman kindly taught me how to use instruments and Dr. Kye-Young Kim helped me a lot to get used to work in the Schanze group. Dr. Xiaoyong Zhao always shared his skills for polymer synthesis with me and encouraged me to overcome difficulties in the lab. Dr. Hui Jiang helped me to learn about the photochemistry with pleasure. Dr. Yongjun Li has been a great classmate and labmate since I joined the chemistry department at UF. Dr. Yan Liu has been a good friend and shared her knowledge for sensor projects. Seoung Ho Lee has always been available for me to discuss about projects. His friendship and encouragement cheer me up to finish study here. I give my thanks to Julia Keller and Abigail Shelton for managing the orders for group members. Their kindness and smile always make me comfortable during the long tough five years. Jonathan Sommer and Jarrett Vella have showed their sense of humor, which always make me laugh in the lab.

I would like to thank Dr. Jon Stewart and Dimitri Dascier. They let me use their instruments to finish my projects. Dimitri Dascier also has supported me to overcome difficulties in a different country. I would like to express my appreciation to Dr. William Dolbier, one of my committee members, for his kindness in writing a recommendation letter for me. I am also thankful to other committee members, Dr. Lisa McElwee-White, Dr. Valeria D. Kleiman and Dr. Stephen Hagen for their time and suggestions.

Finally, I am grateful to my family for their support and love. They always have provided me with the best conditions for my education. Without them, I can't continue my education and come to this far. I am sincerely thankful to my two grandmothers for their love. I am also really sorry to them because they passed away when I was here so I couldn't attend their funeral.

TABLE OF CONTENTS

	<u>page</u>
ACKNOWLEDGMENTS	4
LIST OF TABLES	10
LIST OF FIGURES	11
ABSTRACT.....	16
CHAPTER	
1 INTRODUCTION	18
Conjugated Polyelectrolytes	18
Amplified Fluorescence Quenching of Conjugated Polyelectrolytes.....	19
Fluorescence Quenching	19
Amplified Quenching	22
Aggregation of Conjugated Polyelectrolytes.....	24
Synthetic Helical Conjugated Polyelectrolytes	26
History of Helical Polymers	26
Self-Assembly of Meta-Linked Phenylene Ethynylenes: Helical Folding.....	28
Application of Conjugated Polyelectrolytes.....	34
Optical Sensors.....	34
Superquenching mechanism.....	34
Fluorescence resonance energy transfer (FRET) mechanism	35
Conformation change	37
Biocidal Activity	38
Scope of the Present Study	39
2 SENSING OF PROTEASE ACTIVITY USING META-LINKED POLY (PHENYLENE ETHYNYLENE) SULFONATE	41
Introduction.....	41
Results and Discussion	43
Overview of Protease Turn-on Assay.....	43
Peptidase Activity Sensing	43
Concentration Effect of Polymer and Buffer on Fluorescence Quenching	45
Summary and Conclusions	47
Experimental.....	48
Materials	48
Instrumentation.....	48
General Methods	48

3	FLUORESCENCE QUENCHING OF HELICAL CONJUGATED POLYELECTROLYTE BY RHENIUM-BIOTIN COMPLEX AS QUENCHER-TETHER-LIGAND (QTL) PROBE	50
	Introduction.....	50
	Results.....	54
	Synthesis of Re complexes.....	54
	Photophysical Properties of Re complexes	54
	Fluorescence Quenching of mPPESO ₃ with Re(dppz) and Re(dppz)-biotin.....	55
	Avidin Interactions with mPPESO ₃ /Re(dppz)-biotin	57
	Fluorescence Quenching of mPPESO ₃ with Pre-formed Re(dppz)-biotin/avidin Complex.....	58
	Effect of Specific Protein on Fluorescence Quenching of mPPESO ₃ by Re(dppz)-biotin	58
	Discussion.....	62
	Summary and Conclusions	63
	Experimental.....	64
	Materials.....	64
	Instrumentation.....	64
	General Methods	64
	Fluorescence quenching	64
	Fluorescence recovery.....	65
	Synthetic Procedures	65
4	FLUORESCENCE RESONANCE ENERGY TRANSFER FROM HELICAL CONJUGATED POLYELECTROLYTE TO CHARGED FLUORESCENT DYE-LIGAND CONJUGATED (DLC) MOLECULE	68
	Introduction.....	68
	Results.....	70
	Photophysical Properties.	70
	FRET from mPPESO ₃ to Biocytin-TMR.....	71
	Anisotropy Measurements.....	76
	Fluorescence Quenching of PPESO ₃ by Biocytin-TMR	77
	Avidin binding to Biotin on Biocytin-TMR/CPEs complex	78
	Fluorescence Quenching of mPPESO ₃ by Pre-formed Biocytin-TMR/avidin complex.....	80
	Discussion.....	84
	Summary and Conclusions	85
	Experimental.....	86
	Materials.....	86
	Instrumentation.....	86
	General Methods	87

5	META-LINKED POLY (PHENYLENE ETHYNYLENE) SULFONATE CONTAINING PYRIDINE.....	88
	Introduction.....	88
	Results and Discussion	93
	Synthesis.....	93
	Photophysical Characterization	93
	Fluorescence Quenching of mPPE-SO ₃ -py by Metal ions in water	95
	Protonation and Metal Complexation with Pd ²⁺	96
	Experimental.....	100
	Materials.....	100
	Instrumentation.....	100
	General Methods	100
	Synthetic Procedures	101
6	POLY (PHENYLENE ETHYNYLENE) WITH TETRA ALKYLAMMONIUM SIDE GROUPS FOR LIGHT-INDUCED BIOCIDAL ACTIVITY.....	102
	Introduction.....	102
	Results and Discussion	107
	Synthesis.....	107
	Polymer Characterization	107
	¹ H NMR and pulse gradient echo (PSGE) NMR	107
	Photophysical Characterization.....	109
	UV-vis and fluorescence spectroscopy	109
	Transient absorption spectroscopy	112
	Singlet Oxygen Production.....	112
	Biocidal Activity.....	116
	Mechanism for Biocidal Activity	118
	Experimental.....	121
	Materials.....	121
	Instrumentation.....	121
	General Methods	122
	Synthetic Procedures	123
7	CONJUGATED POLYAMPHOLYTES BASED ON POLY(PHENYLENE ETHYNYLENE)	128
	Introduction.....	128
	Results and Discussion	132
	Synthesis.....	132
	Properties of Conjugated Polyampholytes	135
	Summary and Conclusions	147
	Experimental.....	147
	Materials.....	147
	Instrumentation.....	148

General Methods	148
Synthetic Procedures	148
8 CONCLUSIONS	152
Intercalation of Intercalator Quenchers to mPPESO3	152
Helical Self-Assembly of mPPESO3-py	153
Biocidal Activity of Cationic CPEs	153
Conjugated Polyampholytes	153
LIST OF REFERENCES	155
BIOGRAPHICAL SKETCH	167

LIST OF TABLES

<u>Table</u>		<u>page</u>
2-1	Stern-Volmer Quenching constants for mPPESO3 and PPESO3 fluorescence quenching by K- <i>p</i> NA.....	47
3-1	Stern-Volmer quenching constants for mPPESO3 and PPESO3 fluorescence quenching by Re complexes	55
4-1	Photophysical properties of mPPESO3, PPESO3 and biocytin-TMR in 1 mM phosphate buffer solution (pH 7.4).....	70
5-1	Photophysical properties of mPPE-SO3-py.....	95
6-1	Photophysical properties of cationic CPEs.....	115
7-1	Photophysical properties of conjugated polyampholytes	137
7-2	Stern-Volmer constant (K_{SV}) for P1 and P2 fluorescence quenching upon addition of MV ²⁺ and NDS in water and DMF.....	140

LIST OF FIGURES

<u>Figure</u>	<u>page</u>
1-1 Structures of some classes of conjugated polymers.....	18
1-2 Structures of conjugated polyelectrolytes (CPEs).....	20
1-3 Jablonski diagram	20
1-4 Comparison of dynamic and static quenching	22
1-5 Structures of conjugated polymer, monomer and quencher (MV^{2+}) used by Swager's group.	22
1-6 Amplification of fluorescence quenching of MPS-PPV with MV^{2+}	23
1-7 Stern–Volmer plots of polyfluorene quenching by 5-nm gold nanoparticles.....	24
1-8 Structures of a PPP-type CPE, a PPV-type CPE, and their neutral analogous polymers.....	25
1-9 Structures of PPE-type CPE PPESO3.....	27
1-10 Absorption and fluorescence spectra of PPE-type CPE PPESO3 in methanol, methanol/water (1:1) and water	27
1-11 Schematic illustration of face-face π - π stacking of PPESO3.....	27
1-12 Structures of OPEs studied by Moore's group and a space-filling model showing the conformationalequilibrium for OPE of length $n = 18$	28
1-13 Postulated association equilibrium between OPEs and chiral molecules.....	29
1-14 Structures of amphiphilic mPPEs studied by Tew's group	29
1-16 UV-vis absorption and emission spectra of mPPESO3 in MeOH/H ₂ O at different compositions	30
1-17 Emission spectra of $[Ru(bpy)_2(dppz)]^{2+}$ in absence and presence of mPPE-Ala	32
1-18 Circular dichroism spectra of mPPE-Ala in methanol, water and methanol/water mixtures.....	33
1-19 Emission quenching of mPPESO3by MV^{2+} in a 7:3 methanol/water mixture	34
1-20 Detection of avidin using CPE based on the superquenching mechanism	35
1-21 Structures of CPEs studied by Bazan and co-workers.....	36

1-22	Schematic representation for the use of PF1/PNA-C* to detect a complementary ssDNA.....	36
1-23	Structures of poly(thiophene) derivatives used in CPE-based sensor via conformational change mechanism.....	37
1-24	Schematic illustration for the detection of ssDNA sequences using poly(thiophene).....	38
1-25	Structure of cationic CPE used by the Whitten group	39
1-26	Phase contrast and fluorescence microscope images of CPE-treated <i>E. coli</i> and CPE-treated <i>B. anthracis</i> Stern spores	39
2-1	Mechanism of the “turn-on” and “turn-off” CPE-based enzyme assays	42
2-2	Structures of CPEs and quencher substrates used for CPE-based enzyme assays	42
2-3	Structures for a polymer and a quencher substrate and mechanism of the “turn-on” mPPESO3-based sensor.....	44
2-4	Fluorescence spectroscopic changes observed during turn-on assay	44
2-5	Stern-Volmer plots for fluorescence quenching of mPPESO3 with K- <i>p</i> NA and <i>p</i> -nitroaniline	46
2-6	Stern-Volmer plots of at different concentrations of mPPESO3 with K- <i>p</i> NA.....	47
3-1	Three binding modes of a metal complex with DNA.....	52
3-2	The light-switch effect of dppz-based metallo-intercalators	52
3-3	Structures and acronyms of polymers and Re complexes	54
3-4	Fluorescence spectra of mPPESO3 in the presence of Re(dppz) and Re(dppz)-biotin	56
3-5	Stern-Volmer plots for mPPESO3 quenching by Re(dppz)-biotin, pre-formed Re(dppz)-biotin/avidin complex (avidin:Re(dppz)-biotin = 1:4) and avidin.....	59
3-6	Stern-Volmer plots for PPESO3 quenching by Re(dppz)-biotin and pre-formed Re(dppz)-biotin-avidin complex (avidin:Re(dppz)-biotin = 1:4).	59
3-7	Stern-Volmer plots for mPPESO3 quenching by different ratios of pre-formed Re(dppz)-biotin/avidin complex and quenching percent of mPPESO3 by pre-formed Re(dppz)-biotin/avidin complex containing different concentrations of avidin.....	60
3-8	Stern-Volmer plots of mPPESO3 quenching by Re(dppz)-biotin, pre-mixed Re(dppz)-biotin-BSA mixture (BSA: Re(dppz)-biotin = 1:4) and BSA	61
3-9	Cross-linking of mPPESO ₃ and avidin by using Re(dppz)-biotin.....	63

3-10	Binding of Re(dppz)-biotin and pre-formed Re(dppz)-biotin/avidin complex to mPPESO3	63
4-1	Structures and acronyms of conjugated polyelectrolytes and dye-ligand conjugate used in this study.....	70
4-2	Energy transfer from mPPESO3 to biocytin-TMR.....	71
4-3	Normalized absorption spectrum of biocytin-TMR and normalized fluorescence spectra of biocytin-TMR and CPEs	73
4-4	Normalized fluorescence spectra of mPPESO3 upon addition of biocytin-TMR	74
4-5	Normalized fluorescence spectra of biocytin-TMR in the absence and presence of mPPESO3	75
4-6	Excitation spectrum of mPPESO3/biocytin-TMR complex.....	76
4-7	Excitation anisotropy of biocytin-TMR/mPPESO3 complex and biocytin-TMR.....	77
4-8	Normalized fluorescence spectra of PPESO3 upon addition of biocytin-TMR	78
4-9	Fluorescence spectra of mPPESO3 solution upon addition of biocytin-TMR and avidin.....	79
4-10	Fluorescence spectra of biocytin-TMR upon addition of avidin	80
4-11	Stern-Volmer plots of mPPESO3 and PPESO3 fluorescence quenched by biocytin-TMR or pre-formed biocytin-TMR/avidin complex.....	82
4-12	Sensitized biocytin-TMR fluorescence intensity at 590 nm after addition of biocytin-TMR or pre-formed biocytin-TMR/avidin complex to CPEs.....	82
4-13	SV plots for fluorescence quenching of mPPESO3 at 450 nm and polymer-sensitized biocytin-TMR fluorescence at 590 nm upon addition of pre-formed biocytin-TMR/avidin complex	83
5-1	Structures of phenylene ethynylene (PE) based macrocycle and oligomers used for π -stacked self-assemblies	89
5-2	Schematic diagram illustrates the self-assembly of disk-shaped phenylene ethynylene macrocycles and oligomers.....	89
5-3	Structures of conjugated polymers containing bipyridyl and terpyridyl ligands.....	90
5-4	Structures of poly(pyridyl/phenyl ethynylene) polymers with varying ratios of <i>para</i> -/ <i>meta</i> -linked constitutional units.....	91

5-5	Structures of a poly(<i>p</i> -phenylene ethynylene) derivative containing <i>meta</i> -substituted monopyridyl groups	92
5-6	Structure of a <i>meta</i> -poly(phenylene ethynylene) containing pyridine units (<i>m</i> -PPY).....	92
5-7	Synthesis of mPPE-SO ₃ -py	93
5-8	Normalized absorption and emission spectra of mPPE-SO ₃ -py in water, methanol and mixture of the two solvents	94
5-9	Stern-Volmer plots for mPPE-SO ₃ -py fluorescence quenching by metal ions in water ...	97
5-10	Fluorescence responses of mPPE-SO ₃ -py to metal ions in water	97
5-11	Absorption and emission spectra of mPPE-SO ₃ -py in water and in methanol with addition of HCl solution.....	98
5-12	Absorption and emission spectra of mPPE-SO ₃ -py in water and in methanol with addition of Pd ²⁺	99
6-1	Pathway of type I and Type II reaction of light absorbing photosensitizer	104
6-2	Structure of PPE-NMe ₃ -OR8 and phase contrast and fluorescent microscope images of polymer-treated <i>E.coli</i> and polymer-treated <i>B. anthracis</i> Sterne spores	105
6-3	Structures and acronyms of cationic conjugated polyelectrolytes investigated in this study	106
6-4	General synthetic scheme for monomer 5, 9 and 12.....	108
6-5	General synthetic scheme for polymer 13a, 14 and 16	109
6-6	Absorption and emission spectra of CPEs in methanol and water	110
6-7	Transient absorption spectroscopy of cationic CPEs in methanol and water.....	113
6-8	Pathway for PPE-sensitized singlet oxygen generation.....	114
6-9	Singlet oxygen emission sensitized by CPEs in CD ₃ OD.....	114
6-10	Peroxidation of CHDDE by singlet oxygen (¹ O ₂)	117
6-11	UV-visible spectra of CHDDE and PPE-NMe ₃ -OR8, PPE-NMe ₃ -Th, PPE-4+ or PPE-C6-NMe ₃ -OR8 in D ₂ O solution containing phosphate buffer (100 μM, pH 7) as a function of the irradiation time	117
6-12	Images of single SGCP-particle with captured bacteria	118
6-13	Confocal fluorescence images of SGCP-13b with <i>C. marina</i> in ambient air.....	119

6-14	Dead/live ratios of <i>C. marina</i> exposed to 5 μm SGCP-13b under various conditions	120
6-15	Mechanism of biocidal action.....	120
7-1	Structures of the four subclasses of polyampholytes.....	129
7-2	Structures of polyampholytes that have been synthesized.....	130
7-3	Structures of conjugated polyampholytes.....	131
7-4	Synthesis of monomers 4, 6, 8, 9 and 13	133
7-5	Synthesis of conjugated polyampholytes.....	134
7-6	^1H NMR spectrum of P1 and P2 in DMSO- d_6	136
7-7	Absorption and emission spectra of P1 and P2 in methanol and water	138
7-8	Structures of a cationic and an anionic quencher used in this study.....	139
7-9	Emission spectra of P1 and P2 in water upon addition of a cationic and an anionic quencher.....	140
7-10	Absorption and emission spectra of P1 and P2 in DMF	142
7-11	Emission spectra of P1 and P2 in DMF upon addition of a cationic and an anionic quencher.....	143
7-12	Absorption and emission spectra of PPE-NMe ₃ -COOH as a function of pH in aqueous solution.....	144
7-13	Absorption and emission spectra of PPE-NMe ₃ -COOH in methanol upon addition of HCl solution	145
7-14	Emission spectra of PPE-NMe ₃ -COOH upon addition of an anionic quencher, NDS at different pH solutions.....	146

Abstract of Dissertation Presented to the Graduate School
of the University of Florida in Partial Fulfillment of the
Requirements for the Degree of Doctor of Philosophy

CONJUGATED POLYELECTROLYTES: SYNTHESIS, PHOTOPHYSICAL STUDIES AND
APPLICATIONS TO SENSORS AND BIOCIDAL ACTIVITY

By

Eunkyung Ji

August 2009

Chair: Kirk S. Schanze
Major: Chemistry

This dissertation is focused on the design, synthesis, photophysical characterization and application of conjugated polyelectrolytes (CPE)s including anionic *meta*-linked poly(phenylene ethynylene)s (PPEs) such as mPPESO3 and mPPE-SO3-py, and cationic PPEs featuring quaternary ammonium side groups. We also introduce the synthesis and characterization of PPE-based polyampholytes bearing both anionic and cationic side groups.

First, we have investigated the application of mPPESO3 for sensing of protease activity based on the amplified fluorescence quenching of the polymer. Since the polymer is folded into a helix in water, we have studied a mechanism for the interaction between the polymer and cationic intercalator quenchers. In this study, Re(dppz)-biotin and biocytin-TMR have been used as biotin-functionalized quenchers. The polymer fluorescence is quenched by both quenchers; however, addition of the target protein avidin does not recover the fluorescence from the quenched polymer. We also found that pre-formed avidin-quencher complexes less efficiently quench the polymer fluorescence compared to the only quenchers.

Second, a PPE featuring *meta*-linked pyridine rings on the polymer backbone (mPPE-SO3-py) was designed and synthesized. The polymer is shown to undergo a conformational change

from a random-coil to a helix by solvent polarity, protonation and metal complexation. The polymer also shows high sensitivity and selectivity for the Pd²⁺ ion.

Third, a series of cationic CPEs with quaternary ammonium side groups has been synthesized and examined their biocidal activity. The photophysical studies in solution shows that direct excitation of the polymers produces a triplet state, sensitizing effectively singlet oxygen generation. Therefore, the polymer effectively kills bacteria such as *Cobetia marina* and *Pseudomonas aeruginosa*.

Finally, a series of new conjugated polyampholytes containing both anionic and cationic side groups has successfully synthesized. These polymers show different behavior depending on the nature of ionic groups, the ratio of anionic to cationic groups, and pH. The polymer with 1:1 ratio of ammonium to sulfonate groups shows very low solubility in water and organic solvents; however, when the ratio is smaller, the polymers behave like CPEs. The polyampholyte bearing carboxyl and ammonium side groups shows pH- dependent photophysical changes.

CHAPTER 1 INTRODUCTION

Conjugated Polyelectrolytes

Conjugated polymers (CPs) are organic semiconducting polymers containing a base structure of alternating single and double/triple bonds. Since Shirakawa, MacDiarmid and Heeger discovered the electrically conducting polymer, polyacetylene doped with halogen in 1977,¹ much effort has been directed to a variety of other CPs with different backbone structures based on aromatic, heteroaromatic, vinylic or acetylenic π -systems including poly(*para*-phenylene) (PPP)², polyfluorene (PF),³ polypyrrole (PPy),⁴ polythiophene (PT),⁵ polyaniline (PANI),⁶ poly(phenylene ethynylene) (PPE),⁷ poly(phenylene vinylene) (PPV)⁸ as shown in Figure 1-1. In the past three decades, the CPs have been important materials for applications in light-emitting diodes (LEDs),⁸ light-emitting electrochemical cells (LECs),⁹ plastic lasers,¹⁰ solar cells,¹¹ field-effect transistors (FETs),¹² and sensors.^{13, 14} Each class of CP is prepared by its own synthetic methodology. Metal-catalyzed reaction has been widely used for synthesis of CPs, including PPPs by the Suzuki, Stille and Yamamoto coupling reaction;¹⁵ PPVs by the

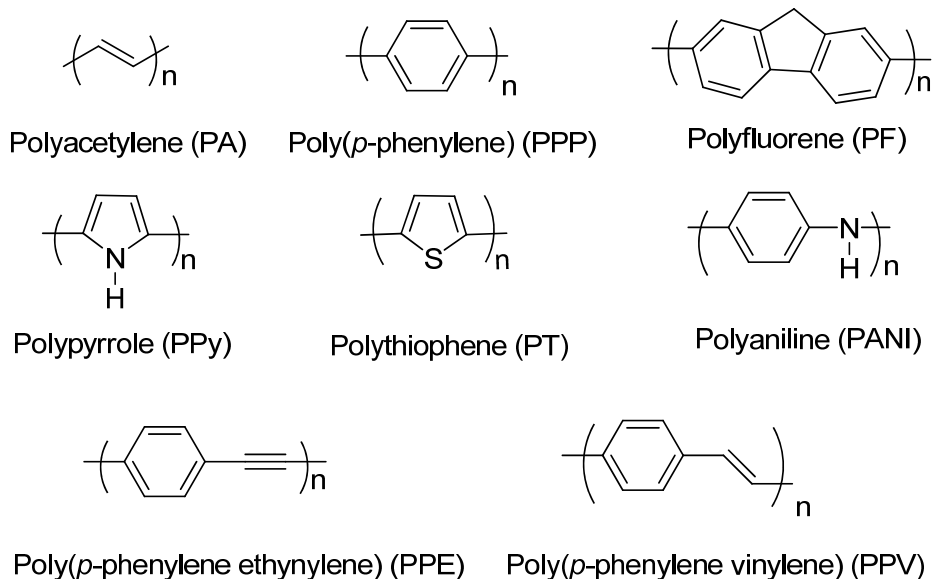


Figure 1-1. Structures of some classes of conjugated polymers.

Wittig-Horner and Heck reactions, or the Gilch and Wessling routes;¹⁶ and PPEs by the Sonogashira coupling and alkyne methathesis reactions.^{7,17} The various palladium-catalyzed coupling methods such as Suzuki, Stille, Heck and Sonogashira allow mild reaction conditions, wide functional group tolerance, and flexibility of solvent used for the polymerization.

These methods are also used for the synthesis of CPs featuring ionic side groups which make the CPs soluble in water and other polar solvents.^{18,19} Shi and Wudl reported the synthesis of water soluble PPV.²⁰ The synthesis of water soluble PPP was reported by Wallow and Novak.²¹ These early reports were important initial contribution to this area. In the decade, several synthetic methods have been developed, resulting in structurally diverse of conjugated polyelectrolytes (CPEs). Most CPEs contain PPV, PPP or PPE backbone with ionic functional groups such as sulfonate (SO_3^-), carboxylate (CO_2^-), phosphate (PO_4^{2-}) and ammonium (NR_3^+) (Figure 1-2). In addition, CPEs feature strong light absorption and strong fluorescence in solution and in solid state.

Amplified Fluorescence Quenching of Conjugated Polyelectrolytes

Fluorescence Quenching

Recently CPEs have been studied for application in chemo- and biosensors^{13, 22-28} because of their amplified quenching by oppositely charged small molecules. Before we present the details of amplified quenching of CPEs, it is necessary to provide a brief overview of photophysical processes which occurs between the absorption and emission of light. These processes can be illustrated with a Jablonski Diagram (Figure 1-3). Following light absorption, molecules are excited from singlet ground state of S_0 to singlet excited state of S_1 , or higher levels of S_2 or S_3 . Molecules relax from higher vibrational level of S_2 to the lowest energy level of S_0 and this is called internal conversion. This process generally occurs within 10^{-12} s or less, which is much less than fluorescence lifetime. Therefore, fluorescence emission generally arises

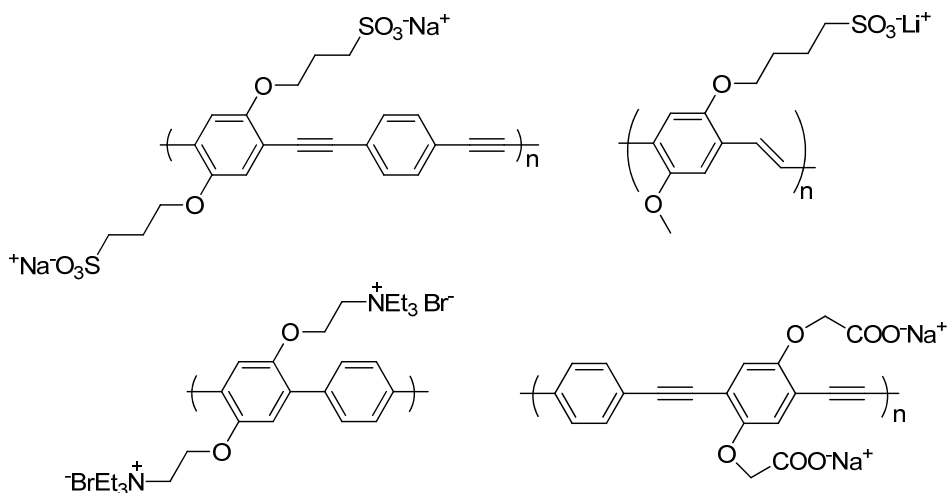


Figure 1-2. Structures of conjugated polyelectrolytes (CPEs).

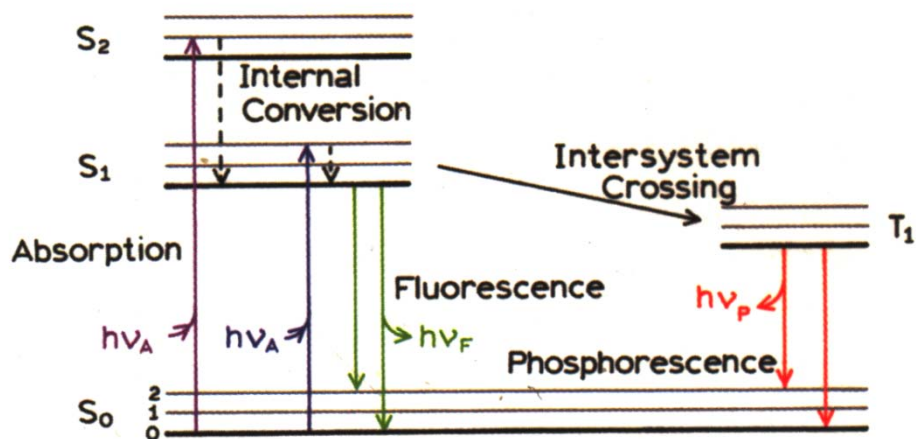
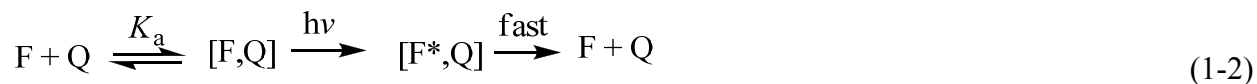


Figure 1-3. Jablonski diagram. Figure was taken from ref. 29.

from the lowest energy vibrational level of S_1 . Besides fluorescence emission, excited molecule is returned to ground state S_0 from the excited state by various competing pathways, including non-radiative decay to release heat and intersystem crossing to a triplet state T_1 . Emission from T_1 is termed phosphorescence. Fluorescence quenching is another important competing process, in which the intensity of fluorescence is decreased by either collision quenching (Eq. 1-1) or static quenching (Eq. 1-2).²⁹ In Eq. 1-1 and 1-2, F^* is an excited-state fluorophore, Q is a quencher, k_q is the bimolecular quenching rate constant and K_a is the association constant for



formation of the ground-state complex [F, Q]. Collision quenching, which is also called dynamic quenching, occurs when the excited state fluorophores contact with quenchers to deactivate and return to the ground state S_0 without fluorescence emission. Static quenching occurs when a non-fluorescent ground state complex is formed between a fluorophore and a quencher. When this complex absorbs light, it immediately returns to the ground state without fluorescence emission.

Both dynamic quenching and static quenching are described by Stern-Volmer (SV) equation:

$$I_0/I = 1 + K_{SV}[Q] \quad (1-3)$$

where I_0 and I are the fluorescence intensities in the absence and presence of a quencher,

respectively, $[Q]$ is the quencher concentration and K_{SV} is the Stern-Volmer quenching constant.

When the quenching is dominated by a dynamic process, $K_{SV} = k_q\tau_0$, where τ_0 is the fluorescence lifetime of F^* ; however, when a static quenching is dominant, $K_{SV} = K_a$. The dependence of

dynamic and static quenching on temperature and viscosity, or lifetime measurement can be used

to distinguish between these two quenching mechanisms (Figure 1-4). At higher temperature

diffusion is faster, and hence a larger amount of collision quenching occurs whereas weakly

bound complex is dissociated, and hence a smaller amount of static quenching occurs. For static

quenching $\tau_0/\tau = 1$. In contrast, for dynamic quenching $F_0/F = \tau_0/\tau$, where F_0 and F are the

fluorescence intensities in the absence and presence of quencher, respectively. Linear SV plots of

I_0/I vs $[Q]$ are observed when quenching is dominated by either purely static or dynamic

pathways. However, SV plots are curved upward in many situations due to various processes

including mixed static and dynamic quenching, variation in the association constant with quencher concentration and chromophore (or polymer) aggregation.

Amplified Quenching

Amplified quenching was first investigated by Swager and co-workers.^{30, 31} They observed amplified fluorescence quenching in a neutral, organic soluble poly(phenylene ethylene) (PPE) functionalized with cyclophane receptors, which form complexes with N,N'-dimethyl-4,4'-bipyridium (MV^{2+}), resulting in fluorescence quenching. This study also showed that the

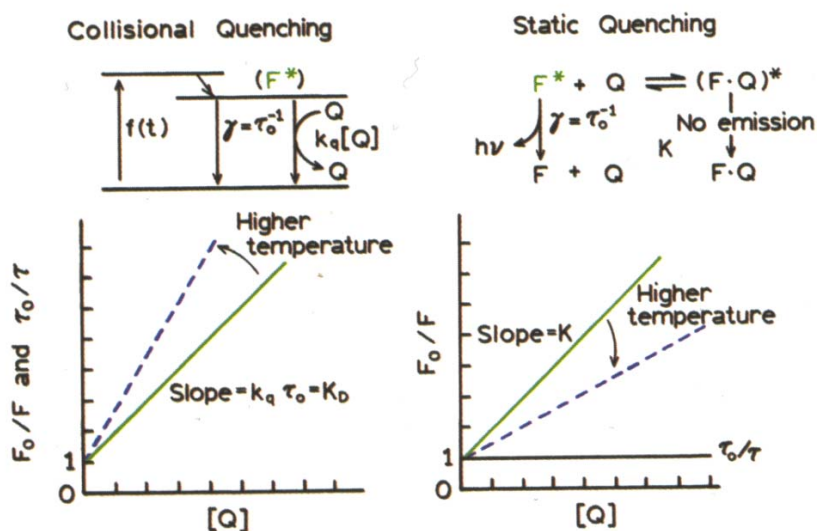


Figure 1-4. Comparison of dynamic and static quenching. Figure was taken from ref. 29.

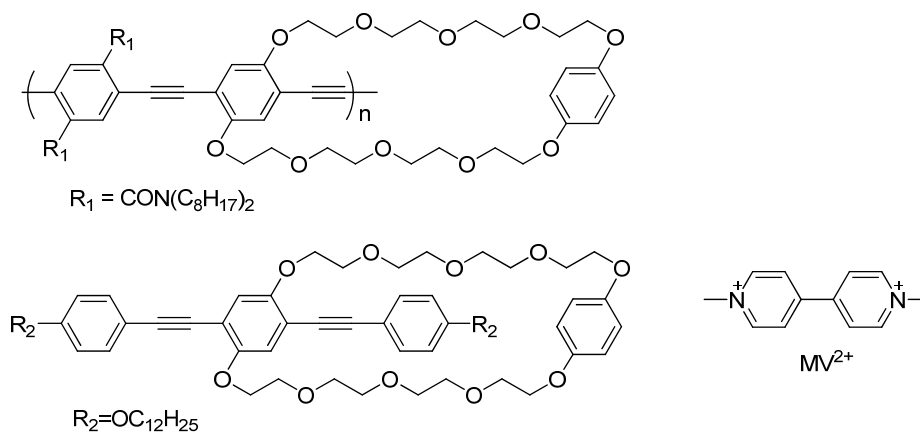


Figure 1-5. Structures of conjugated polymer, monomer and quencher (MV^{2+}) used by Swager's group.

fluorescence of the polymer is quenched about 60 times more efficiently compared to an analogous monomer. Amplified quenching is explained by complex formation between the quencher and the polymer, and rapid diffusion and/or delocalization of singlet exciton within the polymer (“molecular wire effect”).

Recently, amplified fluorescence quenching has been extended to CPEs.^{22, 23} The fluorescence of CPEs is efficiently quenched by oppositely charged quencher ions. Chen et. al. first reported the amplified quenching of CPEs, where K_{SV} of 10^7 M^{-1} was observed in the fluorescence quenching of poly(2-methoxy-5-propyloxysulfonate phenylene vinylene) (MPS-PPV) by methyl viologen (MV^{2+}) (Figure 1-6).²² The quenching constant is six orders of magnitude greater than that for dilute solution of stilbene and four orders of magnitude greater than that of for stilbene in micelles. In most CPE/quencher systems, SV plots show a linear behavior at low concentration followed by superlinear behavior at high concentration as shown in Figure 1-7.³²⁻³⁵ The superlinear quenching behavior is attributed to several factors including ion-pair complex formation between the polymer and the quencher,^{22, 33, 34, 36} efficient singlet exciton migration within the polymer,^{22, 33, 34, 37, 38} efficient long-range Förster energy transfer between the polymer and the quencher³⁴, and aggregation of polymer chains induced by the quencher.^{22, 33-37}

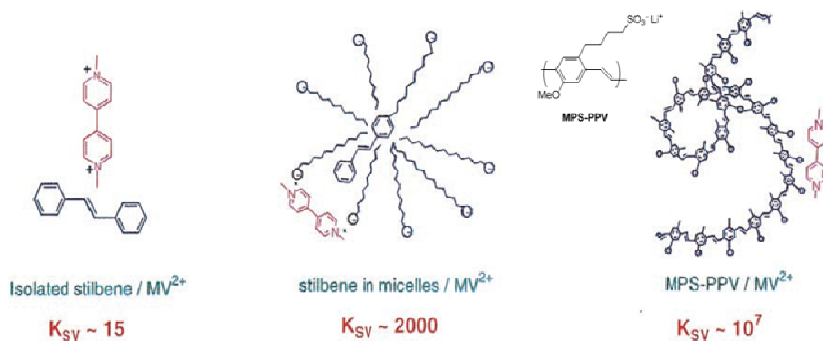


Figure 1-6. Amplification of fluorescence quenching of MPS-PPV with MV^{2+} . Figure was taken from Chen et al.²²

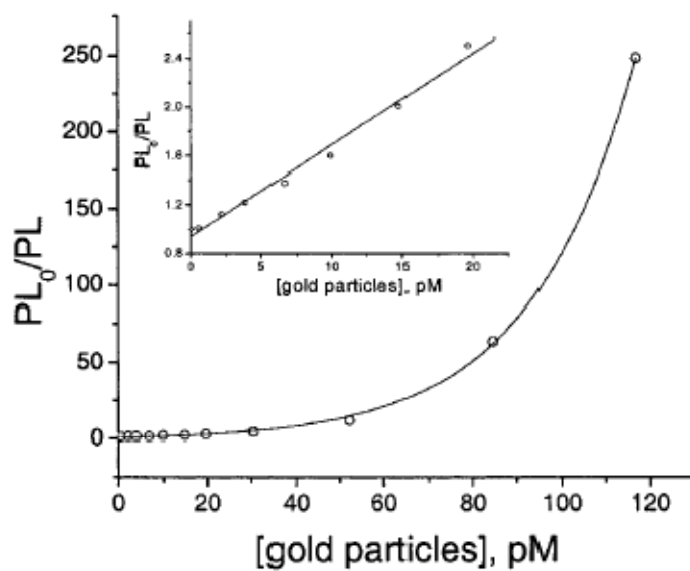


Figure 1-7. Stern–Volmer plots of polyfluorene (1.0×10^{-6} M in monomer repeat units) quenching by 5-nm gold nanoparticles. (Inset) Linear range in the low quencher concentration regime. Figure was taken from Fan et. al.³⁴

Aggregation of Conjugated Polyelectrolytes

It is well known that amphiphilic polymers self-assemble into various supramolecular architectures including micelles, vesicles and liquid-crystalline phases.^{39, 40} The amphiphilic characteristics of CPEs also make them self-assemble into supramolecular aggregates. When CPEs exist in solution in a non-aggregated state, their photophysical properties are similar to those of a neutral analog dissolved in a non-polar organic solvent. For example, Reynolds and co-workers reported that sulfonated PPE-type CPE PPP-OPSO3 (Figure 1-8) in a dilute aqueous solution displays a fluorescence maximum of 410 nm and quantum yield of 0.60.⁴¹ These values are similar to the fluorescence maximum of 406 nm and quantum yield of 0.70 of structurally analogous, neutral PPP with alkyloxy side group, PPP-OR11 (Figure 1-8) in chloroform.⁴² On the other hand, the aggregation of CPEs in aqueous solution strongly influences the photophysical properties of the polymers. For example, Whitten and co-workers reported that sulfonated PPV (MPS-PPV) (Figure 1-8) exhibits a fluorescence maximum that is relatively red-

shifted and has a significantly decreased fluorescence quantum yield compared to the neutral analog MEH-PPV (Figure 1-8) in solution.^{22, 43} These changes arise due to inter-chain aggregation, producing excimer-like states.

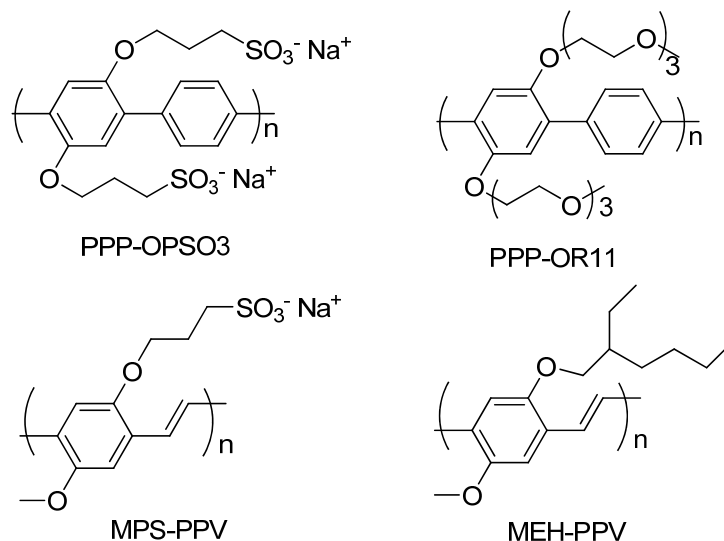


Figure 1-8. Structures of a PPP-type CPE, a PPV-type CPE, and their neutral analogous polymers.

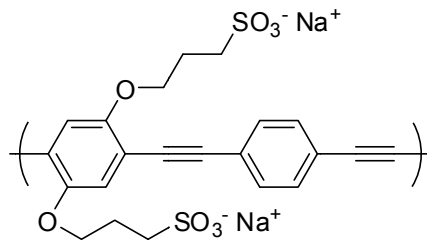
Previously, our group reported that the solvent dependence of the absorption and fluorescence spectra of PPE-type of CPE, PPE- SO_3 (Figure 1-9).³⁶ As shown in Figure 1-10, as the amount of water increases, the absorption red-shifts and narrows. The fluorescence red-shifts and broadens, and the fluorescence quantum yield decreases with increasing water content. All of these features provide clear evidence that PPE- SO_3 aggregates in water, while it exists in a non-aggregated state in methanol. Specifically, the absorption changes are consistent with increased structural order and conjugation length in the PPE backbone. The red-shifted and broad fluorescence band is attributed to the formation of an excimer-like state, which arises from inter-chain π - π stacks. In aggregated polymer, the chains align with their long axis parallel and the phenylene rings in each chain must be nearly co-planar to optimize hydrophobic interactions and π - π stacking (Figure 1-11).

Synthetic Helical Conjugated Polyelectrolytes

History of Helical Polymers

Biopolymers such as proteins and nucleic acids fold into well-defined three-dimensional structures in solution. Synthetic helical polymers have been of interest for understanding the mechanism for helix formation in biopolymers.^{39, 44} Synthetic helical polymers also have been attractive because of their potential applications including molecular recognition, a molecular scaffold function for controlled special alignment of functional groups or chromophores, and ordered molecular alignment in the solid phase such as that in liquid crystalline materials.⁴⁴ The history of helical polymers goes back to the finding of the conformation of some natural polymers.

Among the helical polymers, π -conjugated materials have been of interest because they are potentially useful in areas such as polarization-sensitive electro-optical materials, asymmetric electro-synthesis, nonlinear optics, polarized photo- and electroluminescence and enantioselective sensing.⁴⁵ The materials feature primary structures that allow folding of backbones into a helical secondary structure. Optically active polyacetylenes with chiral side groups are an early example of this class of materials.⁴⁶ Since the first report of such polyacetylenes, a variety of monosubstituted⁴⁷⁻⁵⁰ and disubstituted⁵¹⁻⁵⁴ diacetylenes were synthesized from the monomers with chiral side groups. Yashima et. al. found that polyacetylenes bearing achiral side groups exhibit induced optical activity by interaction with chiral molecules that selectively binds to one form of the helix.^{48, 55} In addition to polyacetylenes, various conjugated polymers have been reported to form helical conformation in poor solvents or in the solid state. The helical polymers includes oligo- and polythiophenes,⁵⁶⁻⁶⁰ oligo- and polyfluorenes,⁶¹⁻⁶³ poly(*p*-phenylene)s,^{64, 65}



PPESO3

Figure 1-9. Structures of PPE-type CPE PPESO3.

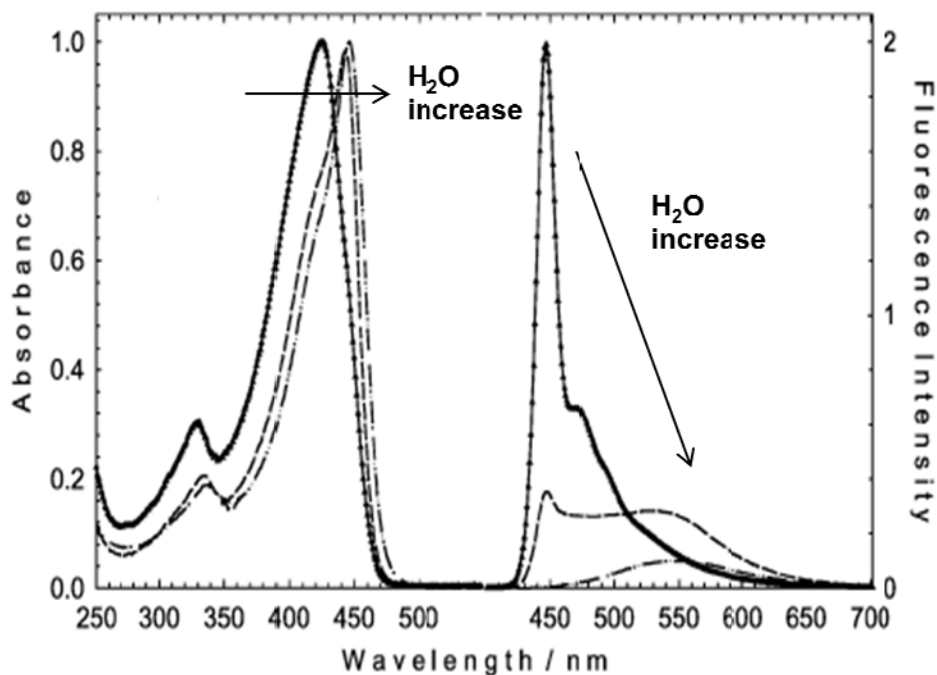


Figure 1-10. Absorption (left) and fluorescence (right) spectra of PPE-type CPE PPESO3 in methanol, methanol/water (1:1) and water. Arrows show the direction of change with water content. Figure was taken from Tan *et. al.*³⁶

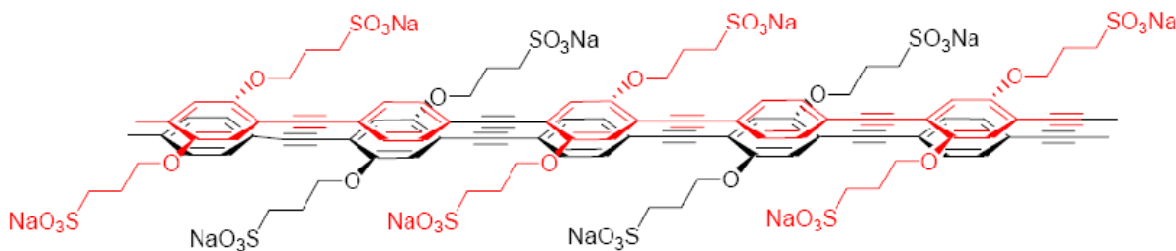


Figure 1-11. Schematic illustration of face-face π - π stacking of PPESO3.

polycarbazoles,⁶⁶ poly(p-phenylene ethylene)s,⁶⁷⁻⁷⁰ and poly(p-phenylene vinylene)s⁷¹⁻⁷³ with optically active side groups.

Self-Assembly of Meta-Linked Phenylene Ethynyls: Helical Folding

Moore and co-workers demonstrated that *meta*-linked oligo(phenylene ethylene)s (OPEs) with longer chains than 8 monomer units fold into a helical conformation in a polar solvent such as acetonitrile.⁷⁴ However, the oligomers exist in an expanded form in a non-polar solvent such as chloroform. This helical conformation is thermodynamically driven by solvophobic effects.^{74, 75} Figure 1-12 shows the structures of OPEs and a space-filling model of the extended coil form of OPEs in chloroform and a helical conformation in acetonitrile. Their folding process was studied using ¹H NMR, UV absorption and fluorescence spectra.^{74, 75} When the percent of acetonitrile in chloroform (by volume) is increased, the polar side chains are extended to the environment and the non-polar backbone folds into a helical conformation, which is stabilized by the π - π stacking interactions between the phenyl rings. The folded conformation of OPEs also create a tubular cavity, which acts as a host to recognize different chiral compounds (Figure 1-13).⁷⁶ Reversible 1:1 association of chiral guests to folded OPEs induces circular dichroism (CD)

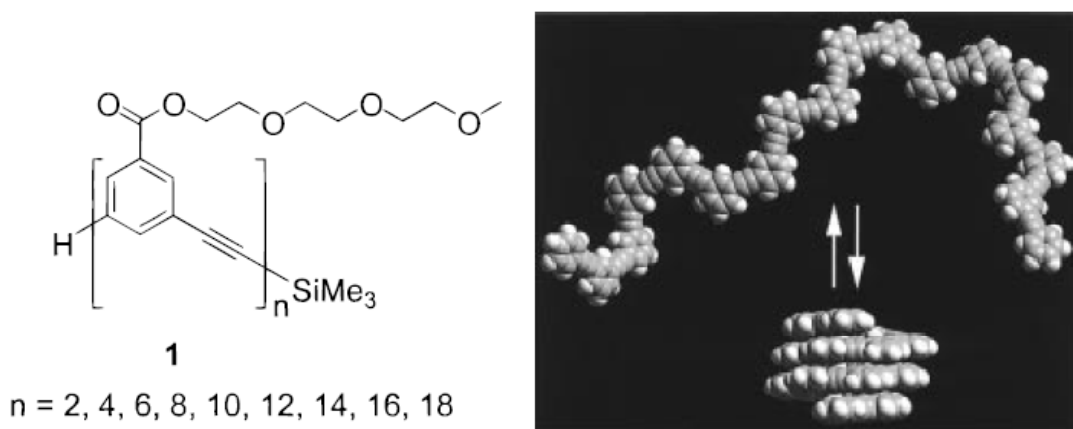


Figure 1-12. Structures of OPEs studied by Moore's group and a space-filling model showing the conformational equilibrium for OPE of length $n = 18$. Side chains are not shown for clarity. Figure was taken from Prince et.al.⁷⁵

signal in UV regions where the polymer absorbs light. This probes the interaction of a chiral molecule with a achiral OPE resulting in induced chirality on OPEs.

Tew and co-workers observed a helical conformation for amphiphilic *meta*-linked poly(phenylene ethylene)s (mPPEs) containing ionic side groups in 90 % H₂O/DMSO solution (Figure 1-14).⁷⁷ mPPE bearing long alkyl chains self-assemble into ordered bilayers. The mPPE is too large for interior cavity formed by the helix; therefore it cannot adopt a helical conformation. In contrast, mPPE bearing no alkyl chains shows similar changes in absorption and fluorescence spectra as spectra obtained by Moore and co-workers, suggesting that this mPPE folds into a helical conformation in 90 % H₂O/DMSO.

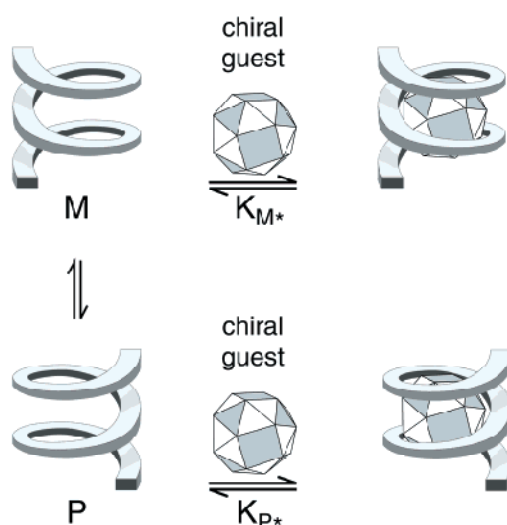


Figure 1-13. Postulated association equilibrium between OPEs and chiral molecules. Figure was taken from Prince *et.al.*⁷⁶

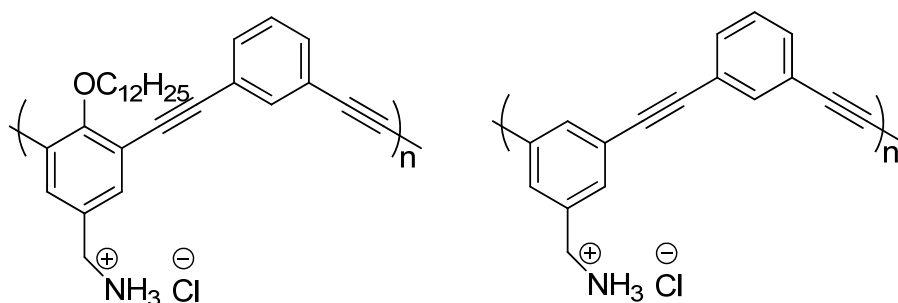


Figure 1-14. Structures of amphiphilic mPPEs studied by Tew's group.⁷⁷

Our group also has been interested in the synthesis and photophysical properties of meta-linked PPE-type CPEs with sulfonate (SO_3^-), carboxylate (CO_2^-) and L-alanine (Ala) as shown in Figure 1-15. The solvent effect on the absorption and fluorescence suggests that the *meta*-linked polymers fold into a helical conformation in water (Figure 1-16).⁷⁸⁻⁸⁰ In the absorption spectra, a decrease in oscillator strength and red-shift of the band (hypochromic effect) are observed as the amount of water in the solvent mixture (water/methanol) increases. These are attributed to π -

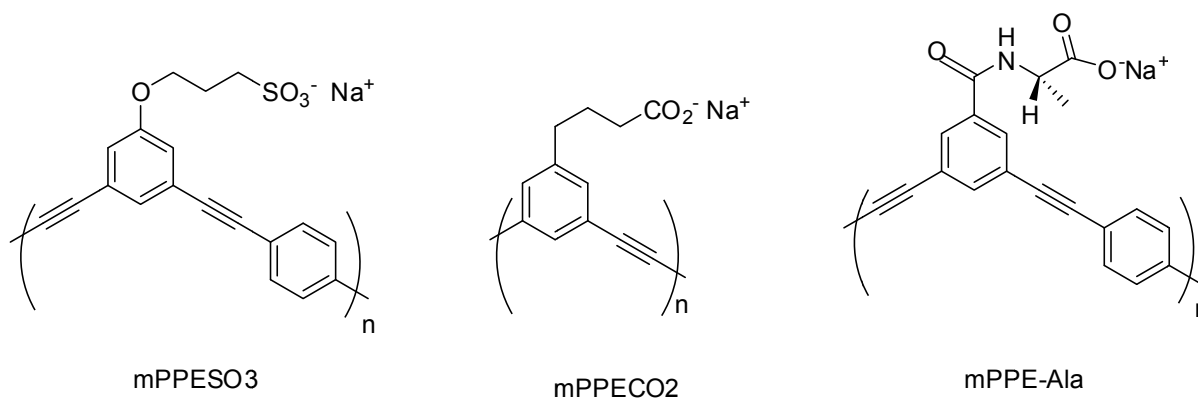


Figure 1-15. Structures of mPPE studied by Schanze's group.⁷⁸⁻⁸⁰

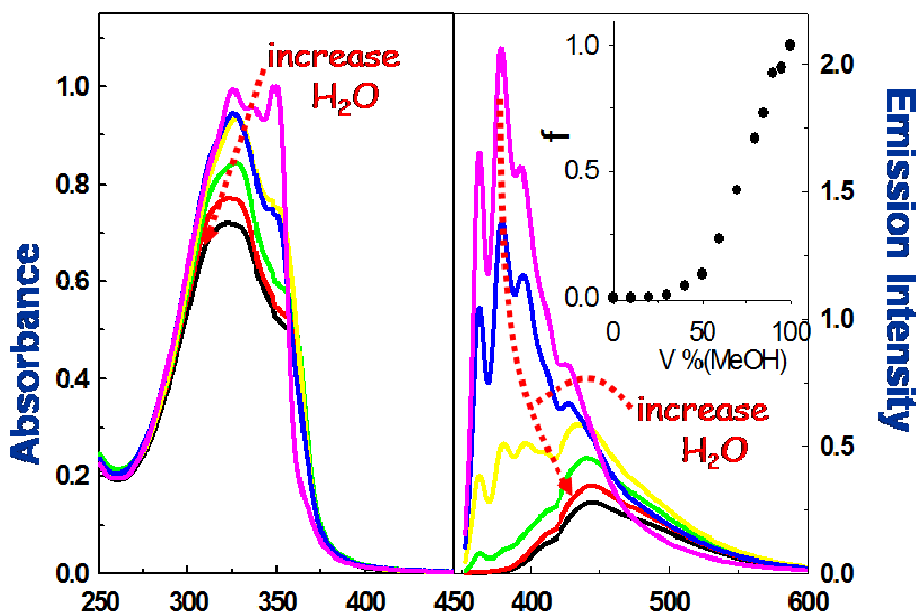


Figure 1-16. UV-vis absorption and emission spectra of mPPESO3 in MeOH/ H_2O at different compositions. Inset illustrates how the fraction of the random-coil conformation varies with solvent composition. Figure was taken from Tan et. al.⁷⁹

stacking interactions in the helical conformation. The changes in fluorescence spectrum provide additional evidence for the solvent-induced transition of mPPEs. With the increase of water amount, the intensity of the structured near-UV emission decreases and it is replaced with a less intense, broad, structureless and red-shifted emission. The broad and structureless “excimer-like” emission band arises due to π -stacking interactions in the folded, helical conformation of mPPEs. Given this structural similarity between double-helical DNA and helical conformation of our anionic mPPEs (i.e. both are helical polyanions which contains aromatic units that are π -stacked along the helical axis), small molecule DNA intercalators were expected to interact in a similar manner with mPPEs. A well-known example of intercalative binding to DNA is the metal complex $[\text{Ru}(\text{bpy})_2(\text{dppz})]^{2+}$, where bpy = 2,2'-bipyridine and dppz = dipyrido[3,2-a:2',3'-c]phenazine. This complex has been of particular interest due to the “light-switch effect”. It is non-luminescent in water; however, it shows strong photoluminescence when it is bound with DNA via intercalation of the dppz ligand.^{81, 82} The luminescence quenching is believed to arise due to H-bond interactions between water and nitrogen on the phenazine ring, resulting in rapid non-radiative decay of $^3\text{MLCT}$.⁷⁹ However, the dppz ligand is shielded from the water when the complex is intercalated, and hence the complex displays strong luminescence. Interestingly, the interaction between the Ru complex and mPPEs also shows the “light-switch effect”. As shown in Figure 1-17, in water $[\text{Ru}(\text{bpy})_2(\text{dppz})]^{2+}$ is non-emissive; however, the $^3\text{MLCT}$ emission from the complex increases upon addition of mPPEs. The emission from $[\text{Ru}(\text{bpy})_2(\text{dppz})]^{2+}$ saturates when a ratio of polymer concentration (in polymer repeat units, PRU) per $[\text{Ru}(\text{bpy})_2(\text{dppz})]^{2+}$ is approximately 6:1. This suggests that the intercalated Ru complex occupies a “binding site” corresponding to one turn of the mPPE helix (there are 6 PRUs per turn).

Circular dichroism (CD) is the most useful technique to study chiral structures. Either an enantiomeric excess of chiral molecules or the existence of a chiral environment is required for a CD signal. When achiral oligomers or polymers fold into a helical structure, racemic mixtures of the right- and left-handed forms (P and M forms, respectively) would be expected; therefore, CD signal cannot be observed. To provide a clear probe of the solvent effect on the folding process using CD spectroscopy, chirality is introduced to achiral oligomers or polymers by interacting with chiral molecules. Previously, Moore and co-workers used CD to explain the helical conformation of *meta*-linked OPEs where chiral guest molecules added to the achiral OPEs or chiral groups incorporated into conjugated oligomer backbones to produce an enantiomeric excess in the helical conformation.⁷⁶ In our previous studies, a small chiral molecule (-)- α -pinene

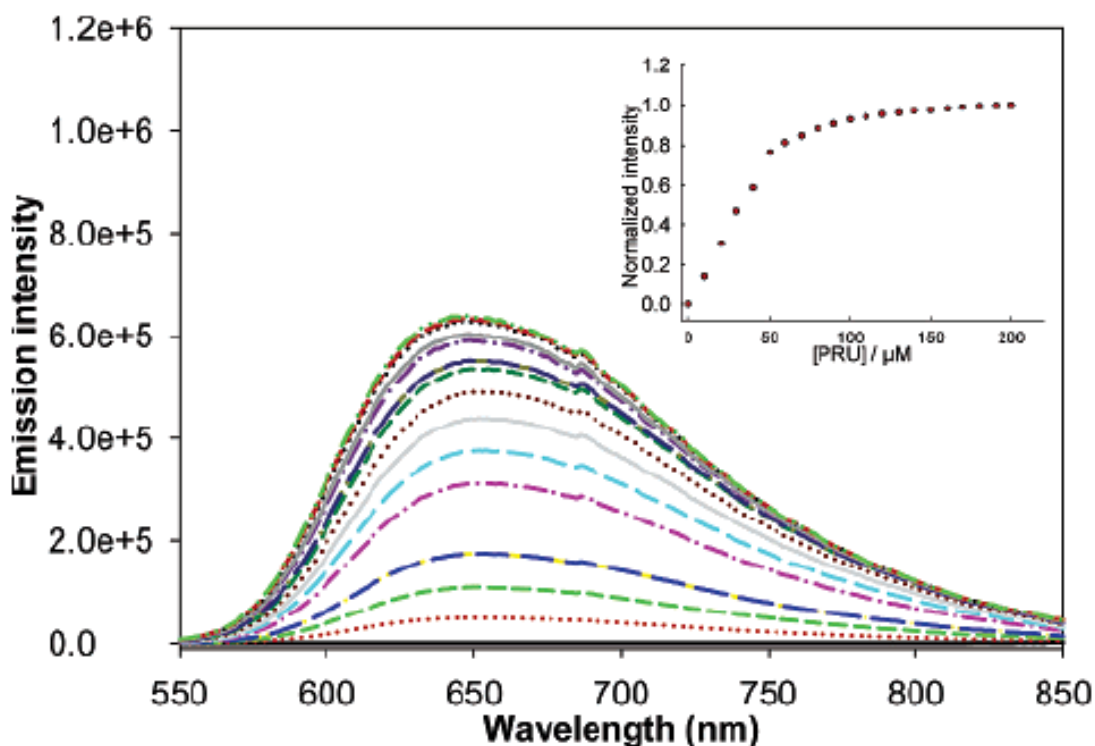


Figure 1-17. Emission spectra of $[\text{Ru}(\text{bpy})_2(\text{dppz})]^{2+}$ (15 μM), in absence (solid black line) and presence of mPPE-Ala (0 -120 μM polymer repeat units). The inset illustrates the $[\text{Ru}(\text{bpy})_2(\text{dppz})]^{2+}$ emission intensity with increasing the concentration of mPPE-Ala. Figure was taken from Zhao et. al.⁸⁰

interacts with our two polymers mPPESO3 and mPPECO2 resulting in CD signals.⁷⁸ For mPPE-Ala with chiral and optical active sidechains, a strong bisignate CD spectrum was observed because the alanine side chain induces an enantiomeric excess in the M-form of the helical conformation (Figure 1-18).

We also examined the effect of helical conformation on the amplified quenching in mPPE-SO3. N,N'-dimethyl-4,4'-bipyridium (MV^{2+}) was added to the random-coil and helical conformation of the polymer. Interestingly, the random-coil conformation of mPPE-SO3 is quenched less strongly than the helical conformation of the polymer at any given $[MV^{2+}]$ (Figure 1-19). This effect might be explained by two factors. The first one is an increased “exciton length” in the helical conformation due to delocalization between π -stacked segments. The second one is the fact that MV^{2+} quencher can interact with a large fraction of the chain when it is folded into the helical conformation.⁷⁹

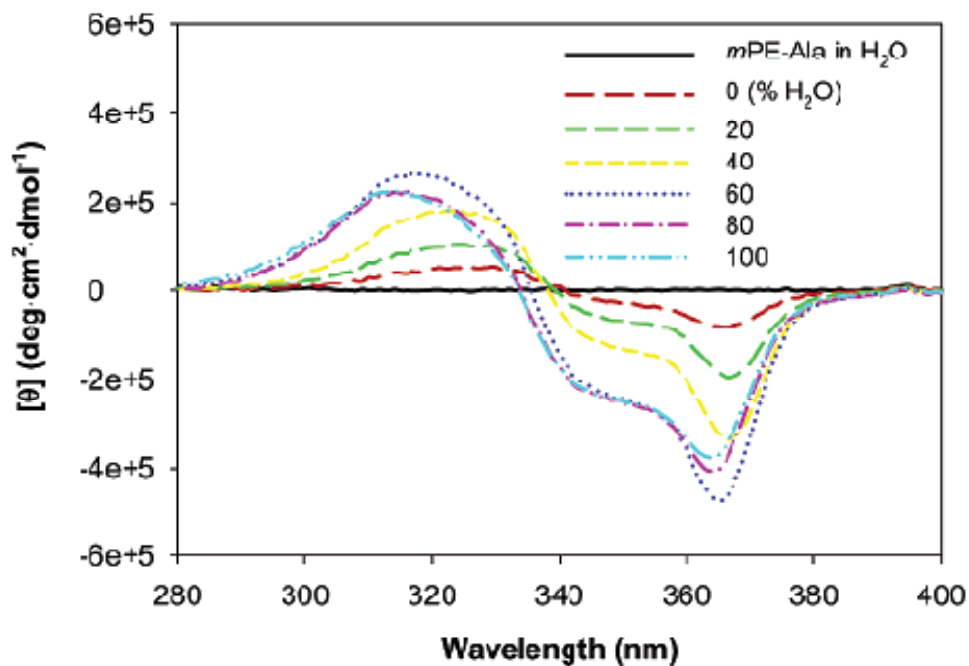


Figure 1-18. Circular dichroism spectra of mPPE-Ala in methanol, water and methanol/water mixtures. Figure was taken from Zhao *et. al.*⁸⁰

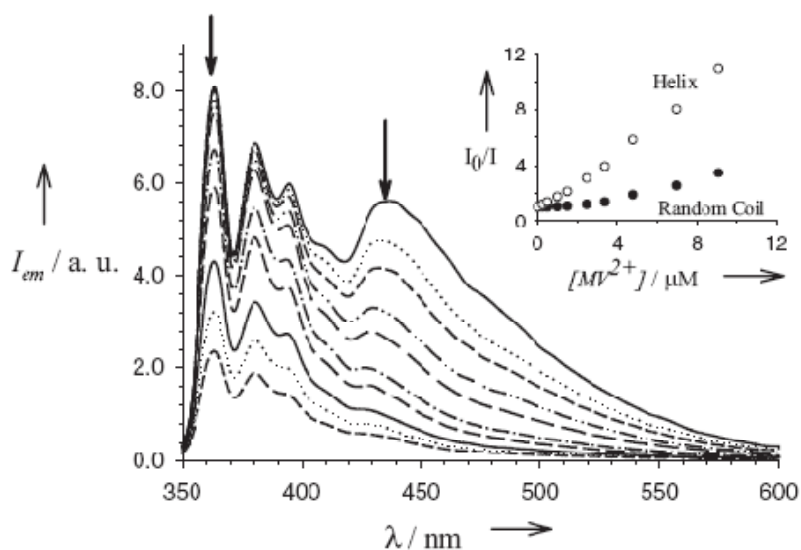


Figure 1-19. Emission quenching of mPPESO3 by MV^{2+} in a 7:3 methanol/water mixture. Arrows show how the intensity changes with increasing $[MV^{2+}]$. The inset shows the Stern-Volmer plots of random-coil state and helix using emission intensities at 363 nm and 445 nm. Figure was taken from Tan *et. al.*⁷⁹

Application of Conjugated Polyelectrolytes

Optical Sensors

One of the most exciting applications of CPEs is highly sensitive fluorescence-based sensors for chemical and biological targets due to amplified quenching by small molecules with opposite charge.¹⁴ CPEs have been used as sensors in different formats, including homogeneous aqueous solution,⁸³ glass-slide supported CPEs⁸⁴ and particle supported CPEs.²⁶ In most of the CPE-based sensors, fluorescence is either enhanced (“turn-on” approach) or quenched (“turn-off” approach) by interacting with targets. Both approaches are based on three mechanisms: superquenching, fluorescence resonance energy transfer (FRET) and conformation change.

Superquenching mechanism

In the superquenching strategy, a quencher-tether-ligand (QTL) complex is synthesized by combining a quencher to biologically interesting ligands. A fluorescence response is produced when the ligands bind to their specific targets. Whitten and co-workers reported the first example

of CPE-based sensor using QTL systems.²² They covalently linked MV²⁺ to a biotin molecule by a short but flexible tether. Biotin has been well-known as an excellent receptor for biotin-binding proteins such as avidin and streptavidin. Addition of biotin-methyl viologen (B-MV) to MPS-PPV (Figure 1-8) results in quenching of the polymer fluorescence. The quenched fluorescence is recovered by adding avidin through avidin-biotin complex formation (Figure 1-20). Based on the QTL systems, Whitten and co-workers also developed CPE-coated particles to detect enzymatic activity and DNA hybridization.²⁶

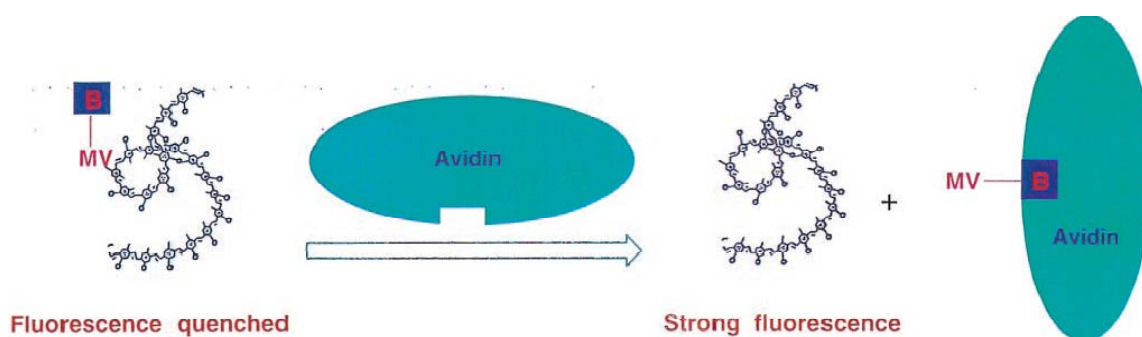


Figure 1-20. Detection of avidin using CPE based on the superquenching mechanism. Figure was taken from Chen *et. al.*²²

Fluorescence resonance energy transfer (FRET) mechanism

FRET is the non-radiative transfer of photon energy from an excited fluorophore (donor) to another fluorophore (acceptor) via dipole-dipole interaction. The FRET efficiency depends on the distance and orientation of the donor and acceptor, and the overlap between the emission of the donor and the absorption of the acceptor. CPEs have been used as light harvesting molecules that transfer excitations to signaling fluorophores attached to biomolecular probes, therefore providing enhanced signal intensities and sensitivities. Specific examples of FRET-based sensors were reported by Bazan and co-workers.^{24, 83} Cationic CPEs based on polyfluorene (PF) (Figure 1-21) were used for the detection of DNA. These CPEs display relatively high fluorescence quantum yields in aqueous solution compared to other CPEs, therefore increasing sensitivity.

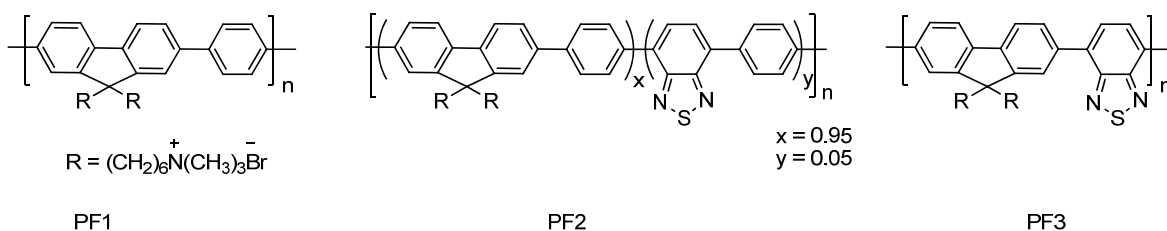


Figure 1-21. Structures of CPEs studied by Bazan and co-workers.

Figure 1-22 shows a schematic representation of a sensing system based on FRET. This system contains PF1 and a peptide nucleic acid (PNA) strand labeled with fluorescein (C^*) as a probe. Since PNA- C^* is neutral, there is no electrostatic interaction between the PF1 and PNA- C^* , and the distance between them is too large for effective FRET. Upon addition of complementary ssDNA into the solution of PNA- C^* /PF1, PNA hybridized with ssDNA (shown in red). The hybridization provides a hybrid complex bearing C^* with negative charges, resulting in formation of complex between PF1 and the hybrid complex via electrostatic interaction.

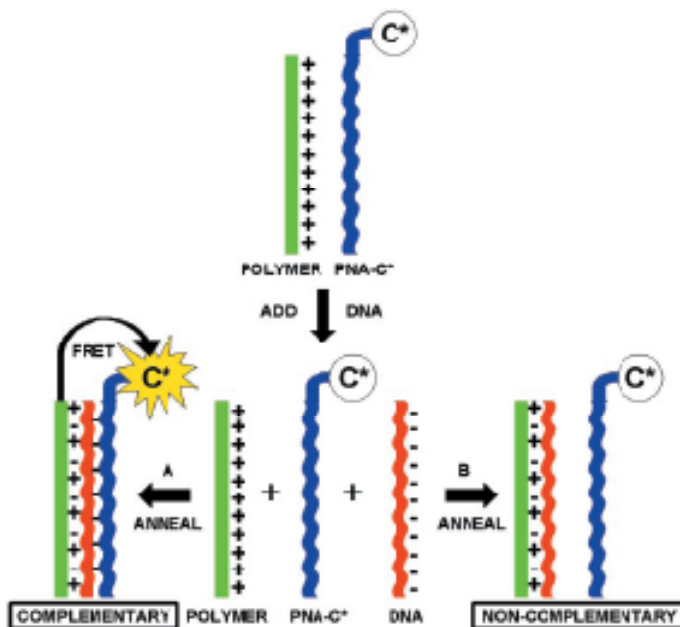


Figure 1-22. Schematic representation for the use of PF1/PNA- C^* to detect a complementary ssDNA. Figure was taken from Gaylord *et al.*²⁴

The distance between PF1 and PNA-C* decreases allowing for efficient FRET. When noncomplementary ssDNA is added, hybridization does not occur and the distance between PF1 and PNA-C* remains too large for FRET. The enhanced emission of fluorescein (C*) provides a probe for the presence of a target ssDNA.

Conformation change

This sensing mechanism is based on conformational change of the conjugated polymer backbone upon complexation with different analytes, inducing chromic changes, both in the absorption and fluorescence of CPEs. Water soluble poly(thiophene)s have been the most commonly used (Figure 1-23).⁸⁵⁻⁸⁸ Leclerc and co-workers reported the detection of ssDNA sequences using cationic poly(thiophene), PT2.^{85, 86} This sensing system is based on different electrostatic interactions and conformational structures between electroactive and photoactive cationic poly(thiophene) derivatives, and single-stranded oligonucleotides or double-stranded (hybridized) nucleic acids. PT2 exist as a random coil conformation before addition of ssDNA (Figure 1-24). Addition of ssDNA forms an electrostatic complex, called duplex between the PT2 and ssDNA, where PT2 exists as a highly conjugated, planar conformation. When a complementary ssDNA is added to the duplex solution, triplex form is observed and it displays

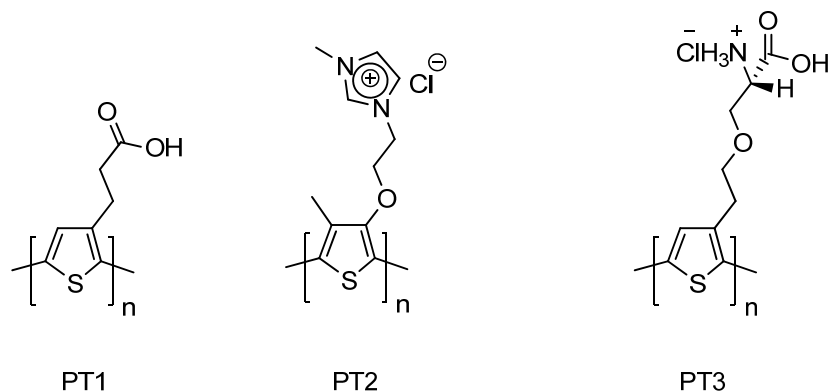


Figure 1-23. Structures of poly(thiophene) derivatives used in CPE-based sensor via conformational change mechanism.

less conjugated non-planar conformation. Depending on the conformational change, PT2 shows different absorption and fluorescence spectra. By monitoring changes in photophysical properties of the polymer, ssDNA sequences can be detected.

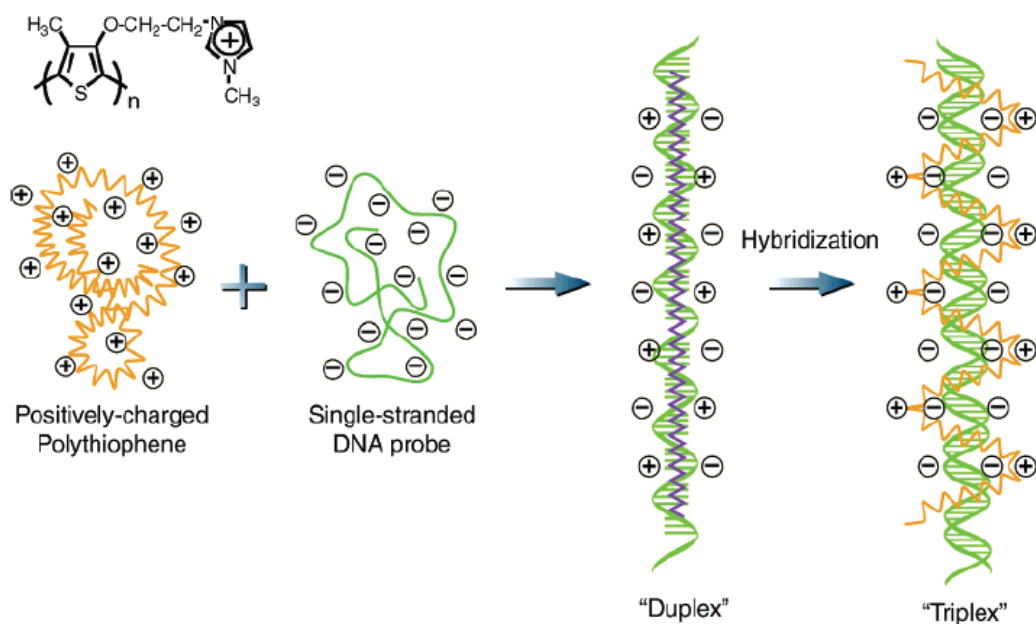


Figure 1-24. Schematic illustration for the detection of ssDNA sequences using poly(thiophene). Figure was taken from Ho *et.al.*⁸⁶

Biocidal Activity

Whitten and co-workers reported that a cationic CPE (Figure 1-25) shows light-induced biocidal activity against Gram negative bacteria (*Escherichia coli*, *E. coli*, BL 21) and Gram positive bacterial spores (*Bacillus anthracis*, Sterne, *B. anthracis*, Sterne).⁸⁹ Phase contrast and fluorescence microscopy indicates that polymer is taken up by both microorganisms, and polymer coated on either bacteria or spores displays strong fluorescence (Figure 1-26). Incubation of bacteria with the polymer under the light shows reduction of bacterial survival. The biocidal activity arises due to the association of the polymers with the cell surface of the bacteria and light-induced activation of the cell surface coated polymer.

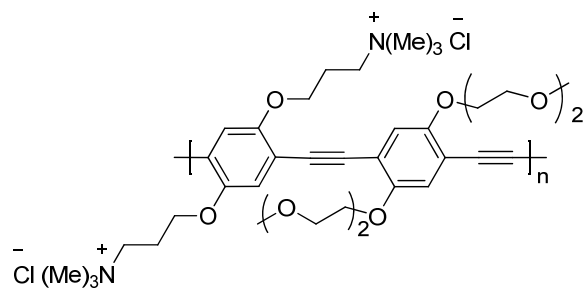


Figure 1-25. Structure of cationic CPE used by the Whitten group.

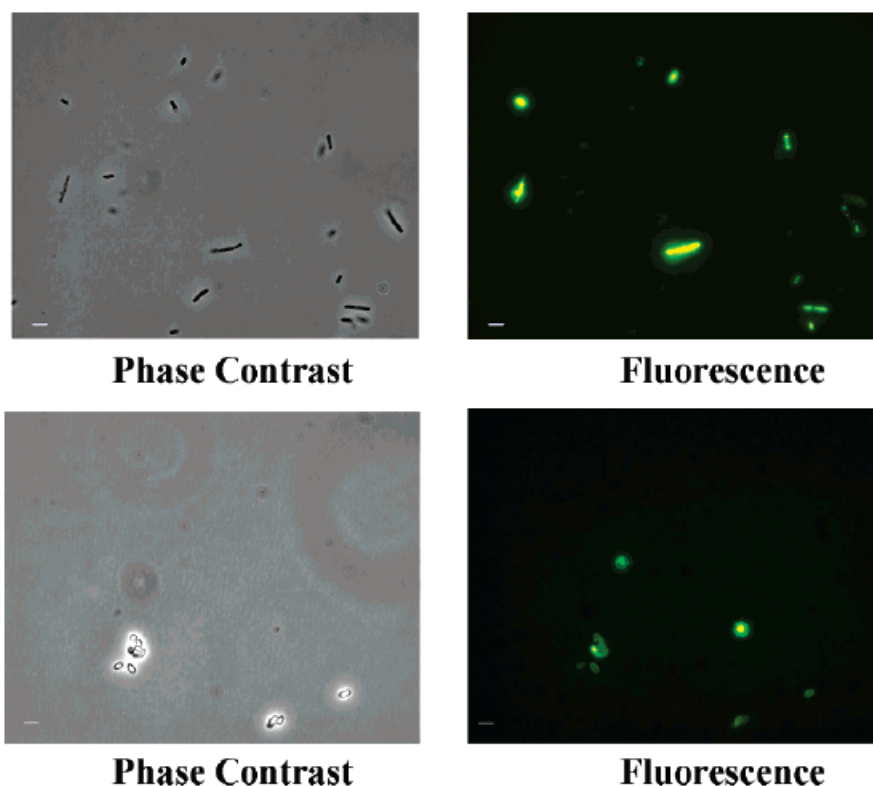


Figure 1-26. Phase contrast and fluorescence microscope images of CPE-treated *E. coli* (upper panel) and CPE-treated *B. anthracis* Stern spores (lower panel). Figure was taken from Lu *et.al.*⁸⁹

Scope of the Present Study

The aim of the present study is the synthesis of poly(arylene ethynylene) conjugated polyelectrolytes with different chemical structures, the investigation of their photophysical properties in solution, and their application to sensors and antimicrobials.

Chapter 2 describes a fluorescent assay for the detection of enzymes using mPPESO3. The assay is based on the quenching mechanism. Quencher-tether-ligand (QTL) system is added to the CPE, resulting in fluorescence quenching. The fluorescence is recovered by addition of target enzymes or carbohydrates.

Chapter 3 and 4 are focused on fundamental understanding of the mechanism of amplified quenching in helical conformational mPPESO3 with cationic intercalator quenchers. Both quenchers are functionalized with biotin ligands, which form strong complexes with proteins such as avidin and streptavidin.

We have also been interested in helical structured CPEs in aqueous solution. In Chapter 5, a *meta*-linked CPE containing pyridine was synthesized. The self-assembly behavior in solution was studied using absorption and emission spectroscopy. The helical structure of the polymer was confirmed by the titration experiment using $[\text{Ru}(\text{bpy})_2(\text{dppz})]^{2+}$ and the polymer. Quenching experiments were carried out using various metals.

In Chapter 6, a series of cationic CPEs with backbones based on a poly (arylene ethynylene) repeat unit and tetraalkylammonium side groups were designed and synthesized. Their photophysical properties were studied in solution. We investigated the biocidal activity of the cationic CPEs and the mechanism for the light induced bacterial killing by the CPEs.

In Chapter 7, we synthesized conjugated polyampholytes carrying both cationic and anionic groups. Their photophysical properties and quenching behaviors were studied in solution.

CHAPTER 2

SENSING OF PROTEASE ACTIVITY USING META-LINKED POLY (PHENYLENE ETHYNYLENE) SULFONATE

Introduction

Enzymes are important targets for the screening of noxious toxins and pathologies associated with their presence, and for the development of effective and selective therapeutics. Proteases^{90, 91} are specially relevant because they conduct proteolysis, which is the final step in the expression of the activity of a variety of proteins.⁹²

Colorimetric and fluorescence-based homogeneous method assays have been validated for a variety of proteases.⁹³ These assays are based on the development of color or fluorescence in solution as a result of substrate hydrolysis. Although the methods have been commonly used, their sensitivity is limited to micromolar or submicromolar range, and hence it is difficult to measure the initial rates at ultralow substrate concentrations or at low enzyme activity.

To improve sensitivity in proteolytic enzyme assays, CPE-based enzyme assays have been reported.^{94, 95} Incorporation of CPEs into assays leads to amplification of sensory response. The strategy using CPEs also contains an enzyme-cleavable peptide substrate covalently bound to a quencher (an electron and/ or energy acceptor) that associates with CPEs due to electrostatic interaction, leading to fluorescence quenching of the CPEs. In the presence of enzyme, the substrate is cleaved and the uncharged quencher is released from CPEs, turning on the fluorescence of CPEs (“turn-on” mechanism) (Figure 2-1). For example, Pinto and co-workers used a cationic peptide labeled with a *p*-nitroanilide (*p*-NA) unit and anionic PPESO₃ (Figure 2-2). The *p*-NA moiety strongly quenches CPE fluorescence via electrostatic interaction between them. Addition of protease induces the hydrolysis of the *p*-NA group, which is neutral and its quenching ability is eliminated. Pinto and co-workers also reported a fluorescence “turn-off” assay to monitor protease activity. In the turn-off assay, the bis-Arg derivative of Rhodamine 110

(Rho-Arg-2) was used. The Rho-Arg-2 is colorless and non-fluorescent and it also does not quench PPECO2 fluorescence. However, addition of protease induces the hydrolysis of one of amide linkage in Rho-Arg2, producing a mono amide derivative (Rho-Arg), which strongly quenches the polymer fluorescence by FRET (Figure 2-1).

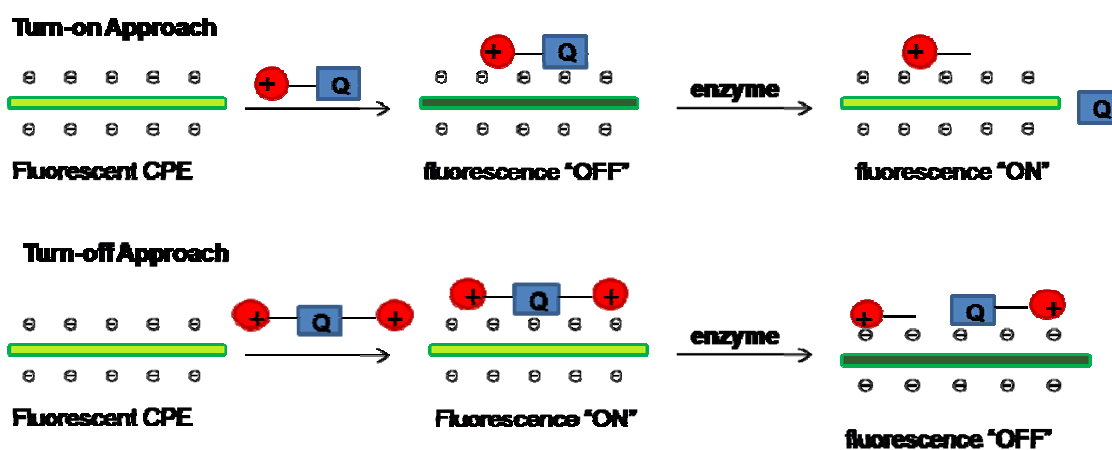


Figure 2-1. Mechanism of the “turn-on” and “turn-off” CPE-based enzyme assays.

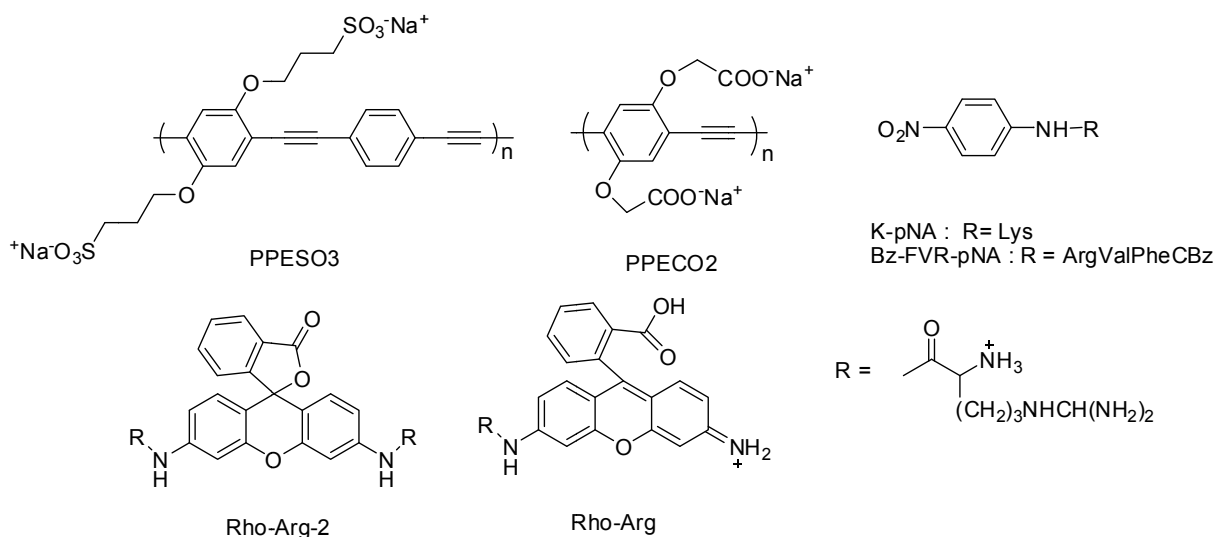


Figure 2-2. Structures of CPEs and quencher substrates used for CPE-based enzyme assays.

In this chapter, we describe a CPE-based enzyme assay using the helical conformation of mPPESO3 in an aqueous solution. This assay is based on a fluorescence turn-on sensor for proteolytic enzyme, peptidase using a *p*-NA labeled peptide, L-Lys-*p*-nitroanilide (K-*p*NA) as shown in the previous study with PPESO3. Amplified quenching of the mPPESO3 fluorescence

is observed with K-*p*NA. Introduction of peptidase reverses the fluorescence quenching concomitant with peptide hydrolysis. To investigate the effect of helical structure on the polymer fluorescence quenching Stern-Volmer quenching constants of helical mPPESO3 by K-*p*NA are compared with those of linear PPESO3 in buffer solutions of varying concentration. mPPESO3 displays more efficient quenching than PPESO3. Additionally, the less effect of concentrated buffer on the fluorescence quenching is observed in mPPESO3 compared to PPESO3.

Results and Discussion

Overview of Protease Turn-on Assay

A fluorescence turn-on sensor was investigated to monitor enzyme activity with mPPESO3 and a cationic peptide labeled with *p*-nitroanilide (*p*-NA) unit (Figure 2-3). mPPESO3 is an anionic meta-linked poly(phenylene ethylene) (PPE) featuring sulfonate side chains. In aqueous solution, the polymer absorbs at $\lambda_{\text{max}} = 320$ nm and it exhibits an intense fluorescence at $\lambda_{\text{max}} = 450$ nm. The *p*-NA moiety strongly quenches the polymer fluorescence because the cationic peptide ion-pairs with the anionic polymer. In this investigation, L-Lys-*p*-nitroanilide dihydrobromide (K-*p*NA) is chosen as an enzyme substrate, which contains a cationic amino acid residue, lysine. The amplified quenching of the polymer fluorescence is recovered by the addition of peptidase. Upon introduction of peptidase to a mixture of the *p*-NA peptide and mPPESO3 hydrolysis of the *p*-NA group is induced. Since the cleaved *p*-NA group is not charged, its quenching ability is eliminated. Therefore, quenching reversal is observed with the peptide hydrolysis.

Peptidase Activity Sensing

As shown in Figure 2-4, fluorescence spectral changes are observed after addition of K-*p*NA and peptidase, respectively. The initial fluorescence from 15 μM of mPPESO3 (black

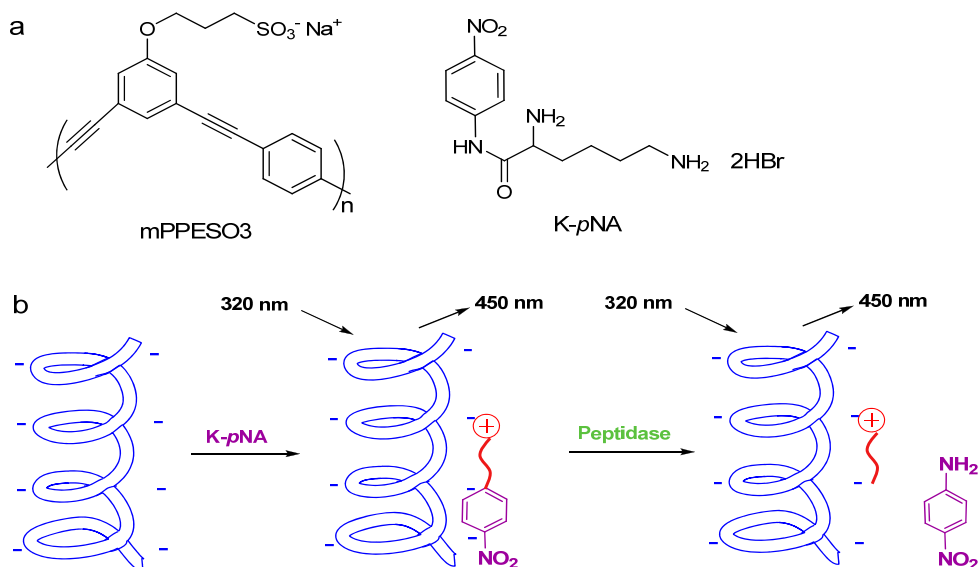


Figure 2-3. (a) Structures for a polymer and a quencher substrate. (b) Mechanism of the “turn-on” mPPESO3-based sensor.

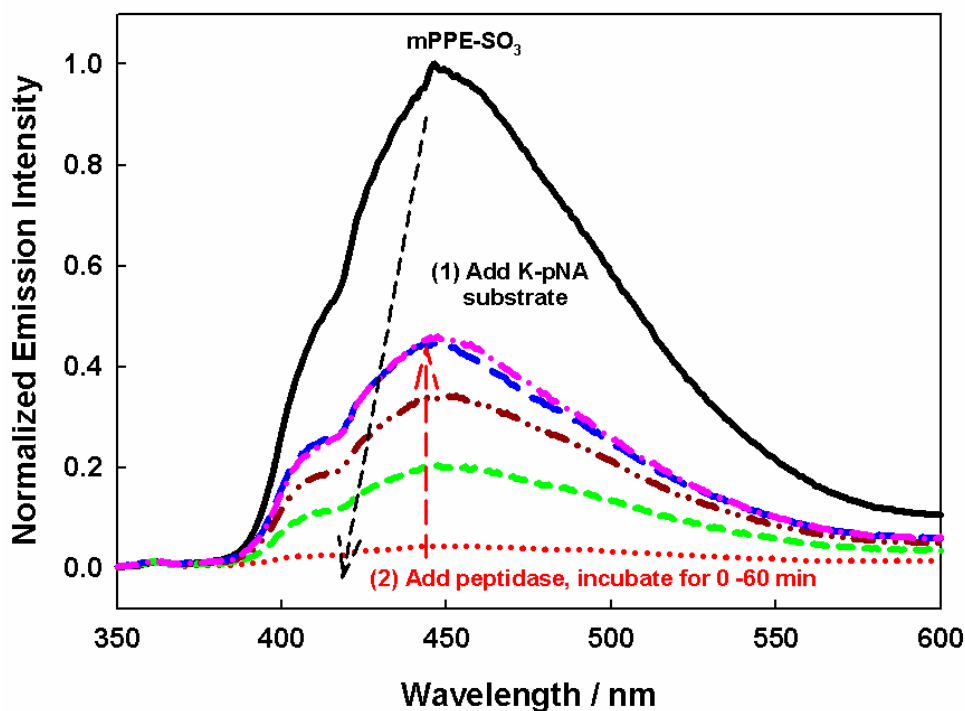


Figure 2-4. Fluorescence spectroscopic changes observed during turn-on assay. Initial fluorescence of mPPESO3 (15 μ M) (—) in phosphate buffer solution (1.0 mM, pH 7.1); fluorescence after addition of 2 μ M of K-pNA (···). Fluorescence intensity of as a function of time after addition of peptidase (0.13 mg / mL): 5 (---), 20 (-·-·-), 40 (- - -), 60 (-·-·-) min. λ_{ex} = 320 nm.

solid line) is quenched up to ~ 90 % by 2 μM of K-*p*NA (red dotted line). After addition of 0.13 mg/ mL of peptidase to the quenched polymer solution, the hydrolysis of K-*p*NA is detected by an increase in fluorescence intensity as a function of incubation time. Approximately 45 % of the initial intensity of mPPESO3 is recovered. The fluorescence of mPPESO3 is not completely recovered by addition of peptidase due to nonspecific interaction of peptidase with the polymer. This can be supported by the observation, that addition of peptidase lowers the initial fluorescence from the polymer by ~ 45 %.

Addition of peptidase to a mixture of the polymer and K-*p*NA induces hydrolysis of *p*NA-groups. The quenching efficiency of *p*-nitroaniline is determined by Stern-Volmer quenching experiments and then compared with the quenching efficiency of K-*p*NA. To obtain the same extent of quenching by K-*p*NA, much higher concentration of *p*-nitroaniline is required as shown in Figure 2-5. Therefore, the quenching ability of the hydrolyzed *p*-NA group is negligible.

Concentration Effect of Polymer and Buffer on Fluorescence Quenching

Sensitivity of mPPESO3 was determined by quenching experiments with K-*p*NA at various concentrations of the polymer solutions. The quenching efficiency increases with a decrease in the concentration of the polymer as shown in Figure 2-6. 5 μM of the polymer solution exhibits the most efficient quenching.

To investigate the effect of buffer ions on fluorescence quenching, the quenching experiments were carried out by using 5 μM of PPESO3 or mPPESO3, and K-*p*NA at various concentrations of buffer solutions. Table 2-1 represents the Stern-Volmer constants (K_{sv}) obtained for quenching mPPESO3 or PPE-SO₃ by K-*p*NA. K_{sv} was acquired at low concentration of quencher (linear regime). In the previous study, we reported that the quenching constants of PPESO3 by K-*p*NA decreased with increasing buffer concentration.⁹⁴ This arises due to an

electronic screening effect of the added ions. However, the helical conformation of mPPESO3 prevents the effect of increased ions on the mPPESO3 fluorescence quenching by K-*p*NA.

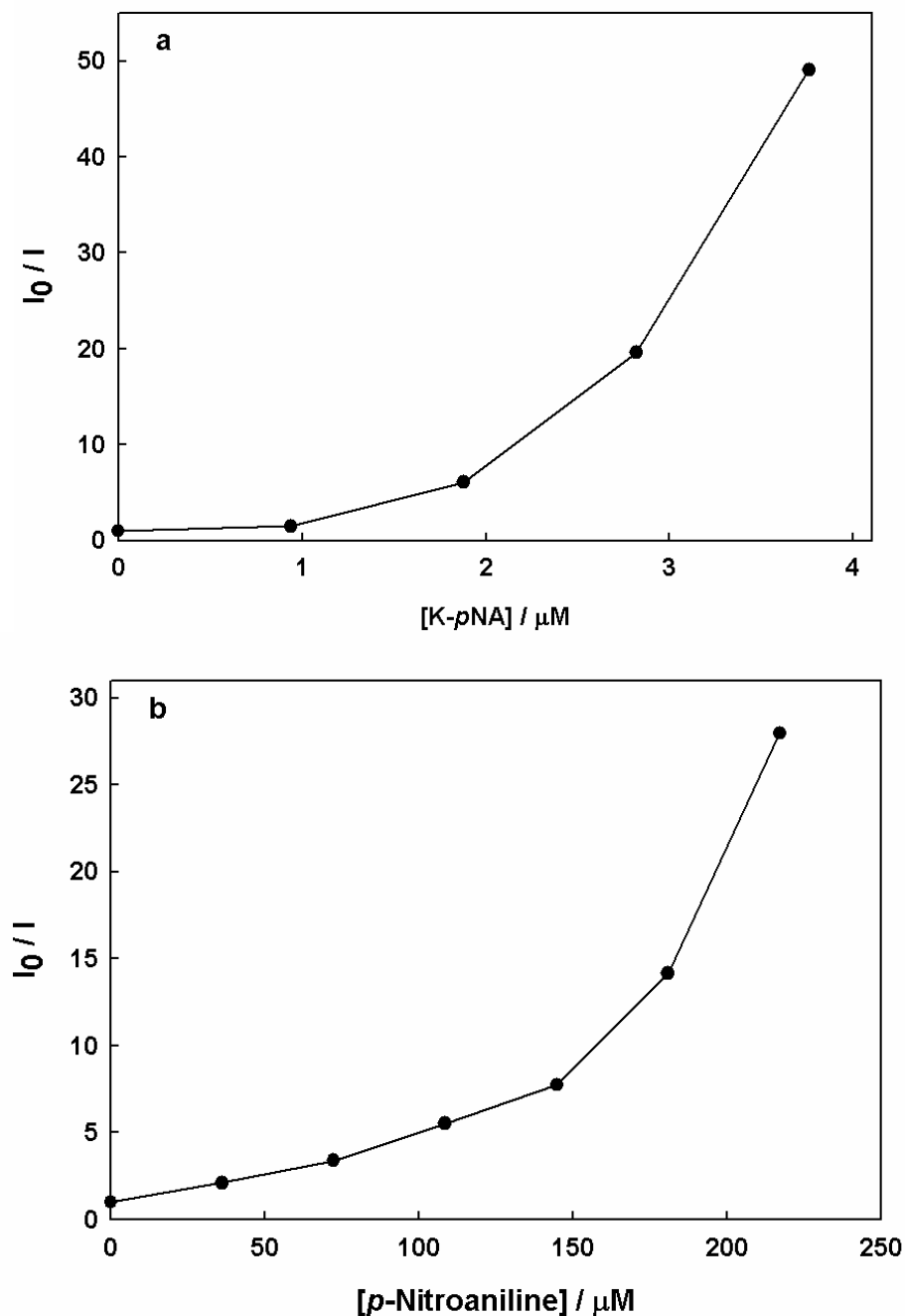


Figure 2-5. Stern-Volmer plots for fluorescence quenching of mPPESO3 with K-*p*NA (a) and *p*-nitroaniline. (b). $[mPPE-SO_3] = 15 \mu M$, 1.0 mM Potassium phosphate buffer solution, pH7.1. ($\lambda_{ex} = 320 \text{ nm}$, $\lambda_{em} = 450 \text{ nm}$)

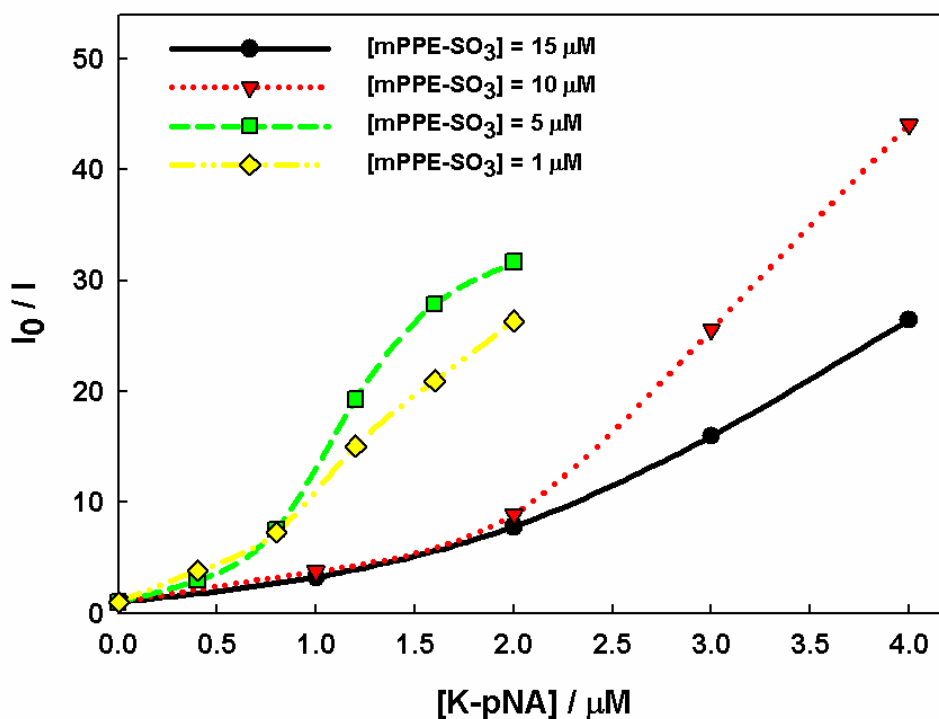


Figure 2-6. Stern-Volmer plots of at different concentrations of mPPESO3 with K-*p*NA in 1.0 mM of potassium phosphate buffer (pH 7.1) ($\lambda_{\text{ex}} = 320 \text{ nm}$, $\lambda_{\text{em}} = 450 \text{ nm}$).

Table 2-1. Stern-Volmer Quenching constants for mPPESO3 and PPESO3 fluorescence quenching by K-*p*NA

[Buffer], mM	$K_{\text{SV}}, \text{M}^{-1}$	
	mPPESO3	PPESO3
1	1.54×10^7	4.79×10^6
5	1.60×10^7	2.18×10^6
10	1.53×10^7	8.20×10^5
100	9.50×10^5	7.38×10^4

Summary and Conclusions

This chapter demonstrates the application of mPPESO3 for detection of proteolytic enzyme activity. The polymer fluorescence is quenched strongly by K-*p*NA and peptidase reverses the fluorescence from the quenched polymer solution concurrent with peptide hydrolysis. mPPESO3 is more efficiently quenched by K-*p*NA compared to PPESO3. More

interestingly, the polymer still shows amplified quenching at even high concentration of buffer solution while PPESO3 shows a reduced quenching efficiency with increasing buffer concentration. Typically, CPEs show a significantly reduced quenching efficiency in the concentrated buffer solution because the buffer ions screen the Coulomb interactions, removing quenchers from the vicinity of CPEs. These two results are believed to arise due to the intercalation of quenchers into the helical conformation of mPPESO3 giving less ion-screening effect on the Coulomb interaction as well as an enhanced quenching efficiency.

Experimental

Materials

mPPESO3 was synthesized by the Sonogashira reaction as described in the literature.⁷⁹ All solutions were prepared by using water that was distilled and then purified by a Millipore purification system. Buffer solutions were prepared with reagent grade chemicals before use. Concentrated aqueous polymer solutions were diluted with buffer to a final concentration. Avidin, K-*p*NA, and peptidase were purchased from Sigma-Aldrich Inc. All solutions were prepared in an appropriate buffer solution before use in the fluorescence assay.

Instrumentation

Absorption spectra were obtained on a Varian-Cary 100 UV-visible absorption spectrometer. Fluorescence spectra were recorded on a Jobin Yvon-SPEX Industries Fluorolog-3 Model FL3-21 spectrofluorometer and corrected by using correction factors generated in-house with a primary standard lamp.

General Methods

The solutions of mPPESO3, K-*p*NA, and peptidase in 1.0 mM sodium phosphate buffer (pH 7.1) were prepared before use. Enzyme assay was conducted at 37°C. The 2 mL of polymer solution (15 μ M) was placed in a poly (methyl methacrylate) cuvette with 10 mm path length and

the initial fluorescence intensity was recorded. The polymer solution was incubated with K-*p*NA solution for 10 minutes and then the fluorescence intensity was measured again. A peptidase solution was added into the mixture of the polymer and K-*p*NA. Fluorescence intensity was then recorded at 5 min intervals. Fluorescence intensity was acquired at 450 nm after it was excited at 320 nm.

CHAPTER 3
FLUORESCENCE QUENCHING OF HELICAL CONJUGATED POLYELECTROLYTE BY
RHENIUM-BIOTIN COMPLEX AS QUENCHER-TETHER-LIGAND (QTL) PROBE

Introduction

Since the structure of double helical DNA was elucidated,⁹⁶ the design of small molecules that recognize and react at specific DNA sites has been of considerable interest.⁹⁷ Over the past twenty five years, transition metal complexes have been studied as reversible DNA binding agents. Metal complexes bind with DNA in several different non-covalent modes including electrostatic and groove binding, intercalation and insertion (Figure 3-1).⁹⁸ Transition metal complexes are attractive because of the second specific advantages: (1) they exhibit a well-defined coordination geometry because the metal center acts as an anchor, holding in place a rigid, three dimensional scaffold of ligands that can, if desired, bear recognition elements. (2) They also possess unique photophysical and electrochemical properties to enhance the functionality of the binding agents.⁹⁸ The unique properties of transition metal complexes have been used in a wide range of areas including fluorescent labels, DNA foot-printing agents and electrochemical probes.⁹⁹ Much of the work in this area originated from the earliest study of Pt(II) complexes.¹⁰⁰ Stimulated by the early work by Barton, Turro and co-workers, a variety of metal complexes including those of Ru(II), Rh(III), Cu(I) with polynuclear aromatic chelate ligands such as 1,10-phenanthroline have been investigated as physical and chemical tools for probing and modifying the structures of nucleic acids.¹⁰¹⁻¹¹² There has been particular interest in transition metal complexes that contain the ligand dipyrido[3,2-a:2',3'-c]phenazine (dppz), which bind strongly to DNA via intercalation of the dppz ligand. One of the interesting properties of these complexes is that intercalation into DNA, resulting in a change in their photophysical properties.^{81, 113} Specifically, they exhibit weak luminescence in aqueous solution

due to solvent-induced quenching of the luminescent $^3\text{MLCT}$ state; however, when bound to DNA, they are moderately luminescent (Figure 3-2).

Previously, we reported that $[\text{fac}-(\text{dppz})\text{Re}^{\text{I}}(\text{CO})_3(4\text{-MePy})]^+$ (where 4-MePy = 4-methylpyridine) binds to DNA via intercalation. By analogy to $\text{Ru}(\text{bpy})_2\text{dppz}^{2+}$, the $\text{Re}(\text{I})$ complex is non-luminescent in water, but becomes emissive from $^3\pi,\pi^*$ intraligand excited state upon intercalation.¹¹³ In 2004, Lo and co-workers reported bifunctional $\text{Re}(\text{I})$ complexes that contain both an extended planar diimine ligand and a biotin moiety and hence they can bind to both nucleic acid and proteins to develop new biorecognition reagents.¹¹⁴ These biofunctional $\text{Re}(\text{I})$ complexes display a significant emission enhancement in the presence of either DNA or avidin.

We have been interested in the optical and self-assembly properties of water-soluble conjugated polyelectrolytes (CPEs), which feature poly(phenylene ethynylene) (PPE) backbones with ionic side chains.^{23, 36, 79, 80, 115-118} These polymers exhibit strong light absorption, efficient fluorescence, and good transport properties for charge carriers and excitons. One property that has been of particular interest in our studies is solvent-induced self-assembly.^{36, 79, 80} For example, the anionic conjugated polyelectrolyte PPESO₃, which has a *para*-linked (linear chain) PPE backbone, self-assembles into π -stacked aggregates in H₂O (a “poor” solvent) while it exists in a monomeric state in MeOH (a “good” solvent).³⁶ This result is based on the study of solvent effects on the spectroscopic properties. The polymer also exhibits a stronger quenching efficiency by oppositely charged quenchers in H₂O compared to MeOH. This effect has been termed “amplified quenching”³⁰ and arises due to rapid interchain exciton migration in the aggregated PPESO₃ chains. The amplified quenching allows CPEs to be used as a unique platform for the development of highly sensitive fluorescence-based sensor for biological

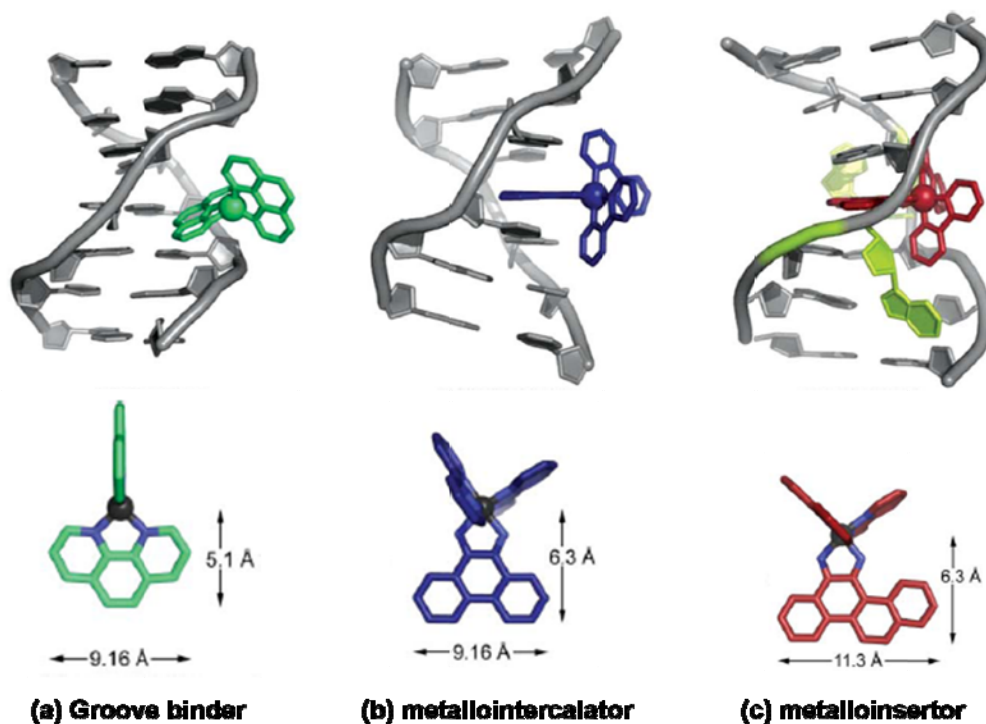


Figure 3-1. Three binding modes of a metal complex with DNA: (a) groove binding, (b) intercalation and (c) insertion and geometries of (a) groove binder, (b) intercalator and (c) metalloinsertor. Figure was taken from Zeglis *et. al.*⁹⁸

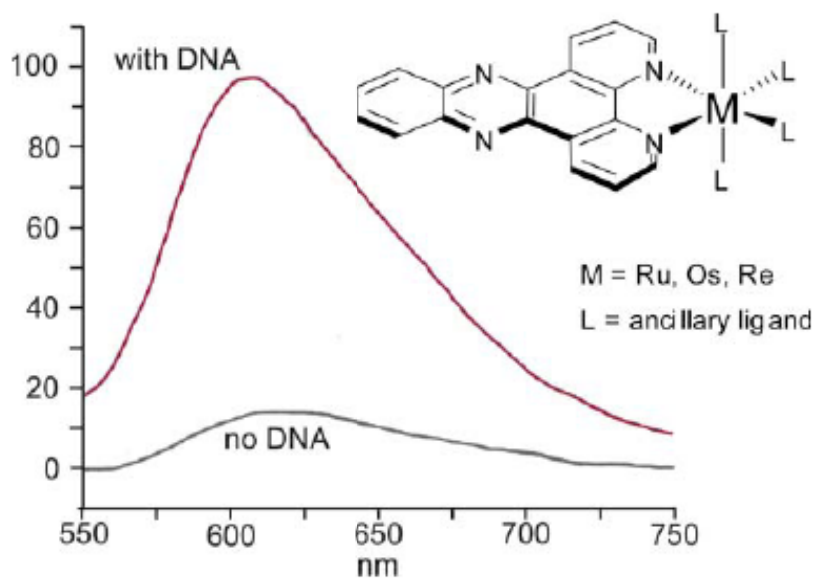


Figure 3-2. The light-switch effect of dppz-based metallo-intercalators. Figure was taken from Zeglis *et. al.*⁹⁸

targets^{22, 24, 94, 95, 119-124}. In contrast to the *para*-linked PPESO3, the *meta*-linked PPE-type polymer mPPESO3 folds into a helical conformation in H₂O while it exists in a random coil conformation in MeOH.⁷⁹ The fluorescence of the helical conformation of the polymer is quenched by oppositely charged quenchers more efficiently, suggesting either an increase of exciton length in the helical conformation, which results from delocalization between π -stacked segments, or the fact that the quencher ion can interact with a larger fraction of the chain when it is helical.

Given the structural similarity between the helical conformation of mPPESO3 and double helical DNA (i.e., both feature aromatic residues that are π -stacked along the helical axis and they present negatively charged side groups to the surrounding solvent environment), DNA intercalators are expected to interact in a similar manner with the polymer. Interestingly, [Ru(bpy)₂(dppz)]²⁺, where bpy = 2,2'-bipyridine and dppz = dipyrido[3,2-a:2',3'-c]phenazine binds to helical mPPESO3 via intercalation of the dppz ligand into the π -stacked phenylene ethynylene units. The intercalated complex is strongly luminescent and it also quenches the polymer fluorescence.⁷⁹

In this chapter, we investigated the interaction between mPPESO3 and two Re(I) complexes. One complex contains the dppz ligand and the second contains the dppz ligand and a pyridine ligand covalently linked to biotin. Both Re(I) complexes bind to mPPESO3 via intercalation of the dppz ligand into the polymer, resulting in amplified quenching of the polymer fluorescence. The Re(I) complex containing biotin ligands specifically interact with avidin. Effect of avidin-biotin complexation on the interaction between the polymer and the Re(I)-biotin complex was also investigated by observing changes in the polymer fluorescence. Scheme 4-3 shows the structures of CPEs and Re complexes used in this study.

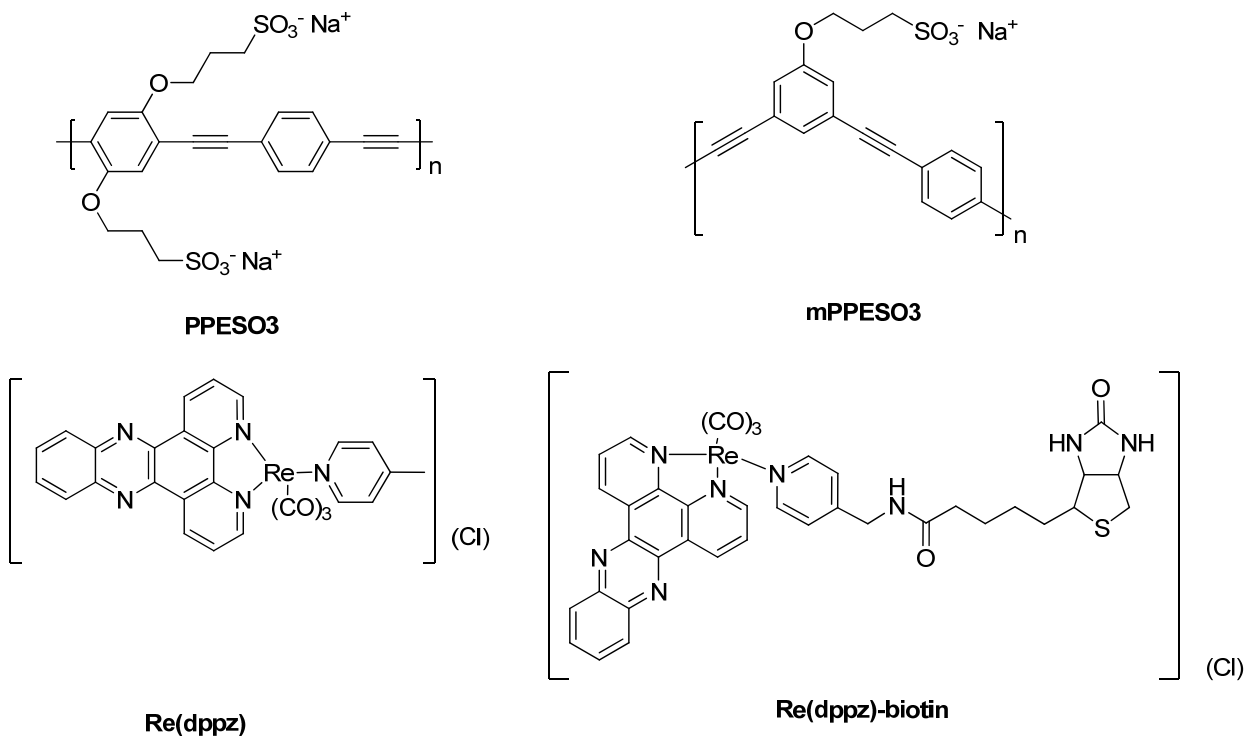


Figure 3-3. Structures and acronyms of polymers and Re complexes.

Results

Synthesis of Re complexes

Re(dppz) (PF₆) was prepared from the reaction of [*fac*-(dppz)Re^I(CO)₃](Cl) and 4-methylpyridine in DMF containing AgPF₆. Re(dppz)-biotin (PF₆) was prepared from the reaction of [*fac*-(dppz)Re^I(CO)₃(CH₃CN)](CF₃SO₃) and the ligand py-CH₂NH-biotin in THF/MeOH and followed by metathesis with NH₄PF₆. The PF₆ salts of two Re complexes were purified by column chromatography and characterized by ¹H NMR and positive-ion ESI-MS, and then metathesized to Cl⁻ form.

Photophysical Properties of Re complexes

The Re(dppz) complex displays moderately intense absorption band with two maxima at 366 nm and 384 nm in aqueous solution. The absorption of Re(dppz)-biotin also appears in the near UV as a moderate intense band with two maxima at 368 nm and 385 nm. Both of Re(dppz)

and Re(dppz)-biotin are non-luminescent in aqueous solution because their luminescent $^3\text{MLCT}$ and $^3\pi,\pi^*$ excited states are strongly quenched in aqueous solution by proton transfer (or H-bond formation) from H_2O to one of the phenazine nitrogens in the dppz ligand.^{81, 82}

Fluorescence Quenching of mPPESO3 with Re(dppz) and Re(dppz)-biotin

Transition metal cations, such as Pd^{2+} , Ru^{2+} , Cu^{2+} , and Pt^{2+} possess high quenching efficiency to conjugated polymer fluorescence via electron transfer or energy transfer mechanism.^{123, 125, 126} Therefore, cationic transition metal Re(I) was chosen to design Re complex containing a dppz ligand, which can bind to mPPESO3 through both electrostatic interaction and intercalation of a dppz ligand to the polymer. The intercalating and quenching properties of Re(dppz) were studied by emission titration experiments. Upon addition of Re(dppz) (0–0.48 μM) to mPPESO3 aqueous solution, the polymer emission at 450 nm is quenched (Figure 3-4). Similar changes are also observed for quenching of the polymer emission by Re(dppz)-biotin. The fluorescence of mPPESO3 is strongly quenched by both Re(dppz) and Re(dppz)-biotin at low concentration. The fluorescence quenching constants (K_{sv}) of mPPESO₃ by Re(dppz) and Re(dppz)-biotin are $7.56 \times 10^6 \text{ M}^{-1}$ and $7.38 \times 10^6 \text{ M}^{-1}$, respectively (Table 3-1). The K_{sv} values were obtained in the linear range of 0–0.32 μM for Re(dppz) and 0–0.34 μM for Re(dppz)-biotin.

Table 3-1. Stern-Volmer quenching constants for mPPESO3 and PPESO3 fluorescence quenching by Re complexes

	$K_{\text{sv}} (10^6 \text{ M}^{-1})^{\text{a}}$						
	Re(dppz)-biotin			Re(dppz)		Only protein	
	-	avidin	BSA	-	avidin	avidin	BSA
mPPESO3	7.38 ^b	1.37 ^c	9.66 ^c	7.56 ^d	3.41 ^c	0.22 ^e	0.23 ^e
PPESO3	1.00 ^f	1.10 ^g	-			-	-

^a K_{sv} values are obtained from the linear region of the SV plots. ^b 0–0.34 μM . ^c 0–0.40 μM .

^d 0–0.32 μM . ^e 0–0.60 μM . ^f 0–1.02 μM . ^g 0–0.50 μM

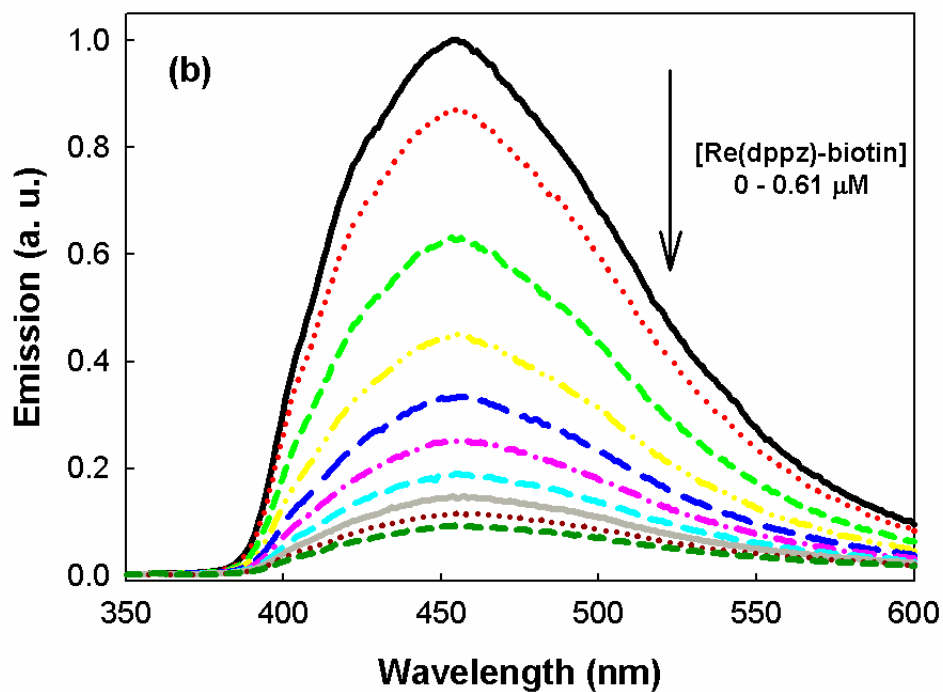
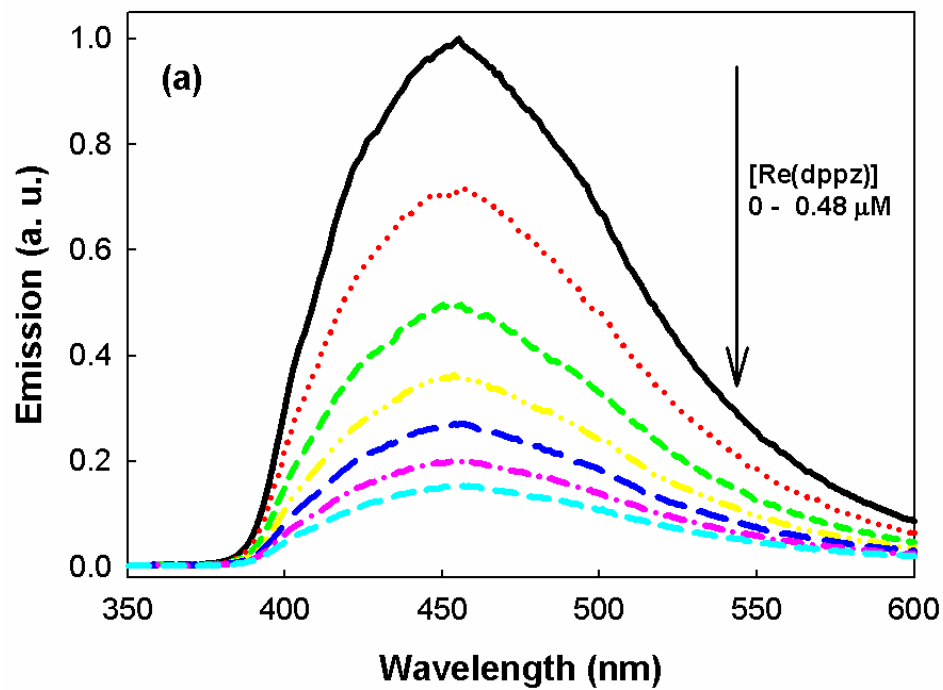


Figure 3-4. Fluorescence spectra of mPPESO3 (15 μM) in the presence of (a) Re(dppz) (0– 0.48 μM) and (b) Re(dppz)-biotin (0 – 0.61 μM) in a 1 mM phosphate buffer solution (pH 7.4).

The effect of polymer structure on the fluorescence of polymer/Re(dppz)-biotin complex was investigated using *para*-linked PPESO3. PPESO3 self-assembles linearly into π -stacked aggregates in contrast to helical structured mPPESO3 in aqueous solution. PPESO3 also contains sulfonate side groups to complex with positively charged quenchers via electrostatic interactions.³⁶ The fluorescence quenching experiment was carried out under previously described conditions for mPPESO3. As shown in Table 3-1, PPESO3 is less strongly quenched by Re(dppz)-biotin compared to mPPESO3.

Avidin Interactions with mPPESO3/Re(dppz)-biotin

The specific biosensor system QTL (quencher-tether-ligand, QTL)²² has been developed to detect biological targets^{94, 95} in which organic cations such as MV²⁺ (*N,N'*-dimethyl-4,4'-bipyridinium) and MV⁺ (*N*-methyl-4,4'-pyridylpyridium) are frequently used as a quencher. Whitten's group reported a violgen-type quencher linked to a biotin molecule, which is an excellent acceptor for proteins such as avidin and streptavidin. Recently, Ai's group used metal cation rhenium(I) to design a biotin-rhenium (I) complex as a QTL probe to detect avidin and streptavidin.¹²⁵ Both studies demonstrate that the fluorescence of polymers is quenched by quencher-biotin molecules and then addition of avidin to the quenched solution reverses the quenching. Avidin is known to bind strongly with biotin ($K \approx 10^{15} \text{ M}^{-1}$).¹²⁷ In addition, at neutral pH, avidin (pI 10–10.5)¹²⁸ is negatively charged and therefore it can be expected to be electrostatically bound to mPPESO3.

Knowing the Re(dppz)-biotin binds to avidin through the biotin moiety, we were interested in the fluorescence change of mPPESO₃ upon addition of avidin to the polymer-intercalated Re(dppz)-biotin. For this experiment the polymer/Re(dppz)-biotin complex was pre-formed to induce quenching polymer's fluorescence and then avidin was added to the quenched polymer solution in a 4:1 ratio of Re(dppz)-biotin/avidin. On contrary to expectation, the recovery of

fluorescence from the quenched polymer solution was not observed after the addition of avidin (data not shown). We conclude from this result that avidin does not displace biotin-Re(dppz) from its mPPESO₃-intercalated form to cause the reversal of fluorescence quenching.

Fluorescence Quenching of mPPESO₃ with Pre-formed Re(dppz)-biotin/avidin Complex

Next, the effect of biotin/avidin complexation on the fluorescence of mPPESO₃ was investigated. The pre-formed Re(dppz)-biotin/avidin complex (avidin:biotin = 1:4) was added to the polymer. Interestingly, the polymer is less efficiently quenched by the pre-formed Re(dppz)-biotin-avidin complex compared to Re(dppz)-biotin (Figure 3-5). For example, addition of 0.6 μM of Re(dppz)-biotin reduces the initial fluorescence of the polymer more strongly (ca. 5-fold) compared to the pre-formed Re(dppz)-biotin/avidin complex. Pre-formed Re(dppz)-biotin-avidin complex also was added to PPESO₃ and then K_{sv} ($1.10 \times 10^6 \text{ M}^{-1}$) was obtained at low concentration of regime by linear fit (Figure 3-6). There is little change in the K_{sv} values compared with the K_{sv} value of the polymer by only Re(dppz)-biotin ($1.14 \times 10^6 \text{ M}^{-1}$).

Similar quenching experiments of mPPESO₃ with different ratios of avidin/Re(dppz)-biotin mixtures were conducted. Each Re(dppz)-biotin sample was pre-mixed with different ratios of avidin (avidin:biotin = 1:1, 1:2, 1:4, 1:8) and added to the polymer. Emission at 450 nm was recorded at various concentrations of Re(dppz)-biotin (Figure 3-7). Re(dppz)-biotin mixed with different ratios of avidin (avidin:biotin = 1:1, 1:2, 1:4, and 1:8) does not show the pronounced difference in fluorescence quenching.

Effect of Specific Protein on Fluorescence Quenching of mPPESO₃ by Re(dppz)-biotin

As shown in Table 1, pre-mixing avidin with Re(dppz) has a distinct effect in the quenching efficiency. This is surprising because this complex does not contain the biotin moiety. The result shows that there is a non-specific interaction between the Re(dppz) and the protein which competes with the Re(dppz) binding to the polymer. K_{sv} value of pre-mixed Re(dppz)-

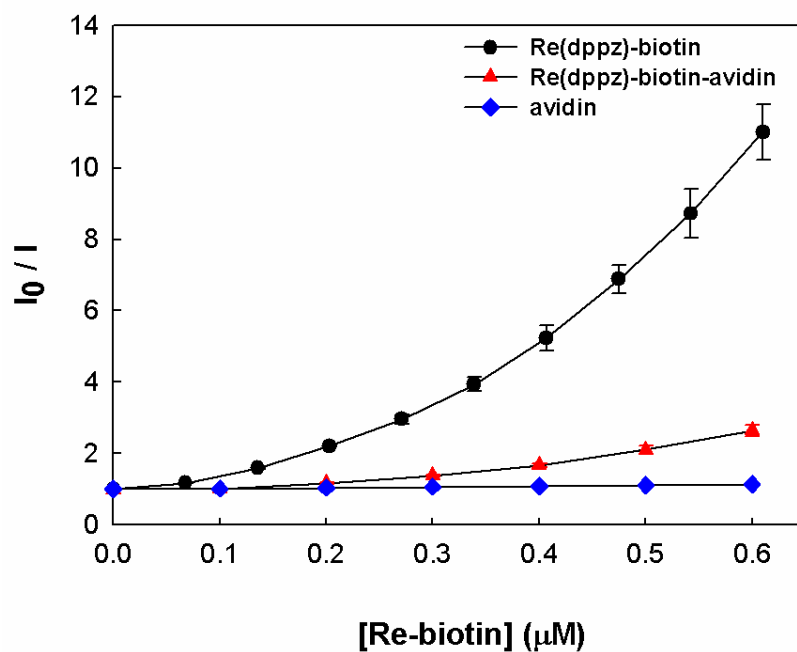


Figure 3-5. Stern-Volmer plots for mPPESO3 (15 μM) quenching by Re(dppz)-biotin, pre-formed Re(dppz)-biotin/avidin complex (avidin:Re(dppz)-biotin = 1:4) and avidin in 1 mM phosphate buffer solution (pH 7.4).

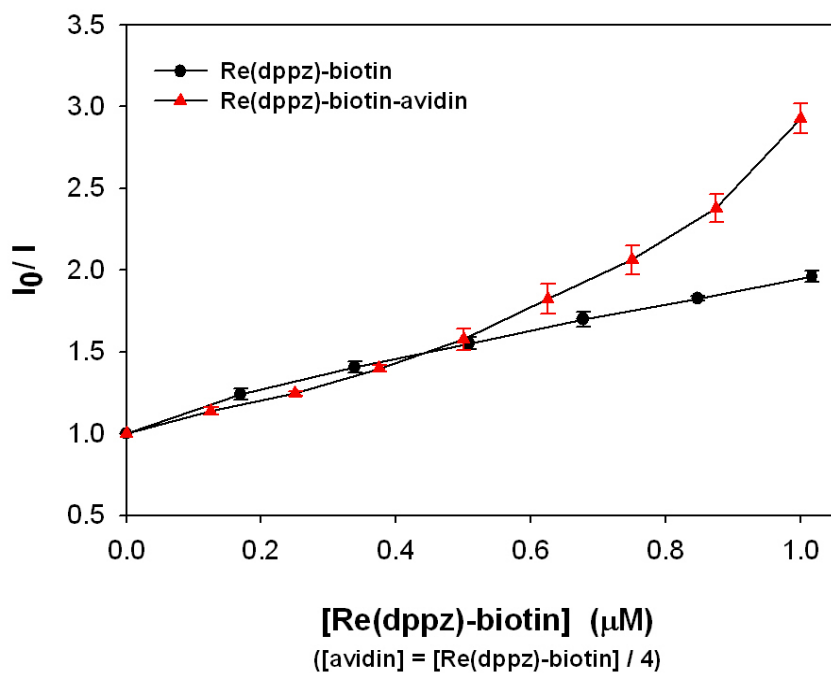


Figure 3-6. Stern-Volmer plots for PPESO3 (15 μM) quenching by Re(dppz)-biotin and pre-formed Re(dppz)-biotin-avidin complex (avidin:Re(dppz)-biotin = 1:4) in a 1 mM phosphate buffer solution (pH 7.4).

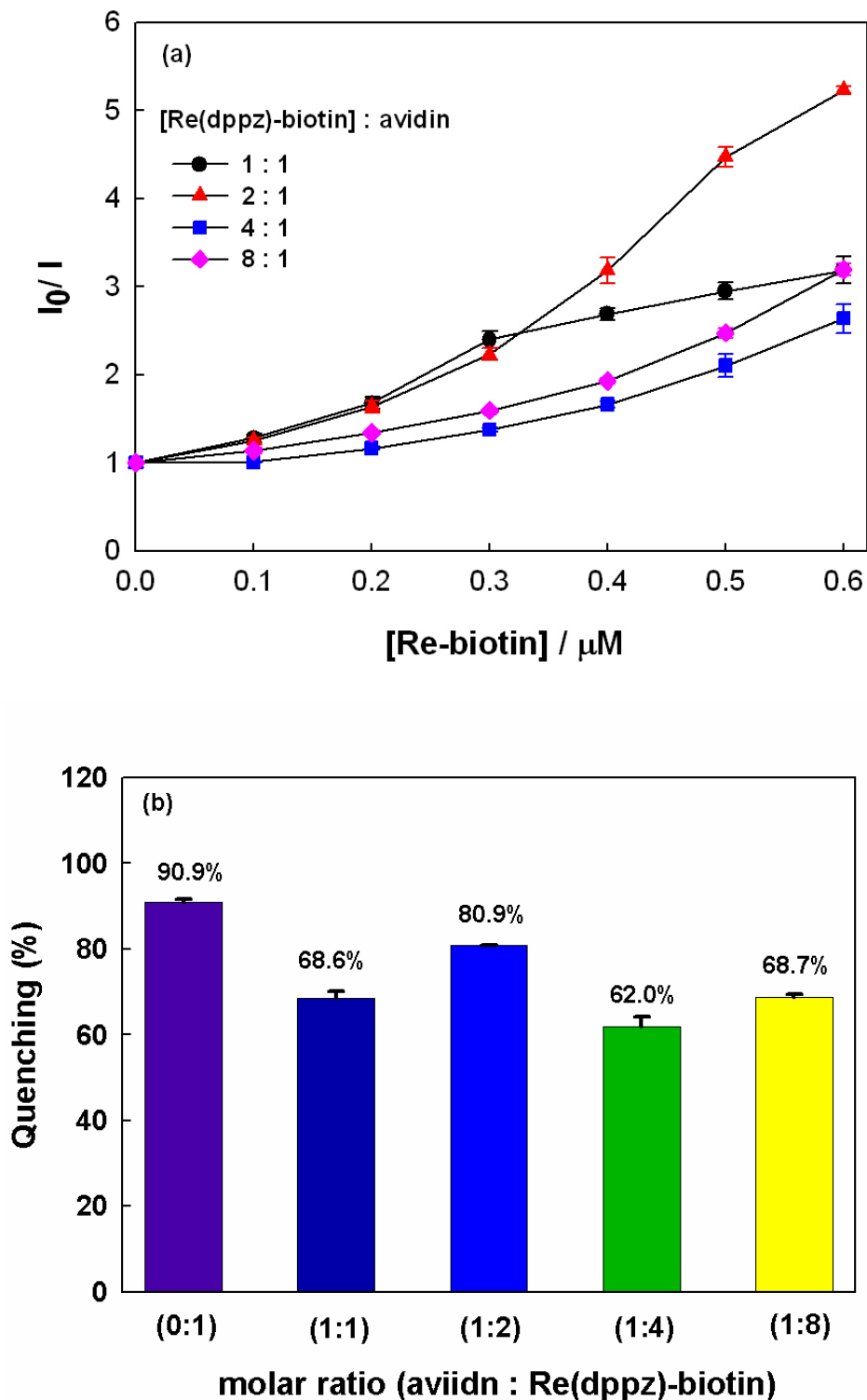


Figure 3-7. (a) Stern-Volmer plots for mPPESO3 (15 μM) quenching by different ratios of pre-formed Re(dppz)-biotin/avidin complex. (b) Quenching percent of mPPESO3 (15 μM) by pre-formed Re(dppz)-biotin (0.6 μM)/avidin complex containing different concentrations of avidin in a 1 mM phosphate buffer solution (pH 7.4).

avidin ($3.41 \times 10^6 \text{ M}^{-1}$) is about two times less than that of Re(dppz) ($7.56 \times 10^6 \text{ M}^{-1}$). Given that avidin nonspecifically disturbs fluorescence quenching by Re(dppz) , we examined influence of protein without biotin binding site on fluorescence quenching by Re(dppz) -biotin (Figure 3-8). BSA (pI 4.7)¹²⁸ was chosen for this experiment. BSA did not cause significant difference in K_{sv} values of pre-mixed Re(dppz) -biotin/BSA ($K_{sv} = 9.66 \times 10^6 \text{ M}^{-1}$) and Re(dppz) -biotin ($7.38 \times 10^6 \text{ M}^{-1}$). These results suggest that the biotin moiety on Re(dppz) -biotin complex specifically binds to avidin, but avidin (pI 10-10.5)¹²⁸ can non-specifically interact with negatively charged mPPESO3 via electrostatic interaction between charged molecules to disrupt polymer quenching by Re(dppz) .

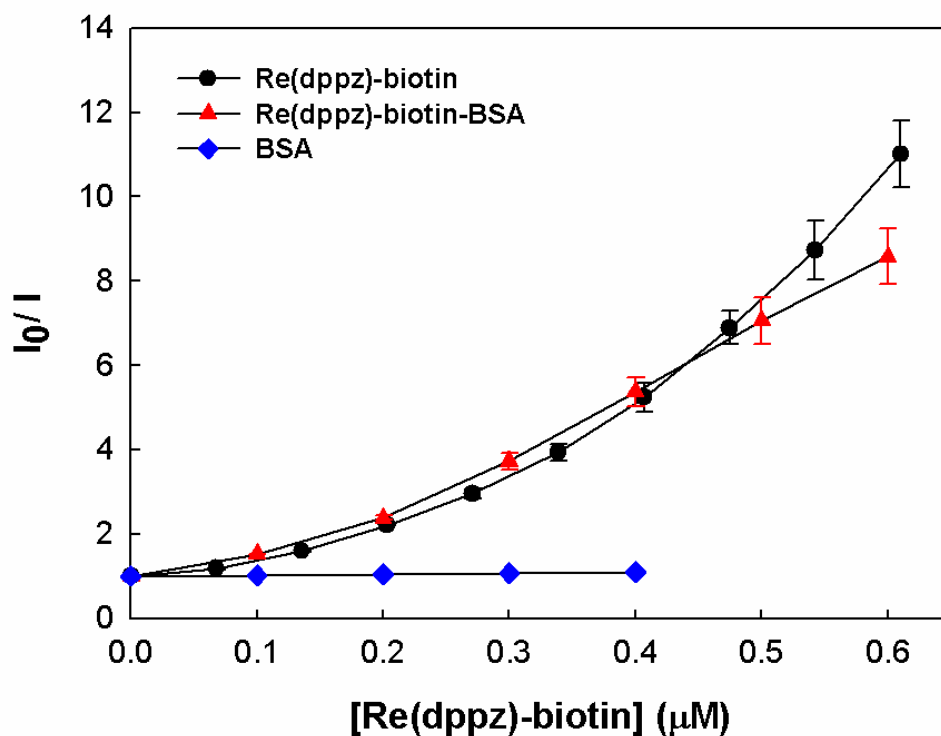


Figure 3-8. Stern-Volmer plots of mPPESO3 (15 μM) quenching in a 1 mM phosphate buffer solution (pH 7.4) by Re(dppz) -biotin, pre-mixed Re(dppz) -biotin-BSA mixture (BSA: Re(dppz) -biotin = 1:4) and BSA.

Discussion

Re(dppz) and Re(dppz)-biotin bind strongly to mPPESO3 via intercalation of the extended planar dppz ligand within π -stacked phenylene ethynylene residues in the helical conformation. This interaction between the polymer and Re complexes induces a pronounced quenching for mPPESO3 compared with PPESO3. The same result was seen previously with Ru(bpy)₂(dppz), which quenched strongly the fluorescence of mPPESO3 via the intercalative binding.⁷⁹ The special quenching effect seen with mPPESO3 provides evidence that intercalation of the Re complex into the helical conformation of the polymer results in stronger polymer-quencher complex association and electrostatic interaction. Therefore, efficient quenching of the polymer fluorescence is observed from mPPESO3.

Addition of avidin to the quenched mPPESO3 solution does not recover the fluorescence of the polymer even though the biotin-avidin complexation is strong ($K \approx 10^{15}$ M). It can be explained by two possibilities. First, the mPPESO₃-intercalated Re(dppz)-biotin complex binds to avidin at the same time (i.e. cross-linking of mPPESO₃ and avidin; Figure 3-9).¹²⁹ When avidin binds to biotin, positively charged avidin sticks to the negatively charged polymer and therefore the quencher remains intercalated to result in no reversal of quenching. Second, Re(dppz)-biotin is hidden due to intercalation and therefore the biotin may not be accessible to avidin. Re(dppz)-biotin remains intercalated to the polymer, but it does not bind to avidin.

Pre-formed Re(dppz)-biotin/avidin (4/1) complex gives weaker quenching of mPPESO3 fluorescence than only Re(dppz)-biotin does. Avidin bound to Re(dppz)-biotin is positively charged at neutral pH and it is attracted to anionic mPPESO3 electrostatically. Therefore, the quencher is close to polymer, but it might not intercalate into the polymer resulting in less efficient quenching (Figure 3-10).

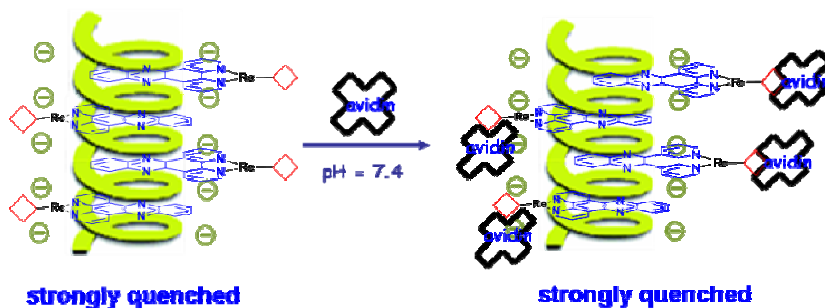


Figure 3-9. Cross-linking of mPPESO₃ and avidin by using Re(dppz)-biotin.

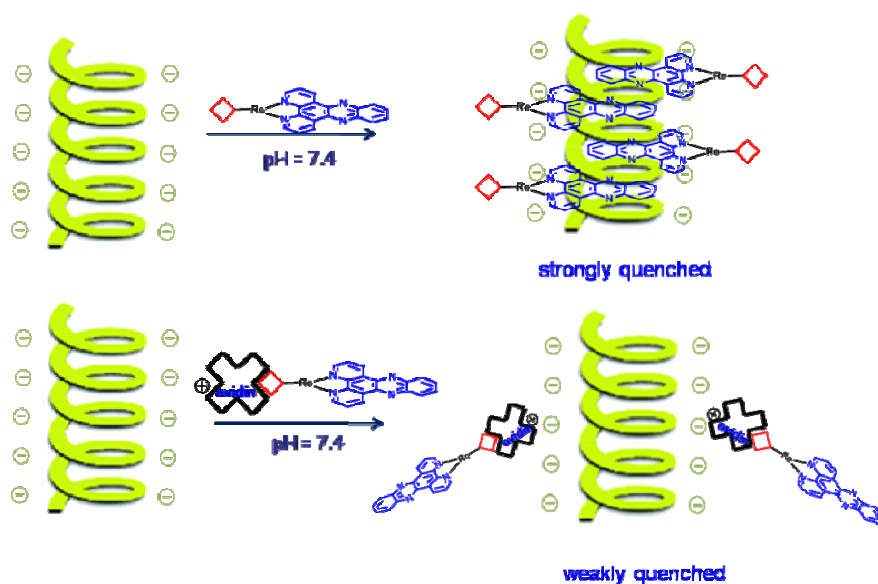


Figure 3-10. Binding of Re(dppz)-biotin and pre-formed Re(dppz)-biotin/avidin complex to mPPESO₃.

Summary and Conclusions

Re(dppz) and Re(dppz)-biotin quenchers strongly quench the mPPESO₃ fluorescence via intercalation and static interaction. However, introduction of avidin to the pre-formed Re(dppz)-biotin-polymer complex gives little effect on the polymer fluorescence. This result conflicts with the earlier work of Whitten's group on QTL and MPS-PPV. This suggests two possibilities. First, biocytin-TMR is buried within the helical structures polymer, and hence avidin is not able to access to biotin, leading to reversal quenching. Second, Re(dppz)-biotin serves as a cross linker for the concurrent binding of the polymer and avidin. When avidin is previously bound to biotin

Re(dppz)-biotin, the Re(dppz)-biotin-avidin complex gives less effect on the fluorescence quenching because of the electrostatic interaction between the oppositely charged polymer and avidin.

Experimental

Materials

All chemicals used for synthesis were of reagent grade and used without purification. Biotin, N-hydroxysuccinimide, 4-picoline and 4-aminomethyl pyridine were purchased from Sigma-Aldrich. 1,10-phenanthroline, 1-ethyl-3-(3-dimethylaminopropyl)-carbodiimide and *o*-phenyldiamine, and silver hexafluorophosphate were obtained from Acros. Rhenium pentacarbonyl chloride and silver trifluoromethanesulfonate were purchased from Strem. Silica gel (Merck, 230-400 mesh) and neutral alumina (Fisher, Brockman grade III) were used for chromatographic purification of Re(dppz) and Re(dppz)-biotin, respectively.

Instrumentation

¹H NMR spectra were recorded on either a Varian VXR 300 or Mercury-300 spectrometer and chemical shifts are reported in ppm relative to TMS. Absorption spectra were obtained on a Varian-Cary 100 UV-visible absorption spectrometer. Steady state fluorescence spectra were recorded on a spectrofluorometer from Photon Technology International and corrected by using correction factors generated with a primary standard lamp.

General Methods

Fluorescence quenching

All fluorescence quenching experiments of mPPESO₃ and PPESO₃ were conducted by titrating the polymer solutions with aliquots of Re(dppz), pre-mixed Re(dppz)-biotin, Re(dppz)-biotin, pre-formed Re(dppz)-biotin-avidin complex and avidin, respectively. The fluorescence intensity was recorded at different concentration of the quenchers. For mPPESO₃, the

fluorescence intensity was acquired with excitation and emission wavelengths of 320 nm and 450 nm, respectively; and for PPESO₃, excitation and emission wavelengths are 420 nm and 540 nm, respectively. The quenching of polymer fluorescence follows a conventional “Stern-Volmer” relationship:

$$\frac{I_0}{I} = 1 + K_{sv}[Q] \quad (3-1)$$

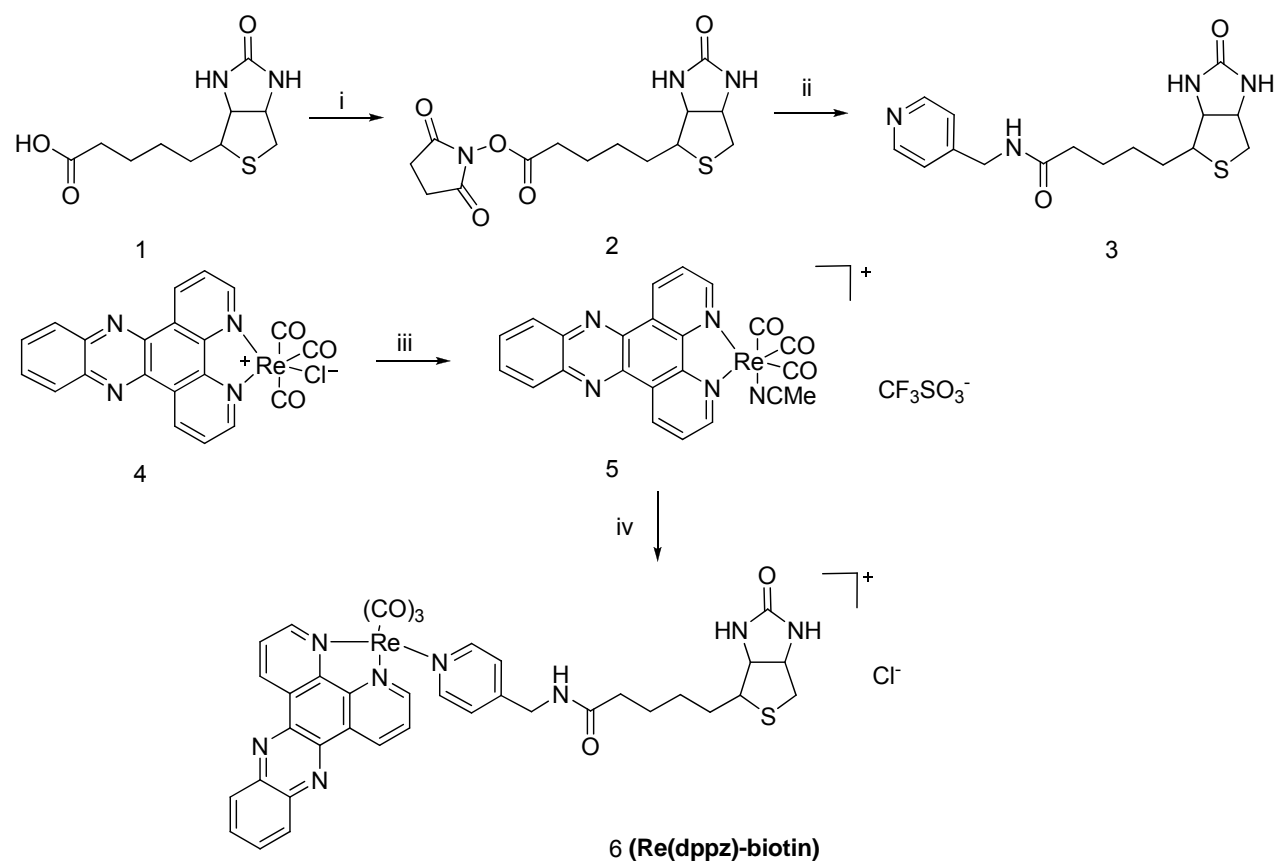
where I_0 and I are the intensities of fluorescence in the absence and presence of quenchers, and $[Q]$ is the concentration of the quencher. Thus, the quenching constant, K_{sv} defines quenching efficiency. The quenching constants were determined from the low concentration range of the Stern-Volmer plots because deviations from the linearity occurred at high quencher concentration.

Fluorescence recovery

mPPESO₃ was titrated with Re(dppz)-biotin to quench the fluorescence followed by the addition of avidin to the quenched mixture solution in a 4:1 ratio of Re(dppz)-biotin/ avidin.

Synthetic Procedures

[*fac*-(dppz)Re^I(CO)₃(4-methylpyridine)] [Cl], Re(dppz). This complex was prepared according to a literature procedure.¹¹³ The following NMR data were obtained by using the PF₆⁻ salt of the complex. ¹H NMR (300MHz, CD₃CN) δ 2.16 (s, 3H), 7.06 (d, 2H), 8.12-17 (m, 4H), 8.26 (m, 2H), 8.45 (m, 2H), 9.65 (d, 2H), 9.90 (d, 2H). Positive-ion ESI-MS calcd for C₂₇H₁₇N₅O₃Re (M⁺) 646.089, found 646.085; calcd for C₂₁H₁₀N₄O₃Re (M⁺-pyridine) 553.031, found 553.028.



i. N-hydroxysuccinimide, 1-Ethyl-3-(3-dimethylaminopropyl)-carbodiimide (EDC), DMF; ii. 4-Aminomethyl pyridine, triethylamine, DMF; iii. 1) Silver triflate, acetonitrile; 2) NH_3PF_6 ; iv. 1) py- CH_2 -NH-biotin, THF/ methanol (3/1, v/v), heat; 2) anion exchange resin.

Figure 3-11. Synthesis of Re(dppz)-biotin.

Biotin succinimide (2). To a solution of biotin (1 g, 4.09 mmol) in anhydrous DMF (25 mL), N-hydroxysuccinimide (0.56 g, 4.91 mmol) and 1-(3-dimethylaminopropyl)-3-ethylcarbodiimide (0.94 g, 4.91 mmol) was added. The solution was stirred for 24 h and was recrystallized in 2-propanol to collect white powder (0.96 g, 2.82 mmol). ^1H NMR (300MHz, $\text{DMSO}-d_6$) δ 1.41-1.62 (m, 6H), 2.56-87 (m, 8H), 3.09-3.11 (m, 1H), 4.13- 4.34 (m, 2H), 6.37 (s, 1H), 6.42 (s, 2H).

Py- CH_2 -NH-biotin (3). Compound 2 (115 mg, 0.34 mmol) was dissolved in dry DMF (5mL) and triethylamine (190 μL , 1.36 mmol) was added. After addition of 4-aminomethyl

pyridine (35 mg, 0.34 mmol) in DMF (5 mL), the mixture was stirred under argon at room temperature. After stirring for 24 h, DMF was removed and recrystallized from MeOH/Et₂O to get white precipitate (0.17g, 0.24 mmol). ¹H NMR (300MHz, DMSO-*d*₆) δ 1.32-1.64 (m, 6H), 2.168 (t, 3H), 2.58 (d, 1H), 2.80 (dd, 1H), 3.09-3.11 (m, 1H), 4.11-4.14 (m, 1H), 4.30-4.32(m, 3H), 6.37 (s, 2H), 6.46 (s, 1H), 7.21 (d, 2H), 8.4-8.48 (m, 3H).

[*fac*-(dppz)Re^I(CO)₃(py-CH₂NH-biotin)][Cl], Re(dppz)-biotin (6). This complex was prepared according to a literature procedure.¹¹⁴ PF₆⁻ salt was metathesized to Cl⁻ form in the same way as Re(dppz).¹¹³ The following NMR data was obtained by using the PF₆⁻ salt of the complex. ¹H NMR (300MHz, DMSO-*d*₆) δ 1.23-1.43 (m, 6H), 2.27 (t, 2H), 2.60 (d, 1H), 2.8 (dd, 1H), 3.05 (m, 1H), 4.14 (m, 3H), 4.30 (m, 1H), 6.40 (m, 2H), 7.18 (d, 2H), 8.17-8.21 (m, 2H), 8.36-8.51 (m, 7H), 9.79 (d, 2H), 9.88 (d, 2H). Positive-ion ESI-MS calcd for C₃₇H₃₂N₈O₅ReS (M⁺) 887.177, found 887.173; calcd for C₂₁H₁₀N₄O₃Re (M⁺- py-CH₂NH-biotin) 553.031, found 553.028.

CHAPTER 4
FLUORESCENCE RESONANCE ENERGY TRANSFER FROM HELICAL CONJUGATED
POLYELECTROLYTE TO CHARGED FLUORESCENT DYE-LIGAND CONJUGATED
(DLC) MOLECULE

Introduction

Conjugated polyelectrolytes (CPEs) are π -conjugated polymers with ionic side groups which make them soluble in water.²³ These materials exhibit strong light absorption, high fluorescence quantum yield and an enhanced quenching effect compared to low molecular weight fluorescence probes.^{30, 36} These interesting properties have proven the CPEs to be useful for fabrication of sensors for biological targets.^{22, 94} Another intrinsic characteristic of CPEs is their ability to self-assemble into supramolecular structures in solution. Previously, our group showed that an anionic conjugated polyelectrolyte mPPESO3, which has a *meta*-linked poly(phenylene ethynylene) (PPE) backbone, self-assembles into a helical conformation in H₂O (a “poor” solvent) while it exists in a random coil conformation in MeOH (a “good” solvent).⁷⁹ It was also demonstrated that the cationic DNA metallo-intercalator, [Ru(bpy)₂(dppz)]²⁺ binds to the helical structure of mPPESO3 via intercalation of the dppz ligand to the π -stacked phenylene ethynylene units. This effect arises due to the structural similarity between the helical conformation of mPPESO3 and double helical DNA (i.e., both feature aromatic residues along the helical axis and they present negatively charged side groups to the surrounding solvent environment). Intercalation induces strong luminescence from the non-luminescent Ru complex as well as fluorescence quenching of the polymer.

We have an interest in fundamental understanding of the mechanism of amplified quenching in mPPESO3 fluorescence with cationic intercalator quenchers. To address this issue, we carried out a detailed photophysical investigation that probes the interaction of the polymer with a quencher. The structures of two different types of CPEs and the quencher used for this

study are shown in Figure 4-1. mPPESO3 and PPESO3 are anionic poly(phenylene ethynylene)s (PPEs) that feature sulfonate side groups. In aqueous solution, mPPESO3 self-assembles into a helical conformation while PPESO3 self-assembles into an aggregate where the chains are aligned.^{36, 79} Biotinylated rhodamine, 5-(and-6)-tetramethylrhodamine biocytin (biocytin TMR), which is a dye-ligand conjugate was selected for this investigation for several reasons. First, biocytin-TMR is a positively charged dye and therefore interacts with anionic CPEs, mPPESO3 or PPESO3 by ion pairing, resulting in fluorescence quenching.^{32, 36} Second, it is well known that rhodamine can intercalate into the helical structure of DNA and therefore it can intercalate into mPPESO3.^{130, 131} Third, because biocytin-TMR absorbs strongly in the visible region, it efficiently quenches the fluorescence of the polymer via energy transfer from the polymer to the dye. Finally, biocytin-TMR is a biotin-functionalized fluorophore, which is capable of binding to avidin. Water soluble CPEs and a dye-modified ligand were used as a donor and an acceptor, respectively.

In this system, the CPEs act as light-harvesting units which transfer excitation via FRET to a signaling dye to enhance the fluorescence signals of dye-modified ligand. Biocytin-TMR intercalates into the helical conformational mPPESO3, resulting in a decrease in the polymer fluorescence. Our efforts concerned FRET experiments to biocytin-TMR upon excitation of mPPESO3 with the fluorescence quenching of the polymer. The Stern-Volmer relation, given by $I_0/I = 1 + K_{sv}[Q]$ (where I_0 and I are the intensity of fluorescence in the absence and presence of a quencher, respectively, K_{sv} is the Stern-Volmer constant, and $[Q]$ is the concentration of a quencher) is used to quantitatively measure the quenching efficiency. The efficiency of energy transfer can be determined by the extent of emission quenching and relative intensities of acceptor emission in the donor alone or the donor-acceptor pair.

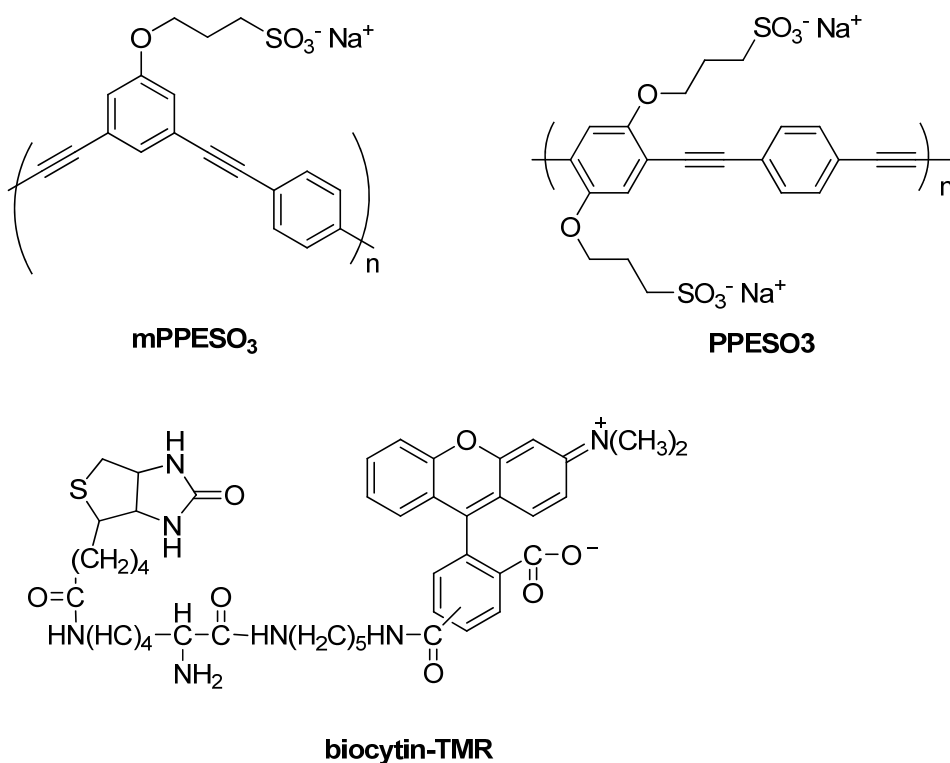


Figure 4-1. Structures and acronyms of conjugated polyelectrolytes and dye-ligand conjugate used in this study.

Results

Photophysical Properties.

The photophysical properties of three CPEs in aqueous solution are shown in Table 4-1. In aqueous solution mPPESO₃ absorbs with $\lambda_{\max} = 320$ nm and shows strong blue fluorescence at $\lambda_{\max} = 450$ nm. PPESO₃ absorbs in the blue of the visible region ($\lambda_{\max} = 420$ nm) and is

Table 4-1. Photophysical properties of mPPESO₃, PPESO₃ and biocytin-TMR in 1 mM phosphate buffer solution (pH 7.4)

	$\lambda_{\max}^{\text{abs}}/\text{nm}$	$\lambda_{\max}^{\text{em}}/\text{nm}$	Φ_{fl}
mPPESO ₃	320 nm	450 nm	0.17 ^a
PPESO ₃	420 nm	540 nm	0.10 ^b
Biocytin-TMR	553 nm	580 nm	-

^a Anthracene in EtOH was used as a standard, $\Phi_{\text{fl}} = 0.27$, see ref. 132, 133. ^b From ref. 36

strongly fluorescent at $\lambda_{\text{max}} = 540$ nm. For biocytin-TMR, the absorption maximum appears at 553 nm and the emission maximum is at 580 nm. The fluorescence quantum yields for the CPEs vary in the sequence mPPESO3 > PPESO3.

FRET from mPPESO3 to Biocytin-TMR

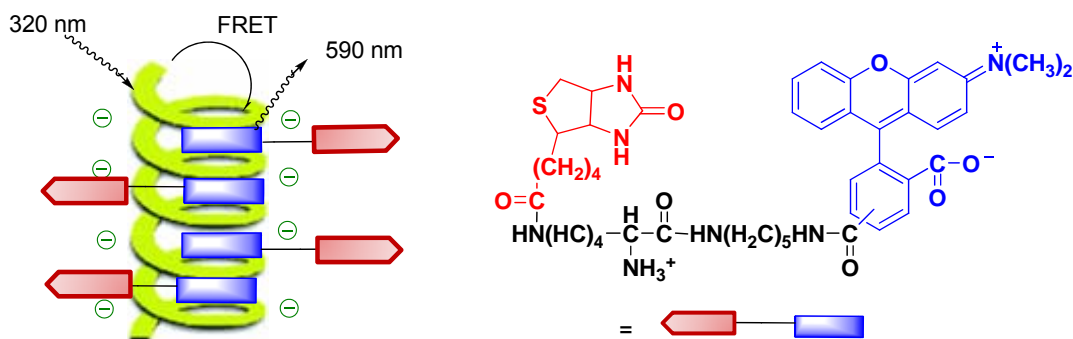


Figure 4-2. Energy transfer from mPPESO3 to biocytin-TMR.

Our strategy for CPE-sensitized biocytin-TMR emission is illustrated in Figure 4-2. Rhodamine is known to have a propensity to intercalate into DNA^{130, 131} and therefore biocytin-TMR is expected to intercalate into the helical structured polymer mPPESO3. This brings biocytin-TMR within close proximity of the polymer. Additionally, biocytin-TMR is a positively charged dye, and hence it forms an electrostatic complex with the polymer. After the excitation of the polymer, biocytin-TMR quenches the fluorescence of mPPESO3 via singlet-singlet energy transfer, where the polymer is the donor and biocytin-TMR is the acceptor. The occurrence of the energy transfer is confirmed by the observation of sensitized fluorescence from biocytin-TMR concomitant with fluorescence quenching of the polymer.

As described by Förster, dipole-dipole interaction leads to long-range resonance energy transfer from a fluorescent donor to an acceptor. The rate of energy transfer ($k_{t(r)}$) depends on the donor-acceptor distance (r), the orientation factor (κ), and the overlap integral ($J(\lambda)$) as described in Eq. 4-1.^{134, 135}

$$k_{t(r)} \propto \frac{1}{\tau_D} \left(\frac{R_0}{r} \right)^6 \quad (4-1)$$

$$R_0 = \left(\frac{9000(\ln 10)Q_D\kappa^2 J(\lambda)}{128 \pi^5 N_A n^4} \right)^{1/6} \quad (4-2)$$

$$J(\lambda) = \frac{\int_0^\infty F_D(\lambda)\varepsilon_A(\lambda)\lambda^4 d\lambda}{\int_0^\infty F_D(\lambda)d\lambda} \quad (4-3)$$

where, τ_D is the lifetime of the donor in the absence of an acceptor, R_0 is the Förster distance, Q_D is the quantum yield of the donor in the absence of an acceptor, N_A is the Avogadro's number, n is the refractive index of the medium, $F_D(\lambda)$ is the donor emission, and $\varepsilon_A(\lambda)$ is the acceptor absorption.

The distance between the donor (mPPESO3) and the acceptor (biocytin-TMR) is controlled by intercalation and electrostatic interaction to satisfy the distance requirement (< 10 nm) for energy transfer. The overlap integral provides the information about how the spectral overlap between the donor emission and the acceptor absorption affects the rate of energy transfer. Figure 4-3 shows the fluorescence of the two CPEs with the absorption and fluorescence of biocytin-TMR in aqueous solution. As a consequence of red-shift of the polymer fluorescence, spectral overlap between the emission of the polymer donor and the absorption of the biocytin-TMR acceptor varies systematically. The PPESO3 fluorescence spectrum is red-shifted compared with the mPPESO3 fluorescence, and hence the overlap between PPESO3 fluorescence and biocytin-TMR absorption spectrum is larger than that between mPPESO3 and biocytin-TMR as seen in Figure 4-3.

Figure 4-4 illustrates the fluorescence spectra of mPPESO3 (15 μM) in aqueous solution during titration with biocytin-TMR (0 to 0.225 μM). As biocytin-TMR is added to the polymer solution, the fluorescence of the polymer is quenched ($\lambda_{\text{em}} = 450 \text{ nm}$) and it is replaced by a red-

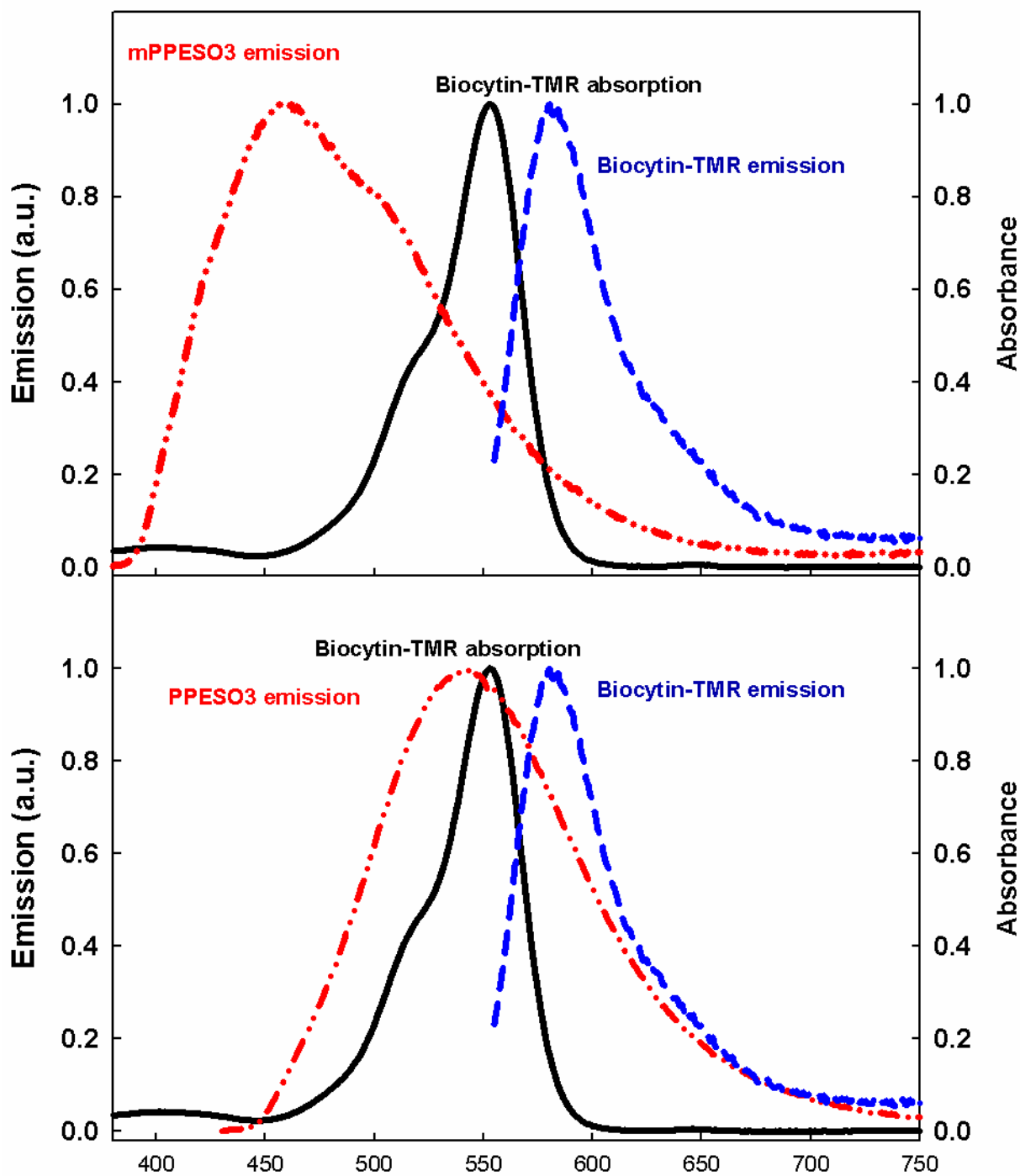


Figure 4-3. Normalized absorption spectrum of biocytin-TMR (—) and normalized fluorescence spectra of biocytin-TMR (---) and CPEs (— · —) in 1 mM phosphate buffer (pH 7.4). $\lambda_{\text{ex}} = 553 \text{ nm}$ for biocytin-TMR, $\lambda_{\text{ex}} = 320 \text{ nm}$ for mPPESO3 and $\lambda_{\text{ex}} = 420 \text{ nm}$ for PPESO3.

shifted fluorescence ($\lambda_{em} = 590$ nm) from biocytin-TMR. Direct excitation of the solution containing only biocytin-TMR at 320 nm provides supplementary information to the energy transfer from the polymer to biocytin-TMR. As seen in Figure 4-5, an 82-fold increase in biocytin-TMR fluorescence intensity is observed in the presence of the polymer, whereas the direct excitation of only biocytin-TMR solution lead to weak fluorescence. The excitation spectrum of biocytin-TMR-intercalated mPPESO3 also supports the premise that the fluorescence at 590 nm originates from the polymer-biocytin-TMR complex (Figure 4-6). The integrated absorption intensity around 320 nm is 24-fold higher than that around 550 nm. This result is consistent with the amplified fluorescence intensity of biocytin-TMR in the presence of the polymer.

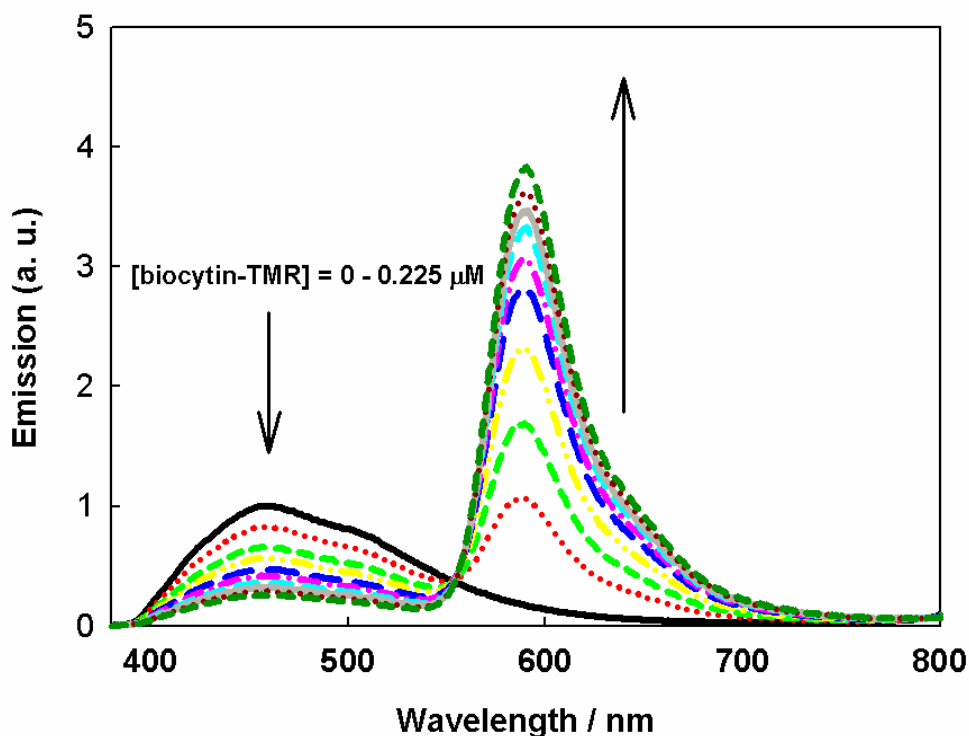


Figure 4-4. Normalized fluorescence spectra of mPPESO3 (15 μ M) upon addition of biocytin-TMR (0–0.225 μ M) in phosphate buffer (1 mM, pH 7.4). $\lambda_{ex} = 320$ nm.

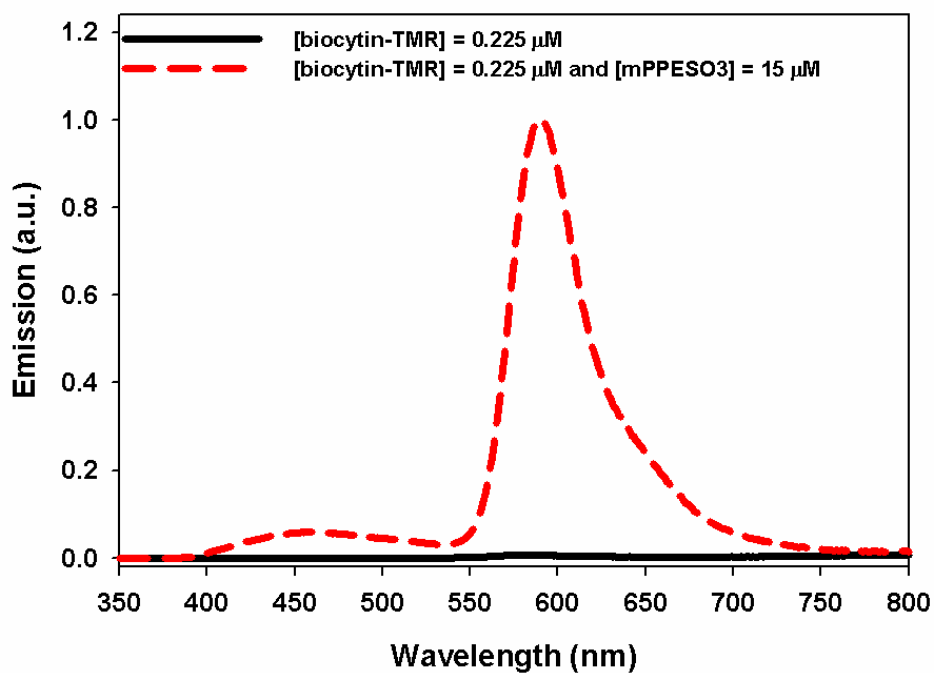
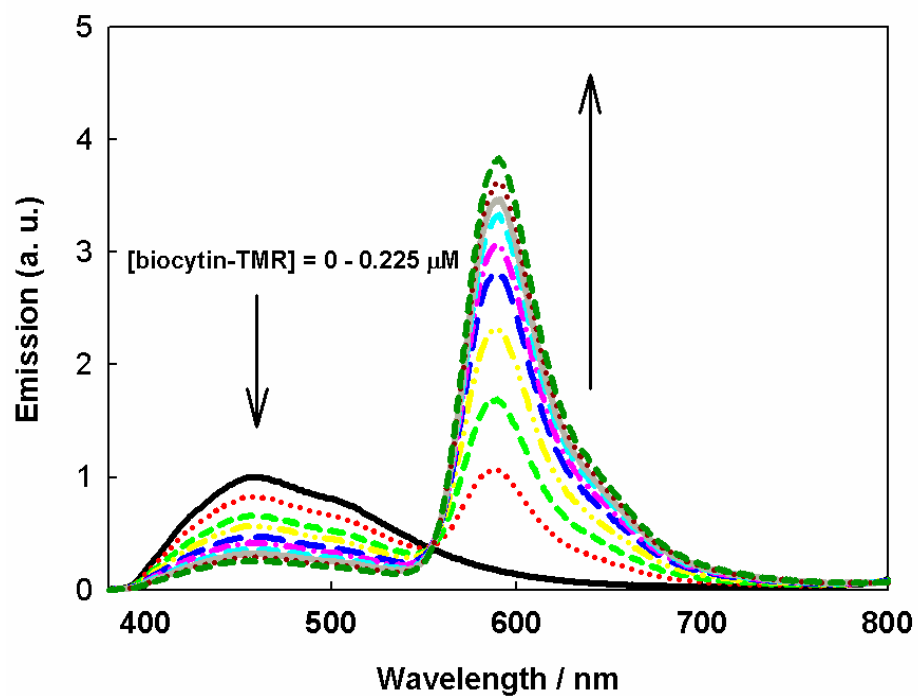


Figure 4-5. Normalized fluorescence spectra of biocytin-TMR (0.225 μM) in the absence (—) and presence (---) of mPPESO3 (15 μM) in phosphate buffer (1 mM, pH 7.4). λ_{ex} = 320 nm.

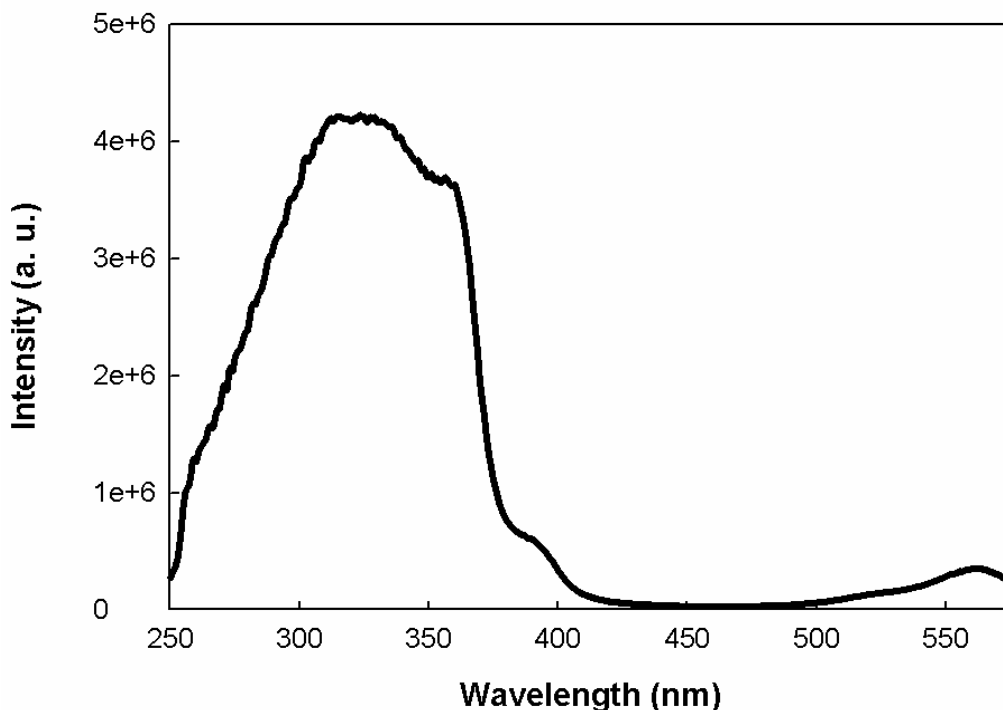


Figure 4-6. Excitation spectrum of mPPESO3 (15 μM)/ biocytin-TMR (0.225 μM) complex in phosphate buffer (1 mM, pH 7.4), $\lambda_{\text{em}} = 590 \text{ nm}$.

Anisotropy Measurements

Fluorescence anisotropy was used to provide insight into the interaction between mPPESO3 and biocytin-TMR (Figure 4-7). Rapid internal rotation and energy transfer are two major mechanisms for a loss of anisotropy. The excitation spectra of both mPPESO3/biocytin-TMR complex and biocytin-TMR were collected in the region of 400–570 nm at the four different polarization configurations: VV, VH, HH, and HV after emission at 580 nm corresponding to the maximum emission wavelength of biocytin-TMR. The anisotropy value, r , at each wavelength was determined from the standard equation given by $r = (I_{\text{VV}} - GI_{\text{VH}})/(I_{\text{VV}} + 2GI_{\text{VH}})$, where I_{VV} and I_{VH} are the vertical and perpendicular emission intensities when vertically polarized excitation is used, and G is an instrumental correction factor, $G = I_{\text{HV}}/I_{\text{HH}}$.¹³⁶ The introduction of the polymer into biocytin-TMR results in an increase in the measured anisotropy

in the absorption range (450 nm–560 nm) of biocytin-TMR. This is due to the decreased rotational rate of biocytin-TMR when it is intercalated into the polymer.¹³⁶ The anisotropy is primarily determined by rotational motion of a fluorophore (biocytin-TMR). In the polymer intercalated-biocytin-TMR, the size of the complex results in an increase in the anisotropy between 450 nm and 560 nm. Therefore, the anisotropy observation provides evidences for the intercalation of biocytin-TMR into the polymer.

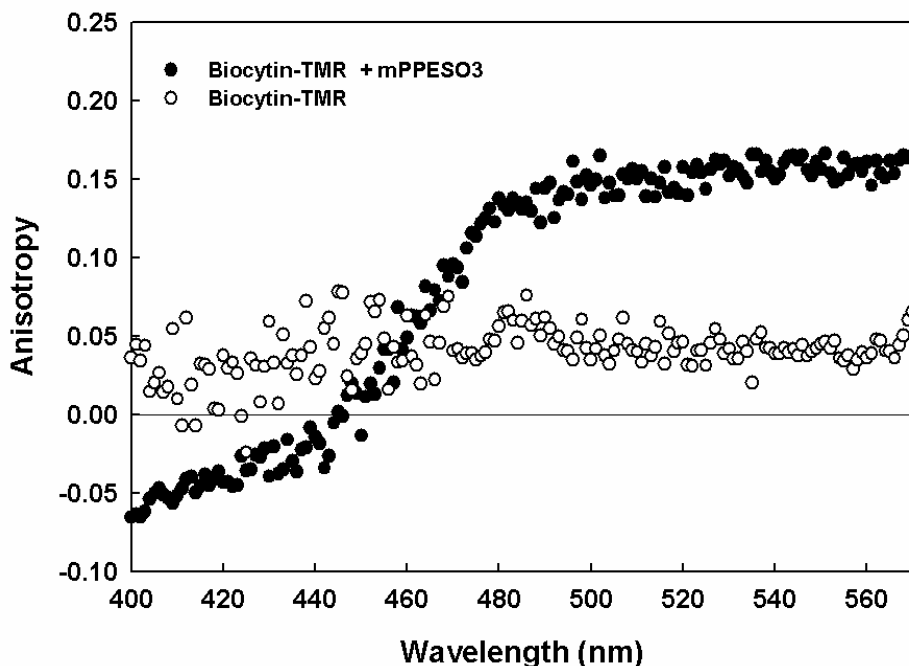


Figure 4-7. Excitation anisotropy of biocytin-TMR/mPPESO3 complex (●●●) and biocytin-TMR (○○○). [mPPESO3] = 15 μ M, [biocytin-TMR] = 0.225 μ M in phosphate buffer (1 mM, pH 7.4), λ_{em} = 580 nm.

Fluorescence Quenching of PPESO3 by Biocytin-TMR

The effect of polymer structure on the fluorescence of polymer/biocytin-TMR complex was examined using PPESO3. This experiment was conducted under the previously described conditions for mPPESO3. As mentioned before, *para*-linked PPESO3 self-assembles linearly into π -stacked aggregates in contrast to helical structured mPPESO3 in aqueous solution.

PPESO3 also contains sulfonate side groups to complex with positively charged quenchers via

electrostatic interactions.³⁶ Changes in the fluorescence intensity of PPESO3 (15 μM) upon addition of biocytin-TMR (0 to 2 μM) were monitored by excitation of the polymer at 420 nm. As seen in Figure 4-8, the sensitized biocytin-TMR fluorescence did not appear, whereas a decrease in the polymer fluorescence intensity was observed (Figure 4-8).

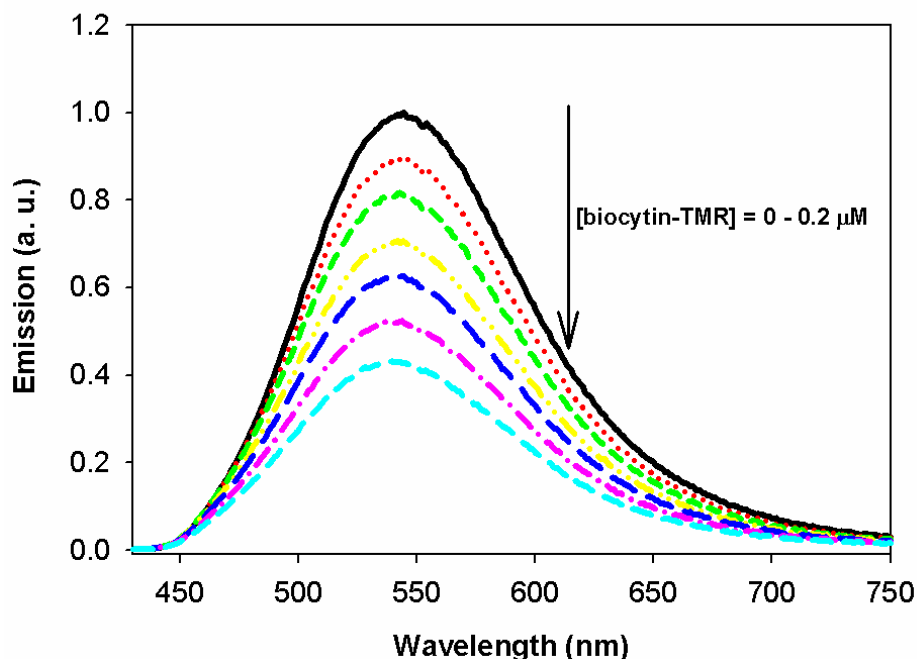


Figure 4-8. Normalized fluorescence spectra of PPESO3(15 μM) upon addition of biocytin-TMR (0 – 0.2 μM) in phosphate buffer (1 mM, pH 7.4). $\lambda_{\text{ex}} = 420$ nm.

Avidin binding to Biotin on Biocytin-TMR/CPEs complex

Quencher-tether-ligand (QTL)-based protein sensors have been widely used because QTL probes are able to undergo competitive binding between CPEs and the target proteins.²² Biotin and avidin were selected as the ligand and the target protein due to their high affinity binding. Avidin contains four identical binding sites for biotin and the binding affinity is known to be very high ($K_a \approx 10^{15} \text{ M}^{-1}$).¹²⁷ In previous studies it has been shown that the CPE fluorescence intensity decreases upon addition of the biotin conjugated quencher, as a result of electrostatic interactions between the CPE and the quencher. Addition of avidin disrupts the CPE/QTL

complex due to the strong binding between the avidin and biotin of the QTL. Once the QTL molecule is trapped by avidin, the quenching process is attenuated, resulting in an increase in the CPE fluorescence intensity.

The results shown above indicate that the fluorescence intensity of mPPESO3 is quenched by the biotin-functionalized QTL probe, biocytin-TMR. Therefore, the recovery of the quenched fluorescence was expected by specific binding between biotin on the biocytin-TMR and avidin. For the experiments of fluorescence recovery, avidin was added to the quenched biocytin-TMR/mPPESO3 complex solution in a 4:1 molar ratio of biocytin-TMR/avidin (Figure 4-9). In contrast to our expectation, the quenched fluorescence was not recovered. A small decrease in sensitized fluorescence intensity from biocytin-TMR at 590 nm was observed upon addition of

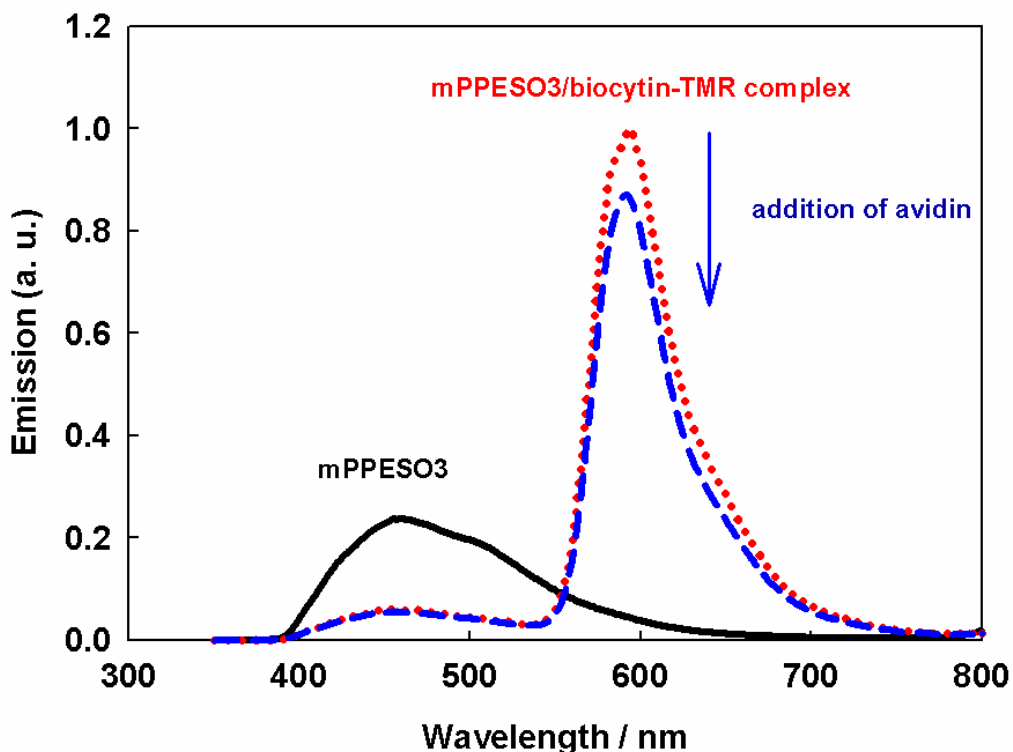


Figure 4-9. Fluorescence spectra of mPPESO3 solution upon addition of biocytin-TMR (•••) and avidin (---). [mPPESO3] = 15 μ M, [biocytin-TMR] = 0.225 μ M and [avidin] = 0.065 μ M in phosphate buffer (1 mM, pH 7.4). λ_{ex} = 320 nm.

avidin. This reduced fluorescence might arise due to the binding interaction between biocytin-TMR and avidin, resulting in quenching of the biocytin-TMR fluorescence as seen in Figure 4-10. Introduction of avidin (0 to 0.05 μM) into only biocytin-TMR solution (0.2 μM) significantly decreases the fluorescence intensity of biocytin-TMR.

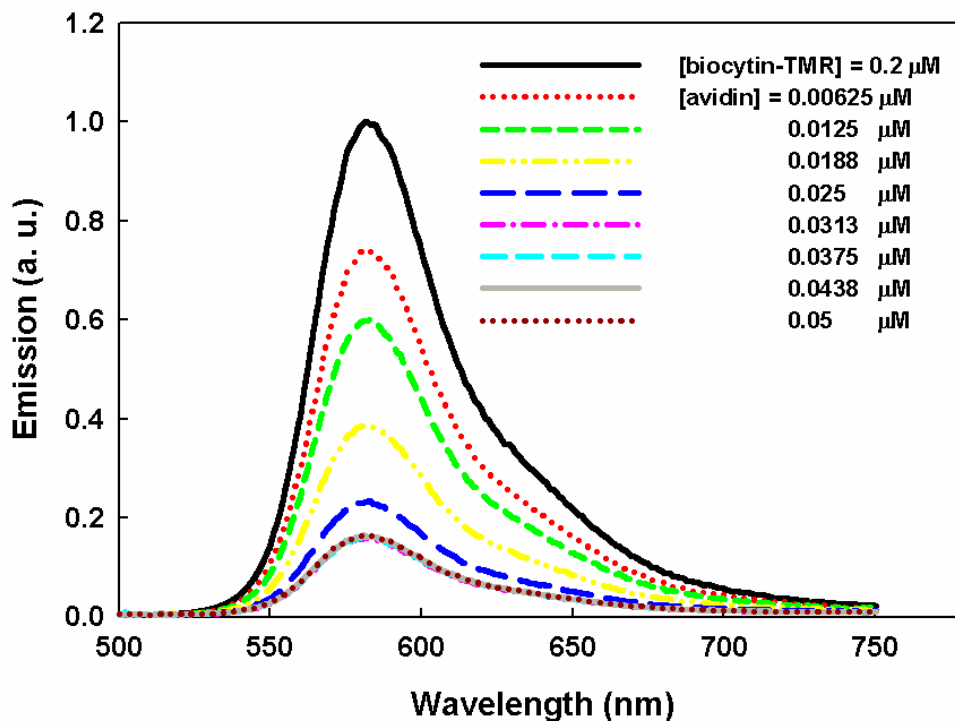


Figure 4-10. Fluorescence spectra of biocytin-TMR (0.20 μM) upon addition of avidin (0–0.05 μM) in phosphate buffer (1 mM, pH 7.4). $\lambda_{\text{ex}} = 550 \text{ nm}$.

Fluorescence Quenching of mPPESO3 by Pre-formed Biocytin-TMR/avidin complex

Since it was found that addition of avidin did not induce an increase in the fluorescence from the quenched mPPESO3/biocytin-TMR complex, we were interested in the interactions between the polymer and a pre-formed biocytin-TMR/avidin complex. For this experiment, the biocytin-TMR/avidin complex (avidin:biocytin-TMR = 1:4) was pre-formed and then it was added to mPPESO3. Changes in mPPESO3 fluorescence intensity at 450 nm were observed after excitation of the polymer at 320 nm. The same experiment was conducted using PPESO3 instead

of mPPESO3. PPESO3 was excited at 420 nm and fluorescence intensities were obtained at 540 nm. Figure 4-11 shows the Stern-Volmer plots for quenching of mPPESO3 and PPESO3 fluorescence with K_{SV} values. Addition of biocytin-TMR/avidin complex strongly quenches the mPPESO3 fluorescence ($K_{SV} = 2.6 \times 10^6$); however the K_{SV} value is 4.2-fold lower than that of the solution containing only biocytin-TMR. For PPESO3, the K_{SV} value of the biocytin-TMR/avidin complex is 10-fold lower compared to biocytin-TMR. Figure 4-12 displays the polymer-sensitized biocytin-TMR fluorescence intensity as a function of the concentration of biocytin-TMR after addition of biocytin-TMR or biocytin-TMR/avidin complex to the polymers. As described before, PPESO3 did not show the sensitized biocytin-TMR fluorescence at 590 nm and there is a little decrease in the fluorescence intensity at 590 nm by both biocytin-TMR and biocytin-TMR/avidin complex. In contrast, mPPESO3 exhibits a 21-fold increase in the fluorescence intensity at 590 nm after addition of 2.0 μ M of biocytin-TMR, whereas the same concentration of avidin bound biocytin-TMR induces only a 5-fold enhancement in the fluorescence intensity at 590 nm. To investigate the influence of an avidin concentration on the polymer fluorescence, different ratios of pre-formed biocytin-TMR/avidin complexes (avidin:biocytin-TMR = 1:1, 1:2, 1:3 and 1:4) were prepared and then added to the mPPESO3 solution. Avidin consists of four identical binding sites and each binding site is capable of binding one biotin ligand. Figure 4-13 (a) shows the Stern-Volmer plots for mPPESO3 fluorescence quenched by different ratios of biocytin-TMR to avidin. When four binding sites bind to biocytin-TMR, the least efficient fluorescence quenching is observed. With an increase in the avidin concentration the extent of the polymer fluorescence quenching increases in the sequence of 1:3 < 1:2 < 1:1. The polymer-sensitized biocytin-TMR fluorescence intensities are also collected at 590 nm. As seen in Figure 4-13 (b), 1:4 ratio of biocytin-TMR/avidin complex

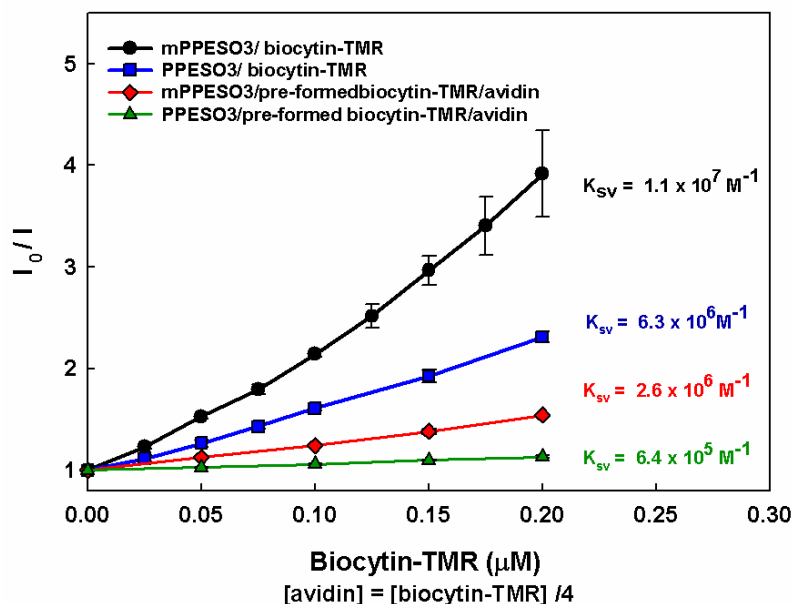


Figure 4-11. Stern-Volmer plots of mPPESO3 (15 μM) and PPESO3 (15 μM) fluorescence quenched by biocytin-TMR or pre-formed biocytin-TMR/avidin complex in phosphate buffer (1 mM, pH 7.4). K_{SV} values were calculated in the range of 0–0.2 μM except mPPESO3/biocytin-TMR (0–0.1 M). $\lambda_{\text{ex}} = 320 \text{ nm}$ and $\lambda_{\text{em}} = 450 \text{ nm}$ for mPPESO3. $\lambda_{\text{ex}} = 420 \text{ nm}$ and $\lambda_{\text{em}} = 540 \text{ nm}$ for PPESO3.

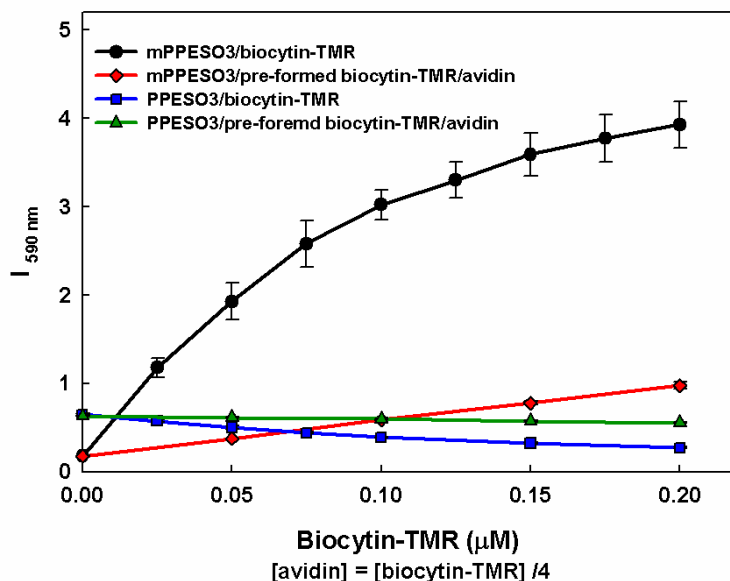


Figure 4-12. Sensitized biocytin-TMR fluorescence intensity at 590 nm after addition of biocytin-TMR or pre-formed biocytin-TMR/avidin complex to CPEs in phosphate buffer (1 mM, pH 7.4). $\lambda_{\text{ex}} = 320 \text{ nm}$ for mPPESO3. $\lambda_{\text{ex}} = 420 \text{ nm}$ for PPESO3.

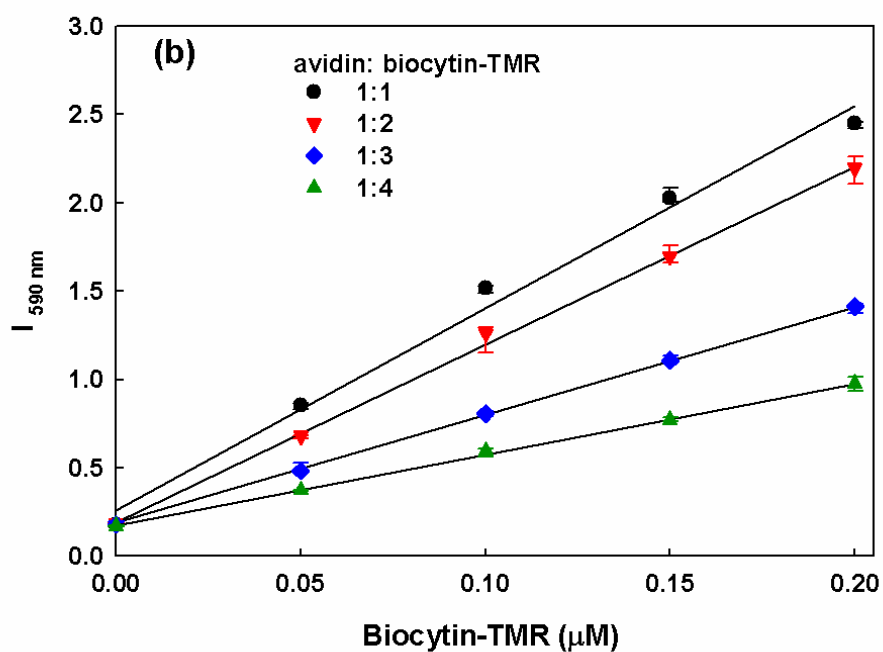
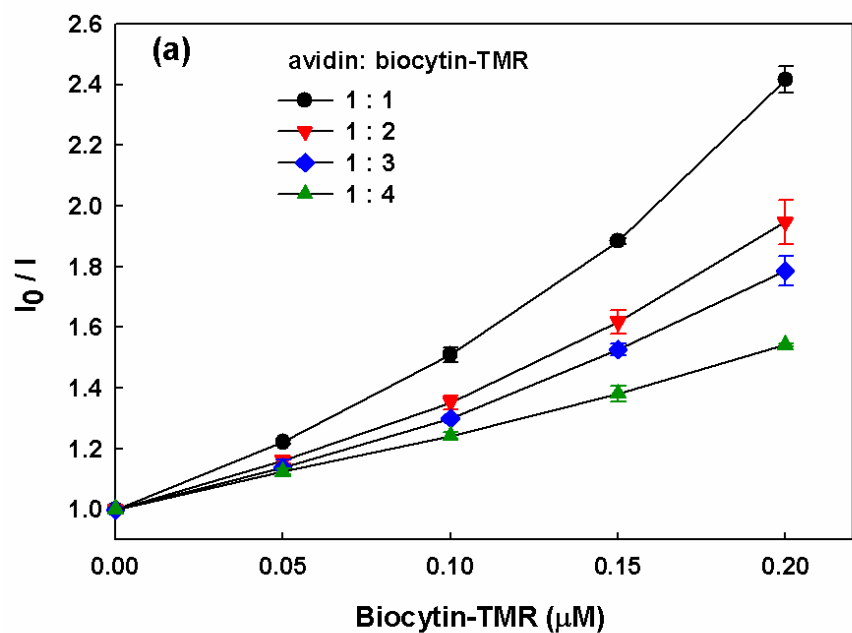


Figure 4-13. (a) SV plots for fluorescence quenching of mPPESO3 (15 μM) at 450 nm and (b) polymer-sensitized biocytin-TMR fluorescence at 590 nm upon addition of pre-formed biocytin-TMR/avidin complex ($[\text{biocytin-TMR}] = 0\text{--}0.20 \mu\text{M}$, avidin:biocytin-TMR = 1:1, 1:2, 1:3 and 1:4) in phosphate buffer (1 mM, pH 7.4). $\lambda_{\text{ex}} = 320 \text{ nm}$.

induces a 5.8-fold increase in the polymer-sensitized fluorescence intensity. An increase in the concentration of avidin enhances the sensitized fluorescence intensity at 590 nm in the order of $1:3 < 1:2 < 1:1$. This result is consistent with the above result where the pre-formed biocytin-TMR/avidin less strongly quenches the polymer fluorescence and induces the weaker FRET signal from biocytin-TMR.

Discussion

Fluorescence quenching and FRET studies shows that CPE-sensitized biocytin-TMR fluorescence is different for helical structured mPPESO3 and linearly π -stacked PPESO3 under the same experimental conditions. Both polymers' fluorescence intensities are quenched by biocytin-TMR; however, only mPPESO3/biocytin-TMR complex displays the sensitized biocytin-TMR fluorescence at 590 nm. FRET occurs through dipole-dipole interactions and the energy transfer rate is given by Eq. 4-1. The difference between the two polymers in the FRET result can be explained using this equation. Since the two polymers have different conformations in aqueous solution, different transition moment orientations between the polymers and biocytin-TMR can be expected. Additionally, the polymers exhibit similar spectral overlaps between the polymer fluorescence and the biocytin-TMR absorption; however, the quantum yield of mPPESO3 is 1.7-fold higher than PPESO3 in aqueous solution. As seen in Eq. 4-2, the quantum yield of the donor (CPEs) Q_D determines the Förster distance R_0 , therefore any variations in the donor quantum yield might influence the energy transfer efficiency. The polymer self-quenching upon complexation with biocytin-TMR due to aggregation of polymer chains gives a negative effect on the polymer-sensitized biocytin-TMR fluorescence.^{32, 137}

More efficient fluorescence quenching and FRET efficiency of mPPESO3 can be explained by the intercalation of biocytin-TMR to the helical polymer. This helix is believed to cause the strong complexation between the polymer and biocytin-TMR via intercalation with

electrostatic interaction. Anisotropy measurements support the binding mechanism between mPPESO3 and the positive intercalator quencher, biocytin-TMR. The polymer-intercalated biocytin-TMR shows an increased anisotropy value due to the change of the complex size via the interaction.

Once mPPESO3 fluorescence is quenched by biocytin-TMR, the fluorescence cannot be recovered by addition of avidin. This suggests that avidin is not able to displace biocytin-TMR from binding to mPPESO3 by intercalation. This result can be explained by two possibilities. First, the mPPESO₃-intercalated biocytin-TMR complex binds to avidin at the same time (i.e., cross-linking of mPPESO₃ and avidin).¹²⁹ When avidin binds to biotin, positively charged avidin is attached to the negatively charged polymer and therefore the quencher remains intercalated, resulting in no reversal of quenching. Second, biocytin-TMR is “hidden” due to intercalation and therefore the biotin may not be accessible to avidin. Biocytin-TMR remains intercalated to the polymer, but it does not bind to avidin.

Pre-formed biocytin-TMR/avidin quenches less strongly the two polymer fluorescence intensities. This complex also induces the weaker sensitized fluorescence from the biocytin-TMR compared to the solution containing only biocytin-TMR. Such difference is attributed to the positive charge of avidin at neutral pH. The positively charged avidin interacts with the polymers electrostatically. Therefore, the quencher might not intercalate to the polymer even though it is close to the polymer. This results in less efficient fluorescence quenching and weaker FRET emission signals.

Summary and Conclusions

In this study, fluorescence quenching and FRET of the anionic conjugated polyelectrolytes, mPPESO3 and PPESO3, were investigated in aqueous solution to understand the mechanism of amplified quenching of mPPESO3 by a cationic intercalator quencher. We have shown that

mPPESO3 possibly takes advantage of its helical conformation as a fluorescence resonance gate to transfer the polymer excitation to biocytin-TMR intercalated within the polymer. Therefore, biocytin-TMR fluorescence can be very efficiently sensitized by mPPESO3 and the energy transfer results in amplified fluorescence quenching of mPPESO3. Once the biocytin-TMR intercalates to mPPESO3, avidin is not able to displace the biocytin-TMR from the polymer. This result suggests that either biocytin-TMR is hidden within the polymer or serves as a cross linker for the concomitant binding of the polymer and avidin. Pre-formed biocytin-TMR/avidin give a little effect on the fluorescence quenching and FRET because of the electrostatic interaction between the oppositely charged polymer and avidin.

Experimental

Materials

The positively charged 5-(and-6)-tetramethylrhodamine biocytin (biocytin TMR) and avidin were purchased from Invitrogen TM and Sigma, respectively. All chemicals used for synthesis were of reagent grade and purchased from Sigma-Aldrich Chemical Company. All sample solutions were prepared by using water that was distilled and then purified by a Millipore purification system (Millipore Simplicity Ultrapure Water System). Buffer solutions were prepared with reagent-grade materials (Fisher). The polymer stock solution was diluted with buffer to a final concentration of 15 μM . All concentrations of polymers are provided in polymer repeat unit concentration (PRU). A concentrated stock solution of biocytin-TMR and avidin was prepared in buffer to obtain the desired concentrations. All assays were conducted in 1.0 mM potassium phosphate buffer (pH 7.4).

Instrumentation

NMR spectra were recorded on either a Varian VXR 300 or Mercury-300 spectrometer and chemical shifts are reported in ppm relative to TMS. Absorption spectra were obtained on a

Varian-Cary 100 UV-visible absorption dual beam spectrophotometer, with a scan rate of 300 nm/min. Steady state fluorescence spectra were recorded on a spectrofluorometer from Photon Technology International and corrected by using correction factors generated with a primary standard lamp.

General Methods

Fluorescence quenching experiments were carried out by microtitration in a fluorescence cuvette. In titration quenching experiments, 2 mL of polymer solution was placed in 1 cm fluorescence cuvette. Then fluorescence spectra were repeatedly acquired after addition of microliter aliquots of a concentrated solution that contained biocytin-TMR, avidin or pre-formed biocytin-TMR/avidin complex.

CHAPTER 5 META-LINKED POLY (PHENYLENE ETHYNYLENE) SULFONATE CONTAINING PYRIDINE

Introduction

Many natural molecules self-assemble into different conformations in solution, such as the helical, double-stranded form of DNA. These ordered conformations are stabilized by noncovalent interactions including hydrogen bonding, hydrophobic, and van der Waals forces.¹³⁸ The self-organization of nonbiological macromolecules has been challenged using the noncovalent interactions. Folded structures induced by hydrogen bonds or metal-ligand coordination interactions have been well understood,¹³⁹⁻¹⁴² however, there are a few reports on the solvophobic^{74, 77, 79, 143} or π - π interactions^{144, 145} used to control ordered conformations.

Supramolecular π -stacked assemblies have been observed in phenylene ethynylene architectures bearing a flexible polar group substituted to a rigid, aromatic backbone. Figure 5-1 shows representative examples including hexameric macrocycles, *para*-linked rigid rod segments, and the more conformationally diverse *ortho*- and *meta*-linked oligomers.¹⁴⁶ For example, hexameric macrocycles with appropriate side chains form stacked dimers and higher order aggregates in solution due to π -stacking interactions.¹⁴⁷ The strength of π -stacking interactions has been known to be strongly dependent on solvent polarity.¹⁴⁶ For *meta*-linked oligo(phenylene ethynylene)s with a polar tri(ethylene glycol) ester-linked side chains they self-assemble into a π -stacked helical conformation in polar solvents due to solvophobic interactions.^{75, 146} The conformational transition is monitored by absorption and fluorescence spectroscopy.

Solvent-induced self-assembly of *meta*-linked PPEs into a helical conformation was also reported in our group.⁷⁹ On the basis of solvent effects on the spectroscopic properties, we conclude a *meta*-linked poly(phenylene ethynylene) (PPE)-type CPE adopts a random coil

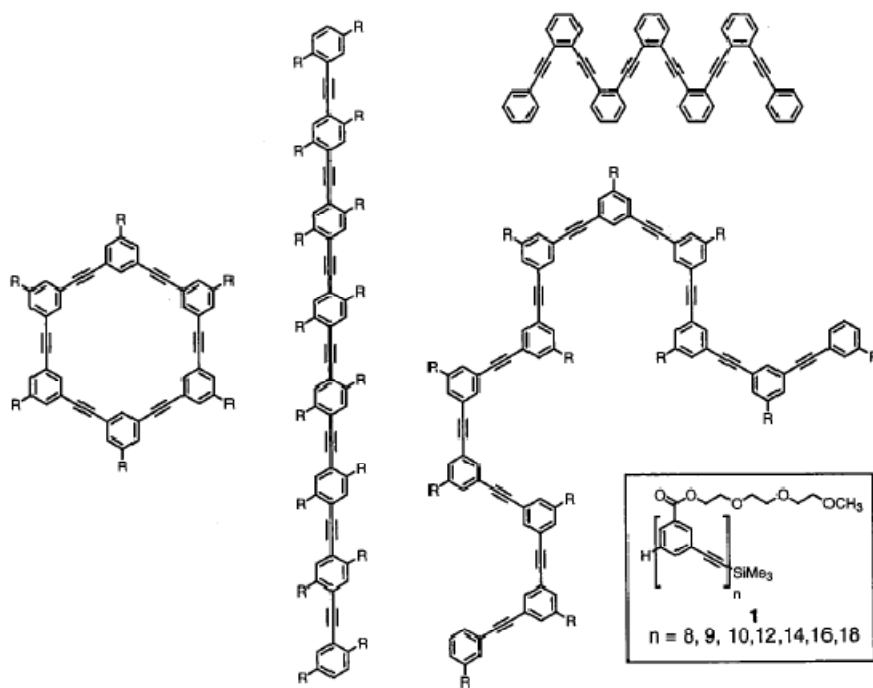


Figure 5-1. Structures of phenylene ethynylene (PE) based macrocycle and oligomers used for π -stacked self-assemblies. Figure was taken from Prest *et.al.*¹⁴⁶

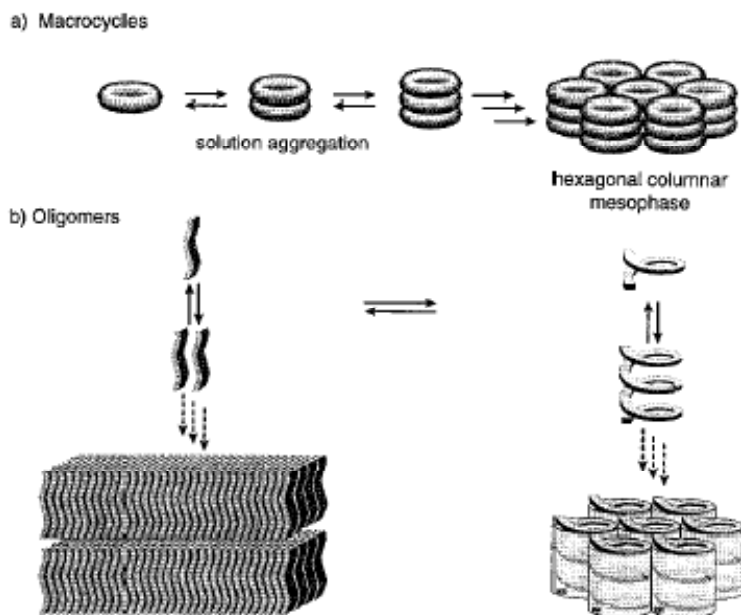


Figure 5-2. Schematic diagram illustrates the self-assembly of disk-shaped phenylene ethynylene macrocycles (a) and oligomers (b). Figure was taken from Prest *et.al.*¹⁴⁶

conformation in methanol and a helical conformation in water. As the amount of water in the mixture of the two solvent system increases, a long wavelength absorption band is red-shifted with a decrease in oscillator strength. A less intense, broad, unstructured and red-shifted emission is also observed in the fluorescence spectrum. These spectral changes are consistent with the spectra obtained by Moore and co-workers for helical conformations. The changes arise due to the π -stacking between phenylene ethynylene rings in the helical conformation. Additionally, fluorescence quenching is more strongly amplified in the helical conformation due to the delocalization of singlet exciton in the helix.

A variety of conjugated polymers have been studied as chemosensory materials for an ions, metal cations and acids. Conjugated polymers with pyridine units in the backbone provide the possibility of tuning their optical properties by electron accepting ability, N-protonation, N-oxidation, N-alkylation, and metal complexation of pyridyl nitrogen. Conjugated polymers containing 2,2'-bipyridyl and terpyridyl ligands (Figure 5-3) display changes in their absorption and fluorescence bands upon addition of metals.^{148, 149} These changes arise due to the electron density changes within the polymer backbone, when the polymers interact with metal ions.

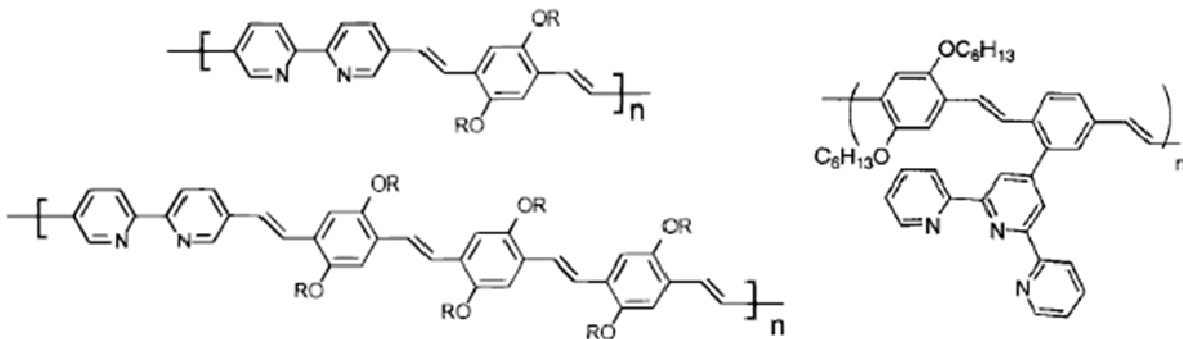


Figure 5-3. Structures of conjugated polymers containing bipyridyl and terpyridyl ligands. Figure was taken from Wang *et. al.* and Kimura *et. al.*^{148, 149}

Incorporation of meta substituents into poly(phenylene ethynylene) polymers backbone improves the solubility and processability of the polymers.¹⁵⁰ This incorporation also can modify the molecular conformation of the polymers from a rigid rod-like conformation into a flexible coil-like conformation. Winter et. al. reported that poly(pyridyl/phenyl ethynylene) polymers showed different rigidity/flexibility depending on the ratio of *para*- to *meta*-pyridine linkages within the polymer backbone (Figure 5-4).¹⁵¹ The polymer containing 100 % *para*-pyridine linkages shows linear conformation. With increasing proportion of *meta*-pyridine linkages, the linearity of the conformation decreased, and hence blue shift of the absorption and the emission maximum was observed.

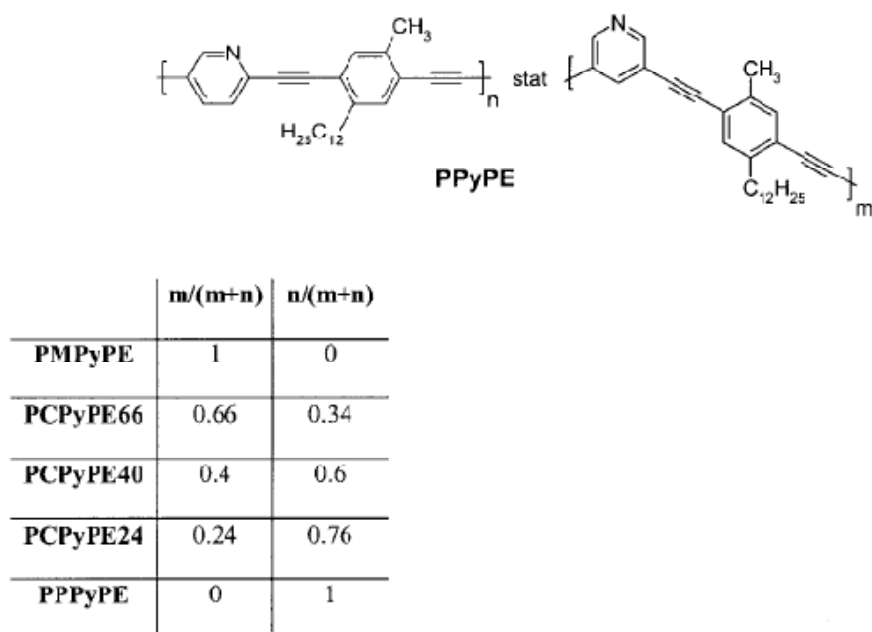


Figure 5-4. Structures of poly(pyridyl/phenyl ethynylene) polymers with varying ratios of *para*-/*meta*-linked constitutional units. Figure was taken from Winter *et.al.*¹⁵¹

In 2004, Huang et. al. designed and synthesized a poly(p-phenylene ethynylene) derivative containing *meta*-substituted monopyridyl groups (Polymer **1** in Figure 5-5).¹⁵² The polymer binds selectively with Pd²⁺ ions over other metal ions and forms interpolymer interaction through the palladium-pyridyl coordination, resulting in fluorescence quenching.

Three years later, Li et.al. reported a *meta*-poly(phenylene ethynylene) containing pyridine units (*m*-PPY) (Figure 5-6)¹⁵³ The polymer undergoes a solvent-induced conformational transition from an extended coil structure to a helical structure. Interestingly, the polymer also shows the conformational change by protonation or complexation with a metal ion (Ag^+).

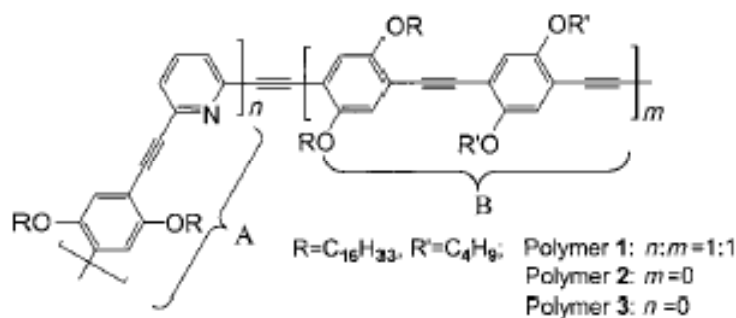


Figure 5-5. Structures of a poly(*p*-phenylene ethynylene) derivative containing *meta*-substituted monopyridyl groups. Figure was taken from Huang *et.al.*¹⁵²

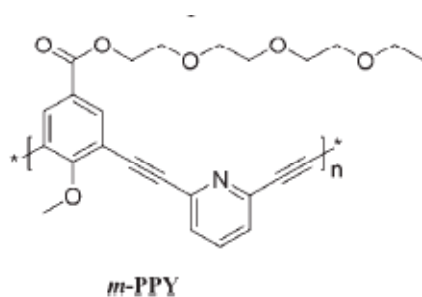


Figure 5-6. Structure of a *meta*-poly(phenylene ethynylene) containing pyridine units (*m*-PPY). Figure was taken from Li et. al.¹⁵³

In this chapter, we synthesized mPPE-SO₃-py, which is a PPE-type CPE containing *meta*-linked pyridine rings in the polymer backbone. The solvent-dependent conformational transition of this polymer was studied by absorption and fluorescence spectroscopy. The incorporation of the *meta*-substituted monopyridyl units can improve the spatial matching for selective binding. The polymer shows a great affinity for the Pd^{2+} ion. The conformational change was also observed upon protonation and metal complexation of the pyridine rings on the polymer backbone.

Results and Discussion

Synthesis

The synthesis of mPPE-SO₃-py containing pyridyl units in the polymer backbone was carried out with 2,6-pyridyldiacetylene (**1**) and sodium 3-(3,5-diiodophenoxy)propane-1-sulfonate (**2**) under Sonogashira coupling conditions (Figure 5-7). The structure of the polymer was characterized by using ¹H NMR and ¹³C NMR in DMSO-d₆.

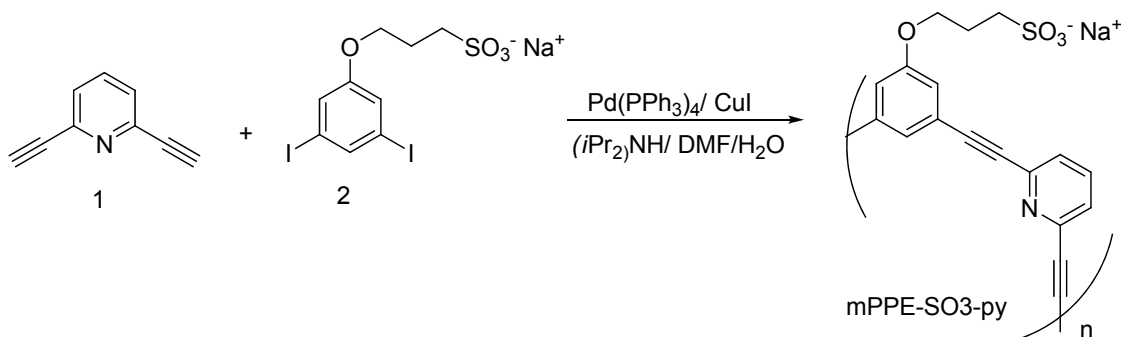


Figure 5-7. Synthesis of mPPE-SO₃-py.

Photophysical Characterization

Previously, the water-methanol solvent system was used for the investigation of CPE folding behavior.^{36, 79} The same solvent system was used to investigate solvent-induced helical folding of mPPE-SO₃-py. Table 5-1 summarizes the photophysical properties of the polymer. The absorption spectrum of mPPE-SO₃-py exhibits two featured absorption bands at 387 nm and 306 nm in methanol (Figure 5-8). With an increasing amount of water in the methanol-water solvent mixture, the oscillator strength decreases. And a more pronounced decrease is observed in the long wavelength band. Thus, the ratio of oscillator strength for 387 nm and 306 nm is smaller in water than that in methanol. Additionally, the long wavelength band is red-shifted from 387 nm to 396 nm. These spectral changes support that the polymer undergoes a random-coil to a helix. The reduced oscillator strength and red-shifted bands (hypochromic effect) is believed to arise due to π -stacking interactions in the helix conformation.

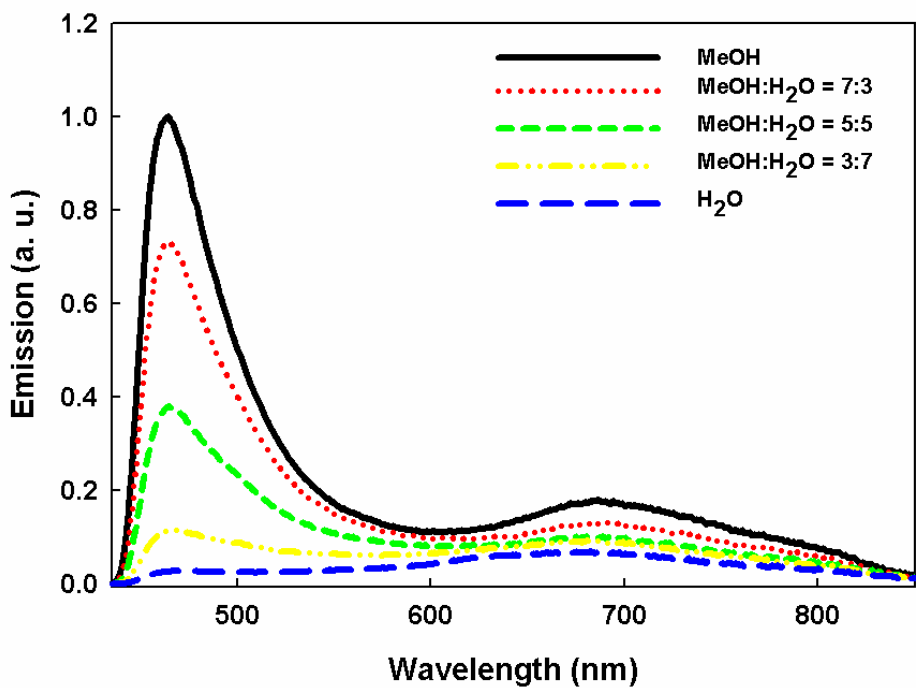
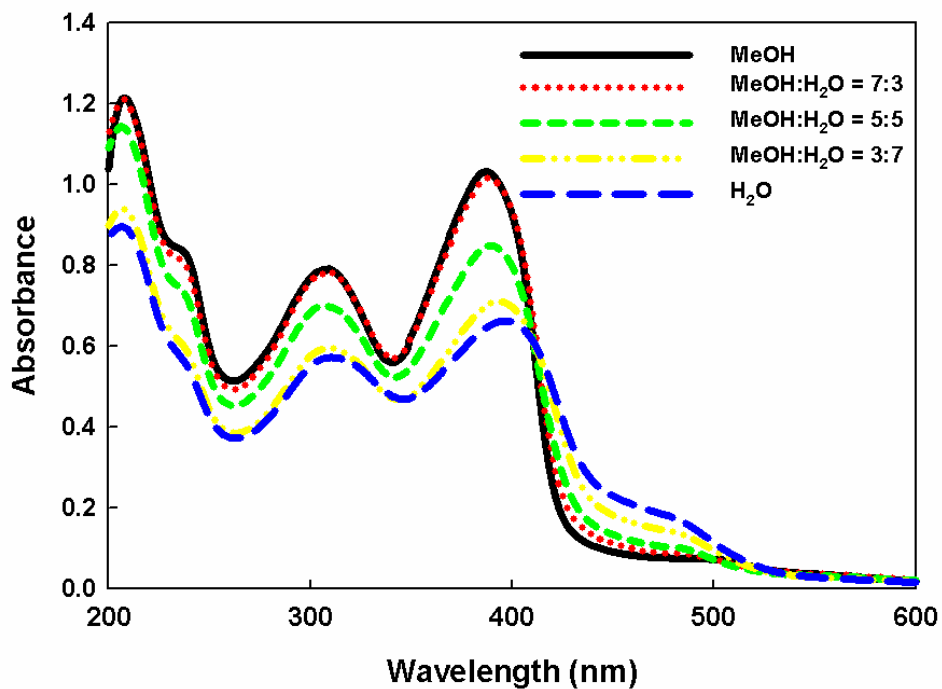


Figure 5-8. Normalized absorption and emission spectra of mPPE-SO₃-py (15 μM) in water, methanol and mixture of the two solvents. $\lambda_{\text{ex}} = 390$ nm.

Table 5-1. Photophysical properties of mPPE-SO3-py

	$\lambda_{\max}^{\text{abs}}/\text{nm}$	$\lambda_{\max}^{\text{fl}}/\text{nm}^{\text{b}}$	Φ_{fl}
MeOH	306, 387	464, 680	$0.015 \pm 0.001^{\text{a}}$
H ₂ O	310, 396	680	$0.003 \pm 0.0003^{\text{a}}$

^a Coumarine 30 in MeOH as standard, $\Phi_{\text{fl}} = 0.307$ (ref.154).

The solvent-induced conformational change of the polymer is also supported by the changes in the polymer fluorescence spectrum (Figure 5-8). In methanol the polymer fluorescence ($\Phi_{\text{fl}} = 0.015$) is characterized by a structured band centered at 464 nm with a weak and very broad “excimer like” emission band around 680 nm. The fact that the structured emission dominates in methanol solution suggests that the polymer exists mainly in a random coil; however, the broad excimer like emission indicates that a fraction of the polymer exists in a helical conformation even in pure methanol solution.⁸⁰ Interestingly, as the amount of water increases in the methanol-water solvent mixture, the intensity of structured emission is significantly reduced. In water, the structured emission is completely quenched and the broad emission is dominant ($\Phi_{\text{fl}} = 0.003$). This is consistent with the changes in the absorption spectrum. These spectral results suggest that the polymer predominantly exists in a random coil conformation in methanol whereas the polymer is mostly folded into a helical conformation in water.

Fluorescence Quenching of mPPE-SO3-py by Metal ions in water

The absorption and fluorescence spectra already showed that mPPE-SO3-py folded into a helix by π -stacking interactions in water. In this helix, nitrogen atoms of the pyridine rings are located inside the pore, whereas negatively charged side chains extend outside. Due to the good complexation ability of pyridine nitrogen atoms inside the pore of the polymer helix, the significant response of mPPE-SO3-py to various metal ions was expected. To investigate the

interaction of the polymer with metal ions, aliquots of solutions of metal ions were added to the polymer solution in water and then changes in the polymer fluorescence intensity were observed. As seen in Figure 5-9, addition of Pd^{2+} metal ions to the polymer results in strong fluorescence quenching with an excellent selectivity for Pd^{2+} over other metal ions. This quenching is believed to arise due to a photo-induced electron transfer (PET) process or energy transfer (ET) process.¹⁵⁵ Cu^{2+} , Fe^{3+} and Cr^{3+} slightly quench the polymer fluorescence compared to Pd^{2+} whereas Ni^{+} and Li^{+} does not show any quenching ability. Additionally, Ag^{+} , Ca^{2+} , Cd^{2+} , Zn^{2+} , K^{+} and Mg^{2+} relatively enhanced fluorescence intensity compared with the fluorescence intensity of the polymer in the absence of metal ions. Figure 5-10 shows the ratio of fluorescence intensities for the absence (I_0) and presence of 20 μM of metal ions (I).

Protonation and Metal Complexation with Pd^{2+}

As shown in Figure 5-11, protonation does not lead to any effect on the absorption and fluorescence spectrum of the polymer solution in water. The helical structured polymer shows stability to introduction of HCl solution. However, mPPE-SO₃-py in methanol undergoes a significant reduction of oscillator strength in the long wavelength band. Thus, the ratio of oscillator strengths for the 387 nm and 307 nm is smaller with an increasing concentration of HCl solution. Additionally, with an increasing concentration of HCl solution the polymer emission intensity decreases with appearance of the excimer like emission, which is typical of π -stacked aromatic residues.¹⁵⁶ These spectral observations suggest the conformation transition of the polymer from a random-coil conformation to a helix structure in methanol by addition of HCl solution.

The hypothesis of conformational transition is further supported by the response of mPPE-SO₃-py to Pd^{2+} ions in methanol. Since a monopyridyl group has been known to exhibit a strong affinity for Pd^{2+} ions and selectively bind by self-assembly,¹⁵² titration experiments of Pd^{2+}

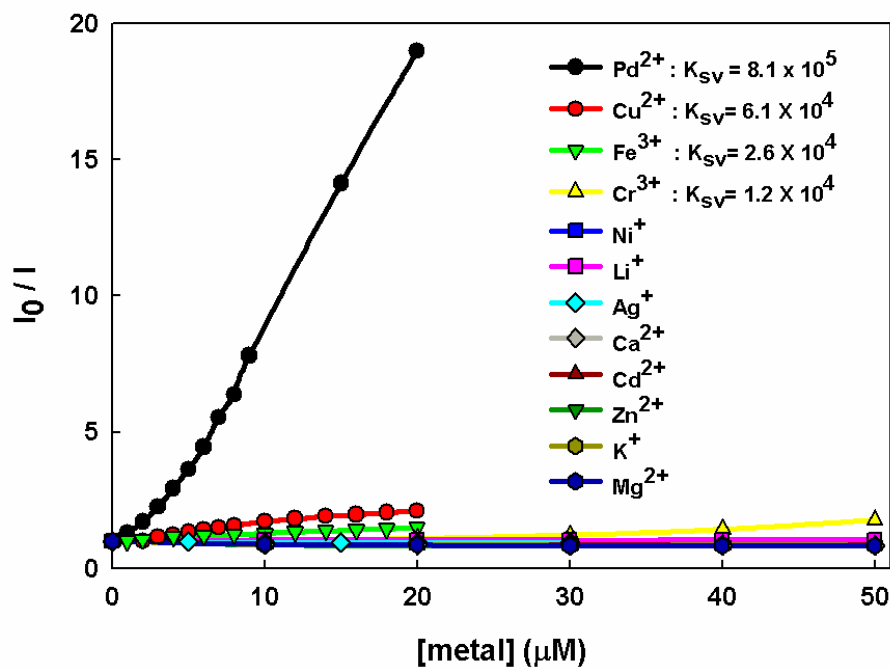


Figure 5-9. Stern-Volmer plots for mPPE-SO₃-py fluorescence quenching by metal ions in water. $\lambda_{\text{ex}} = 400 \text{ nm}$ and $\lambda_{\text{em}} = 680 \text{ nm}$.

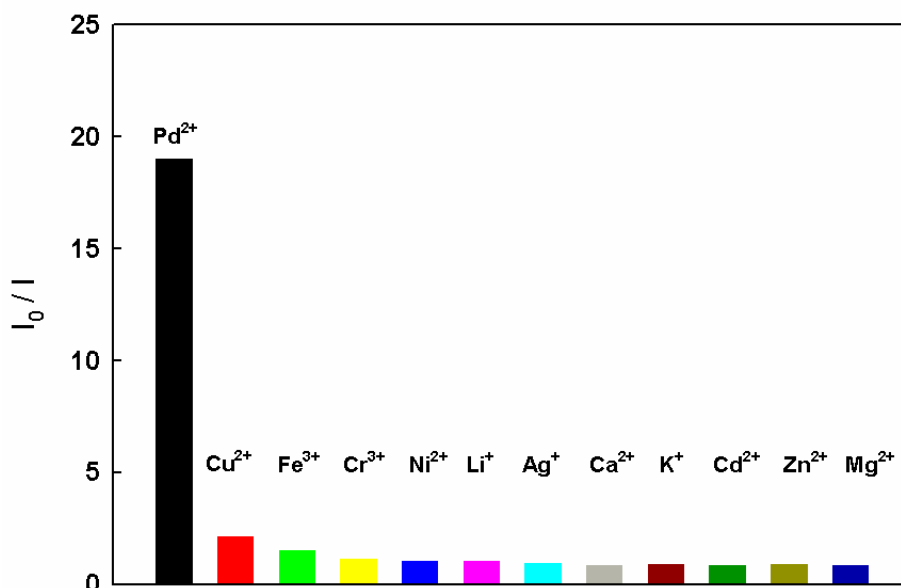


Figure 5-10. Fluorescence responses of mPPE-SO₃-py to metal ions (20 μM) in water. I_0 and I represent the fluorescence intensity in the absence and presence of a metal ion. $\lambda_{\text{ex}} = 400 \text{ nm}$ and $\lambda_{\text{em}} = 680 \text{ nm}$.

ions to the polymer were conducted in methanol. Introduction of Pd^{2+} ions to the polymer induces the spectral changes of the polymer (Figure 5-12 (c) and (d)). The absorption spectrum shows reduced oscillator strengths with red-shift of the absorption maximum from 387 nm to 414 nm (hypochromic effect). mPPE-SO₃-py also exhibits an isosbestic point in the absorption spectra upon metal complexation, indicating the coexistence of two kinds of conformations. The emission maximum at 458 nm is progressively quenched and very broad emission at 680 nm is dominant. These spectral changes are similar to those observed for the polymer when the amount

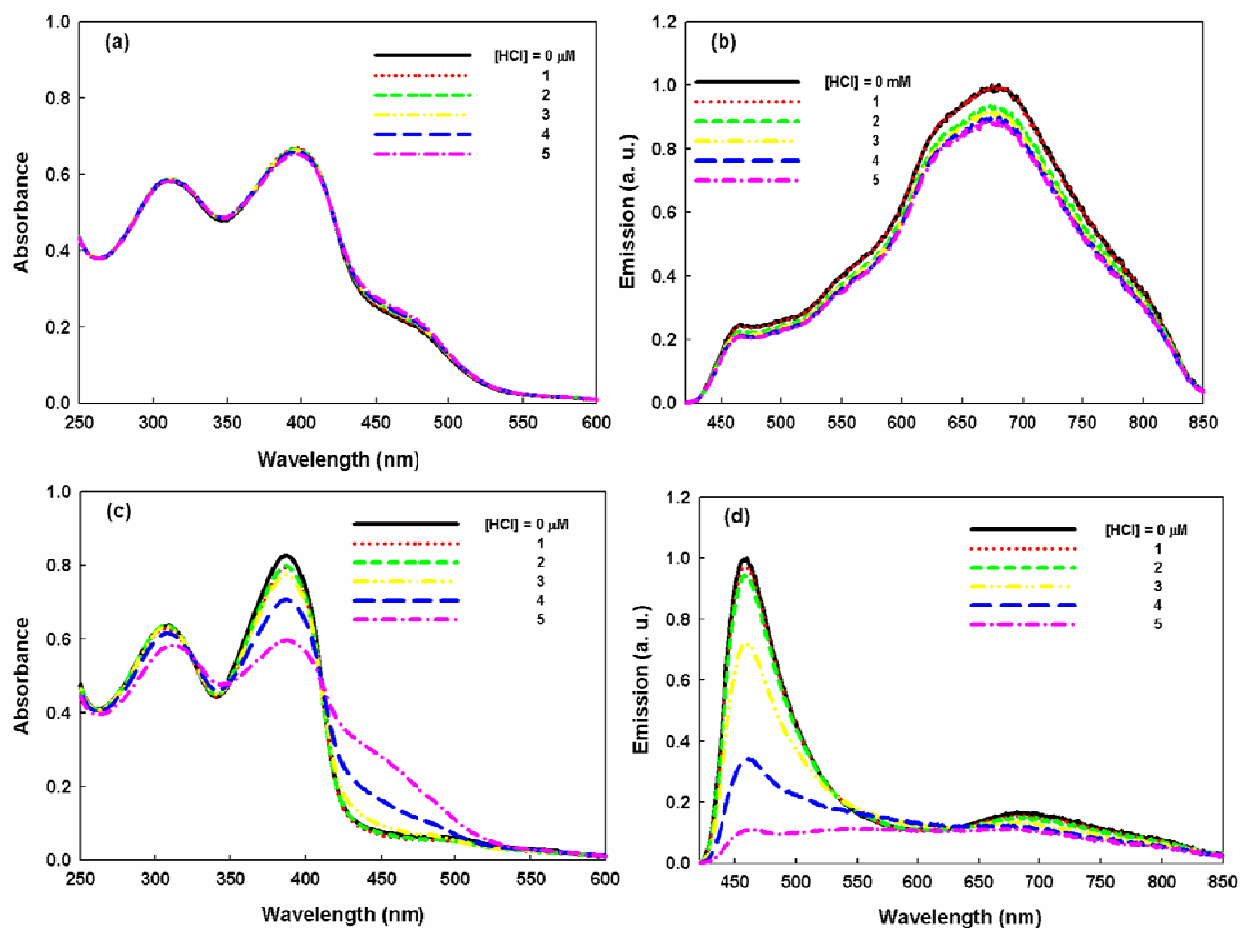


Figure 5-11. Absorption and emission spectra of mPPE-SO₃-py (15 μM) (a and b) in water and (c and d) in methanol with addition of HCl solution. $\lambda_{\text{ex}} = 400$ nm in water and $\lambda_{\text{ex}} = 410$ nm in methanol.

of water increases in the methanol-water solvent mixture. These results suggest that suggest that the complexation of mPPE-SO₃-py with Pd²⁺ induces the helical conformation of the polymer even in methanol because the metal complex favors aromatic π - π face-to-face interactions.¹⁵⁷ After addition of Pd²⁺ to the polymer solution in water, similar changes in the absorption spectrum were observed (Figure 5-10 (a)) with those in methanol, suggesting that metal complex enforces π -stacking interactions and stabilizes the helical conformation in water.

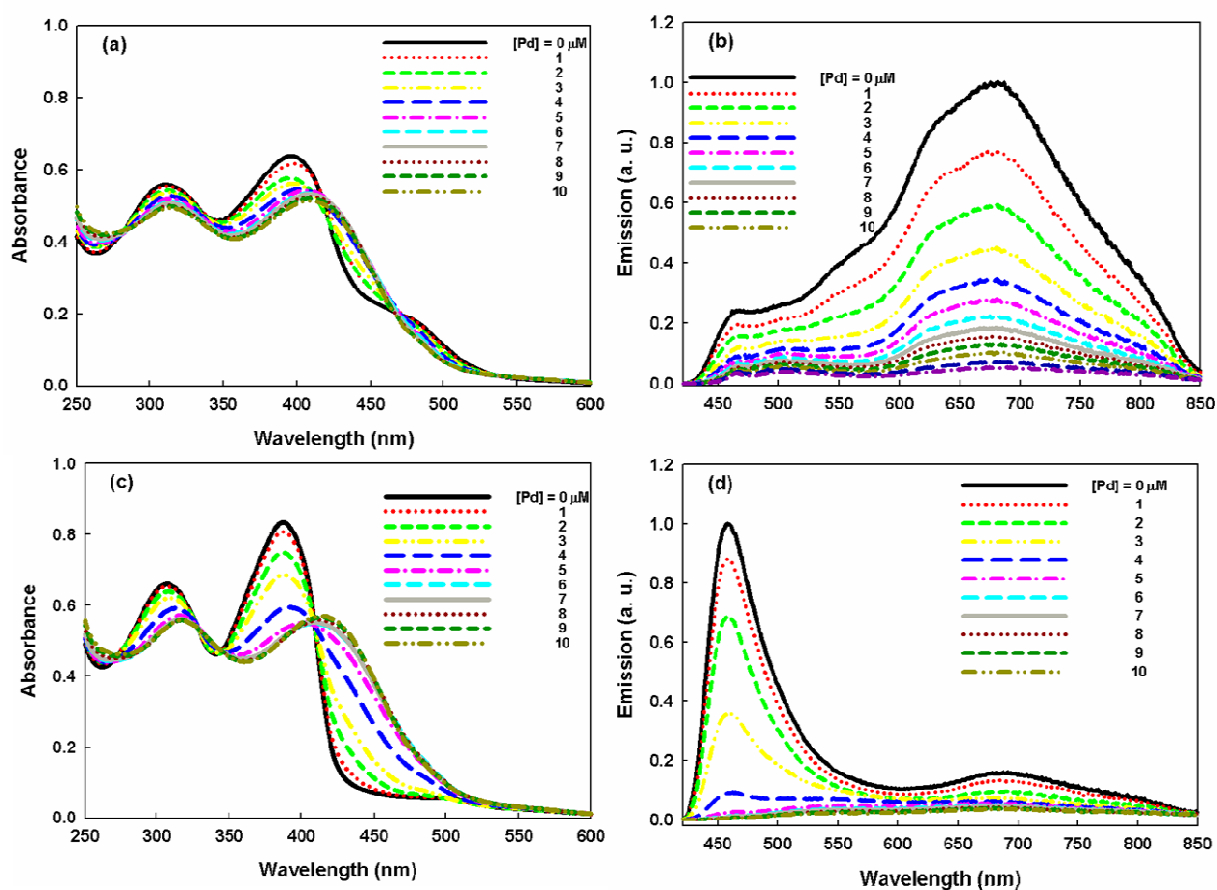


Figure 5-12. Absorption and emission spectra of mPPE-SO₃-py (15 μM) (a and b) in water and (c and d) in methanol with addition of Pd²⁺. $\lambda_{\text{ex}} = 400$ nm in water and $\lambda_{\text{ex}} = 408$ nm in methanol.

Experimental

Materials

2,6-Pyridyldiacetylene (**1**)¹⁵⁸ and sodium 3-(3,5-diiodophenoxy)propane-1-sulfonate (**2**)⁷⁹ were synthesized according to previously described procedures. Pd(PPh₃)₄ was purchased from Strem Chemical Company and used as received. The solutions of metal ions were prepared from their chloride salts, except for AgNO₃, ZnBr₂ and NiBr₂. Except PdCl₂, all metal sample solutions were prepared by using water that was distilled and then purified by a Millipore purification system (Millipore Simplicity Ultrapure Water System). A stock solution of PdCl₂ was prepared in methanol. The polymer stock solution was diluted with water or methanol to a final concentration of 15 μM. All concentrations of polymers are provided in polymer repeat unit (PRU) concentration.

Instrumentation

NMR spectra were recorded on either a Varian VXR 300 or Mercury-300 spectrometer and chemical shifts are reported in ppm relative to TMS. Absorption spectra were obtained on a Varian-Cary 100 UV-visible absorption dual beam spectrophotometer, with a scan rate of 300 nm/min. Steady state fluorescence spectra were recorded on a spectrofluorometer from Photon Technology International and corrected by using correction factors generated with a primary standard lamp.

General Methods

Titration experiments were carried out in a fluorescence cuvette. In a typical titration experiment, 3 mL of a polymer solution was placed in a 1 cm quartz fluorescence cuvette with a small magnetic stir bar. The UV-visible absorption and fluorescence spectra were recorded at room temperature. Then fluorescence and/or absorption spectra were repeatedly acquired subsequent to the addition of microliter aliquots of a concentrated solution containing the

quencher. The polymer is soluble in water and insoluble in methanol. For measurements in methanol, stock solution of the polymer is diluted with methanol to a final concentration of 15 μM .

Synthetic Procedures

mPPE-SO₃-py. A solution of 2,6-pyridyldiacetylene (**1**) (26 mg, 0.2 mmol) and sodium 3-(3,5-diiodophenoxy)propane-1-sulfonate (**2**) (98 mg, 0.2 mmol) in 7 mL of DMF/H₂O/*i*Pr₂NH (v/v/v = 5/1/1) was placed inside a Schlenk flask. The resulting solution was degassed with argon for 15 minutes. Then Pd(PPh₃)₄ (7 mg, 6 μmol) and CuI (1 mg, 6 μmol) powder were added under the protection of argon. The solution was degassed with argon for 15 minutes and then stirred at 60°C for 24 hours. The reaction mixture was poured into the 200 mL of acetone. The precipitated polymer was dissolved in an aqueous solution containing NaCN and the resulting solution was filtered through a 25 μm glass filter followed by dialysis against deionized water using 6-8 kD MWCO cellulose membrane for 2 days. The polymer solution was lyophilized to yield a brown solid (36 mg, 50%). ¹H NMR (300 MHz, DMSO-d₆) δ 2.09 (broad, 2H), 2.71 (broad, 2H), 4.20 (broad, 2H), 7.82-7.89 (broad, 6H). ¹³C NMR (75 MHz, DMSO-d₆) δ 25.30, 48.15, 68.23, 85.79, 93.95, 112.99, 117.32, 122.46, 127.28, 137.89, 142.92, 153.47.

CHAPTER 6
POLY (PHENYLENE ETHYNYLENE) WITH TETRA ALKYLAMMONIUM SIDE GROUPS
FOR LIGHT-INDUCED BIOCIDAL ACTIVITY

Introduction

Antimicrobials have gained interest in various areas, such as medical devices, healthcare products, water purification systems, hospital, dental office equipment, food packaging, food storage, household sanitation, etc.^{159, 160} because contamination by microorganisms such as bacteria is a great concern in those areas. Antimicrobials are materials capable of killing pathogenic microorganisms.¹⁶¹ Conventionally, such antimicrobial materials have been usually prepared by incorporation of leachable antiseptic into a polymeric surface matrix. Antimicrobials are gradually released and kill the microorganism by diffusing into and disrupting the cell.¹⁶² Typical leaching microbial materials contain antibiotics, halogens or heavy metals like silver or mercury. However, these conventional antimicrobial reagents have the limitation of residual toxicity since they are liquids or gases of low molecular weight. Antimicrobial reagents of low molecular weight also suffer from short-term antimicrobial activity as the leachable components eventually become exhausted. Furthermore, the gradually decreasing level of the released compound leads to subinhibitory concentration of antimicrobials in the surrounding, which provides conditions for resistance development of bacteria.

To overcome these disadvantages of conventional antimicrobials, polymeric materials with antimicrobial activities have been suggested as an alternative. Previous studies have shown that cationic polymers with pendant cationic groups, especially quaternary ammonium salts possess effective antimicrobial activity.¹⁶³⁻¹⁶⁶ Tilter et al. have found that immobilized cationic groups on the surface of glass or SiO₂-coated plastic kill bacteria on contact.^{167, 168} The biocidal polymers are covalently immobilized onto the surface of substrates, which prevents uncontrolled material release to the environment and enables them to be reused after cleaning.^{163, 165, 169, 170}

The antibacterial ability of the cationic polymers has been attributed to penetration of cationic groups into bacteria membrane resulting in the cell damage and death. The following sequential steps have been proposed for this mechanism: (1) adsorption of cationic groups onto negatively charged cell surfaces; (2) penetration into the cell wall; (3) binding to the cytoplasmic membrane; (4) disruption of the cytoplasmic membrane; (5) release of K^+ ions and constituents of the cytoplasmic membrane; and (6) death of the cell.^{163, 171, 172}

Increasing bacteria resistance to antibiotics requires the development of new antibacterial strategies. Photodynamic killing of bacteria is one of new promising strategies. It utilizes light with a photosensitizer to induce a phototoxic reaction, which is identical to the use of photodynamic therapy for skin.¹⁷³⁻¹⁷⁵ A large number of compounds with photodynamic activity such as phenothiazines, phthalocyanines and phophyrins have been used as light induced biocides against Gram-positive and Gram-negative bacteria.¹⁷⁶⁻¹⁷⁹ Light absorption by a photosensitizer initiates photosensitization mechanism. Absorbed light excites a photosensitizer to an excited state and the excited photosensitizer undergoes an intersystem cross-over to the excited state. From the excited stated photosensitizer either charge (type I reaction) or energy (type II reaction) is transferred to substrate or molecular oxygen to generate reactive oxygen species (Figure 6-1). In photodynamic actions, singlet oxygen (1O_2) is considered to play a crucial role via type II reaction since this reactive form of oxygen initiates further oxidative reaction of its surroundings such as cell wall, lipid membranes, enzymes or nucleic acids.¹⁸⁰⁻¹⁸⁴ Therefore, photodynamic inactivation of bacteria is based on the concept that a photosensitizer can accumulate in significant amount in or at the cytoplasmic membrane, which is the critical target to induce an irreversible damage in bacteria after irradiation.¹⁷⁶

Lu et. al. previously showed that a cationic conjugated polyelectrolyte (CPE) with

quaternary ammonium groups (PPE-NMe₃-OR8) exhibited light-activated biocidal activity against Gram-negative bacteria such as *Escherichia coli* (*E. coli*) and Gram-positive bacterial spores such as *Bacillus anthracis* (*B. anthracis*).⁸⁹ These studies were carried out with an aqueous solution of the polymer and microsphere-coated suspension of the polymer. Due to limited water solubility of CPEs, they spontaneously coat oppositely charged surfaces close to monolayer coverage.^{22, 185, 186} The coating is irreversible, robust and stable both in the presence and absence of interfacial water. As seen in phase contrast and fluorescent microscope images (Figure 6-2), PPE-NMe₃-OR8 is taken by both bacteria and the polymer coated on the bacteria or spores shows strong fluorescence. The polymer coated on the bacteria effectively kills bacteria upon irradiation with white light. In contrast to under white light, there is little or no biocidal activity under yellow light.

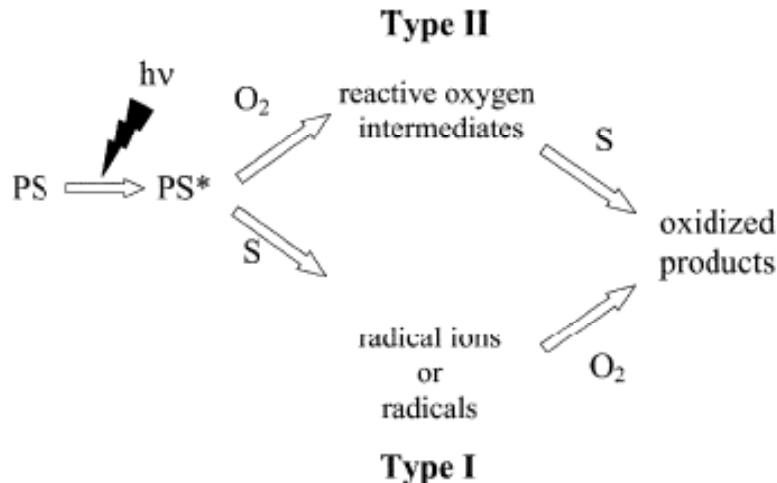
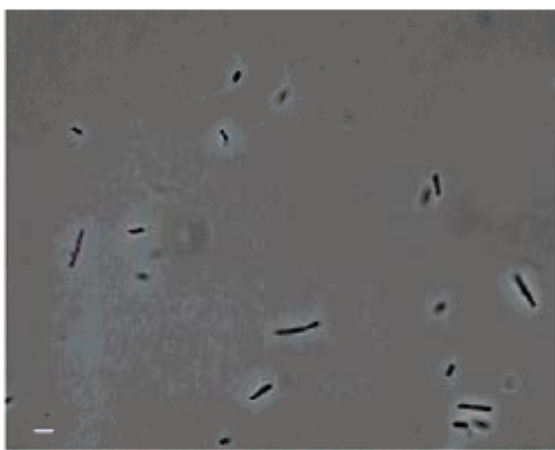
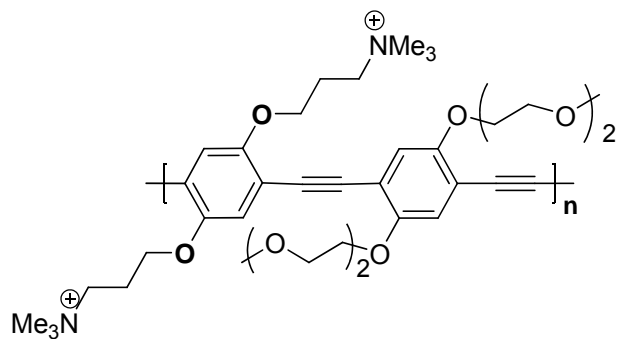
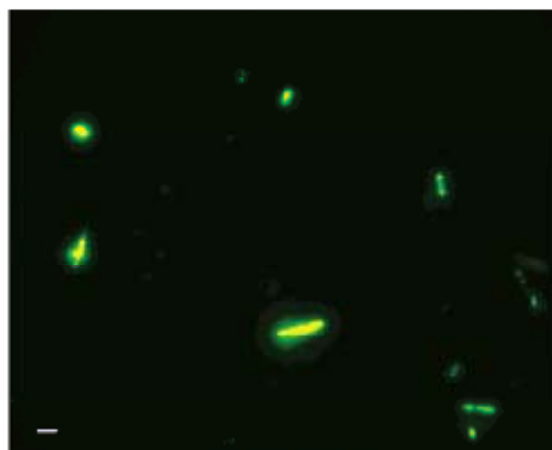


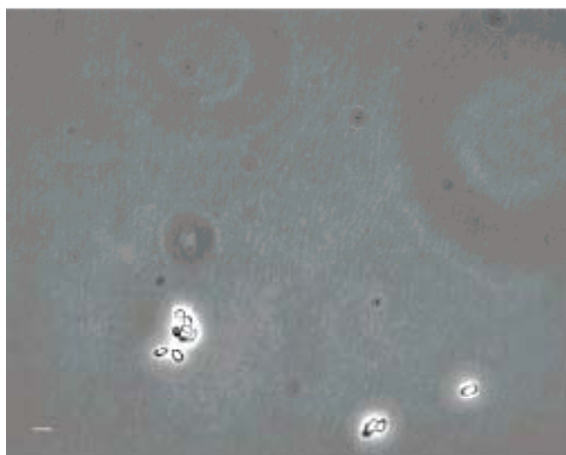
Figure 6-1. Pathway of type I and Type II reaction of light absorbing photosensitizer. After light activating of the ground state of photosensitizer (PS), activated form of PS* can follow two alternative pathways *via* reactive singlet oxygen (¹O₂), hydrogen peroxide, hydroxyl radical (type II) or organic substrate (S) (type I). The intermediates react rapidly with their surroundings: cell wall, cell membrane, peptides and nucleic acids. Figure was taken from Maisch *et al.*¹⁸⁷



Phase Contrast



Fluorescence



Phase Contrast



Fluorescence

Figure 6-2. Structure of PPE-NMe₃-OR8 and phase contrast and fluorescent microscope images of polymer-treated *E. coli* (upper panel) and polymer-treated *B. anthracis* Sterne spores (lower panel). Figure was taken from Lu *et al.*⁸⁹

In this chapter, we designed and synthesized a series of cationic CPEs with backbones based on a poly(phenylene ethynylene) repeat unit and tetraalkylammonium side groups. The biocidal activity of the CPEs and surface grafted conjugated polymer (SGCP) beads with the same repeat unit as PPE-NMe₃-OR11¹⁸⁸ was examined. The biocidal effects of the CPEs were tested against two Gram negative bacteria: *Cobetia marina*, a marine bacterium and *Pseudomonas aeruginosa* strain PA01, a model pathogen. Such biocidal activity is correlated with the photophysical properties of the cationic polymers. Therefore, the photophysical properties of the polymer were studied in solution. We investigated the role of oxygen in the light induced bacterial killing and proposed a mechanism in the biocidal action of the CPEs. The structures of CPEs used for this study are given in Figure 6-3.

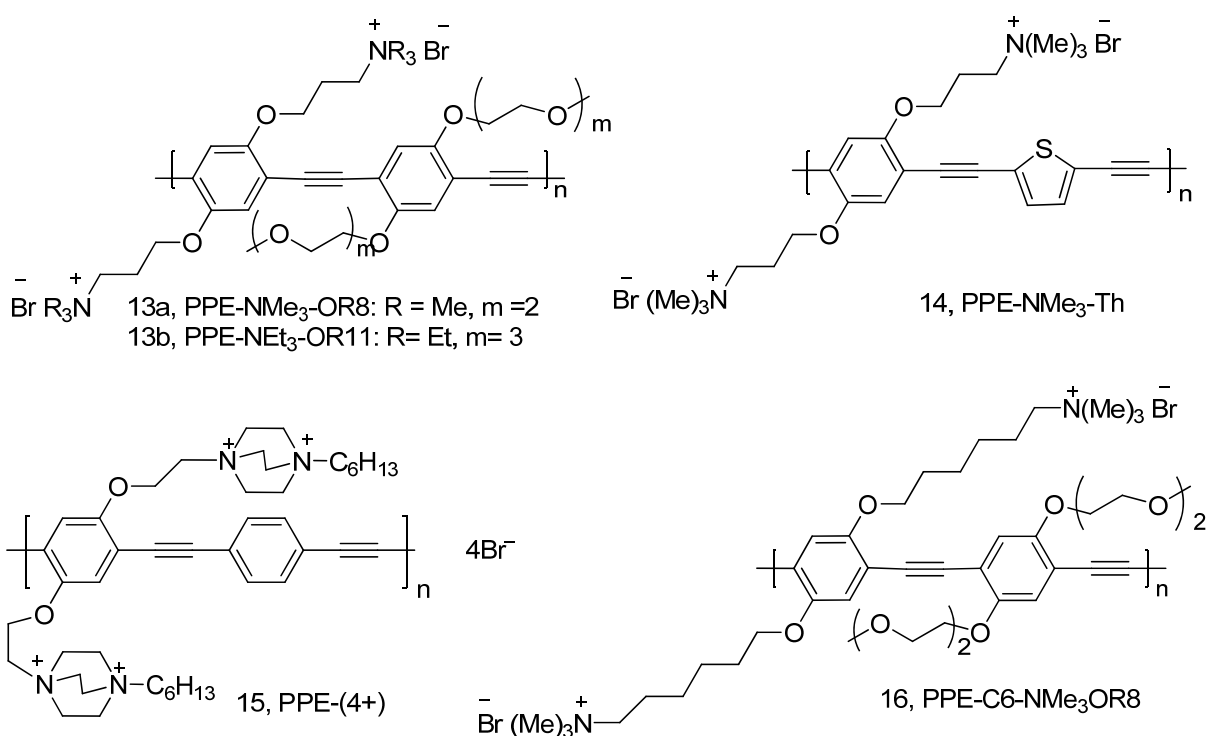


Figure 6-3. Structures and acronyms of cationic conjugated polyelectrolytes investigated in this study.

Results and Discussion

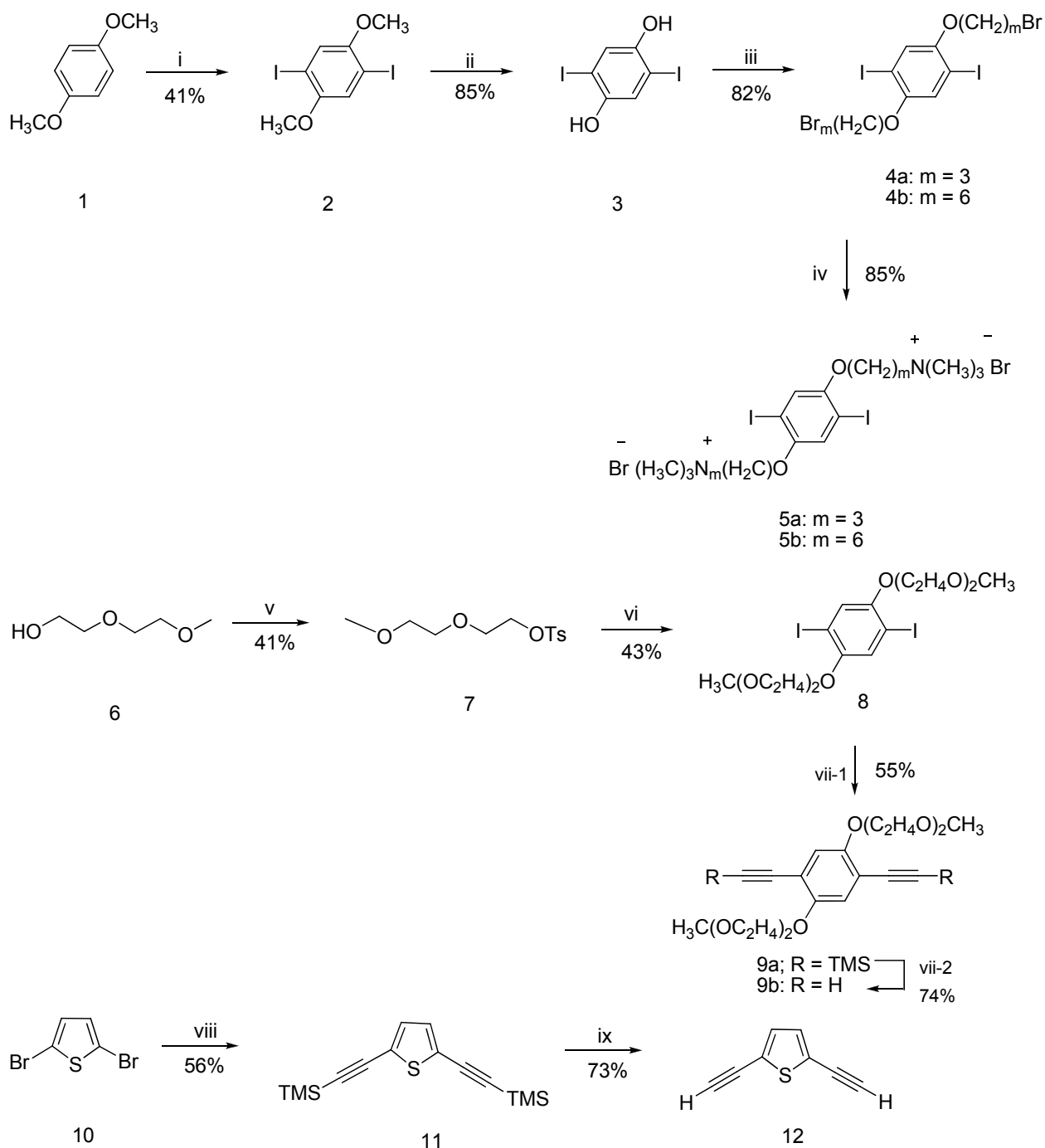
Synthesis

Figure 6-4 illustrates synthesis of the monomers used to synthesize the polymers. 2,5-Diiodohydroquinone **3** was synthesized according to the literature procedure.³⁰ Compounds **4a** and **4b** were obtained by deprotonation of 2,5-diiodohydroquinone **3** with K_2CO_3 and subsequent alkylation with 1,3-dibromopropane and 1,6-dibromohexane, respectively. Subsequently, pendant groups were quaternized with trimethylamine (25 wt. % in water) in a mixture of H_2O /ethanol/ acetone (v/v/v/ =2/3/3) to give the desired cationic monomer **5a** and **5b** in 85% yield. Phenylenediacetylene **9** was made by Sonogashira coupling of trimethylsilylacetylene (TMSA) with compound **8**. The silyl protecting groups were next removed with TBAF. The synthesis of 2,5-diethynylthiophene **12** was accomplished by using procedures analogous to those described for the phenyl derivatives.¹⁸⁹ The reaction of 2,5-dibromothiophene with TMSA resulted in the formation of compound **11** in 56% yield. Deprotection of the two silyl protecting groups was accomplished by treatment of with dilute KOH in degassed methanol. 2,5-Diethynylthiophene **12** was isolated as yellow oil in 73% yield after extraction with pentane. Compound **12** was immediately used for polymerization because it was unstable in air or light. As shown in Figure 6-5, the polymers studied in this chapter were synthesized by polycondensation between bifunctional monomers under Sonogashira coupling conditions. PPE4⁺¹¹⁶ and PPE-NEt₃-OR11¹⁸⁸ were prepared according to literature procedures.

Polymer Characterization

¹H NMR and pulse gradient echo (PSGE) NMR

All polymers were dried by lyophilization technique. They are soluble in water, methanol and DMSO. The structures of all polymers were confirmed by ¹H NMR. Due to their limited solubility, only partial ¹³C NMR was obtained at 54.606 ppm (ammonium methyl groups). The



i. KIO_3 , I_2 , H_2SO_4 , CH_3CO_2H , heat; ii. BBr_3 , CH_2Cl_2 , $-78^\circ C$ $0^\circ C$; iii. $Br(CH_2)_3Br$ or $Br(CH_2)_6Br$, K_2CO_3 , acetone, heat; iv. 25% $N(CH_3)_3$, H_2O , C_2H_5OH , CH_3COCH_3 , heat; v. **3**, K_2CO_3 , KI , $CH_3COC_2H_5$, heat; vi. 1) Trimethylsilylacetylene, $Pd(PPh_3)_4$, CuI , Toluene, $(iPr)_2NH$; 2) TBAF, CH_3OH , RT; viii. Trimethylsilylacetylene, $Pd(PPh_3)_4$, CuI , $(iPr)_2NH$, $0^\circ C$ $75^\circ C$; ix. KOH , CH_3OH , RT

Figure 6-4. General synthetic scheme for monomer 5, 9 and 12.

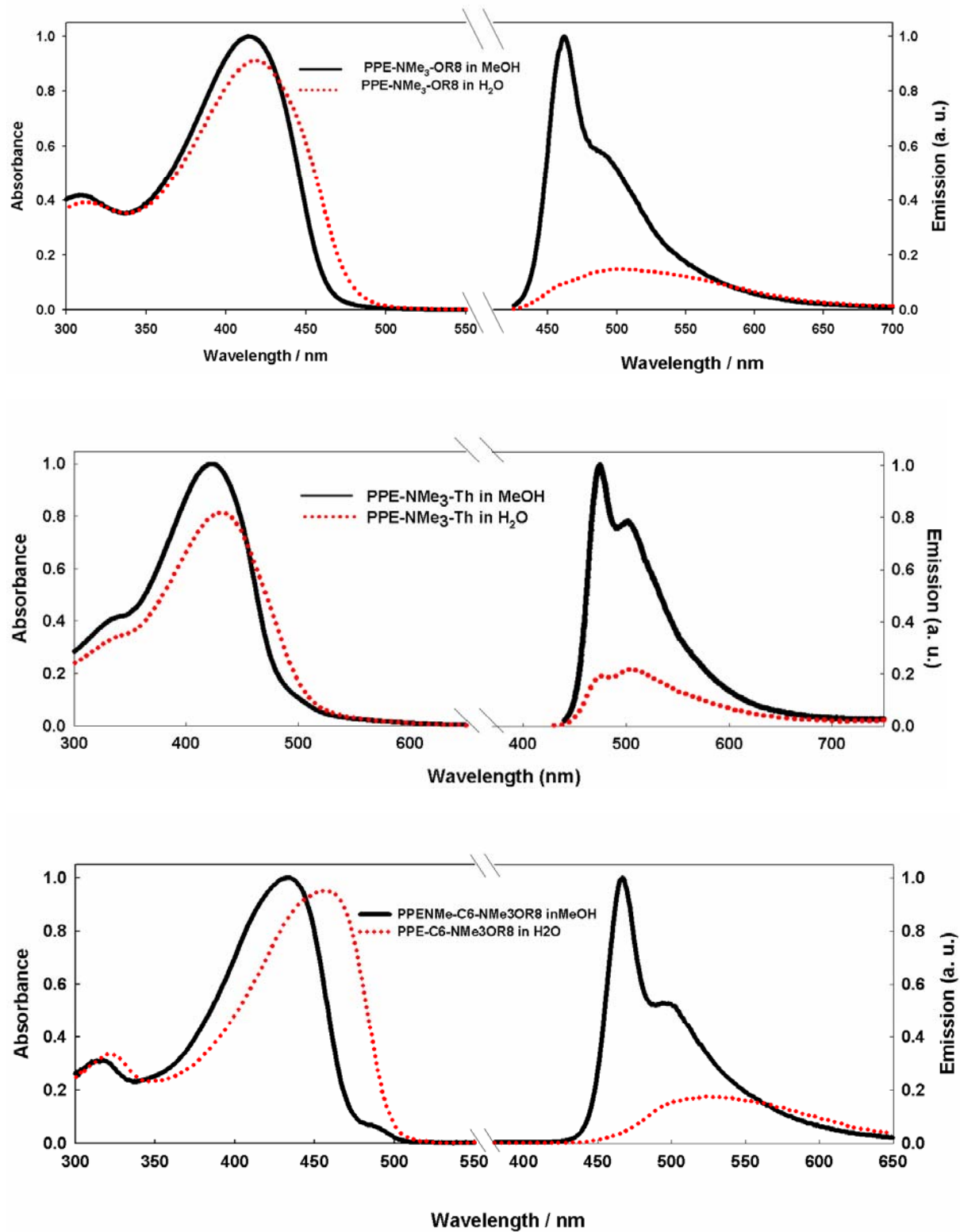


Figure 6-6. Absorption and emission spectra of CPEs in methanol and water. The spectra are normalized according to extinction coefficients (absorption) and relative quantum yield efficiency (emission).

red- shifted to $\lambda_{\text{max}} = 500$ nm and the relative fluorescence quantum efficiency is lower. The solvent-dependent fluorescence behavior is attributed to aggregation of the polymer chains in water and consequent domination of the fluorescence by interchain excitons (analogous to excimer).¹⁸⁸

PPE-NMe₃-Th. As seen in Figure 6-6, a methanol solution of the polymer exhibits a broad absorption band with λ_{max} at 422 nm. In water, the absorption maximum red-shifts to 432 nm and also the absorption extinction coefficient decreases. The emission properties are more dependent on the nature of the solvent. In methanol, the polymer exhibits a narrow emission band at $\lambda_{\text{max}} = 475$ nm with a vibronic band at $\lambda_{\text{max}} = 502$ nm. In aqueous solution, the emission band becomes broader and the quantum efficiency ($\Phi_{\text{fl}} = 0.016$) is lower than that in methanol ($\Phi_{\text{fl}} = 0.045$). Interestingly, the emission maximum is at the same position as in methanol (475 nm) with a shoulder at 502 nm. Such behavior is different from other PPE-based CPEs, which exhibit a large red-shift of emission band in a poor solvent. The lack of a spectral shift for PPE-NMe₃-Th likely is due to the fact that the aggregated state of the polymer has a much lower quantum yield, and therefore its contribution to the total emission spectrum is small.

PPE4+. The photophysical properties of PPE4+ were previously studied and reported in the literature.¹¹⁶

PPE-C6-NMe₃-OR8. As shown in absorption spectrum of other cationic CPEs, the absorption maximum band of PPE-C6-NMe₃-OR8 undergoes a very clear red-shift from 432 nm to 450 nm in water. In methanol the fluorescence is strong and it features a structured band at $\lambda_{\text{max}} = 467$ nm with a shoulder at 500 nm. In water, the quantum efficiency of the polymer decreases and a new red-shifted and broad band appears at 505 nm.

Transient absorption spectroscopy

Molecular oxygen has the relatively small energy difference (94.2 kJ/ mol) between its ground state ($^3\Sigma_g^-$) and excited state ($^1\Delta_g$), and thus singlet oxygen ($^1O_2 (^1\Delta_g)$) can be produced by energy transfer from the lowest triplet state of sensitizers (CPEs) to molecular oxygen. Since the triplet state of CPEs plays an important role in singlet-oxygen generation, transient absorption spectroscopy was utilized to investigate the triplet states of the non-phosphorescent cationic CPEs **13-16**. Direct excitation of PPE-based conjugated polymers produces a triplet state (triplet exciton) with a moderate efficiency.¹⁹³⁻¹⁹⁵ The triplet state is typically detected by its characteristic long-lived transient absorption in the red of the visible region. As shown in Figure 6-7, the triplet states of cationic CPEs **13-16** were confirmed by a broad, intense transient absorption band centered at $\lambda_{\text{max}} \sim 760$ nm which is quite similar to other PPE-based CPEs. A lower lifetime of the transient absorption is observed in methanol compared to that in water. The spectral appearance and long lifetime provide strong evidence that the transient species is due to the triplet states of the cationic CPEs. The lower intensity of transient absorption in water suggests that the triplet yield is lower than that in methanol. Such a lower triplet yield in water can be explained by aggregation of the CPEs, resulting in quenching of the singlet states of CPEs. This result is consistent with reduced fluorescence intensities of CPEs in water compared to in methanol.

Singlet Oxygen Production

The transient absorption results indicate that direct excitation of the cationic CPEs **13-16** affords a triplet state in a moderate yield. Therefore, we expected that these CPEs could sensitize singlet oxygen (1O_2) according to the pathway shown in Figure 6-8. Such singlet oxygen sensitization by the cationic CPEs **13-16** was investigated in CD_3OD by monitoring the emission

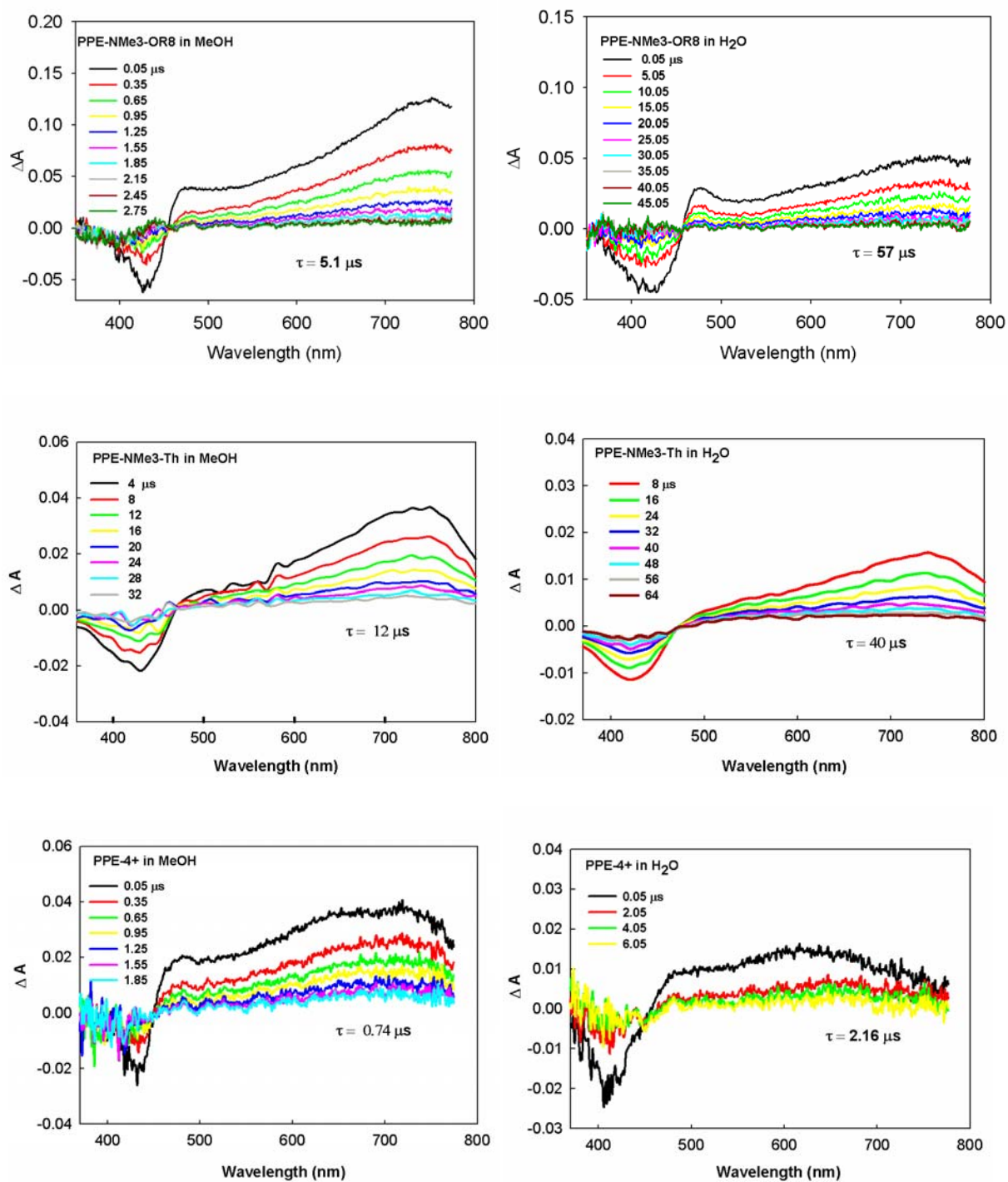


Figure 6-7. Transient absorption spectroscopy of cationic CPs in methanol and water. The Spectra of PPE-NMe3-OR8 and PPE4+ were obtained on the laser system described in ref.196 and those of PPE-NMe3-Th were obtained in the system described in ref.197.

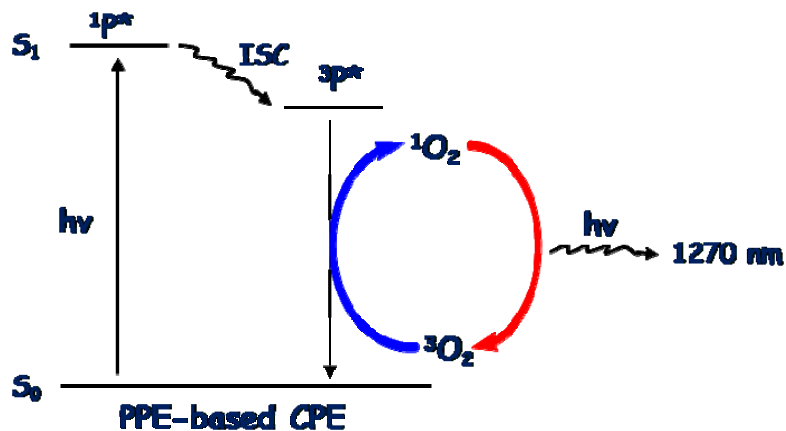


Figure 6-8. Pathway for PPE-sensitized singlet oxygen generation.

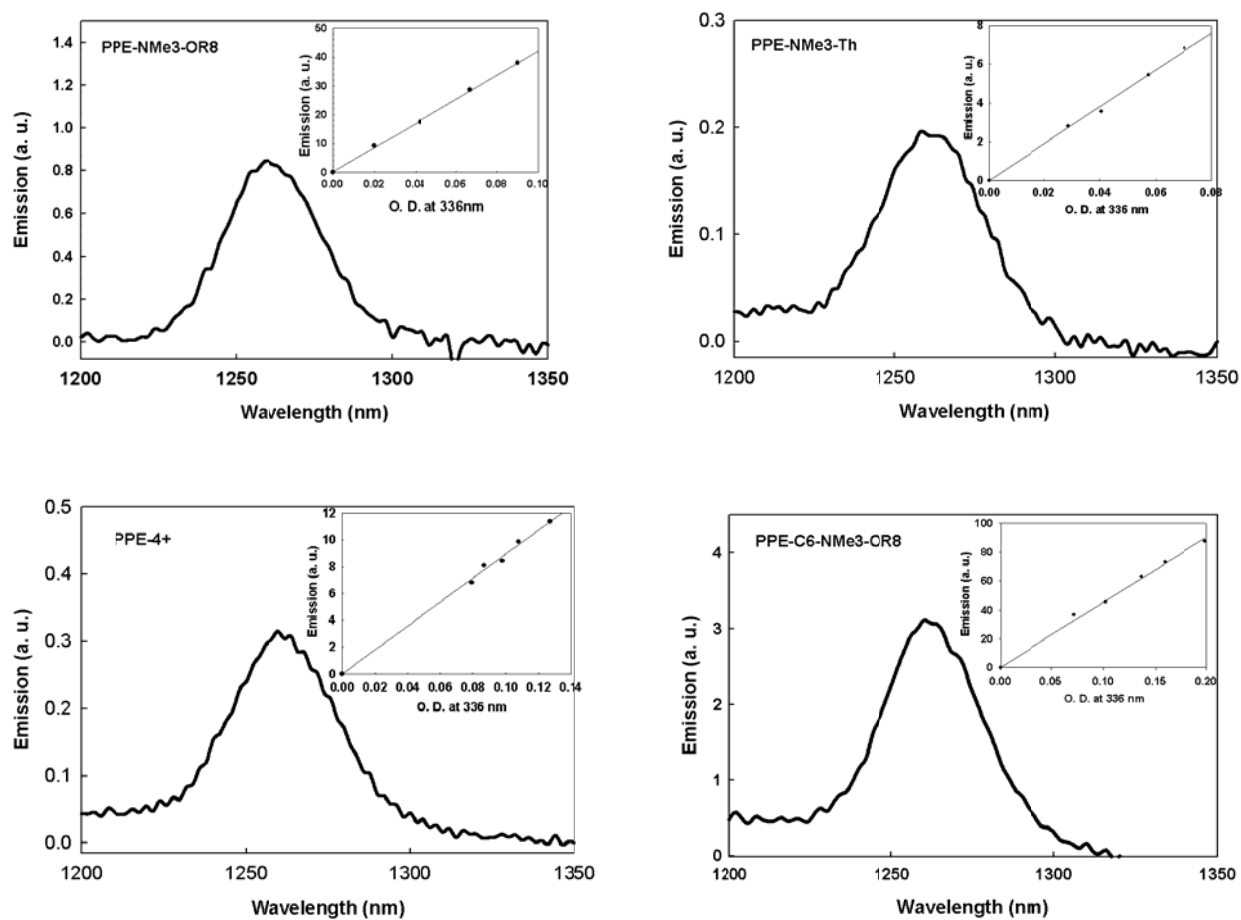


Figure 6-9. Singlet oxygen emission sensitized by CPEs in CD₃OD. Inset: Integrated ¹O₂ emission intensity versus optical density of the polymer solution.

at 1260 nm, which results from the deactivation of singlet oxygen (Figure 6-9). Solvents containing O-H bonds quench the singlet oxygen emission to great extent since the terminal bonds of the solvents absorb the near-infrared emission according to the respective energies of the highest fundamental vibration of that bond.¹⁹⁸ Therefore, solvents containing heavier atoms in the terminal bonds were used for this study. The concentration dependence of the ¹O₂ emission was investigated by varying the polymer concentration and a linear correlation was observed between the polymer concentration and the ¹O₂ emission intensity. The quantum yield of sensitized ¹O₂ emission¹⁹⁹ by the CPEs in CD₃OD was determined using 2'-acetonaphthone as a reference ($\Phi_{\Delta} = 0.79$).²⁰⁰ The quantum yields of singlet oxygen generation from the CPEs are presented in Table 6-1. This observation clearly indicates that PPE-type CPEs are able to sensitize ¹O₂ with moderate efficiency.

Table 6-1. Photophysical properties of cationic CPEs

		$\lambda_{\max}^{\text{abs}}/\text{nm}$	$\lambda_{\max}^{\text{fl}}/\text{nm}$	Φ_{fl}	Φ_{Δ}^{c}
PPE-NMe ₃ -OR8	MeOH	414	460	0.285 ± 0.02 ^a	0.130 ± 0.02 ^d
	H ₂ O	417	500	0.106 ± 0.01 ^a	0.069 ± 0.004 ^d
PPE-NMe ₃ -Th	MeOH	422	475, 502	0.045 ± 0.004 ^a	0.112 ± 0.008 ^d
	H ₂ O	432	475, 502	0.016 ± 0.001 ^a	0.037 ± 0.001 ^d
PPE-4+	MeOH	422	441	0.15 ± 0.01 ^b	0.091 ± 0.005 ^d
	H ₂ O	394	436	0.047 ± 0.004 ^b	0.320 ± 0.039 ^d
PPE-C6-NMe ₃ -OR8	MeOH	432	467	0.239 ± 0.02 ^a	0.079 ± 0.007 ^d
	H ₂ O	450	505	0.131 ± 0.01 ^a	-

^a Coumarin 30 in MeOH as standard, $\Phi_{\text{fl}} = 0.307$ (ref.154). ^b From ref.116. ^c Quantum yield of singlet oxygen. ^d Oxygen atmosphere.

Since the biocidal experiments were carried out in aqueous solution, the same experiments were carried out in D₂O to provide evidence that the cationic PPE-type CPEs will sensitize ¹O₂ in

water. However, near-infrared emission spectroscopy did not afford any detectable emission from $^1\text{O}_2$ in D_2O . This is likely due to the fact that the quantum efficiency for $^1\text{O}_2$ emission is considerably less in D_2O , making it more difficult to detect in this medium.²⁰¹ Thus, a second approach was used to detect the sensitization of $^1\text{O}_2$ by the polymer. This method is based on the use of a water-soluble chemical trap, 1,3-cyclohexadiene-1,4-diethanoate (CHDDE), which forms a stable endoperoxide when it reacts with $^1\text{O}_2$ (Figure 6-10).²⁰¹ In these experiments disappearance of CHDDE was monitored by decrease of its absorption at 270 nm as a function of irradiation time (Figure 6-11). The quantum yields of singlet oxygen generation were determined following a literature procedure using 5,10,15,20-tetrakis(4-sulfonatophenyl)-porphyrin (TPPS) as a reference ($\Phi_{\Delta} = 0.66$).²⁰¹ This result confirms that the production of $^1\text{O}_2$ is sensitized in water, but with reduced efficiency compared to that in methanol. The decreased efficiency is consistent with the photophysical experiments which show that the triplet yield of the CPEs is lower in water relative to methanol, presumably due to quenching of the singlet excited state by aggregation. The maximum absorption band for PPE-C6-NMe₃-OR8 is reduced with the $^1\text{O}_2$ generation and hence the quantum efficiency for $^1\text{O}_2$ emission is not obtained in D_2O .

Biocidal Activity.

In collaboration with Dr. Whitten and his co-workers at the University of New Mexico, the biocidal activity of the cationic CPEs was studied using silica particles with surface grafted conjugated polyelectrolyte (SGCP) **13b**. For live-dead assays of bacteria exposed to the CPE-coated particles in the light and dark, suspensions of CPE-coated particles, bacteria and two DNA stains, SYTO-60 and SYTOX Green stains were examined by confocal fluorescence microscopy. SYTO 60 is a red fluorescent (~650 nm) nucleic acid stain that is cell permeant and used to stain both live and dead cells. SYTOX Green is a green-fluorescent (~ 530 nm) nuclear

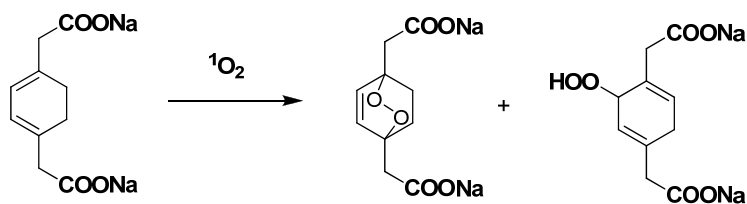


Figure 6-10. Peroxidation of CHDDE by singlet oxygen ($^1\text{O}_2$).

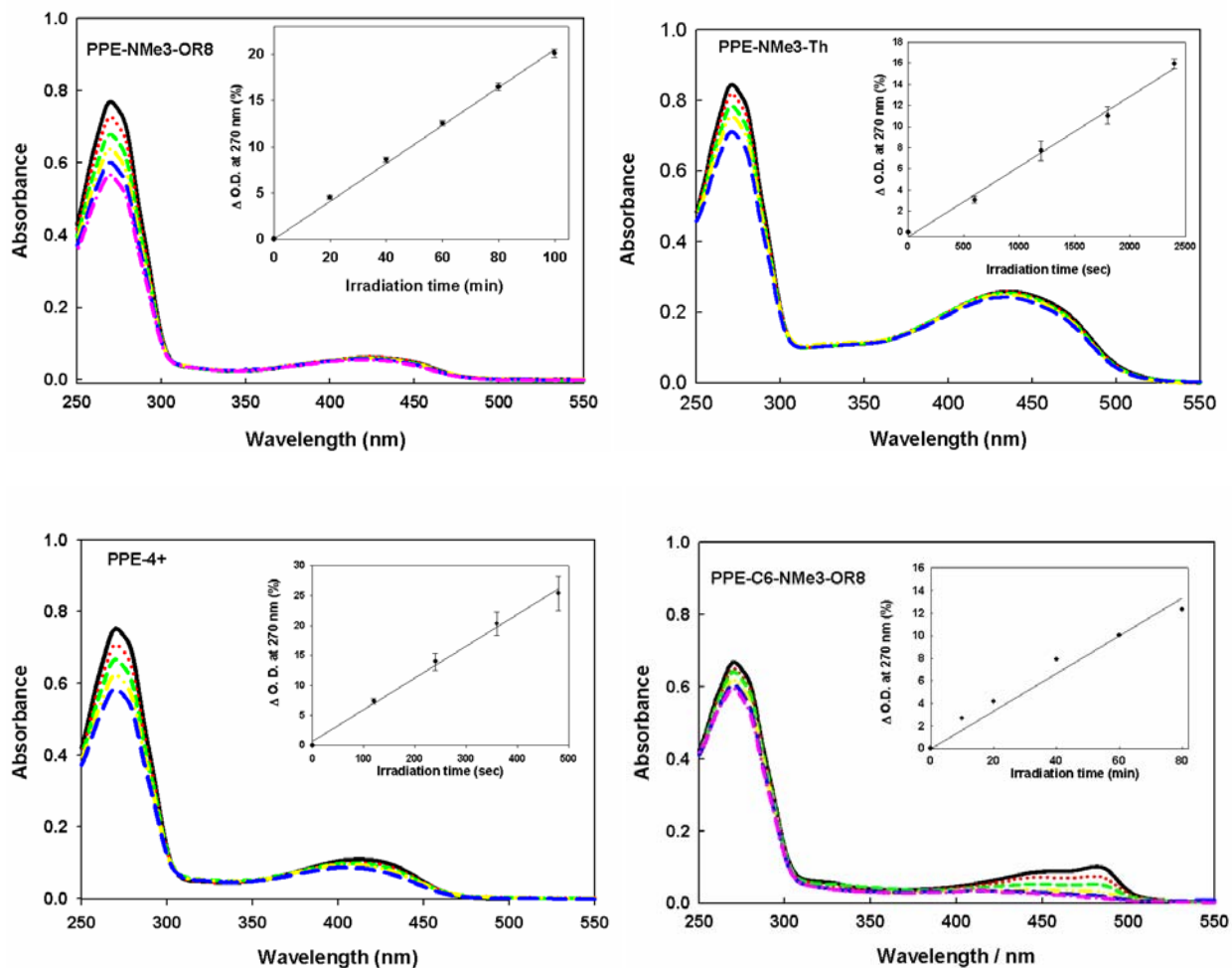


Figure 6-11. UV-visible spectra of CHDDE (100 μM) and PPE-NMe₃-OR8 (2 μM), PPE-NMe₃-Th (10 μM), PPE-4+ (2 μM) or PPE-C6-NMe₃-OR8 (2 μM) in D₂O solution containing phosphate buffer (100 μM , pH 7) as a function of the irradiation time. Inset: decrease of absorbance at 270 nm (%) as a function of irradiation time.

and chromosome counterstain that is impermeant to live cells but stains the chromatin of dead cells with compromised membranes, indicating cell death. Figure 6-12 shows that *C. marina* is captured by the particles and several (7–12) bacteria associate with a single particle. As shown in

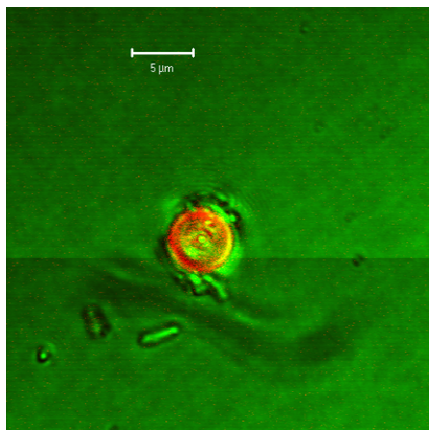


Figure 6-12. Images of single SGCP-particle with captured bacteria. Data from ref. 202, experiments were done at the University of New Mexico.

Figure 6-13(b), irradiation of the suspensions containing particles, bacteria and dyes induce to form a cluster of particles and bacteria. And most of bacteria in the cluster are dead and green fluorescence from the dye (SYTOX Green) is dominant on the confocal fluorescence image.

Live/dead counting assays were performed from the confocal fluorescence images to quantify the dead/live ratio under various conditions (Figure 6-14). Light-exposed suspension in ambient air shows a small increase in the number of dead bacteria compared to suspension in the dark. However, suspensions purged with oxygen and irradiated with visible light displays large increased dead/live ratio. In contrast, deoxygenated suspensions exhibit low dead/live ratio both in dark and when irradiated. This observation clearly indicates the role of oxygen in biocidal activity.

Mechanism for Biocidal Activity

Figure 6-15 summarizes the possible mechanism of biocidal action. First, CPE-coated particles adhere to bacteria cell wall and they bind to the inner bacteria membrane (i). Second, singlet oxygen is produced at the polymer/bacteria interface after irradiation of the polymer (ii and iii). The singlet oxygen or subsequently produced reactive oxygen intermediates interact with bacteria resulting in bacteria death (iv). Finally, bacterial remains during the physical

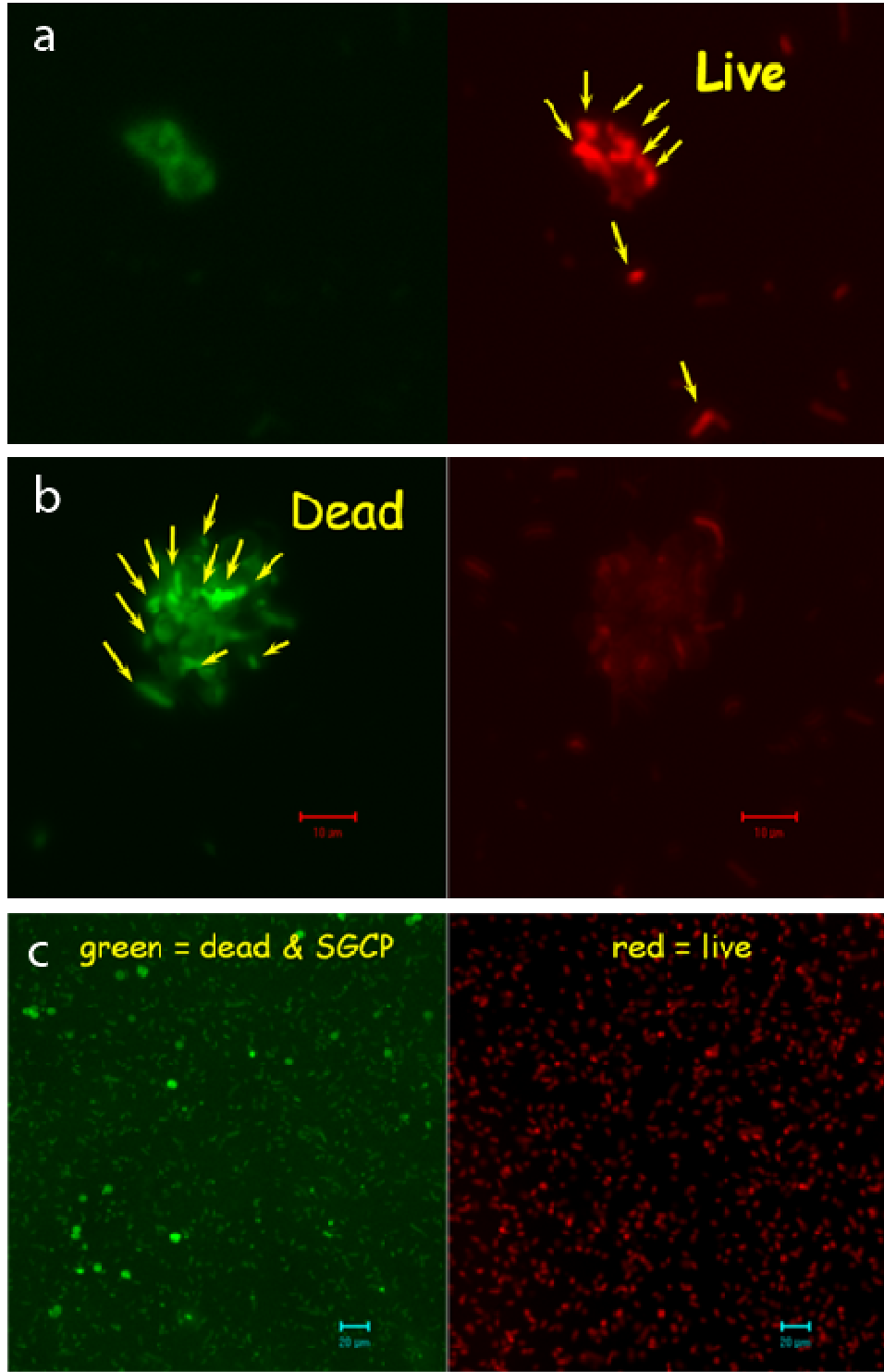


Figure. 6-13. Confocal fluorescence images of SGCP-13b with *C. marina* in ambient air. a) Before irradiation, b) after irradiation and c) a large field of view. Left panels show green channel corresponding to dead bacteria and polymer emission; right panels show red channel corresponding to live bacteria. Data from ref. 202, experiments were done at the University of New Mexico.

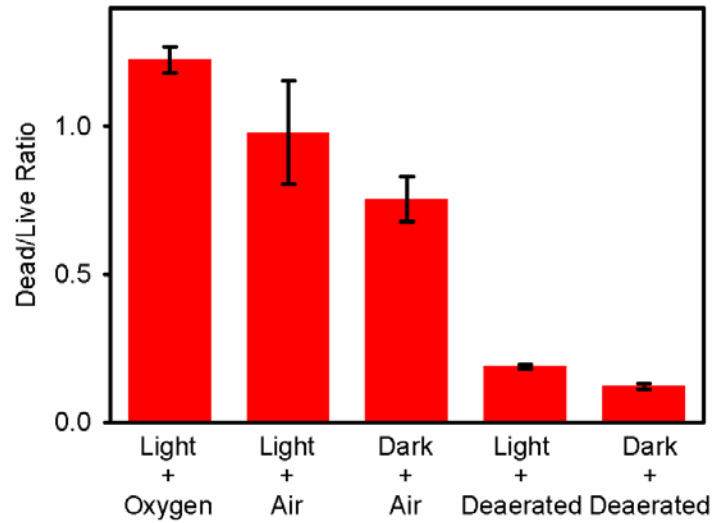


Figure 6-14. Dead/live ratios of *C. marina* exposed to 5 μm SGCP-13b under various conditions. Data from ref. 202, experiments were done at the University of New Mexico.

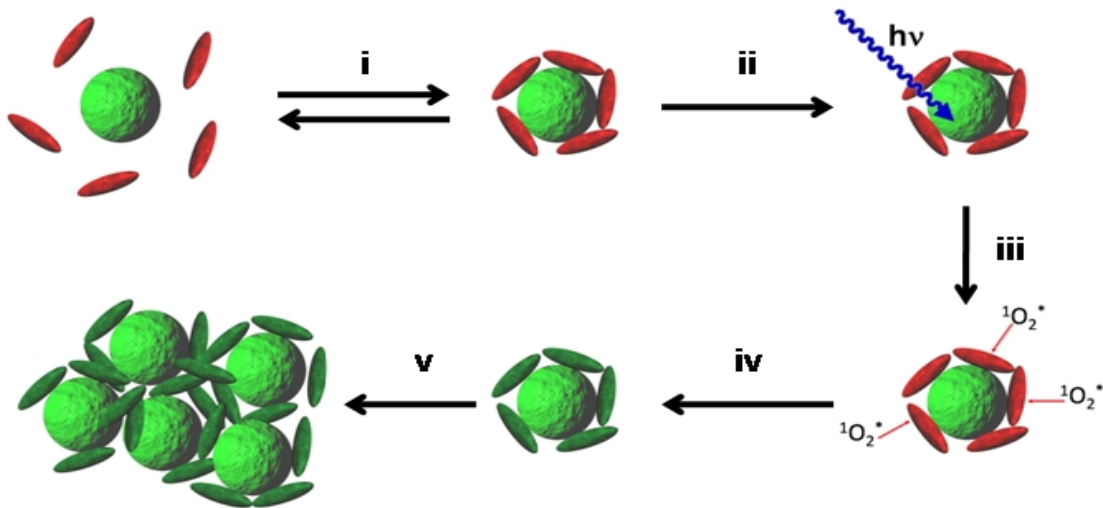


Figure 6-15. Mechanism of biocidal action.

destruction of the bacteria form large clusters of dead bacteria and particles shown in Figure 6-13 (b) and Figure 6-15 (v).

The biocidal activity experiments show that the deaerated suspensions of bacteria and CPE-coated particles induce little bacterial death in the dark and when irradiated. On the contrary, the suspensions that were oxygenated and irradiated result in more pronounced

bacterial death. This clearly proves efficient light-induced biocidal activity of CPE-coated particles and the role of oxygen in the biocidal action. As mentioned before, photophysical studies of CPEs show that direct excitation of CPEs produces efficiently a long-lived triplet excited state (exciton) with a moderate yield, and the triplet state can sensitize singlet oxygen. Oxygen is required for the light-induced biocidal activity. These results suggest that singlet oxygen generated on the CPE/bacteria interface is the key role in the light-induced biocidal activity.

Experimental

Materials

Polymer **15**,¹¹⁶ and 1,3-cyclohexadiene 1,4-diethanoate (CHDDE)²⁰³ were synthesized according to literature procedures. 2'-Acetonaphthone and 5,10,15,20-tetrakis(4-sulfonatophenyl)porphyrin (TPPS) were purchased from J. T. Baker and Sigma-Aldrich Chemical Company, respectively. CPE-coated particles were prepared according to procedures described in the previous literature.¹⁸⁸

Instrumentation

¹H and ¹³C NMR spectra were recorded on either a VXR 300 or Varian Mercury-300 spectrometer and chemical shifts are reported in ppm relative to TMS. UV-vis absorption spectra were obtained with samples contained in a 1 cm quartz cuvette on a Varian Cary 100 spectrometer. Steady state fluorescence emission spectra were recorded on a PTI (Photon Technology International) fluorometer and corrected by using correction factors generated with a primary standard lamp. Transient absorption spectra were collected using laser systems that are described elsewhere.^{196, 197} The polymer solutions were prepared in water or methanol, and purged with argon for 30 min before each transient absorption measurement. Steady-state near-IR phosphorescence spectra recorded on SPEX-2 fluorescence spectrophotometer equipped with

an Indium-Gallium-Arsenide (InGaAs) detector. A long pass filter (LP850) was placed before the emission monochromator to eliminate UV and visible light.

General Methods

Singlet Oxygen Phosphorescence Quantum Yield. Oxygen gas was bubbled into CD₃OD solutions of CPEs in the dark for 15 min with stirring. The oxygen-saturated polymer solutions were excited at 336 nm and steady-state near-IR phosphorescence spectra recorded.

The singlet oxygen quantum yield of a sample can be calculated by the Eq. 6-1.¹⁹⁹

$$\Phi_{\Delta s} = \frac{I_r}{I_s} \frac{I_{\Delta s}}{I_{\Delta r}} \frac{\tau_r}{\tau_s} \Phi_{\Delta r} \quad (6-1)$$

where I_s and I_r are the absorbed incident light, $I_{\Delta s}$ and $I_{\Delta r}$ are the integrated singlet oxygen emission intensities of the sample (CPEs) and the reference (2'-acetonaphthone), respectively, τ_s and τ_r are the singlet oxygen phosphorescence lifetime in the reference and the sample solvents, and $\Phi_{\Delta r}$ is the singlet oxygen quantum yield ($\Phi_{\Delta} = 0.79$)²⁰⁰ of the reference compound.

Quantum Yields of Singlet Oxygen Generation by Chemical Trap. Oxygen gas was bubbled into aqueous (D₂O) solutions containing CHDDE (100 μ M), phosphate buffer (100 μ M, pH 7.0), and CPEs in the dark for 15 minutes with stirring. Solutions were irradiated at 365 nm with stirring using a xenon short arc lamp equipped with a monochromator. Duration of irradiation was recorded and UV-visible spectra collected on Cary 100 UV-Vis Spectrophotometer. The disappearance of CHDDE was monitored as a decrease in absorption at 270 nm. The quantum yields of singlet oxygen generation were determined following Eq. 6-2 using 5,10,15,20-tetrakis(4-sulfonatophenyl)porphyrin (TPPS) as a reference ($\Phi_{\Delta} = 0.66$).²⁰¹

$$\Phi_s = \Phi_r \times \frac{t_r}{t_s} \quad (6-2)$$

where t_r and t_s are irradiation time to induce the oxidation of the same amount of CHDDE and CPEs, respectively, and Φ_r is the singlet oxygen quantum yield of the reference compound (TPPS). The irradiation time for 10 % loss of CHDDE absorbance at 270 nm was obtained from the linear plots for both TPPS and for CPEs. And then the quantum yield singlet oxygen generation by CPEs is calculated.

Synthetic Procedures

2, 5-Diiodohydroquinone (3). This compound was synthesized using a literature procedure³⁰ modified for easier work-up. 2,5-Diiodo-1,4-dimethoxybenzene (4.64 g, 11.9 mmol) was dissolved in dry CH_2Cl_2 (100 mL) in a three-necked flask fitted with a condenser and additional flask. The solution was cooled to $-78\text{ }^\circ\text{C}$ in a dry ice-acetone bath. Boron tribromide (2.24 mL, 23.8 mmol) solution in CH_2Cl_2 (20 mL) was added slowly. After addition, the mixture was warmed to room temperature and stirred for 24 hours. The resulting solution was hydrolyzed by mixing with 150 mL of water. After addition of water, a white powder was formed and it was recrystallized in benzene. (yield: 3.87 g, 9.87 mmol, 83%). $^1\text{H NMR}$ (300 MHz, acetone- d_6): δ 7.28 (s, 2H), 8.98 (s, 2H).

1,4-Bis(3-bromopropoxy)-2,5-diiodobenzene (4a). 1,3-Dibromopropane (4.69 g, 23.22 mmol), K_2CO_3 (5.35 g, 38.7 mmol), and acetone (150 mL) were added to a three-neck, round bottomed flask equipped with a condenser and an additional flask. 2,5-Diiodohydroquinone (1.4 g, 3.87 mmol) was dissolved in 150 mL of acetone and added dropwise to the mixture solution at $70\text{ }^\circ\text{C}$. The reaction was stirred overnight and cooled to room temperature. K_2CO_3 was removed by filtration through Celite and the solvent was removed. The resulting solid was dissolved in chloroform and washed with 10 % NaOH, water, and saturated NaCl solution. The organic layer was dried with sodium sulfate, filtered and concentrated. The resulting solid was crystallized

from ethylacetate and hexane. The white solid was dissolved in hot ethanol and insoluble solid was removed using hot filtration. The solution was concentrated to yield a white solid (2 g, 82 %). $^1\text{H NMR}$ (300 MHz, CDCl_3): δ 2.29 (m, 4H), 3.70 (t, 4H), 4.09 (t, 4H), 7.32 (s, 1H).

1,4-Bis(6-bromohexyloxy)-2,5-diiodobenzene (4b). This compound was synthesized using the same procedure described for compound **4a** except replacing 1,3-dibromopropane with 1,6-dibromohexane (Yield: 80%). $^1\text{H NMR}$ (300 MHz, CDCl_3): δ 1.52 (m, 8H), 1.87 (m, 8H), 3.41 (t, 3H), 3.92 (t, 4H), 7.17 (s, 1H).

3,3'-(2,5-Diiodo-1,4-phenylene)bis(oxy)]bis[N,N,N-trimethylpropan-1-aminium] (5a). Compound **4** (1.56 g, 2.47 mmol) was suspended in 25 % trimethylamine in water (80 mL), ethanol (120 mL), and acetone (120 mL) and heated to 120 °C. The reaction was refluxed overnight. The solvent was removed and the white solid recrystallized from ethanol to yield 1.52 g (85 %). $^1\text{H NMR}$ (300 MHz, CD_3OD): δ 2.26 (m, 4H), 3.15 (s, 18H), 3.57 (m, 4H), 4.04 (t, 4H), 7.30 (s, 1H).

3,3'-(2,5-Diiodo-1,4-phenylene)bis(oxy)]bis[N,N,N-trimethylpropan-1-aminium] (5b). This compound was synthesized using the same procedure described for compound **5a** except replacing compound **4a** with compound **4b** (Yield: 91%). $^1\text{H NMR}$ (300 MHz, CD_3OD): δ 1.36 (m, 12H), 1.72 (m, 4H), 3.06 (s, 18H), 3.26 (m, 4H), 3.89 (t, 4H), 7.21 (s, 1H).

1,4-Diiodo-2,5-bis[2-(2-methoxyethoxy)ethoxy]benzene (8). 2,5-Diiodohydroquinone (2.00 g, 5.53 mmol) and diethylene glycol monomethyl ether *p*-toluenesulfonate (6.07 g, 22.12 mmol) in 120 mL of methylethylketone was placed under argon. To this solution K_2CO_3 (3.06 g, 22.12 mmol) and KI (0.09 g, 0.55 mmol) was added. The reaction mixture was refluxed at 100 °C for 48 hours and then cooled to room temperature. The solvent was removed and the solid was dissolved in CH_2Cl_2 (200 mL), followed by washing with 100 mL of 10 % KOH solution,

water, and saturated NaCl solution. The organic layer was dried with sodium sulfate and concentrated to give a gold color oil. Flash chromatography on silica gel (80 % CH₂Cl₂/ 10 % hexane/ 10% ethyl acetate) yielded a white solid (1.35 g, 43 %). ¹H NMR (300 MHz, CDCl₃): δ 3.40 (s, 6H), 3.58 (m, 4H), 3.78 (m, 4H), 3.88 (m, 4H), 4.11 (m, 4H), 7.23 (s, 2H). ¹³C NMR (75 MHz, CDCl₃): δ 59.5, 69.9, 70.7, 71.4, 72.4, 86.7, 123.8, 153.4.

1,4-Bis(trimethylsilyl)ethynyl-2,5-bis[2-(2-methoxyethoxy)ethoxy]benzene (9a).

Schlenk flask equipped with compound **8** (1.29g, 2.27 mmol), CuI (0.013 g, 0.068 mmol), and Pd(PPh₃)₄ (0.052 g, 0.045 mmol) was placed under argon. And then 20 mL of toluene and 40 mL of diisopropylamine were added and argon bubbled through the solution for 30 minutes. To this solution, (trimethylsilyl)acetylene was added and the solution stirred at 70 °C for 3 days. The solvent was removed and the residue was dissolved in CH₂Cl₂ and filtered through one-inch silica gel using ethyl acetate. The filtrate was concentrated and purified by flash chromatography on silica gel (8 % CH₂Cl₂/ 67 % hexane/ 25% ethyl acetate) to yield a gold oil, which solidified slowly at room temperature (0.87 g, 76 %). ¹H NMR (300 MHz, CDCl₃): δ 0.25 (s, 18H), 3.93 (s, 6H), 3.56 (m, 4H), 3.77 (m, 4H), 3.80 (t, 4H), 4.17 (t, 4H), 6.92 (s, 2H).

1,4-Diethynyl-2,5-bis[2-(2-methoxyethoxy)ethoxy]benzene (9b). A two-necked flask with compound **9a** (0.8 g, 1.58 mmol, 1 eq.) and methanol (45 mL) was placed and argon bubbled through the solution for 30 minutes. Tetrabutylammonium fluoride (1M in THF, 3.79 mL) was then added to the flask under the argon and the mixture was stirred at room temperature for 9 hours. The solvent was removed and the solid was purified by flash chromatography on silica gel (5% methanol/95% methylene chloride) to yield a light yellow solid (0.42 g, 1.16 mmol, 73%). ¹H NMR (300 MHz, CDCl₃): δ 3.32 (s, 2H), 3.39 (s, 6H), 3.55 (m, 4H), 3.74 (m,

4H), 3.86 (t, 4H), 4.15 (t, 4H), 7.00 (s, 2H). ^{13}C NMR (75 MHz, CDCl_3): δ 59.4, 69.9, 69.9, 71.3, 72.4, 79.9, 83.1, 113.9, 118.6, 154.4.

2,5-Bis((trimethylsilyl)ethynyl)thiophene (11). 2,5-Dibromothiophene (4.00 g, 16.53 mmol), CuI (0.38 g, 1.98 mmol), $\text{Pd}(\text{PPh}_3)_2\text{Cl}_2$ (0.69 g, 0.98 mmol), and 120 mL of diisopropylamine were placed in a Schlenk flask and the solution was degassed with stirring for 30 min under ice-bath by bubbling argon gas. To this solution, (trimethylsilyl)acetylene (6.49 g, 66.12 mmol) was added. The solution was stirred under an ice-bath for 1 hour. Temperature was raised to room temperature and the mixture was kept stirring for an additional 1 hour. The resulting solution was heated to 75 °C and stirred for 20 hours. The solvent was removed and the solid was purified by flash chromatography on silica gel with hexane to yield a yellow solid **7** (2.54 g, 55.5 %). ^1H NMR (300 MHz, CDCl_3): δ 0.24 (s, 18H), 7.04 (s, 2H).

2,5-Diethynylthiophene (12). To a suspension of compound **7** (0.4 g, 1.45 mmol) in deoxygenated methanol (20 mL) was added 0.1 mL of 0.5 M aqueous KOH solution. The mixture was stirred at room temperature under argon for 40 min. The solution was diluted with water (50 mL) and extracted with *n*-pentane (2 x 50 mL). The combined organic solution was dried over Na_2SO_4 and the solvent was removed at reduced pressure to yield a viscous oil **8** (0.14 g, 73 %). ^1H NMR (300 MHz, CDCl_3): δ 3.32 (s, 2H), 7.09 (s, 1H). ^{13}C NMR (75 MHz, CDCl_3): δ 132.6, 123.6, 82.1, 76.2.

PPE-NMe₃-OR8 (13a). Compound **5** (0.1 g, 0.14 mmol), compound **10** (0.05 g, 0.14 mmol), DMF (5 mL), and water (5 mL) were placed into a Schlenk flask and degassed with argon for 30 min. In a separate flask, CuI (1 mg, 0.005 mmol), $\text{Pd}(\text{PPh}_3)_4$ (4.8 mg, 0.004 mmol), DMF (2.5 mL), and triethylamine (2.5 mL) were degassed with argon for 30 minutes and added to the degassed solution containing compound **5** and compound **10**. The reaction mixture was

stirred at 60 °C for 22 hours. The DMF solution was added to 200 mL of acetone to form a precipitate. The collected yellow precipitate was dissolved in an aqueous solution containing NaCN, filtered using a 25 µm glass filter, and followed by dialysis against deionized water using 6-8 kD MWCO cellulose membrane for 2 days. The polymer solution was lyophilized to yield a dark yellow solid (72 mg, 62 %). ¹H NMR (300 MHz, CD₃OD): δ 2.54 (b, 4H), 3.16 (s, 18H), 3.39 (s, 6H), 3.53 (b, 4H), 3.65 (b, 8H), 3.89 (b, 4H), 4.26 (b, 4H), 7.25 (b, 4H).

PPE-NMe₃-Th (14). A solution of compound **5a** (100 mg, 0.15 mmol), CuI (4 mg, 0.02 mmol), and Pd(PPh₃)₄ (10 mg, 0.01 mmol) in 8.5mL of DMF/H₂O/(*i*Pr)₂NH (v/v/v/ = 9/6/2) was deoxygenated with argon for 30 minutes. Then, compound **12** was added to the mixture solution under argon. The resulting solution was heated at 70 °C for 22 hours. The reaction mixture was poured into 200 mL of acetone. The precipitate was dissolved in small amount of Millipore water and treated with NaCN, filtered using a 25 µm glass filter and followed by dialysis against deionizer water using 6-8 kD MWCO cellulose membrane for 2 days. The polymer solution was lyophilized to yield a yellow-tan solid (46 mg, 51 %). ¹H NMR (300 MHz, CD₃OD): 2.38 (br, 4H), 3.21 (br, 18H), 3.63 (br, 4H), 4.22 (br, 4H), 7.23 (br, 2H), 7.33 (br, 2H).

PPE-C6-NMe₃-OR8 (16). This polymer was synthesized in the same procedure described for PPE-NMe₃-OR8 (**13a**) using compound **5b** (78 mg, 0.1 mmol), compound **9b** (36 mg, 0.1mmol). Yield: 45 mg, 49%. ¹H NMR (300 MHz, DMSO-d₆): δ 1.37 (br, 18H), 3.05 (s, 18H), 3.22 (s, 6H), 3.30 (br, 4H), 3.45 (br, 4H), 3.67 (br, 4H), 3.81 (br, 4H) 4.08 (br, 4H), 4.22 (br, 4H) 7.15 (br, 4H).

CHAPTER 7 CONJUGATED POLYAMPHOLYTES BASED ON POLY(PHENYLENE ETHYNYLENE)

Introduction

Polymers containing ionic groups are divided into two groups: polyelectrolytes and polyampholytes.²⁰⁴ The former contain either anionic or cationic groups along the polymer chain while latter contain both anionic and cationic groups. Polyelectrolytes show ability to obtain large hydrodynamic volumes in deionized water at low concentrations because of Coulombic repulsion between charged groups along the polymer chain forcing the polymer chain into a rod-like conformation. However, the addition of electrolytes or changes in pH screens the Coulombic repulsions allowing the polymers to more random conformation with a subsequent decrease in the hydrodynamic volume. In contrast to polyelectrolytes, structure-property relationship of polyampholytes is controlled by Coulombic attraction between anionic and cationic groups on different monomer units. When either anionic or cationic groups are in sufficient excess ($\geq 10\text{--}15\text{ mol}\%$), charge repulsion forces the chains into an extended conformation showing typical behavior of polyelectrolytes. However, when the molar ratio of anionic and cationic groups is close to unity, Coulombic interactions induce globular-like conformation and, in most cases, insolubility in deionized water. The addition of electrolytes and change in pH screens these attractive interactions allowing a random coil conformation, often improving solubility. This behavior is called as “antipolyelectrolyte effect”. Therefore, the property of polyampholytes in aqueous solution depends on both the chemical structure and the composition of the polymer. Essentially, there are four subclasses of polyampholytes based on their pH responses (Figure 7-1).^{204, 205} First, the polyampholytes contain a carboxylate group as the anionic species and an amine hydrohalide group as the cationic species and both species may be neutralized (Figure 7-1a). Second, the anionic groups may be neutralized while the cationic groups remain charged

over the whole range of pH (i.e., quaternary alkyl ammonium groups) (Figure 7-1 b). Third, the cationic groups may be neutralized while the anionic groups remain unchanged over the whole range of pH (i.e., sulfonate groups) (Figure 7-1c). Finally, both the anionic and cationic groups are insensitive to pH changes.

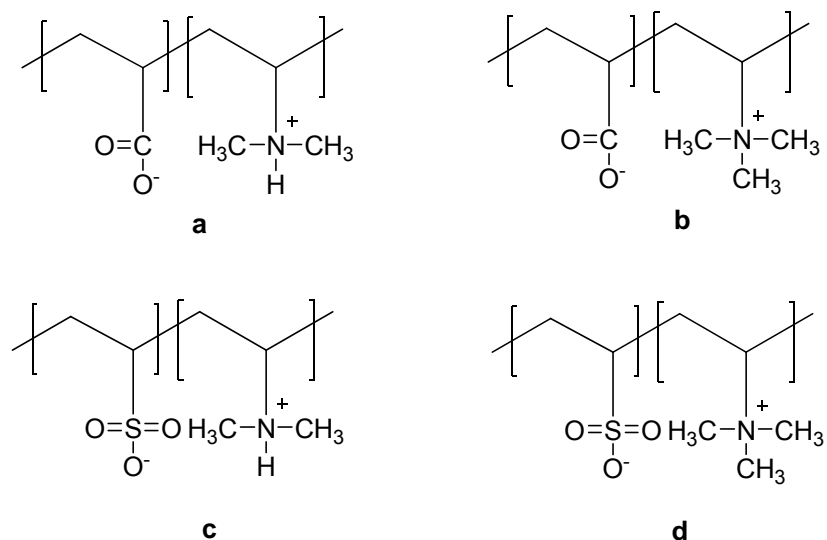


Figure 7-1. Structures of the four subclasses of polyampholytes.

The first synthetic polyampholytes were reported in 1950s by Alfrey and Katchalsky.²⁰⁶⁻²⁰⁹ The first synthesized polyampholytes are copolymers of acrylic (or methacrylic) acid and vinylpyridine. They are typically synthesized via radical copolymerization of acidic and basic monomers because of their different reactivity. A typical example is copolymerization of 2-vinylpyridine (weak base) and methacrylic acid (weak acid), which results in the formation of statistical copolymers. Since these early reports, many researchers have studied the synthesis and properties of a wide range of statistical polyampholytes (Figure 7-2).²⁰⁵ The polyampholytes have been of interest because they are synthetic analogous proteins. Therefore they can contribute to understanding the aqueous solution behavior of biological molecules such as proteins and be applied to various areas of biotechnology, medicine, and hydrometallurgy.^{204, 210}

Particularly, they have been used to absorb and deliver metals, drugs, amino acids, and nucleic acids.²¹⁰

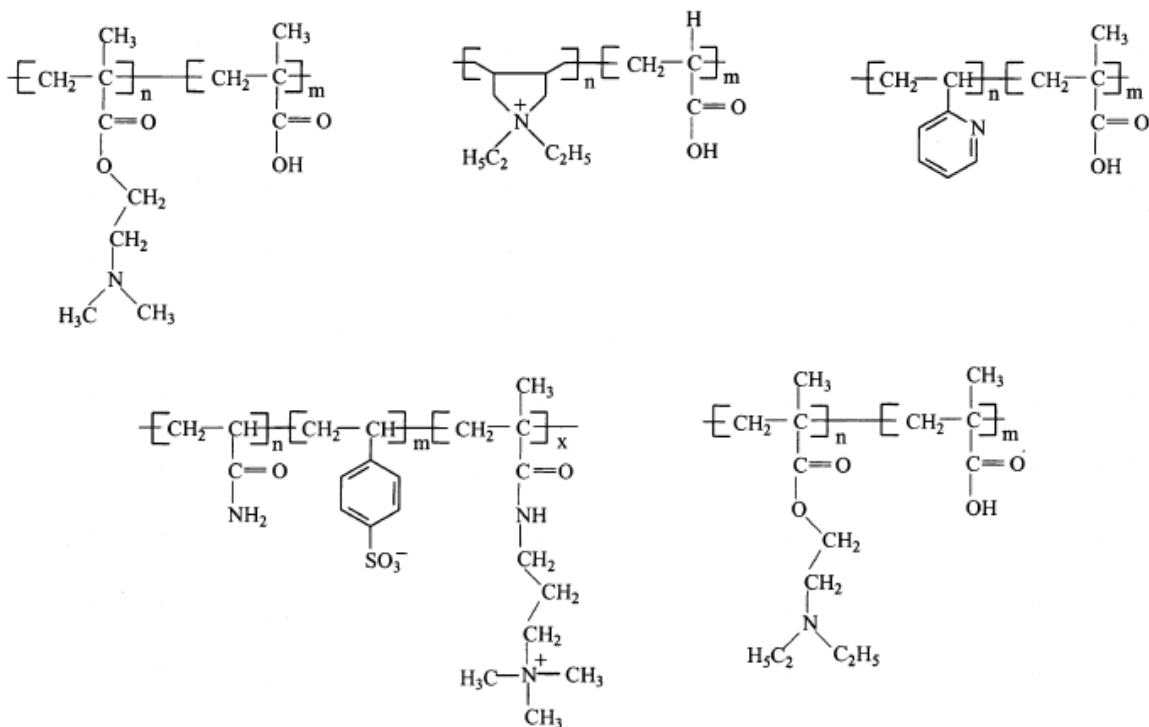


Figure 7-2. Structures of polyampholytes that have been synthesized. Figure was taken from Lowe et.al.²⁰⁵

The polyampholytes containing both anionic and cationic groups along their backbone can form polyanion-polycation complex formation (“symplex formation”) via two pathways.²¹¹ First, “homosymplex” is formed by interactions between the anionic and cationic groups of the polyampholytes without a participation of another macroion. Second, “heterosymplex” formation occurs by interactions between either the anionic or cationic groups of the polyampholytes with an oppositely charged macroion added to the polyampholytes. These homo- and heterosymplex formation are dependent on pH, the kind of ionic groups, the ratio of anionic to cationic groups within the polyampholytes, and the distribution of both groups along the polyampholyte backbone. The properties of polyampholytes have been investigated mostly by means of

viscometry and turbidimetry.^{204, 210, 212} Most of synthetic polyampholytes possess an isoelectric point (IEP) at given pH. The IEP is determined by a minimum viscosity and at this IEP point there are strong Coulombic interactions between oppositely charged groups, and hence the polyampholytes are electoneutral and a highly compact structure of the polymer is expected. When the pH is changed and either cationic or anionic groups become neutral or when electrolytes are added, Coulombic repulsion induces chain expansion of the polymer.

In this chapter, we report that synthesis of conjugated polyampholytes carrying both cationic and anionic groups (Figure 7-3). The polyampholytes contain different molar ratios of

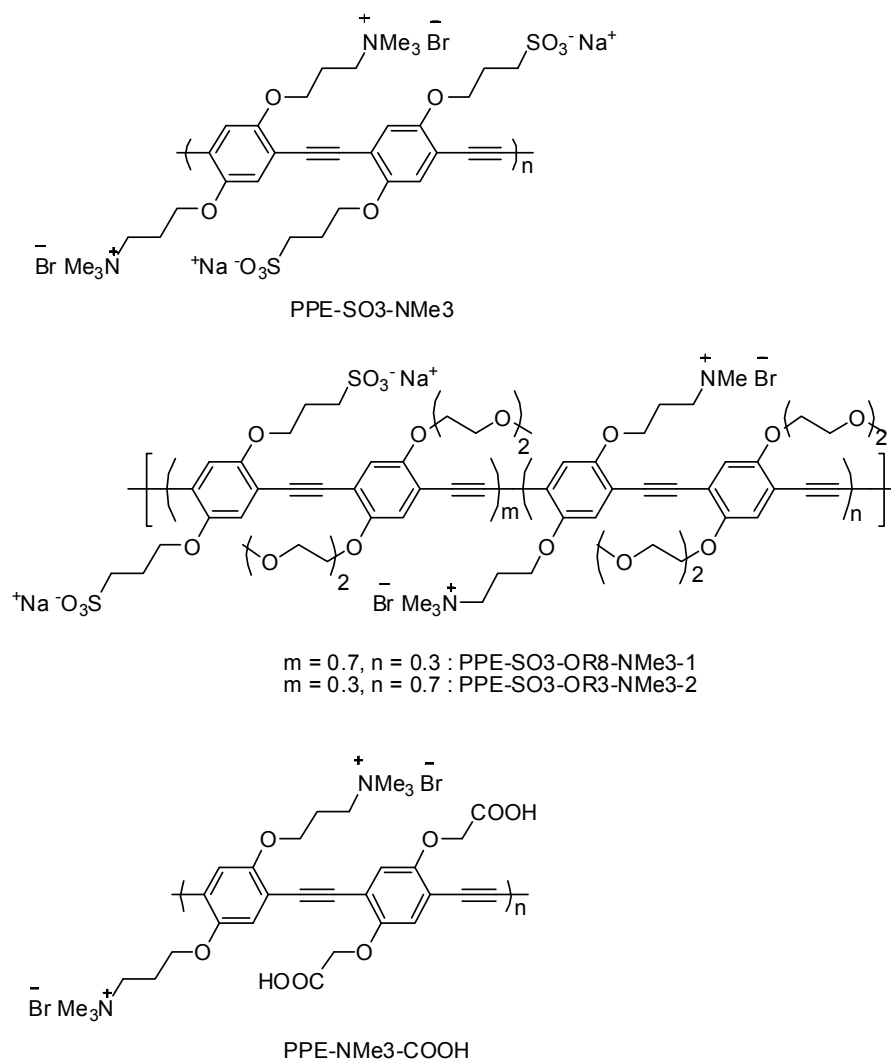


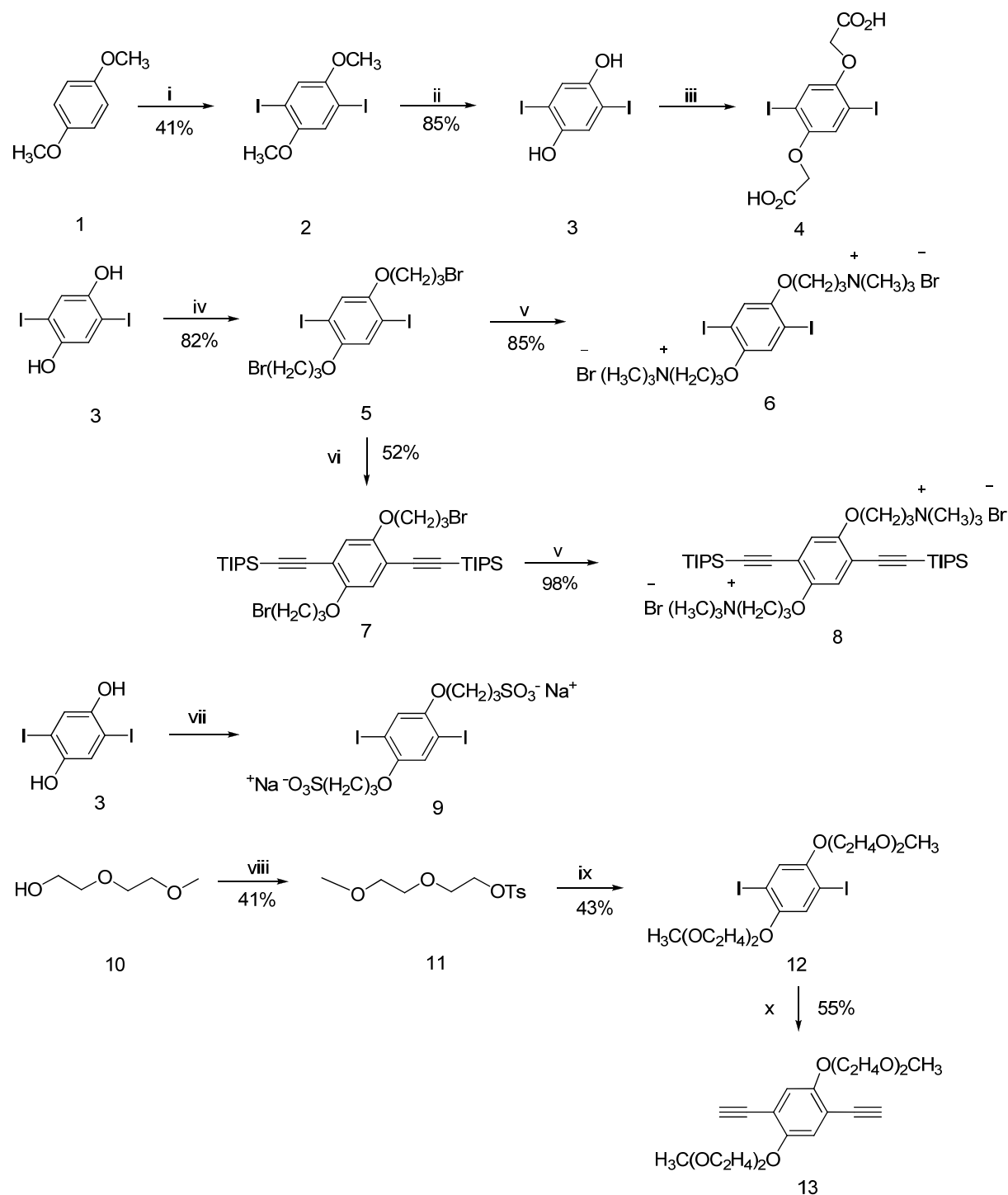
Figure 7-3. Structures of conjugated polyampholytes.

anionic to cationic groups and show different behavior in solution. The solution properties of polyampholytes were studied using absorption and fluorescence spectroscopy. PPE-NMe₃-SO₃ with 1:1 ratio of cationic to anionic groups exhibits the low solubility in deionized water due to the static interaction between oppositely charged side groups. On the other hand, PPE-SO₃-NMe-OR₈ with low ratio (< 1) of cationic to anionic groups shows good solubility in deionized water with the similar solution properties with those observed for cationic or anionic conjugated polyelectrolytes (CPEs). The highlight of this study is the finding that the competition between homo- and heterosymplex formation is dependent on the pH of the PPE-NMe₃-COOH solution containing quaternary ammonium and carboxyl groups. The polymer shows the pH dependent optical properties.

Results and Discussion

Synthesis

Figure 7-4 illustrates the synthetic route for the monomers. The synthesis started with commercially available 1,4-dimethoxybenzene **1**, which was converted to 2,5-diiodohydroquinone **3** according to the procedures described previously.³⁰ Substitution reaction of 2,5-diiodohydroquinone **3** with bromoacetic acid yielded compound **4** with procedures adapted from the previous literature.¹⁸⁹ Reaction of 1,3-dibromopropane with compound **3** afforded compound **5** and subsequent quaternization of pendant groups gave the desired cationic monomer **6** in 85% yield. Substitution of both iodines of **5** by (triisopropyl)acetylene (TIPSA) was achieved under Sonogashira coupling conditions. Compound **5** was treated with TIPSA in THF with diisopropylamine (*i*Pr)₂NH as base and dichlorobis(triphenylphosphine)palladium (Pd(PPh₃)₂Cl₂) and copper iodide (CuI) as catalysts at room temperature and then quaternization of pendant groups was carried out to give the cationic monomer with TIPS protection group **8** in 98 % yield. The anionic monomer with sulfonate **9** was synthesized following the procedures



i. KIO_3 , I_2 , H_2SO_4 , $\text{CH}_3\text{CO}_2\text{H}$, heat; ii. BBr_3 , CH_2Cl_2 , $-78^\circ\text{C} \rightarrow 0^\circ\text{C}$; iii. 1) NaOH , BrCH_2COOH , heat; 2) HCl ; iv. $\text{Br}(\text{CH}_2)_3\text{Br}$, K_2CO_3 , acetone, heat; v. 25% $\text{N}(\text{CH}_3)_3$, H_2O , $\text{C}_2\text{H}_5\text{OH}$, CH_3COCH_3 , heat; vi. TIPS, $\text{Pd}(\text{PPh}_3)_2\text{Cl}_2$, CuI , $(i\text{Pr})_2\text{NH}$, THF, RT; vii. NaOH , 1,3-propanesultone, 1,4-dioxane, heat; viii. TsCl , NaOH , H_2O , THF, RT; ix. 2,5-diiodohydroquinone **3**, K_2CO_3 , KI , $\text{CH}_3\text{COC}_2\text{H}_5$, heat; x. 1) Trimethylsilylacetylene, $\text{Pd}(\text{PPh}_3)_4$, CuI , Toluene, $(i\text{Pr})_2\text{NH}$; 2) TBAF, CH_3OH , RT

Figure 7-4. Synthesis of monomers 4, 6, 8, 9 and 13.

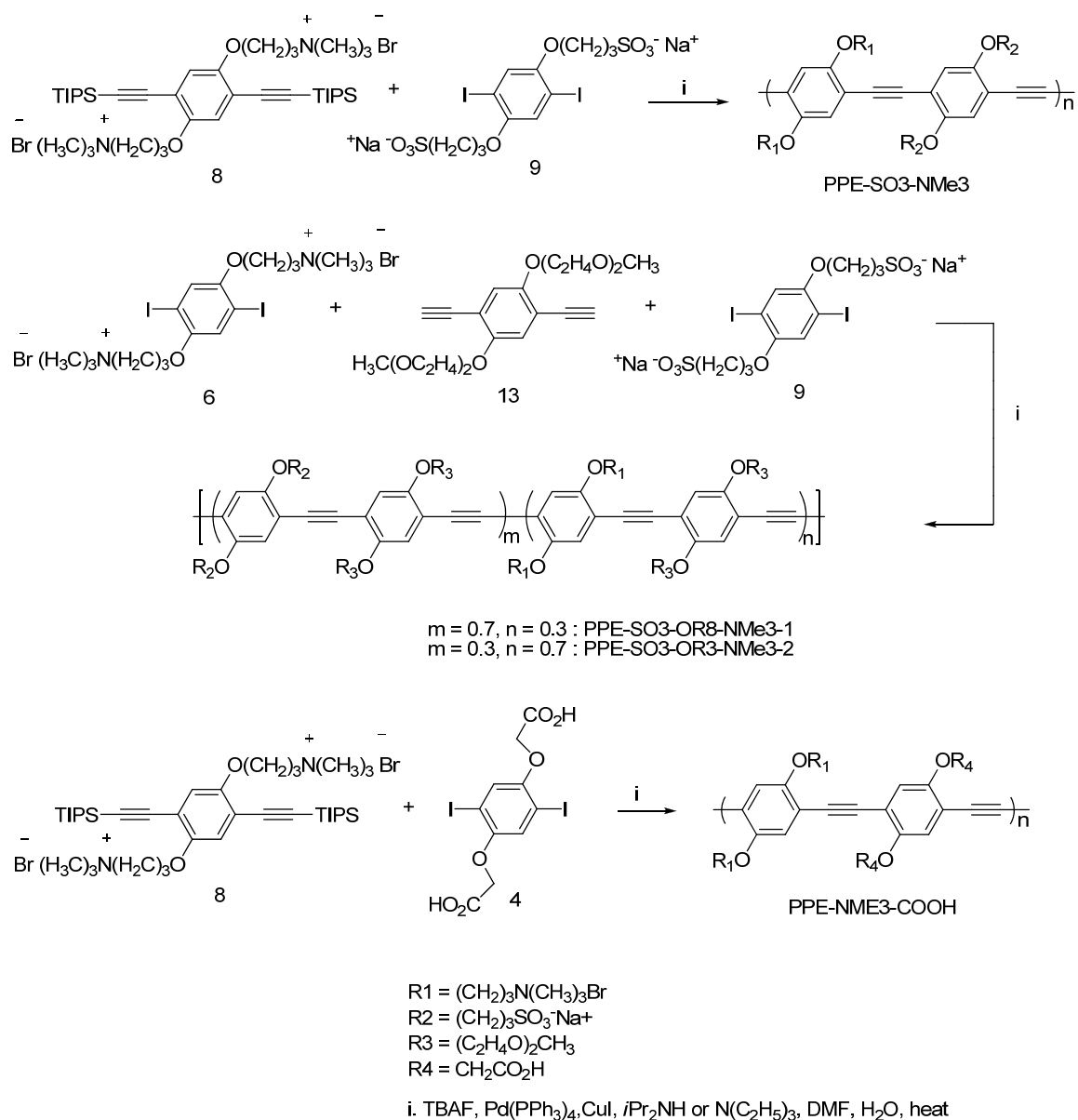


Figure 7-5. Synthesis of conjugated polyampholytes.

described previously.³⁶ Reaction of compound **11** with 2,5-diiodohydroquinone **3** gave diiodobenzene derivative **12** with di(ethyleneoxide) side chains. Phenylacetylene with di(ethyleneoxide) groups **13** was made by Sonogashira coupling of trimethylsilylacetylene (TMSA) with compound **12** and deprotection of the silyl group with TBAF in 55% yield. As shown in Figure 7-5, conjugated polyampholytes were synthesized in the mixture of DMF/H₂O/(*i*Pr)₂NH or N(C₂H₅)₃ with catalytic amount of Pd(PPh₃)₄ and CuI. All polymer

solutions were dried by lyophilization process after dialysis against deionized water and characterized by ^1H NMR spectroscopy. The solubility of PPE-NMe₃-SO₃ in various organic solvents as well as water is too low to obtain ^1H NMR spectra. For two different PPE-SO₃-OR8-NMe₃, ^1H NMR spectra were obtained in DMSO-*d*₆; however, ^{13}C NMR spectra were not able to be measured because of their poor solubility. PPE-NMe₃-COOH shows limited solubility in both DMSO and D₂O (< 1mg/mL). Using a mixture of D₂O/DMSO-*d*₆ (v/v = 1:1), ^1H NMR spectrum was finally obtained after intensive scanning (1024 scans) at room temperature.

Properties of Conjugated Polyampholytes

PPE-NMe₃-SO₃. This polyampholyte is composed of an equimolar ratio of quaternary ammonium (NR_4^+) and sulfonate groups (SO_3^-) along the polymer backbone. The sulfonate group is a strong polyelectrolyte group, and hence it remains fully ionized over a wide pH range in aqueous solution. In the previous studies using polyampholytes with a sulfonate group, the polyampholytes showed interesting rheological behavior in the presence of electrolytes.²¹³⁻²¹⁸ Specifically, polyampholytes in which the cationic/anionic charge ratio is one are insoluble in deionized water. This arises due to the interaction between the anionic and cationic groups of the polymer to form an ionically crosslinked network (“Homosymplex”) without participation of a further macroion.²¹¹ Addition of a critical concentration of salt is required to achieve solubility in aqueous solution.^{215, 216, 218} Similarly, PPE-NMe₃-SO₃ is insoluble (shows turbidity) in water and requires addition of salt to make it water-soluble. This polyampholyte also shows poor solubility in polar organic solvents such as DMSO, DMF and methanol.

PPE-NMe₃-OR8-SO₃. When anionic or cationic groups are in sufficient excess (≥ 10 – 15 mol%), polyampholytes exist in an extended conformation due to charge repulsion, resulting in rheological behavior typical of polyelectrolytes. Here, conjugated polyampholytes with different molar ratios of anionic groups to cationic groups were synthesized. PPE-NMe₃-OR8-SO₃-1 (P1)

and PPE-NMe3-OR8-SO3-2 (P2) contain 3:7 and 7:3 molar ratio of quaternary ammonium to sulfonate groups, respectively. The polymers show good solubility in water, DMSO and DMF whereas they are insoluble in methanol. The ratio of anionic and cationic groups on the polymer backbone was confirmed by integration ratio of protons on CH₂ right next to anionic and cationic groups in the ¹H NMR spectrum. The proton peak next to quaternary ammonium groups appears at 2.2-2.4 ppm while the proton peak next to sulfonate groups shows up around 2.06 ppm (Figure 7-6). Their ratios are about 3:7 and 7:3 for P1 and P2, respectively.

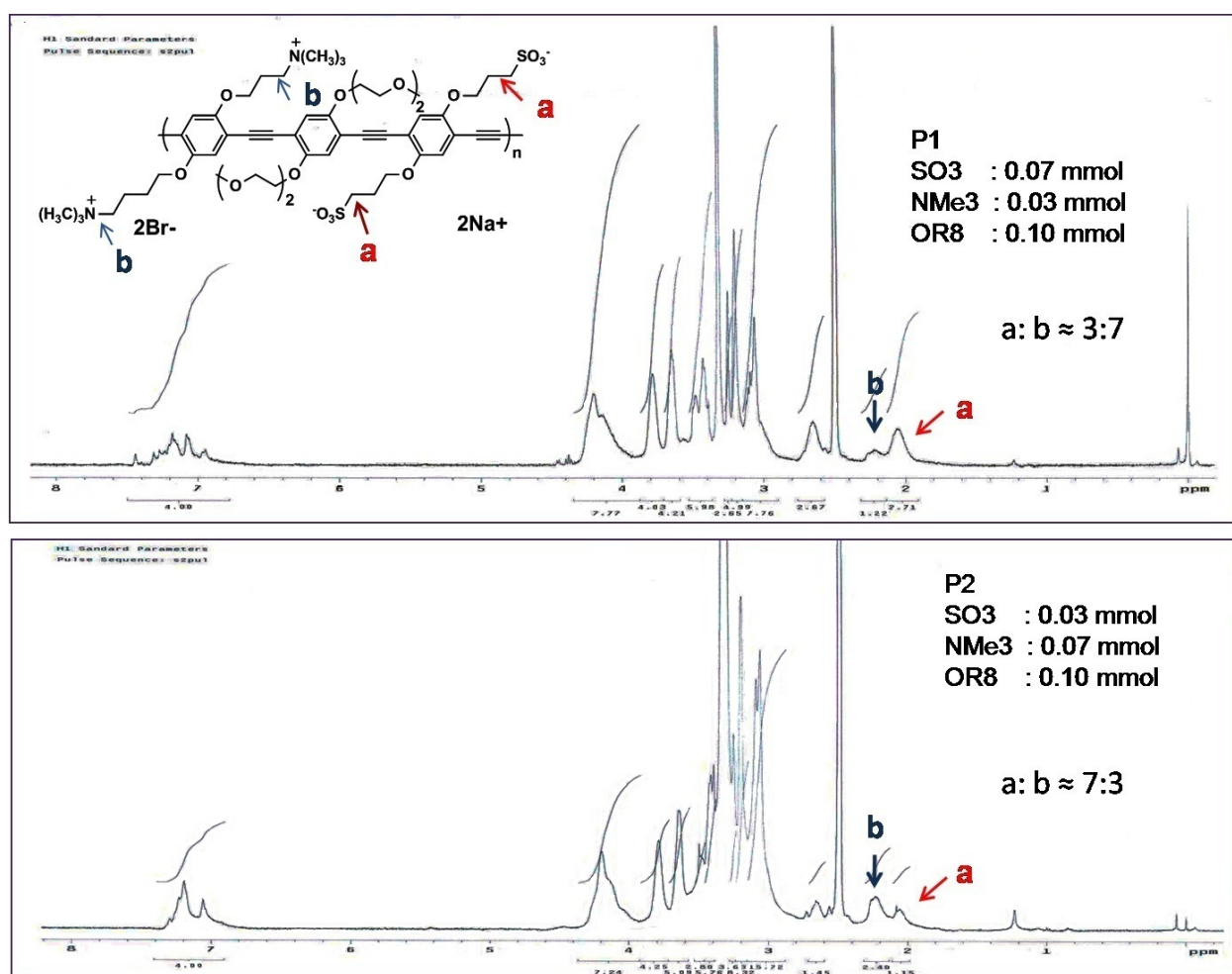


Figure 7-6. ¹H NMR spectrum of P1 and P2 in DMSO-d₆.

The absorption and fluorescence spectra of P1 and P2 in methanol or water are similar to those for conjugated polyelectrolytes (CPEs)^{23, 35, 36, 79} which contain poly(phenylene

ethynylene) (PPE) backbones. As reported previously for PPE-type CPEs, P1 and P2 in water show red-shifted absorption bands from 425 nm to 443 nm for P1 and from 418 nm to 435 nm for P2 with reduced oscillator strength (Figure 7-7). This supports that P1 and P2 exist as aggregates in water like other CPEs. The aggregation of these two polyampholytes is also evidenced by a broad and red-shifted fluorescence band with a relatively low quantum yield in water (Figure 7-7). By contrast, the polyampholytes are not aggregated in methanol as proved by the fact that the polyampholytes feature a structured fluorescence spectrum with a comparatively high quantum yield (Table 7-1). These results suggest that the polyampholytes which contain

Table 7-1. Photophysical properties of conjugated polyampholytes

		$\lambda_{\max}^{\text{abs}}/\text{nm}$	$\lambda_{\max}^{\text{fl}}/\text{nm}$	Φ_{fl}
P1	MeOH ^a	425	470	$0.13 \pm 0.01^{\text{b}}$
	H ₂ O	443	556	$0.08 \pm 0.008^{\text{c}}$
P2	MeOH ^a	418	471, 495	$0.088 \pm 0.008^{\text{b}}$
	H ₂ O	435	524	$0.058 \pm 0.005^{\text{c}}$
PPE-NMe ₃ -COOH	MeOH ^a	420	463	$0.10 \pm 0.01^{\text{b}}$
	H ₂ O	440	561	0.071 ± 0.007 (pH 3.0) ^b
				0.077 ± 0.007 (pH 7.6) ^b
			0.046 ± 0.004 (pH 10.3) ^b	

^a Microliters of a concentrated polymer solution in water was diluted with methanol. ^b Coumarin 30 in MeOH as standard, $\Phi_{\text{fl}} = 0.307$ (ref. 154). ^c Coumarine 6 in EtOH as standard, $\Phi_{\text{fl}} = 0.78$ (ref. 219).

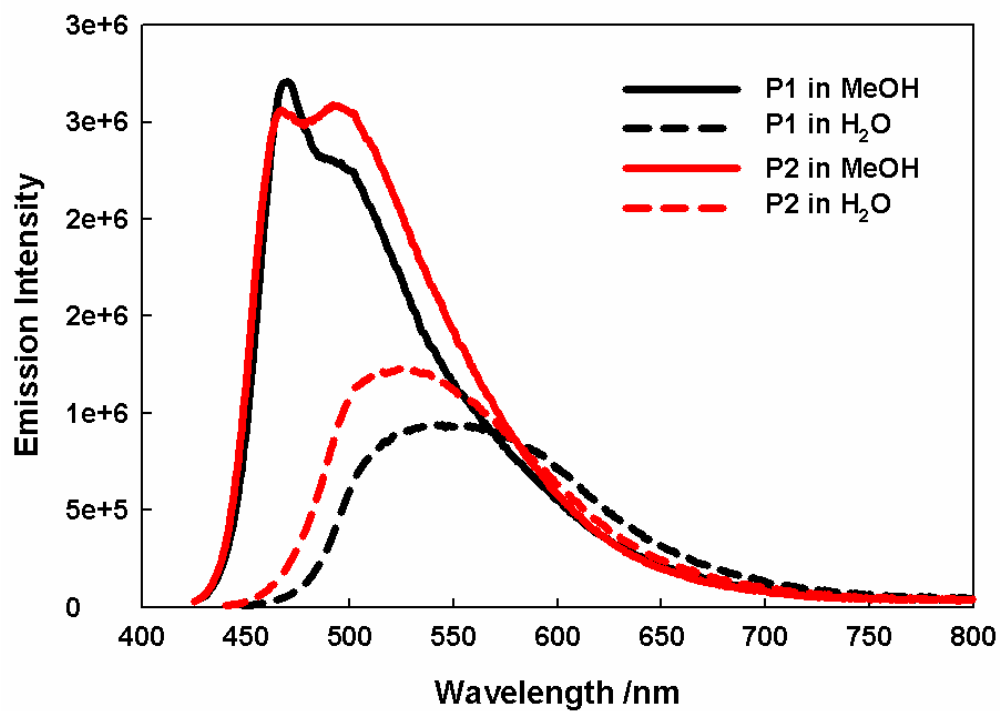
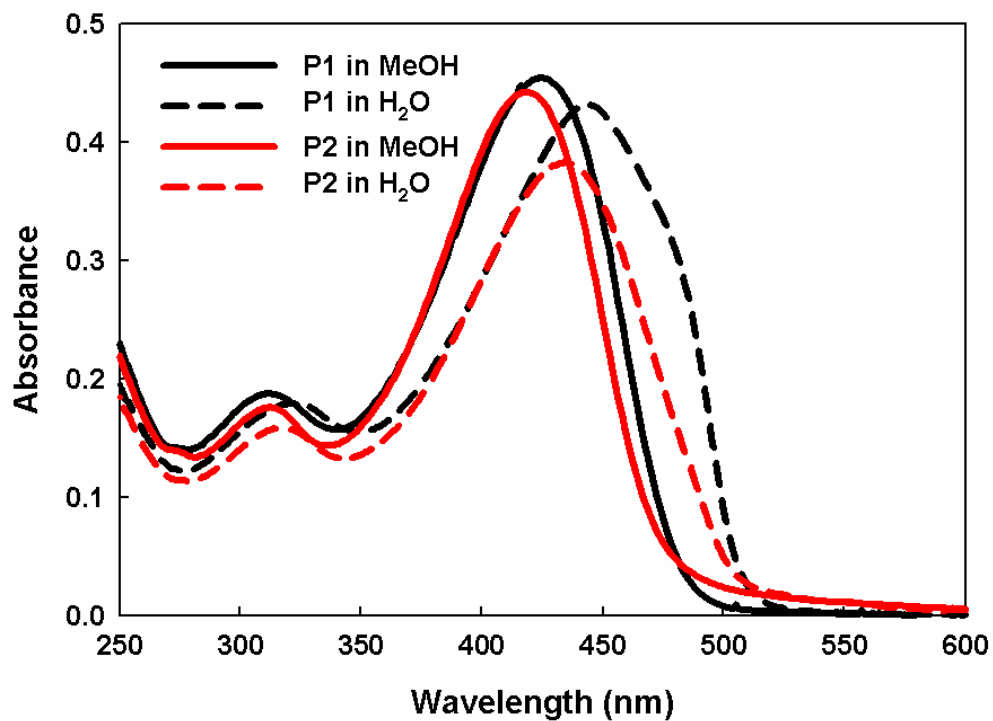


Figure 7-7. Absorption and emission spectra of P1 (10 μ M) and P2 (10 μ M) in methanol and water. Each polymer solution is excited at its own maximum absorption wavelength.

either cationic or anionic groups are in sufficient excess show solvent-dependent photophysical properties similar with those for CPEs.

Titration of P1 and P2 in water with aliquots of N,N'-dimethyl-4,4'-bipyridinium (MV^{2+}) and sodium 1,4,5,8-naphthalenediimide-N,N'-bis(methylsulfonate) (NDS) was conducted to provide the quenching behavior of the two polymers. MV^{2+} and NDS (Figure 7-8) efficiently quench the fluorescence of CPEs in water. MV^{2+} and NDS are known to quench the fluorescence of anionic and cationic CPEs by photoinduced electron transfer, respectively. Therefore, the same quenching mechanism was expected for P1 and P2 since they showed the similar solution behavior as CPEs. First, the quenching efficiency of P1 and P2 by MV^{2+} and NDS were investigated in water. As shown in Figure 7-9, P1 in which sulfonate groups are dominant on the polymer backbone is much more efficiently quenched by a cationic quencher, MV^{2+} ($K_{SV} = 2.1 \times 10^6 M^{-1}$) compared to an anionic quencher, NDS ($K_{SV} = 4.2 \times 10^3 M^{-1}$). In contrast, P2 in which quaternary ammonium groups are dominant is quenched much more strongly by NDS ($K_{SV} = 3.56 \times 10^6 M^{-1}$) than MV^{2+} ($K_{SV} = 1.5 \times 10^3 M^{-1}$). The fluorescence quenching data were analyzed using Stern-Volmer (SV) relation, given by $I_0/I = 1 + K_{SV}[Q]$ (where I_0 and I are the intensity of fluorescence in the absence and presence of a quencher, respectively, K_{SV} is the Stern-Volmer constant, and $[Q]$ is the concentration of a quencher). The Stern-Volmer constant (K_{SV}) is used to quantitatively measure the quenching efficiency. K_{SV} values for P1 and P2

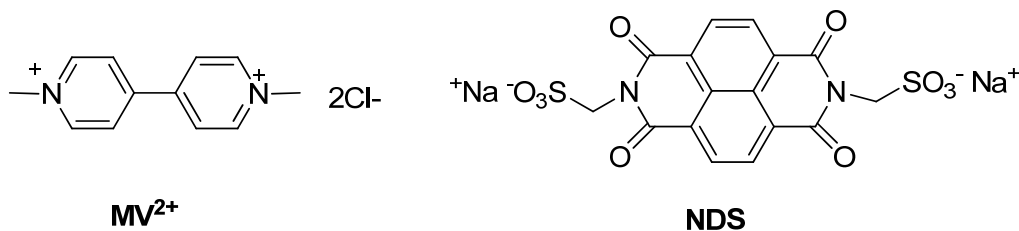


Figure 7-8. Structures of a cationic and an anionic quencher used in this study.

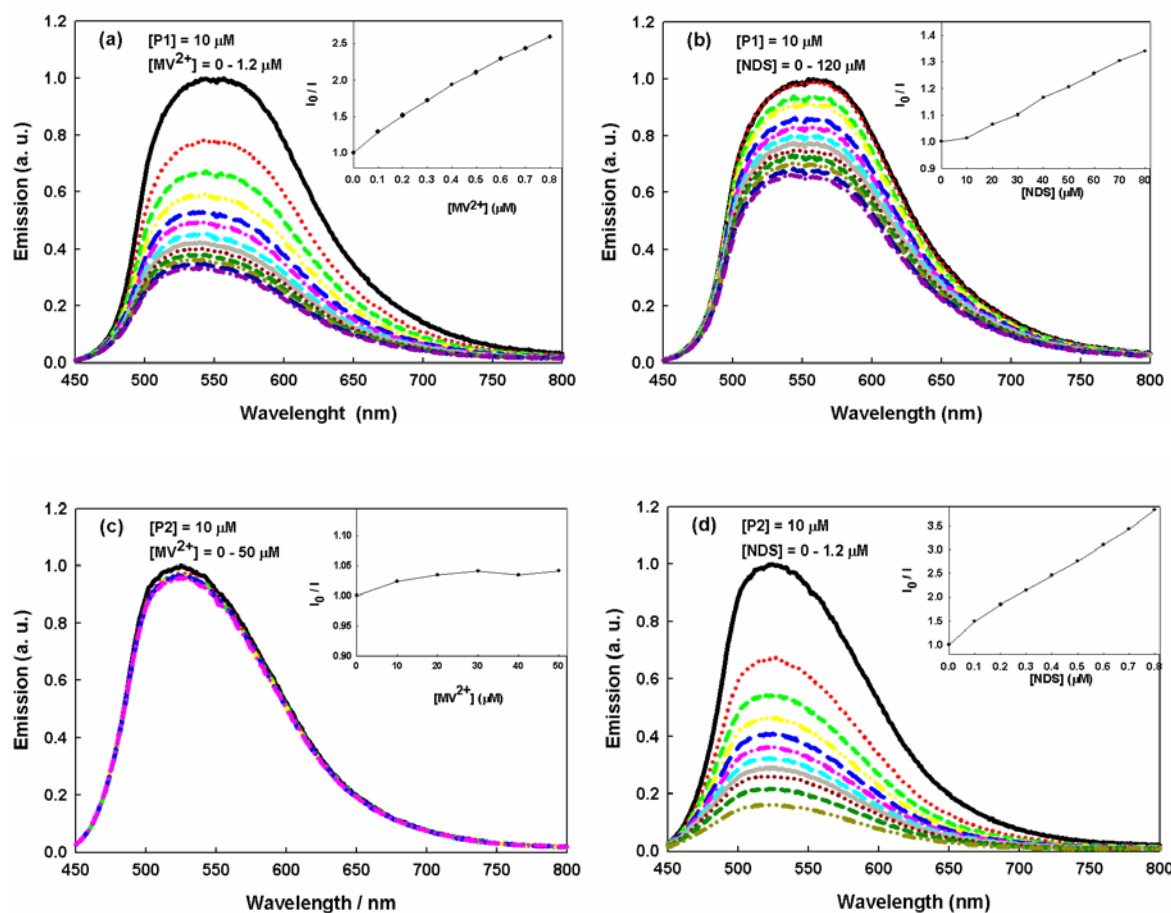


Figure 7-9. Emission spectra of P1 and P2 in water upon addition of a cationic and an anionic quencher. $\lambda_{\text{ex}} = 440 \text{ nm}$ for P1 and $\lambda_{\text{ex}} = 430 \text{ nm}$ for P2. The inset shows the Stern-Volmer plots using emission intensities at 556 nm for P1 and 445 nm for P2.

Table 7-2. Stern-Volmer constant (K_{SV}) for P1 and P2 fluorescence quenching upon addition of MV^{2+} and NDS in water and DMF.

	In water	In DMF
P1- MV^{2+}	$2.1 \times 10^6 \text{ M}^{-1}$	$7.4 \times 10^5 \text{ M}^{-1}$
P1-NDS	$4.2 \times 10^3 \text{ M}^{-1}$	$1.5 \times 10^3 \text{ M}^{-1}$
P2- MV^{2+}	$1.5 \times 10^3 \text{ M}^{-1}$	$4.0 \times 10^2 \text{ M}^{-1}$
P2-NDS	$3.56 \times 10^6 \text{ M}^{-1}$	$8.3 \times 10^5 \text{ M}^{-1}$

quenching were obtained in the linear region of the SV plots. Table 7-2 summarizes the Stern-Volmer constants (K_{sv}).

Figure 7-10 shows the absorption and emission spectra of P1 and P1 in DMF. Compared to the absorption spectra of P1 and P2 in water, relatively blue-shifted absorption maximum appears at 432 nm for P1 and 428 nm for P2. Both polymers feature a well-defined 0-0 band with $\lambda_{max} = 480$ nm for P1 and $\lambda_{max} = 476$ nm with a shoulder band around 510 nm. These spectral properties indicate the non-aggregated states of both polymers in DMF.

The same fluorescence quenching experiments as described above were carried out in DMF (Figure 7-11 and Table 7-2). The results are consistent with those observed in quenching experiments with P1 and P2 solution in water. Interestingly, at any given $[MV^{2+}]$ or $[NDS]$, the aggregated conformation of P1 and P2 is quenched more strongly compared to the non-aggregated conformation of polymers as previously reported for fluorescence quenching of PPE-based CPEs. This is likely due to the ability of the exciton to diffuse rapidly along the polymer chain. These observations provide the evidences for the fact that the polyampholytes with a low anionic-group/cationic-group ratio (< 1.0) on their backbone show similar solution properties with cationic or anionic CPEs.

PPE-NMe₃-COOH. To investigate the effect of the nature of ionic groups on the ampholyte properties, a sulfonate group was replaced with a carboxyl group as an anionic side group. The carboxyl group remains charged or neutralized according to pH changes whereas the quaternary ammonium group is insensitive to pH changes. The spectral changes induced by pH on the absorption and fluorescence spectra of this polymer are shown in Figure 7-12. For the absorption spectra, oscillator strength decreases with a decrease in the pH of the polymer solution. Interestingly, emission intensity and emission quantum efficiency increases in the

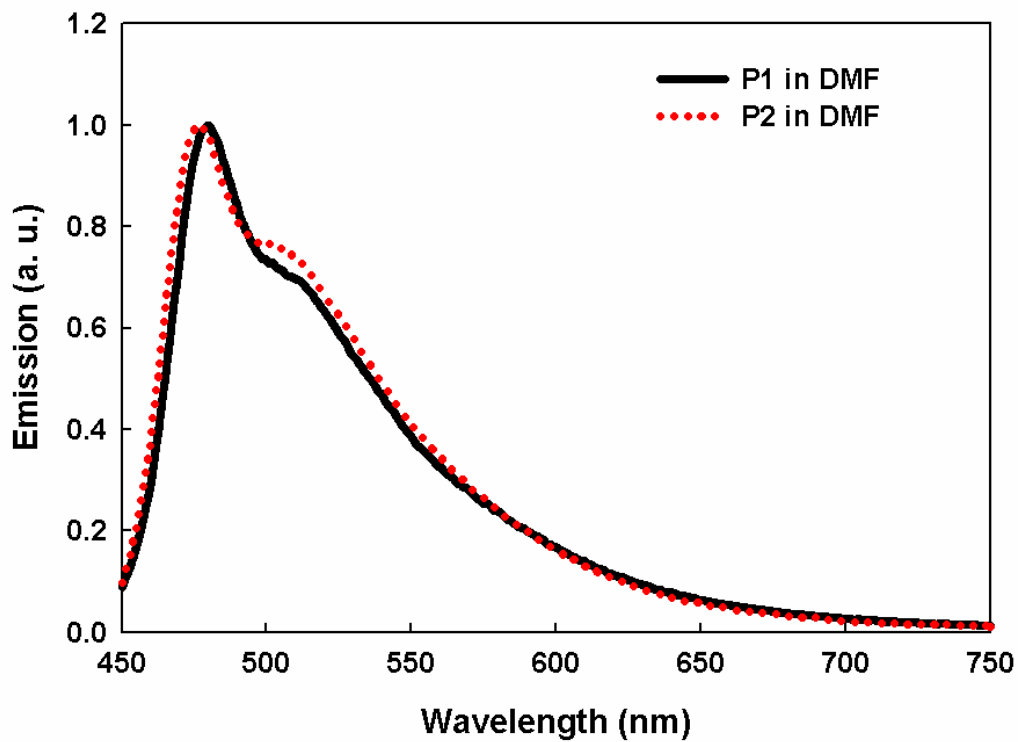
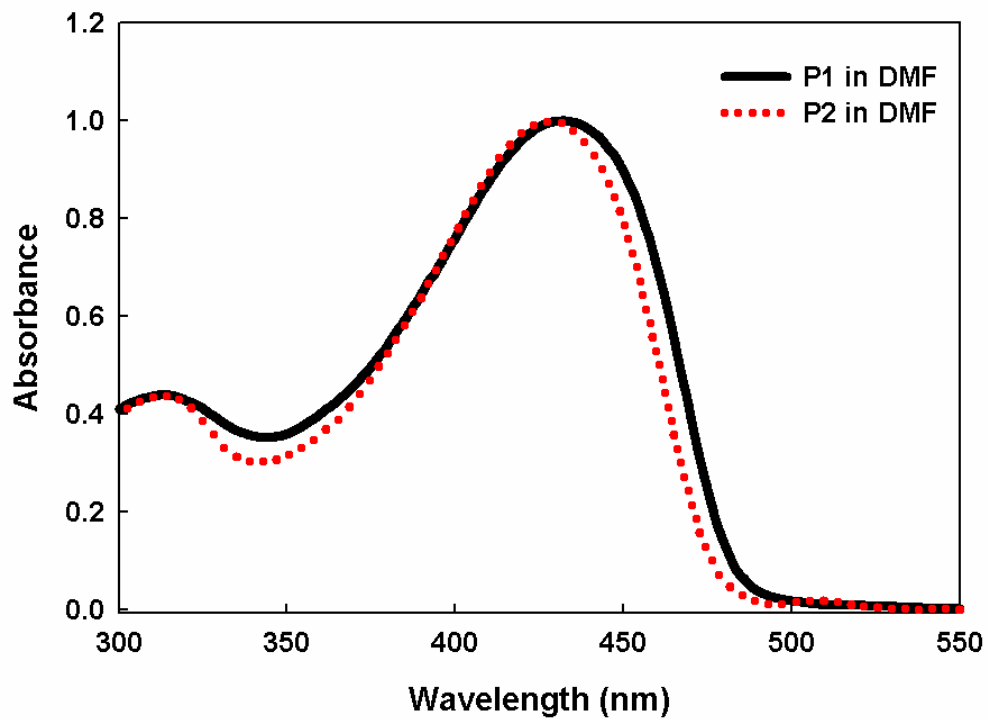


Figure 7-10. Absorption and emission spectra of P1 and P2 in DMF. $\lambda_{\text{ex}} = 430 \text{ nm}$ for both P1 and P2.

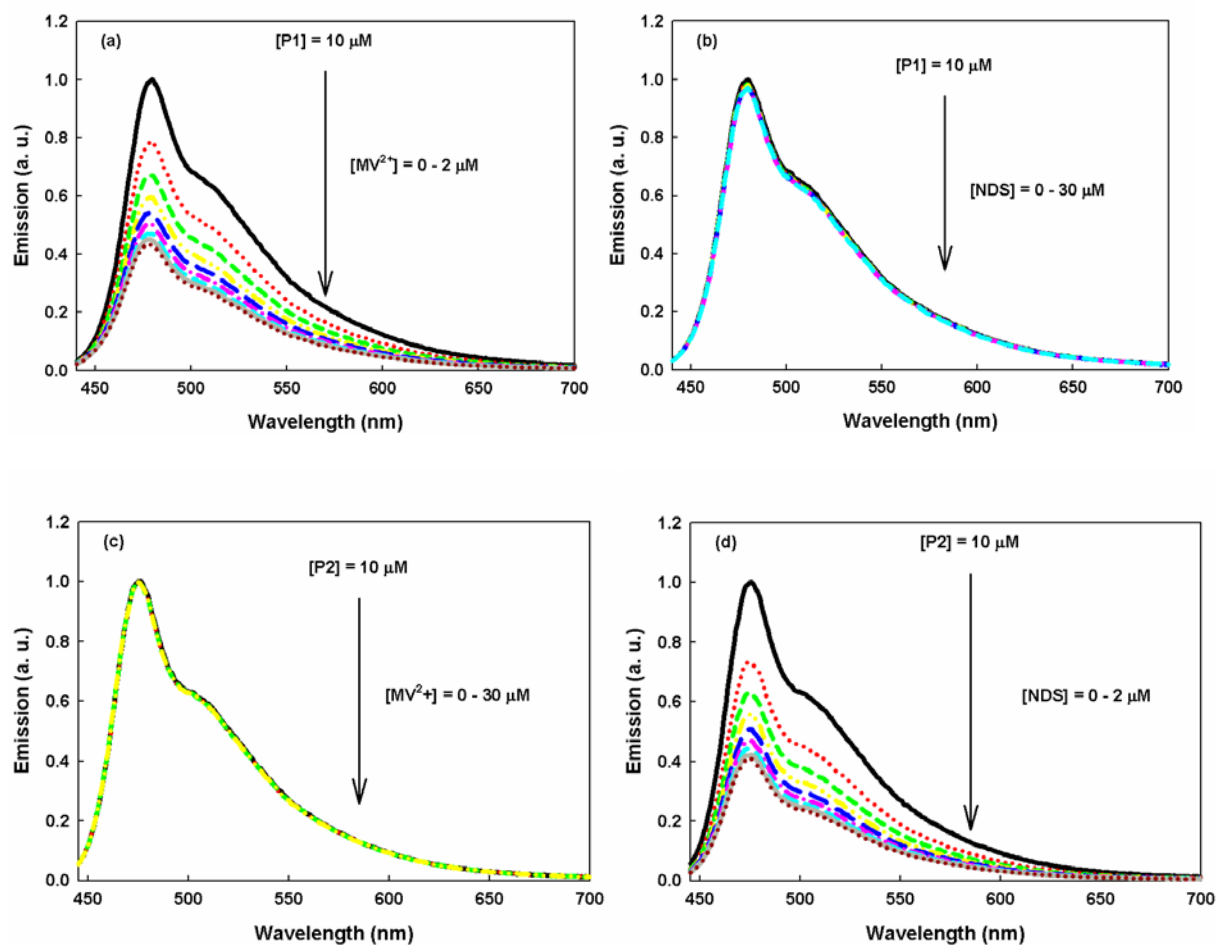


Figure 7-11. Emission spectra of P1 and P2 in DMF upon addition of a cationic and an anionic quencher. $\lambda_{\text{ex}} = 430 \text{ nm}$ for both P1 and P2.

sequence of pH 10.3 ($\Phi_{\text{fl}} = 0.046$) < pH 3.0 ($\Phi_{\text{fl}} = 0.071$) < pH 7.6 ($\Phi_{\text{fl}} = 0.077$). In the emission spectra of PPE-NMe₃-COOH, as pH decreases from 11 to 8, emission intensity sharply increases. At pH 5-8, the emission intensity remains almost constant. With a decrease in pH from 5 to 3, intensity is progressively reduced. At pH > 8, the COO⁻ groups are involved in the formation of zwitterions on the polymer backbone, and hence the attractive interaction between the negatively charged and positively charged groups forms an ionically crosslinked network that forces the polymer chains into a highly compact structure under this basic condition.^{204, 212} This might result in the reduced fluorescence intensity. In a pH range of 5-8, two contrary factors influence the polymer solution.²²⁰ First, COO⁻ - COO⁻ and ammonium-ammonium repulsion prevents

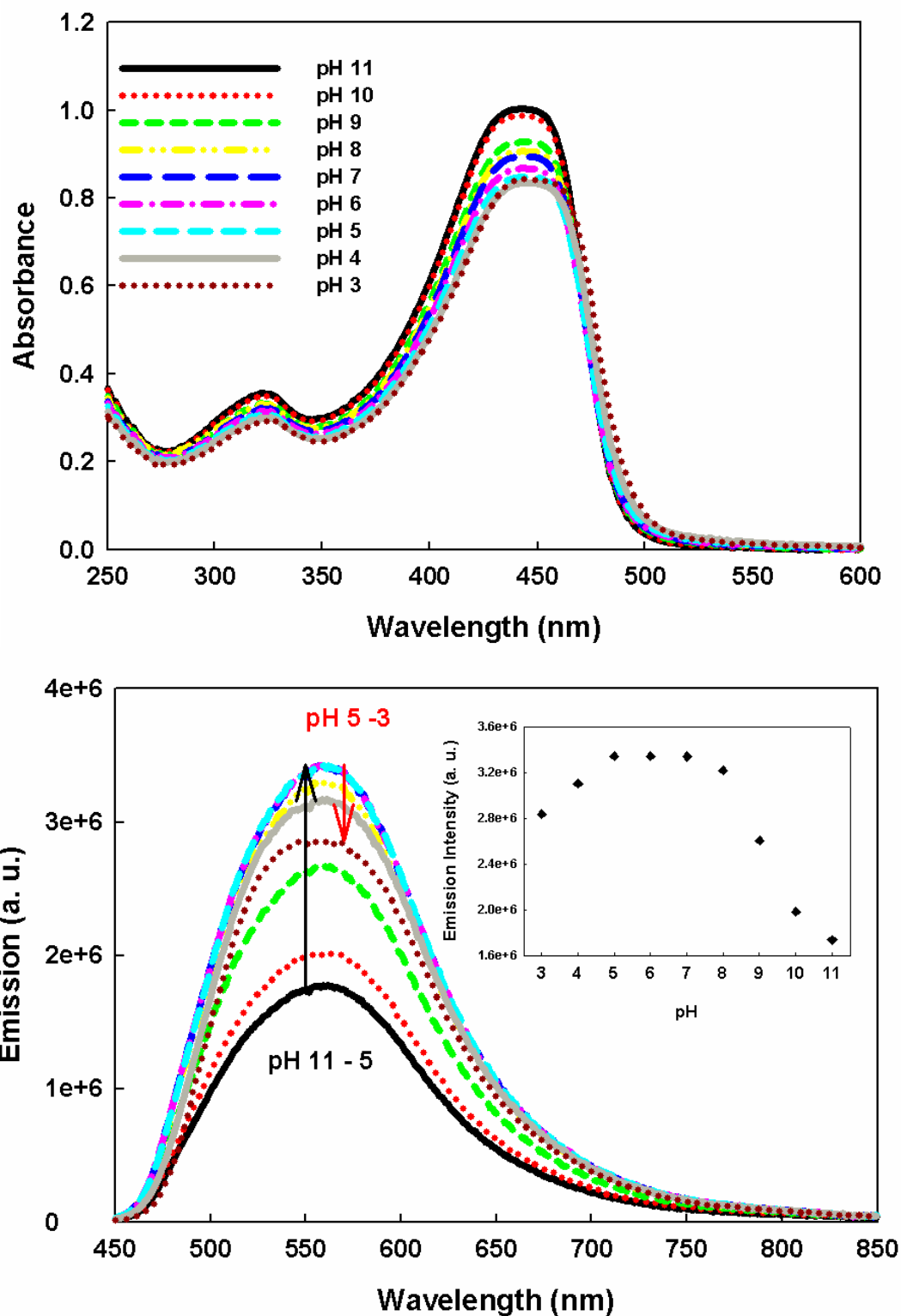


Figure 7-12. Absorption and emission spectra of PPE-NMe₃-COOH (30.72 μM) as a function of pH in aqueous solution. The inset illustrates that emission intensity at 548 nm varies depending on the pH in the polymer solution. $\lambda_{\text{ex}} = 430$ nm.

formation of a crosslinked network that induces the compact structure of polymer. At the same time, the static interaction between the carboxyl and ammonium groups restricts extended conformation of the polymer chain. As a result, the fluorescence intensity remains constant. At $\text{pH} < 4$, $-\text{COOH}$ groups are dominant, reducing the negative charge density on the polymer chain. Thus this reduces the attractive interactions between the oppositely charged groups. The polymer shows the similar behavior with that of cationic or anionic CPEs in water. Therefore, the fluorescence intensity of the polymer is reduced due to aggregation via π -stacking between adjacent polymer chains at this acidic condition.

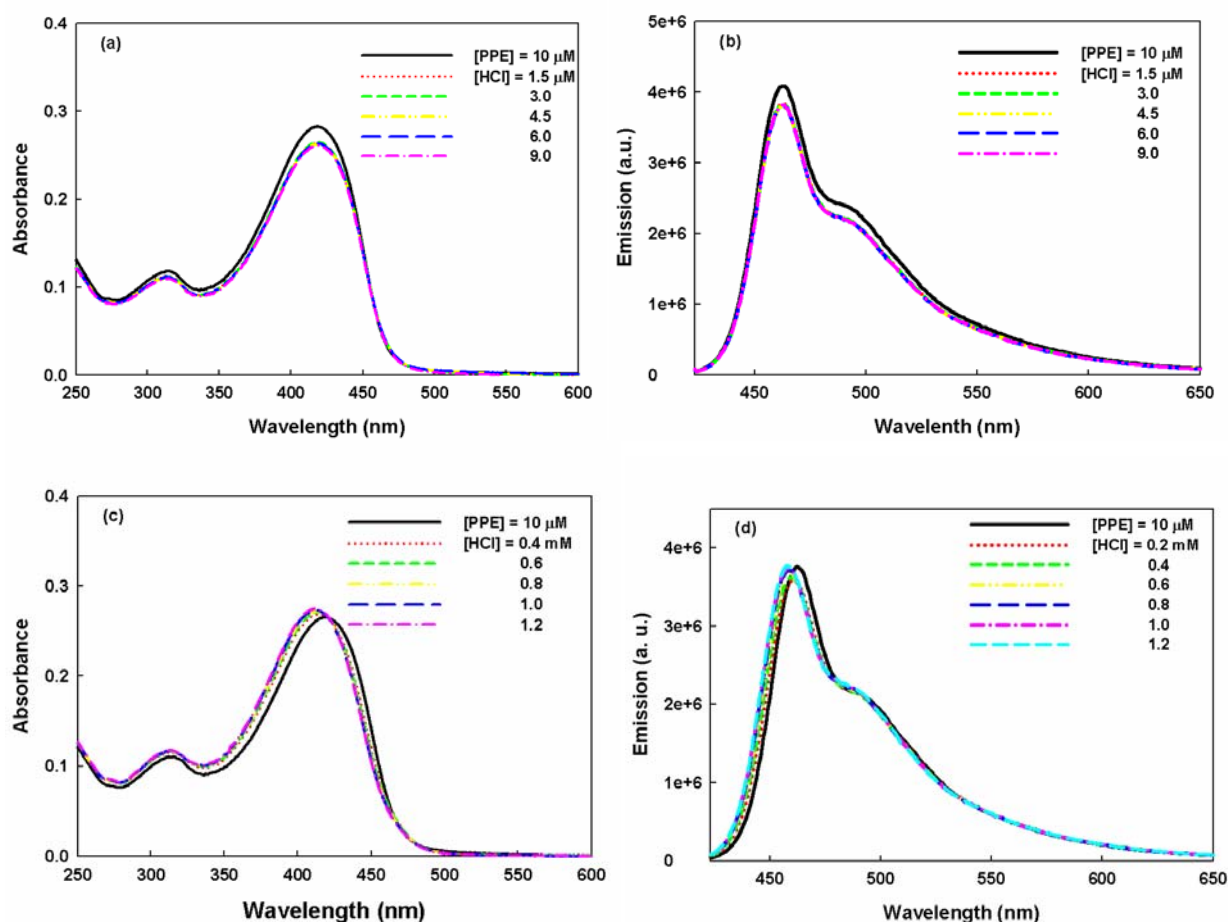


Figure 7-13. Absorption and emission spectra of PPE-NMe₃-COOH (10 μM) in methanol upon addition of HCl solution. (a) and (b) are spectra after addition of low concentration of HCl solution (0–9.0 μM). (c) and (d) are spectra after addition of high concentration of HCl solution (0–1.2 mM). $\lambda_{\text{ex}} = 420 \text{ nm}$.

The effect of HCl on the optical properties is also investigated using the polymer solution in methanol (Figure 7-13). Since the polymer is insoluble, the polymer aqueous solution (pH 11) is diluted with methanol to get the desired concentration of the polymer solution (10 μM). At low concentrations of HCl, the absorption and emission intensity are slightly decreased (Figure 7-13 (a) and (b)). After addition of higher concentration of HCl solution, the absorption and fluorescence spectra slightly red-shift compared to those in the absence of HCl solution (Figure 7-13 (c) and (d)). This suggests that introduction of HCl slightly interrupts the interactions between the oppositely charged side groups, inducing to expand the polymer chains.

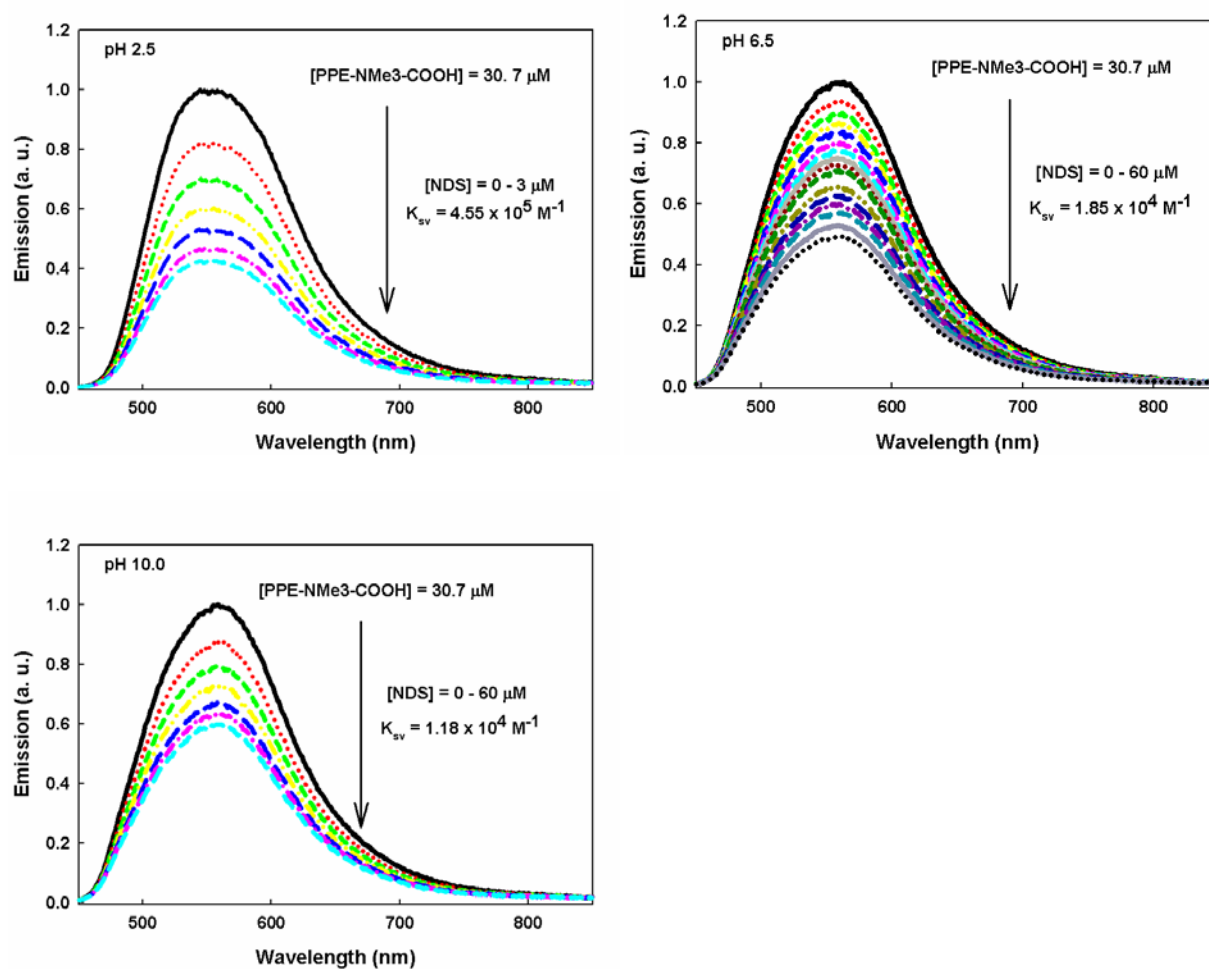


Figure 7-14. Emission spectra of PPE-NMe₃-COOH (30.72 μM) upon addition of an anionic quencher, NDS at different pH solutions. $\lambda_{\text{ex}} = 440 \text{ nm}$.

The quenching efficiency for PPE-NMe₃-COOH by an anionic quencher, NDS is observed at different pH (Figure 7-14). Stern-Volmer constants (K_{SV}) were obtained in a linear region of SV plots. At pH 2.5, most carboxyl groups exist as –COOH, and the negative charge density of ammonium groups is dominant in the polymer solution. Thus, the polymer is the most strongly quenched by NDS ($K_{SV} = 4.55 \times 10^5 \text{ M}^{-1}$). There is little difference between the K_{SV} values at pH 6.5 and pH 10.0.

Summary and Conclusions

In this chapter, we illustrated the effects of molecular architecture of polyampholytes on solution behavior. The nature of charged side groups and composition of the charged groups on the polymer backbone induce different solubility and rheological behavior. PPE-NMe₃-SO₃ bearing an equimolar ratio of ammonium and sulfonate groups shows very poor solubility in water. P1 and P2 containing a low molar ratio of ammonium to sulfonate groups (< 1.0) show similar solution behavior with anionic or cationic CPEs. Depending on the dominant charges on the polymer backbone, the polymers are strongly quenched by oppositely charged molecules. PPE-NMe₃-COOH containing carboxyl groups sensitive to changes in pH behaves as a polyelectrolyte or polyampholyte depending on the pH in aqueous solution. The different solution behavior also leads to changes in the absorption and emission spectra. The quenching efficiency for PPE-NMe₃-COOH varies according to pH.

Experimental

Materials

2,2'-(2,5-Diiodo-1,4-phenylene)bis(oxy)diacetic acid (**4**)¹⁸⁹ and 3,3'-(2,5-diiodo-1,4-phenylene)bis(oxy)dipropene-1-sulfonate (**9**)³⁶ were synthesized according to the literature procedure. 3,3'-[(2,5-Diiodo-1,4-phenylene)bis(oxy)]bis- [N,N,N-trimethylpropan-1-aminium]

(**6**) and 1,4-Diethynyl-2,5-bis[2-(2-methoxyethoxy)ethoxy] benzene (**13**) were synthesized according to the procedures described in Chapter 6.

Instrumentation

^1H and ^{13}C NMR spectra were recorded on either a VXR 300 or Varian Mercury-300 spectrometer and chemical shifts are reported in ppm relative to TMS. UV-vis absorption spectra were obtained with samples contained in a 1 cm quartz cuvette on a Varian Cary 100 spectrometer. Steady state fluorescence emission spectra were recorded on a PTI (Photon Technology International) fluorometer and corrected by using correction factors generated with a primary standard lamp.

General Methods

All sample solutions were prepared by using water that was distilled and then purified by a Millipore purification system (Millipore Simplicity Ultrapure Water System). The polymer stock solutions were diluted with the deionized water to a final concentration. All concentrations of polymers are provided in polymer repeat unit (PRU) concentration. In titration quenching experiments, 3 mL of polymer solution was placed in a 1cm fluorescence cuvette. Then fluorescence spectra were repeatedly acquired after addition of microliter aliquots of a concentrated solution containing a quencher. All experiments using the polymer solutions in methanol, the polymer aqueous solutions were diluted with methanol to obtain the desired concentration.

Synthetic Procedures

1,4-Bis(triisopropylsilylethynyl)-2,5-Bis(3-bromopropoxy)benzene (7). Under an argon atmosphere, THF (20 mL) and diisopropylamine (2.5 mL) were added to compound **5** (98 mg, 1.56 mmol), Pd(PPh₃)₂Cl₂ (62 mg, 0.09 mmol) and CuI (45 mg, 0.234 mmol). The mixture solution was degassed by argon bubbling at room temperature for 20 minutes and this was

followed by the dropwise addition of trisopropylsilylacetylene (0.63 mL, 2.77 mmol). The solution was stirred at room temperature for 40 hours. The solvent was removed and the solid was purified by flash chromatography on silica gel with hexane to yield a white solid **7** (570 mg, 0.80 mmol 51%). ¹H NMR (300 MHz, CDCl₃): δ 1.14 (s, 42H), 2.29 (m, 4H), 3.60 (t, 4H), 4.08 (t, 4H), 6.89 (s, 2H).

3,3'-(2,5-bis((Triisopropylsilyl)ethynyl)-1,4-phenylene)bis(oxy)bis(N,N,N-trimethylpropan-1-aminium) (8). Compound **7** (210 mg, 0.25 mmol) was suspended in 25 % trimethylamine in water (20 mL), ethanol (30 mL), and acetone (30 mL) and heated to 120 °C. The reaction was refluxed overnight. The solvent was removed and the white solid recrystallized from ethanol to yield 200 mg (0.24 mmol, 98%). ¹H NMR (300 MHz, CDCl₃): δ 1.10 (s, 42H), 2.23 (m, 4H), 3.12 (s, 18H), 3.48 (m, 4H), 4.08 (t, 3H), 6.99 (s, 2H).

PPE-SO₃-NMe₃. The solvent mixture (17 mL) of DMF/H₂O/(*i*Pr)₂NH (v/v/v/ = 9/6/2) was degassed with argon for 15 minutes and followed by the addition of compound **8** (100 mg, 0.12 mmol). After argon bubbling through the solution for 15 minutes, 1.0 M tetrabutylammonium fluoride solution in THF (1.60 mmol) was added to the flask under argon and the mixture was stirred at room temperature for 30 minutes. In a separate flask, a solution of CuI (4 mg, 0.02 mmol) and Pd(PPh₃)₄ (11 mg, 0.01 mmol) in DMF was degassed with argon for 30 minutes and added to the degassed solution containing compound **8**. Addition of compound **9** and 15 minute degassing were followed. Finally the solution was stirred under argon atmosphere at 60 °C for 24 hours. The reaction mixture was poured into 200 mL of acetone. The precipitate was dissolved in small amount of Millipore water and treated with NaCN, filtered using 25 μm glass filter and followed by dialysis against deionizer water using 6-8 kD MWCO cellulose membrane. The polymer solution was lyophilized to yield a yellow solid (35 mg, 0.036 mmol, 30

%). ^1H NMR (300 MHz, CD_3OD) and ^{13}C NMR (75 MHz, CD_3OD) spectra were not obtained due to the poor solubility of the compound.

PPE-SO₃-NMe₃-OR8-1. A solution of compound **6** (22 mg, 0.03 mmol), compound **9** (46 mg, 0.07 mmol,) and compound **13** (36 mg, 0.1 mmol) in 15 mL of DMF/water/ triethylamine (v/v/v = 3/2/1) were placed to a Schlenk flask and degassed with argon for 30 minutes. CuI (2 mg, 0.01 mmol) and Pd(PPh₃)₄ (7 mg, 0.006 mmol) were added to the mixture solution containing compound **6** and compound **9**. The reaction mixture was stirred at 60 °C for 26 hours. The resultant solution was added to 200 mL of acetone to form a precipitate. The collected precipitate was dissolved in an aqueous solution containing NaCN (8 mg), filtered using a 25 μm glass filter and followed by dialysis against deionized water using 6-8 kD MWCO cellulose membrane for 2 days. The polymer solution was lyophilized to yield a yellow solid (50 mg, 57%). ^1H NMR (300 MHz, DMSO- d_6): δ 2.06 (br, 2.8H), 2.22 (br, 1.2H), 2.65 (br, 2.8H), 3.01 (br, 5.4 H), 3.25 (br, 6H), 3.43 (br, 4H), 3.66 (br, 5.2 H), 3.79 (b, 4H). ^{13}C NMR (75 MHz, DMSO- d_6) spectrum was not obtained due to the limited solubility of the compound.

PPE-SO₃-NMe₃-OR8-2. This polymer was synthesized by the same procedure described for PPE-SO₃-NMe₃-OR8-1 using compound **6** (51 mg, 0.07 mmol), compound **9** (20 mg, 0.03 mmol) and compound **13** (36 mg, 0.1 mmol). Yield: 12 mg, 13%. ^1H NMR (300 MHz, DMSO- d_6): δ 2.06 (br, 1.2 H), 2.24 (br, 2.8H), 2.66 (br, 1.2H), 3.07 (br, 12.6 H), 3.21 (br, 6H), 3.40 (br, 4H), 3.65 (br, 6.8H), 3.79 (br, 4H). ^{13}C NMR (75 MHz, DMSO- d_6) spectrum was not obtained due to the limited solubility of the compound.

PPE-NMe₃-COOH. The solvent mixture (17 mL) of DMF/water/diisopropylamine (v/v/v/ = 9/6/2) was degassed with argon for 15 minutes and followed by the addition of compound **8** (79 mg, 0.095 mmol). After argon bubbling through the solution for 15 minutes, 1.0 M

tetrabutylammonium fluoride solution in THF (0.95 mmol) was then added to the flask under argon and the mixture was stirred at room temperature for 30 minutes. CuI (2 mg, 0.011 mmol) and Pd(PPh₃)₄ (7 mg, 0.006 mmol) was added to the mixture solution. After 15 minutes of degassing, compound **4** was added and the reaction mixture was stirred under argon at 60 °C for 24 hours. The reaction mixture was poured into 200 mL of acetone. The precipitate was dissolved in small amount of Millipore water and treated with NaCN (8 mg), filtered using 25 µm glass filter and followed by dialysis against deionized water using 6-8 kD MWCO cellulose membrane for 2 days. The polymer solution was lyophilized to yield a yellow solid (10 mg, 15 %). ¹H NMR (300 MHz, CD₃OD/D₂O) δ 2.23 (br, 4H), 3.10 (br, 18 H), 3.59 (br, 4H), 4.23 (br, 4H), 4.62 (br, 4H), 6.82 (br, 4H). ¹³C NMR (75 MHz, CD₃OD) spectra were not obtained due to the limited solubility of the compound.

CHAPTER 8 CONCLUSIONS

In the previous chapters, the synthesis, photophysical characterization and applications of poly(arylene ethynylene)-based conjugated polyelectrolytes (CPEs) have been presented.

Intercalation of Intercalator Quenchers to mPPESO3

Meta-linked poly(phenylene ethynylene)s bearing ionic groups can fold into a helical conformation in water, which is stabilized by π - π stacking and hydrophobic interactions. The helical polymer was used to sense protease activity. The polymer fluorescence is quenched significantly by L-Lys-*p*-nitroanilide (K-*p*NA) and peptidase reverses the fluorescence from the quenched polymer solution concurrent with peptide hydrolysis. More importantly, the polymer still shows amplified quenching at even high concentration of buffer solution up to 100 mM. Typically, CPEs show a significantly reduced quenching efficiency with increasing buffer concentration because the buffer ions screen the Coulomb interactions, removing quenchers from the vicinity of CPEs. This result is likely due to intercalation of quenchers into the helical conformation of the polymer, giving less ion-screening effect on the Coulomb interaction.

By taking the advantage of the helical structure, the polymer was used as a sensor platform with intercalator quenchers containing ligand. For this study, biotin and avidin were chosen as a ligand and a target protein, respectively. Biotin-functionalized quenchers strongly quench the polymer fluorescence via intercalation and static interaction. However, introduction of avidin to the polymer/quencher complexes is not capable of displacing the quenchers from the polymer, which does not increase the polymer fluorescence. Two possibilities are suggested to explain this result. First, biocytin-TMR is hidden within the helical polymer, and hence avidin is not able to be accessible to the biotin, leading to reversal of quenching. Second, the quenchers serve as crosslinkers for the concurrent binding of the polymer and avidin. When avidin is previously

bound to biotin on the quenchers, the quencher/avidin complexes give less effect on the fluorescence quenching. This might arise due to the electrostatic interaction between the oppositely charged polymer and avidin

Helical Self-Assembly of mPPESO3-py

In mPPESO3, phenylene units were replaced with pyridine rings. PPE-SO3-py shows solvent-induced self-assembly into a helix, which is evidenced by the absorption and emission spectra. The polymer also shows strong and selective affinity for Pd²⁺ ions in water. Interestingly, Pd-complexation with the polymer in methanol induces conformation changes into a helix. Changes in the absorption and emission spectra are consistent with those obtained depending on solvent polarity. Protonation of pyridine rings in methanol also leads to self-assembly of the polymer into a helix.

Biocidal Activity of Cationic CPEs

PPE-based cationic conjugated polyelectrolytes with tetraalkylammonium side groups exhibit light-induced biocidal activity. It was found that surface grafted conjugated polymer (SGCP) particles entrap and kill bacteria. Singlet oxygen generation at the polymer/bacteria surface is a crucial step in the biocidal action. This study shows that SGCP particles with bacteria that are oxygenated and irradiated exhibit the most efficient biocidal activity. Photophysical studies of the cationic polymers in solution strongly support the role of oxygen in the biocidal process. Direct excitation of the polymers generates a long-lived triplet state and the triplet state sensitizes singlet oxygen. For the light-induced biocidal activity, oxygen is also required at the polymer/bacteria interface.

Conjugated Polyampholytes

The effects of molecular architecture of polyampholytes on solution behavior were investigated by varying the nature of charged side groups, composition of the charged groups

and changes in pH. As the molar ratio of anionic to cationic groups is one and both charged groups are insensitive to changes in pH, the polyampholyte shows poor solubility in water. For polyampholytes with a low molar ratio of anionic to cationic groups, the polyampholytes show similar solution behavior compared with anionic or cationic CPEs. Depending on the dominant charges, the polymers are strongly quenched by oppositely charged molecules. The polyampholyte containing charged groups (carboxyl groups) that are sensitive to changes in pH behaves as a polyelectrolyte or polyampholyte depending on the pH in aqueous solution. The different solution behavior also leads to changes in the absorption and emission spectra.

LIST OF REFERENCES

1. Shirakawa, H.; Louis, E. J.; Macdiarmid, A. G.; Chiang, C. K.; Heeger, A. J., *J. Chem. Soc., Chem. Commun.* **1977**, (16), 578.
2. Grimsdale, A. C.; Mullen, K., *Emissive Materials: Nanomaterials* **2006**, 199, 1.
3. Scherf, U.; List, E. J. W., *Adv Mater* **2002**, 14, (7), 477.
4. Patil, A. O.; Heeger, A. J.; Wudl, F., *Chem Rev* **1988**, 88, (1), 183.
5. Perepichka, I. F.; Perepichka, D. F.; Meng, H.; Wudl, F., *Adv Mater* **2005**, 17, (19), 2281.
6. MacDiarmid, A. G., *Angew Chem Int Edit* **2001**, 40, (14), 2581.
7. Bunz, U. H. F., *Chem. Rev.* **2000**, 100, (4), 1605.
8. Kraft, A.; Grimsdale, A. C.; Holmes, A. B., *Angew. Chem., Int. Ed.* **1998**, 37, (4), 402.
9. Heeger, A. J., *Solid State Commun.* **1998**, 107, (11), 673.
10. Hide, F.; DiazGarcia, M. A.; Schwartz, B. J.; Heeger, A. J., *Accounts Chem Res* **1997**, 30, (10), 430.
11. Gunes, S.; Neugebauer, H.; Sariciftci, N. S., *Chem. Rev.* **2007**, 107, (4), 1324.
12. Sirringhaus, H., *Adv Mater* **2005**, 17, (20), 2411.
13. McQuade, D. T.; Pullen, A. E.; Swager, T. M., *Chem. Rev.* **2000**, 100, (7), 2537.
14. Thomas, S. W.; Joly, G. D.; Swager, T. M., *Chem. Rev.* **2007**, 107, (4), 1339.
15. Skotheim, T. A.; Elsenbaumer, R. L.; Reynolds, J. R., *Handbook of conducting polymers*. 2nd ed.; M. Dekker: New York, 1998; p 209.
16. Wise, D. L., *Photonic polymer systems : fundamentals, methods, and applications*. M. Dekker: New York, 1998; p 61.
17. Giesa, R., *J. Macromol. Sci., Rev. Macromol. Chem. Phys.* **1996**, C36, (4), 631.
18. Reddinger, J. L.; Reynolds, J. R., *Radical Polymerisation Polyelectrolytes* **1999**, 145, 57.
19. Schluter, A. D., *J. Polym. Sci., Part A: Polym. Chem.* **2001**, 39, (10), 1533.
20. Shi, S. Q.; Wudl, F., *Macromolecules* **1990**, 23, (8), 2119.
21. Wallow, T. I.; Novak, B. M., *J. Am. Chem. Soc.* **1991**, 113, (19), 7411.

22. Chen, L. H.; McBranch, D. W.; Wang, H. L.; Helgeson, R.; Wudl, F.; Whitten, D. G., *Proc. Natl. Acad. Sci. U. S. A.* **1999**, *96*, (22), 12287.
23. Pinto, M. R.; Schanze, K. S., *Synthesis-Stuttgart* **2002**, (9), 1293.
24. Gaylord, B. S.; Heeger, A. J.; Bazan, G. C., *Proc. Natl. Acad. Sci. U. S. A.* **2002**, *99*, (17), 10954.
25. Juan, Z.; Swager, T. M., *Poly(Arylene Ethynylene)S: From Synthesis to Application* **2005**, *177*, 151.
26. Achyuthan, K. E.; Bergstedt, T. S.; Chen, L.; Jones, R. M.; Kumaraswamy, S.; Kushon, S. A.; Ley, K. D.; Lu, L.; McBranch, D.; Mukundan, H.; Rininsland, F.; Shi, X.; Xia, W.; Whitten, D. G., *J. Mater. Chem.* **2005**, *15*, (27-28), 2648.
27. Kim, I. B.; Dunkhorst, A.; Gilbert, J.; Bunz, U. H. F., *Macromolecules* **2005**, *38*, (11), 4560.
28. Cabarcos, E. L.; Carter, S. A., *Macromolecules* **2005**, *38*, (25), 10537.
29. Lakowicz, J. R., *Principles of fluorescence spectroscopy*. 3rd ed.; Springer: New York, 2006.
30. Zhou, Q.; Swager, T. M., *J. Am. Chem. Soc.* **1995**, *117*, (26), 7017.
31. Zhou, Q.; Swager, T. M., *J. Am. Chem. Soc.* **1995**, *117*, (50), 12593.
32. Wang, J.; Wang, D. L.; Miller, E. K.; Moses, D.; Bazan, G. C.; Heeger, A. J., *Macromolecules* **2000**, *33*, (14), 5153.
33. Wang, D. L.; Wang, J.; Moses, D.; Bazan, G. C.; Heeger, A. J., *Langmuir* **2001**, *17*, (4), 1262.
34. Fan, C. H.; Wang, S.; Hong, J. W.; Bazan, G. C.; Plaxco, K. W.; Heeger, A. J., *Proc. Natl. Acad. Sci. U. S. A.* **2003**, *100*, (11), 6297.
35. Tan, C. Y.; Alas, E.; Muller, J. G.; Pinto, M. R.; Kleiman, V. D.; Schanze, K. S., *J. Am. Chem. Soc.* **2004**, *126*, (42), 13685.
36. Tan, C. Y.; Pinto, M. R.; Schanze, K. S., *Chem Commun* **2002**, (5), 446.
37. Gaylord, B. S.; Wang, S. J.; Heeger, A. J.; Bazan, G. C., *J. Am. Chem. Soc.* **2001**, *123*, (26), 6417.
38. Chen, L. H.; McBranch, D.; Wang, R.; Whitten, D., *Chem. Phys. Lett.* **2000**, *330*, (1-2), 27.
39. Cornelissen, J. J. L. M.; Rowan, A. E.; Nolte, R. J. M.; Sommerdijk, N. A. J. M., *Chem. Rev.* **2001**, *101*, (12), 4039.

40. Mueller, A.; O'Brien, D. F., *Chem. Rev.* **2002**, *102*, (3), 727.
41. Kim, S.; Jackiw, J.; Robinson, E.; Schanze, K. S.; Reynolds, J. R.; Baur, J.; Rubner, M. F.; Boils, D., *Macromolecules* **1998**, *31*, (4), 964.
42. Harrison, B. S.; Foley, T. J.; Knefely, A. S.; Mwaura, J. K.; Cunningham, G. B.; Kang, T. S.; Bouguettaya, M.; Boncella, J. M.; Reynolds, J. R.; Schanze, K. S., *Chem. Mater.* **2004**, *16*, (15), 2938.
43. Samuel, I. D. W.; Crystall, B.; Rumbles, G.; Burn, P. L.; Holmes, A. B.; Friend, R. H., *Chem Phys Lett* **1993**, *213*, (5-6), 472.
44. Nakano, T.; Okamoto, Y., *Chem. Rev.* **2001**, *101*, (12), 4013.
45. Pu, L., *Acta Polym.* **1997**, *48*, (4), 116.
46. Ciardelli, F.; Lanzillo, S.; Pieroni, O., *Macromolecules* **1974**, *7*, (2), 174.
47. Moore, J. S.; Gorman, C. B.; Grubbs, R. H., *J. Am. Chem. Soc.* **1991**, *113*, (5), 1704.
48. Yashima, E.; Matsushima, T.; Okamoto, Y., *J. Am. Chem. Soc.* **1995**, *117*, (46), 11596.
49. Nakako, H.; Mayahara, Y.; Nomura, R.; Tabata, M.; Masuda, T., *Macromolecules* **2000**, *33*, (11), 3978.
50. Shinohara, K.; Yasuda, S.; Kato, G.; Fujita, M.; Shigekawa, H., *J. Am. Chem. Soc.* **2001**, *123*, (15), 3619.
51. Aoki, T.; Shinohara, K.; Kaneko, T.; Oikawa, E., *Macromolecules* **1996**, *29*, (12), 4192.
52. Aoki, T.; Kobayashi, Y.; Kaneko, T.; Oikawa, E.; Yamamura, Y.; Fujita, Y.; Teraguchi, M.; Nomura, R.; Masuda, T., *Macromolecules* **1999**, *32*, (1), 79.
53. Lam, J. W. Y.; Dong, Y. P.; Cheuk, K. K. L.; Tang, B. Z., *Macromolecules* **2003**, *36*, (21), 7927.
54. Lam, J. W. Y.; Dong, Y. P.; Cheuk, K. K. L.; Law, C. C. W.; Lai, L. M.; Tang, B. Z., *Macromolecules* **2004**, *37*, (18), 6695.
55. Yashima, E.; Matsushima, T.; Okamoto, Y., *J. Am. Chem. Soc.* **1997**, *119*, (27), 6345.
56. Sakurai, S.; Goto, H.; Yashima, E., *Org. Lett.* **2001**, *3*, (15), 2379.
57. Leclere, P.; Surin, M.; Viville, P.; Lazzaroni, R.; Kilbinger, A. F. M.; Henze, O.; Feast, W. J.; Cavallini, M.; Biscarini, F.; Schenning, A. P. H. J.; Meijer, E. W., *Chem. Mater.* **2004**, *16*, (23), 4452.
58. Yashima, E.; Goto, H.; Okamoto, Y., *Macromolecules* **1999**, *32*, (23), 7942.

59. Nilsson, K. P. R.; Olsson, J. D. M.; Konradsson, P.; Inganas, O., *Macromolecules* **2004**, *37*, (17), 6316.
60. Goto, H.; Yashima, E., *J. Am. Chem. Soc.* **2002**, *124*, (27), 7943.
61. Geng, Y. H.; Trajkovska, A.; Katsis, D.; Ou, J. J.; Culligan, S. W.; Chen, S. H., *J. Am. Chem. Soc.* **2002**, *124*, (28), 8337.
62. Oda, M.; Nothofer, H. G.; Scherf, U.; Sunjic, V.; Richter, D.; Regenstein, W.; Neher, D., *Macromolecules* **2002**, *35*, (18), 6792.
63. Craig, M. R.; Jonkheijm, P.; Meskers, S. C. J.; Schenning, A. P. H. J.; Meijer, E. W., *Adv Mater* **2003**, *15*, (17), 1435.
64. Chen, H. P.; Katsis, D.; Mastrangelo, J. C.; Marshall, K. L.; Chen, S. H.; Mourey, T. H., *Chem. Mater.* **2000**, *12*, (8), 2275.
65. Fiesel, R.; Scherf, U., *Acta Polym.* **1998**, *49*, (8), 445.
66. Zhang, Z. B.; Motonaga, M.; Fujiki, M.; McKenna, C. E., *Macromolecules* **2003**, *36*, (19), 6956.
67. Fiesel, R.; Scherf, U., *Macromol. Rapid Commun.* **1998**, *19*, (8), 427.
68. Wilson, J. N.; Steffen, W.; McKenzie, T. G.; Lieser, G.; Oda, M.; Neher, D.; Bunz, U. H. F., *J. Am. Chem. Soc.* **2002**, *124*, (24), 6830.
69. Zahn, S.; Swager, T. M., *Angew. Chem., Int. Ed.* **2002**, *41*, (22), 4225.
70. Fiesel, R.; Halkyard, C. E.; Rampey, M. E.; Kloppenburg, L.; Studer-Martinez, S. L.; Scherf, U.; Bunz, U. H. F., *Macromol. Rapid Commun.* **1999**, *20*, (3), 107.
71. Peeters, E.; Delmotte, A.; Janssen, R. A. J.; Meijer, E. W., *Adv Mater* **1997**, *9*, (6), 493.
72. Peeters, E.; Christiaans, M. P. T.; Janssen, R. A. J.; Schoo, H. F. M.; Dekkers, H. P. J. M.; Meijer, E. W., *J. Am. Chem. Soc.* **1997**, *119*, (41), 9909.
73. Satrijo, A.; Swager, T. M., *Macromolecules* **2005**, *38*, (10), 4054.
74. Nelson, J. C.; Saven, J. G.; Moore, J. S.; Wolynes, P. G., *Science* **1997**, *277*, (5333), 1793.
75. Prince, R. B.; Saven, J. G.; Wolynes, P. G.; Moore, J. S., *J. Am. Chem. Soc.* **1999**, *121*, (13), 3114.
76. Prince, R. B.; Barnes, S. A.; Moore, J. S., *J. Am. Chem. Soc.* **2000**, *122*, (12), 2758.
77. Arnt, L.; Tew, G. N., *Macromolecules* **2004**, *37*, (4), 1283.

78. Tan, C. Ph.D. Dissertation, University of Florida, 2004.
79. Tan, C. Y.; Pinto, M. R.; Kose, M. E.; Ghiviriga, I.; Schanze, K. S., *Adv Mater* **2004**, *16*, (14), 1208.
80. Zhao, X. Y.; Schanze, K. S., *Langmuir* **2006**, *22*, (10), 4856.
81. Friedman, A. E.; Chambron, J. C.; Sauvage, J. P.; Turro, N. J.; Barton, J. K., *J. Am. Chem. Soc.* **1990**, *112*, (12), 4960.
82. Hartshorn, R. M.; Barton, J. K., *J. Am. Chem. Soc.* **1992**, *114*, (15), 5919.
83. Liu, B.; Bazan, G. C., *Chem. Mater.* **2004**, *16*, (23), 4467.
84. Liu, B.; Bazan, G. C., *Proc. Natl. Acad. Sci. U. S. A.* **2005**, *102*, (3), 589.
85. Dore, K.; Dubus, S.; Ho, H. A.; Levesque, I.; Brunette, M.; Corbeil, G.; Boissinot, M.; Boivin, G.; Bergeron, M. G.; Boudreau, D.; Leclerc, M., *J. Am. Chem. Soc.* **2004**, *126*, (13), 4240.
86. Ho, H. A.; Boissinot, M.; Bergeron, M. G.; Corbeil, G.; Dore, K.; Boudreau, D.; Leclerc, M., *Angew. Chem., Int. Ed.* **2002**, *41*, (9), 1548.
87. Nilsson, K. P. R.; Rydberg, J.; Baltzer, L.; Inganas, O., *Proc. Natl. Acad. Sci. U. S. A.* **2003**, *100*, (18), 10170.
88. McCullough, R. D.; Ewbank, P. C.; Loewe, R. S., *J. Am. Chem. Soc.* **1997**, *119*, (3), 633.
89. Lu, L. D.; Rininsland, F. H.; Wittenburg, S. K.; Achyuthan, K. E.; McBranch, D. W.; Whitten, D. G., *Langmuir* **2005**, *21*, (22), 10154.
90. Hedstrom, L., *Chem. Rev.* **2002**, *102*, (12), 4501.
91. Tong, L., *Chem. Rev.* **2002**, *102*, (12), 4609.
92. Neurath, H., *J. Cell. Biochem.* **1986**, *32*, (1), 35.
93. Eisenthal, R.; Danson, M. J., *Enzyme assays : a practical approach*. 2nd ed.; Oxford University Press: Oxford, OX ; New York, 2002.
94. Pinto, M. R.; Schanze, K. S., *Proc. Natl. Acad. Sci. U. S. A.* **2004**, *101*, (20), 7505.
95. Kumaraswamy, S.; Bergstedt, T.; Shi, X. B.; Rininsland, F.; Kushon, S.; Xia, W. S.; Ley, K.; Achyuthan, K.; McBranch, D.; Whitten, D., *P Natl Acad Sci USA* **2004**, *101*, (20), 7511.
96. Watson, J. D.; Crick, F. H. C., *Nature* **1953**, *171*, (4356), 737.

97. Demeunynck, M.; Bailly, C.; Wilson, W. C., *Small molecule DNA and RNA binders : from synthesis to nucleic acid complexes*. Wiley-VCH: Weinheim, 2003.
98. Zeglis, B. M.; Pierre, V. C.; Barton, J. K., *Chem Commun* **2007**, (44), 4565.
99. Erkkila, K. E.; Odom, D. T.; Barton, J. K., *Chem. Rev.* **1999**, *99*, (9), 2777.
100. Jennette, K. W.; Lippard, S. J.; Vassilia, G.; Bauer, W. R., *Proc. Natl. Acad. Sci. U. S. A.* **1974**, *71*, (10), 3839.
101. Pyle, A. M.; Barton, J. K., *Prog. Inorg. Chem.* **1990**, *38*, 413.
102. Barton, J. K.; Danishefsky, A. T.; Goldberg, J. M., *J. Am. Chem. Soc.* **1984**, *106*, (7), 2172.
103. Barton, J. K.; Dannenberg, J. J.; Raphael, A. L., *J. Am. Chem. Soc.* **1982**, *104*, (18), 4967.
104. Barton, J. K.; Goldberg, J. M.; Kumar, C. V.; Turro, N. J., *J. Am. Chem. Soc.* **1986**, *108*, (8), 2081.
105. Pyle, A. M.; Long, E. C.; Barton, J. K., *J. Am. Chem. Soc.* **1989**, *111*, (12), 4520.
106. Mahnken, R. E.; Billadeau, M. A.; Nikonowicz, E. P.; Morrison, H., *J. Am. Chem. Soc.* **1992**, *114*, (24), 9253.
107. Tamilarasan, R.; Mcmillin, D. R., *Inorg. Chem.* **1990**, *29*, (15), 2798.
108. Grover, N.; Gupta, N.; Thorp, H. H., *J. Am. Chem. Soc.* **1992**, *114*, (9), 3390.
109. Grover, N.; Thorp, H. H., *J. Am. Chem. Soc.* **1991**, *113*, (18), 7030.
110. Gupta, N.; Grover, N.; Neyhart, G. A.; Singh, P.; Thorp, H. H., *Inorg. Chem.* **1993**, *32*, (3), 310.
111. Kalsbeck, W. A.; Thorp, H. H., *J. Am. Chem. Soc.* **1993**, *115*, (16), 7146.
112. Carlson, D. L.; Huchital, D. H.; Mantilla, E. J.; Sheardy, R. D.; Murphy, W. R., *J. Am. Chem. Soc.* **1993**, *115*, (14), 6424.
113. Stoeffler, H. D.; Thornton, N. B.; Temkin, S. L.; Schanze, K. S., *Journal of the American Chemical Society* **1995**, *117*, (27), 7119.
114. Lo, K. K. W.; Tsang, K. H. K., *Organometallics* **2004**, *23*, (12), 3062.
115. Pinto, M. R.; Kristal, B. M.; Schanze, K. S., *Langmuir* **2003**, *19*, (16), 6523.
116. Zhao, X. Y.; Pinto, M. R.; Hardison, L. M.; Mwaura, J.; Muller, J.; Jiang, H.; Witker, D.; Kleiman, V. D.; Reynolds, J. R.; Schanze, K. S., *Macromolecules* **2006**, *39*, (19), 6355.

117. Jiang, H.; Zhao, X. Y.; Schanze, K. S., *Langmuir* **2006**, *22*, (13), 5541.
118. Jiang, H.; Zhao, X. Y.; Schanze, K. S., *Langmuir* **2007**, *23*, (18), 9481.
119. Fan, C. H.; Plaxco, K. W.; Heeger, A. J., *J Am Chem Soc* **2002**, *124*, (20), 5642.
120. DiCesare, N.; Pinto, M. R.; Schanze, K. S.; Lakowicz, J. R., *Langmuir* **2002**, *18*, (21), 7785.
121. Rininsland, F.; Xia, W. S.; Wittenburg, S.; Shi, X. B.; Stankewicz, C.; Achyuthan, K.; McBranch, D.; Whitten, D., *P Natl Acad Sci USA* **2004**, *101*, (43), 15295.
122. Liu, Y.; Ogawa, K.; Schanze, K. S., *Anal Chem* **2008**, *80*, (1), 150.
123. Zhao, X. Y.; Liu, Y.; Schanze, K. S., *Chem Commun* **2007**, (28), 2914.
124. Gaylord, B. S.; Heeger, A. J.; Bazan, G. C., *J Am Chem Soc* **2003**, *125*, (4), 896.
125. Chen, Y. G.; Zhao, D.; He, Z. K.; Ai, X. P., *Spectrochim Acta A* **2007**, *66*, (2), 448.
126. Zhao, D.; Du, J.; Chen, Y. G.; Ji, X. H.; He, Z. K.; Chan, W. H., *Macromolecules* **2008**, *41*, (14), 5373.
127. Livnah, O.; Bayer, E. A.; Wilchek, M.; Sussman, J. L., *Proc. Natl. Acad. Sci. U. S. A.* **1993**, *90*, (11), 5076.
128. Dwight, S. J.; Gaylord, B. S.; Hong, J. W.; Bazan, G. C., *J. Am. Chem. Soc.* **2004**, *126*, (51), 16850.
129. Slim, M.; Durisic, N.; Grutter, P.; Sleiman, H. F., *ChemBioChem* **2007**, *8*, (7), 804.
130. Hou, X. L.; Xu, M.; Wu, L. X.; Shen, J. C., *Colloid Surface B* **2005**, *41*, (2-3), 181.
131. Liu, X. D.; Diao, H. Y.; Nishi, N., *Chem. Soc. Rev.* **2008**, *37*, (12), 2745.
132. Dawson, W. R.; Windsor, M. W., *J. Phys. Chem.* **1968**, *72*, (9), 3251.
133. Eaton, D. F., *Pure Appl. Chem.* **1988**, *60*, (7), 1107.
134. Forster, T., *Ann Phys-Berlin* **1948**, *2*, (1-2), 55.
135. Wang, S.; Gaylord, B. S.; Bazan, G. C., *J. Am. Chem. Soc.* **2004**, *126*, (17), 5446.
136. Lakowicz, J. R., *Principles of fluorescence spectroscopy*. 3rd ed.; Springer Verlag: 2006.
137. Liu, B.; Bazan, G. C., *J. Am. Chem. Soc.* **2006**, *128*, (4), 1188.
138. Friedman, R. A.; Honig, B., *Biophys. J.* **1995**, *69*, (4), 1528.

139. Delnoye, D. A. P.; Sijbesma, R. P.; Vekemans, J. A. J. M.; Meijer, E. W., *J. Am. Chem. Soc.* **1996**, *118*, (36), 8717.
140. Brunsveld, L.; Zhang, H.; Glasbeek, M.; Vekemans, J. A. J. M.; Meijer, E. W., *J. Am. Chem. Soc.* **2000**, *122*, (26), 6175.
141. Bielawski, C.; Chen, Y. S.; Zhang, P.; Prest, P. J.; Moore, J. S., *Chem Commun* **1998**, (12), 1313.
142. Yagi, S.; Sakai, N.; Yamada, R.; Takahashi, H.; Mizutani, T.; Takagishi, T.; Kitagawa, S.; Ogoshi, H., *Chem Commun* **1999**, (10), 911.
143. Lahiri, S.; Thompson, J. L.; Moore, J. S., *J. Am. Chem. Soc.* **2000**, *122*, (46), 11315.
144. Ravve, A., *Principles of polymer chemistry*. Plenum Press: New York, 1995; p xiv, 496 p.
145. Chan, H. S.; Dill, K. A., *Macromolecules* **1989**, *22*, (12), 4559.
146. Prest, P. J.; Prince, R. B.; Moore, J. S., *J. Am. Chem. Soc.* **1999**, *121*, (25), 5933.
147. Shetty, A. S.; Zhang, J. S.; Moore, J. S., *J. Am. Chem. Soc.* **1996**, *118*, (5), 1019.
148. Wang, B.; Wasielewski, M. R., *J. Am. Chem. Soc.* **1997**, *119*, (1), 12.
149. Kimura, M.; Horai, T.; Hanabusa, K.; Shirai, H., *Adv. Mater.* **1998**, *10*, (6), 459.
150. Pang, Y.; Li, J.; Hu, B.; Karasz, F. E., *Macromolecules* **1998**, *31*, (19), 6730.
151. Winter, D.; Eisenbach, C. D., *J. Polym. Sci., Part A: Polym. Chem.* **2004**, *42*, (8), 1919.
152. Huang, H. M.; Wang, K.; Tan, W. H.; An, D.; Yang, X. H.; Huang, S. S.; Zhai, Q.; Zhou, L.; Jin, Y., *Angew Chem Int Edit* **2004**, *43*, (42), 5635.
153. Li, C. H.; Guo, Y. B.; Lv, J.; Xu, J. L.; Li, Y. L.; Wang, S.; Liu, H. B.; Zhu, D. B., *J. Polym. Sci., Part A: Polym. Chem.* **2007**, *45*, (8), 1403.
154. Senthilikumar, S.; Nath, S.; Pal, H., *Photochem. Photobiol.* **2004**, *80*, (1), 104.
155. Fan, L. J.; Jones, W. E., *J. Am. Chem. Soc.* **2006**, *128*, (21), 6784.
156. Birks, J. B., *Photophysics of aromatic molecules*. Wiley-Interscience: London, New York, 1970.
157. Blake, A. J.; Baum, G.; Champness, N. R.; Chung, S. S. M.; Cooke, P. A.; Fenske, D.; Khlobystov, A. N.; Lemenovskii, D. A.; Li, W. S.; Schroder, M., *J Chem Soc Dalton* **2000**, (23), 4285.
158. Dana, B. H.; Robinson, B. H.; Simpson, J., *J. Organomet. Chem.* **2002**, *648*, (1-2), 251.

159. Patel, M. B.; Patel, S. A.; Ray, A.; Patel, R. M., *J. Appl. Polym. Sci.* **2003**, *89*, (4), 895.
160. Park, E. S.; Lee, H. J.; Park, H. Y.; Kim, M. N.; Chung, K. H.; Yoon, J. S., *J. Appl. Polym. Sci.* **2001**, *80*, (5), 728.
161. Kenawy, E. R., *J. Appl. Polym. Sci.* **2001**, *82*, (6), 1364.
162. Denyer, S. P., *Int. Biodeterior. Biodegrad.* **1995**, *36*, (3-4), 227.
163. Cen, L.; Neoh, K. G.; Kang, E. T., *Langmuir* **2003**, *19*, (24), 10295.
164. Ikeda, T.; Yamaguchi, H.; Tazuke, S., *Antimicrob. Agents Chemother.* **1984**, *26*, (2), 139.
165. Kugler, R.; Bouloussa, O.; Rondelez, F., *Microbiology* **2005**, *151*, 1341.
166. Thorsteinsson, T.; Masson, M.; Kristinsson, K. G.; Hjalmarsdottir, M. A.; Hilmarsson, H.; Loftsson, T., *J. Med. Chem.* **2003**, *46*, (19), 4173.
167. Tiller, J. C.; Liao, C. J.; Lewis, K.; Klibanov, A. M., *Proc. Natl. Acad. Sci. U. S. A.* **2001**, *98*, (11), 5981.
168. Tiller, J. C.; Lee, S. B.; Lewis, K.; Klibanov, A. M., *Biotechnol. Bioeng.* **2002**, *79*, (4), 465.
169. Lewis, K.; Klibanov, A. M., *Trends Biotechnol* **2005**, *23*, (7), 343.
170. Lin, J.; Tiller, J. C.; Lee, S. B.; Lewis, K.; Klibanov, A. M., *Biotechnol. Lett.* **2002**, *24*, (10), 801.
171. Kwon, D. H.; Lu, C. D., *Antimicrob Agents Ch* **2006**, *50*, (5), 1623.
172. Johnston, M. D.; Hanlon, G. W.; Denyer, S. P.; Lambert, R. J. W., *J. Appl. Microbiol.* **2003**, *94*, (6), 1015.
173. Fink-Puches, R.; Hofer, A.; Smolle, J.; Kerl, H.; Wolf, P., *J. Photochem. Photobiol., B* **1997**, *41*, (1-2), 145.
174. Hohenleutner, U.; Baumler, W.; Karrer, S.; Michel, S.; Landthaler, M., *Hautarzt* **1996**, *47*, (3), 183.
175. Jeffes, E. W.; McCullough, J. L.; Weinstein, G. D.; Fergin, P. E.; Nelson, J. S.; Shull, T. F.; Simpson, K. R.; Bukaty, L. M.; Hoffman, W. L.; Fong, N. L., *Arch Dermatol* **1997**, *133*, (6), 727.
176. Merchat, M.; Bertolini, G.; Giacomini, P.; Villanueva, A.; Jori, G., *J. Photochem. Photobiol., B* **1996**, *32*, (3), 153.
177. Merchat, M.; Spikes, J. D.; Bertoloni, G.; Jori, G., *J. Photochem. Photobiol., B* **1996**, *35*, (3), 149.

178. Minnock, A.; Vernon, D. I.; Schofield, J.; Griffiths, J.; Parish, J. H.; Brown, S. B., *J. Photochem. Photobiol., B* **1996**, *32*, (3), 159.
179. Zanin, I. C. J.; Goncalves, R. B.; Brugnera, A.; Hope, C. K.; Pratten, J., *J. Antimicrob. Chemother.* **2005**, *56*, (2), 324.
180. Foote, C. S., *Photochem. Photobiol.* **1991**, *54*, (5), 659.
181. Jones, L. R.; Grossweiner, L. I., *J. Photochem. Photobiol., B* **1994**, *26*, (3), 249.
182. Kilger, R.; Maier, M.; Szeimies, R. M.; Baumler, W., *Chem. Phys. Lett.* **2001**, *343*, (5-6), 543.
183. Baumler, W.; Abels, C.; Karrer, S.; Weiss, T.; Messmann, H.; Landthaler, M.; Szeimies, R. M., *Br. J. Cancer* **1999**, *80*, (3-4), 360.
184. Halliwell, B.; Gutteridge, J. M. C., *Lancet* **1984**, *1*, (8391), 1396.
185. Jones, R. M.; Bergstedt, T. S.; McBranch, D. W.; Whitten, D. G., *J. Am. Chem. Soc.* **2001**, *123*, (27), 6726.
186. Lu, L. D.; Jones, R. M.; McBranch, D.; Whitten, D., *Langmuir* **2002**, *18*, (20), 7706.
187. Maisch, T.; Szeimies, R. M.; Jori, G.; Abels, C., *Photochem. Photobiol. Sci.* **2004**, *3*, (10), 907.
188. Ogawa, K.; Chemburu, S.; Lopez, G. P.; Whitten, D. G.; Schanze, K. S., *Langmuir* **2007**, *23*, (8), 4541.
189. Zhao, X. Ph.D. Dissertation, University of Florida, **2007**.
190. Johnson, C. S., *Prog. Nucl. Magn. Reson. Spectrosc.* **1999**, *34*, (3-4), 203.
191. Antalek, B.; Hewitt, J. M.; Windig, W.; Yacobucci, P. D.; Mourey, T.; Le, K., *Magn. Reson. Chem.* **2002**, *40*, S60.
192. Antalek, B., *Concepts Magn. Reson.* **2002**, *14*, (4), 225.
193. Walters, K. A.; Ley, K. D.; Schanze, K. S., *Chem. Commun.* **1998**, (10), 1115.
194. Partee, J.; Frankevich, E. L.; Uhlhorn, B.; Shinar, J.; Ding, Y.; Barton, T. J., *Phys. Rev. Lett.* **1999**, *82*, (18), 3673.
195. Funston, A. M.; Silverman, E. E.; Schanze, K. S.; Miller, J. R., *J. Phys. Chem. B* **2006**, *110*, (36), 17736.
196. Farley, R. T. Ph. D. Dissertation, University of Florida, **2007**.
197. Wang, Y. S.; Schanze, K. S., *Chem. Phys.* **1993**, *176*, (2-3), 305.

198. Ogilby, P. R.; Foote, C. S., *J Am Chem Soc* **1983**, *105*, (11), 3423.
199. Mathai, S.; Smith, T. A.; Ghiggino, K. P., *Photochem. Photobiol. Sci.* **2007**, *6*, (9), 995.
200. Wilkinson, F.; Helman, W. P.; Ross, A. B., *J. Phys. Chem. Ref. Data* **1993**, *22*, (1), 113.
201. Nardello, V.; Brault, D.; Chavalle, P.; Aubry, J. M., *J. Photochem. Photobiol., B* **1997**, *39*, (2), 146.
202. Chemburu, S.; Corbitt, T. S.; Ista, L. K.; Ji, E.; Fulghum, J.; Lopez, G. P.; Ogawa, K.; Schanze, K. S.; Whitten, D. G., *Langmuir* **2008**, *24*, (19), 11053.
203. Nardello, V.; Azaroual, N.; Cervoise, I.; Vermeersch, G.; Aubry, J. M., *Tetrahedron* **1996**, *52*, (6), 2031.
204. McCormick, C. L.; Kathmann, E. E., *Polymeric materials encyclopedia*. CRC Press: Boca Raton, 1996; Vol. 7, p 5462.
205. Lowe, A. B.; McCormick, C. L., *Chem. Rev.* **2002**, *102*, (11), 4177.
206. Alfrey, T.; Fuoss, R. M.; Morawetz, H.; Pinner, H., *J. Am. Chem. Soc.* **1952**, *74*, (2), 438.
207. Alfrey, T.; Morawetz, H., *J. Am. Chem. Soc.* **1952**, *74*, (2), 436.
208. Alfrey, T.; Morawetz, H.; Fitzgerald, E. B.; Fuoss, R. M., *J. Am. Chem. Soc.* **1950**, *72*, (4), 1864.
209. Katchalsky, A.; Miller, I. R., *J. Polym. Sci.* **1954**, *13*, (68), 57.
210. Ibraeva, Z. E.; Hahn, M.; Jaeger, W.; Bimendina, L. A.; Kudaibergenov, S. E., *Macromol. Chem. Phys.* **2004**, *205*, (18), 2464.
211. Kotz, J.; Hahn, M.; Philipp, B.; Bekturov, E. A.; Kudaibergenov, S. E., *Makromol. Chem.* **1993**, *194*, (2), 397.
212. Lee, W. F.; Tsai, C. C., *Polymer* **1995**, *36*, (2), 357.
213. Salamone, J. C.; Watterson, A. C.; Hsu, T. D.; Tsai, C. C.; Mahmud, M. U., *J. Polym. Sci. Polym. Lett. Ed.* **1977**, *15*, (8), 487.
214. Salamone, J. C.; Tsai, C. C.; Watterson, A. C., *J. Macromol. Sci. Chem.* **1979**, *A13*, (5), 665.
215. Salamone, J. C.; Quach, L.; Watterson, A. C.; Krauser, S.; Mahmud, M. U., *J. Macromol. Sci. Chem.* **1985**, *A22*, (5-7), 653.
216. Corpart, J. M.; Candau, F., *Macromolecules* **1993**, *26*, (6), 1333.
217. McCormick, C. L.; Johnson, C. B., *Macromolecules* **1988**, *21*, (3), 694.

218. McCormick, C. L.; Salazar, L. C., *Macromolecules* 1992, 25, (7), 1896.
219. Reynolds, G. A.; Drexhage, K. H., *Opt. Commun.* 1975, 13, (3), 222.
220. Xu, S. M.; Wu, R. L.; Huang, X. J.; Cao, L. Q.; Wang, J. D., *J. Appl. Polym. Sci.* 2006, 102, (2), 986.

BIOGRAPHICAL SKETCH

Eunkyung Ji was born in Onyang in South Korea and grew up there until she graduated a high school in February 1995. In March of that year she moved to Seoul, Korea's capital city and started her academic career in chemical engineering. She graduated from Hanyang University with a bachelor's degree in chemical engineering in February 1999 and then she took a job in Seoul. In March 2001, she restarted her education to achieve master's degree in chemical engineering at Hanyang University. Her research was focused on the development of biosensors using polydiacetylene. After obtaining a master's degree in February 2003, she moved to Gainesville in August 2004 and continued her education in chemistry at the University of Florida toward get Ph. D. During the course of graduate school, she joined the group of Dr. Kirk Schanze. In the past five years, she did research in the area of water-soluble conjugated polymers. After her Ph. D., Eunkyung started her postdoctoral research in the group of Dr. David Whitten at the University of New Mexico.